UC San Diego

UC San Diego Electronic Theses and Dissertations

Title

Characterizing Cetacean Distribution and Density across Two Decades of Environmental Change in the Southern California Current Ecosystem

Permalink

https://escholarship.org/uc/item/6pv6d1ng

ISBN

9798171606893

Author

Alksne, Michaela Noel

Publication Date

2026-10-19

Peer reviewed|Thesis/dissertation

eScholarship.org Powered by the California Digital Library
University of California

UNIVERSITY OF CALIFORNIA SAN DIEGO

Characterizing Cetacean Distribution and Density across Two Decades of Environmental Change in the Southern California Current Ecosystem

A dissertation submitted in partial satisfaction of the
requirements for the degree Doctor of Philosophy

in

Oceanography

by

Michaela Noel Alksne

Committee in charge:

Professor Simone Baumann-Pickering, Chair
Professor Kaitlin Frasier
Professor John A. Hildebrand
Professor Carolyn Kurle
Professor Marie A. Roch
Professor Duncan Watson-Parris

2026

Copyright

Michaela Noel Alksne, 2026

All rights reserved.

The Dissertation of Michaela Noel Alksne is approved, and it is acceptable in quality and form for publication on microfilm and electronically.

University of California San Diego

2026

DEDICATION

For my father, Ward E. Alksne.
I see you dancing in the waves at Blacks, and I know you're still with me.

EPIGRAPH

We know only too well that what we are doing is nothing more than a drop in the ocean.
But if the drop were not there, the ocean would be missing something.

- Mother Teresa

TABLE OF CONTENTS

Dissertation Approval Page iii

Dedication iv

Epigraph v

Table of Contents vi

List of Figures ix

List of Tables xiv

Acknowledgements xvii

Vita xx

Abstract of the Dissertation xxi

Chapter 1 Introduction 1

Bibliography 7

Chapter 2 Biogeographic patterns of Pacific white-sided dolphins based on long-term passive acoustic records 11
2.1 Abstract 11
2.2 Introduction 12
2.3 Methods 15
2.3.1 Data Collection 15
2.3.2 Data Processing 15
2.3.3 Data analysis 18
2.4 Results 20
2.4.1 Classifier Performance 21
2.4.2 Biogeographic Patterns 21
2.5 Discussion 24
2.5.1 Limitations 29
2.5.2 Conclusions 30
2.6 Acknowledgments 31
2.7 Data Availability Statement 31

Bibliography 42
2.8 Supplementary Material 47
2.8.1 Deployment Metadata 47
2.8.2 Automatic vs. Manual Label Comparison 53
2.8.3 Diel Trends 53

Chapter 3 Application of deep learning to estimate blue and fin whale call density in the southern California Current Ecosystem 59
3.1 Abstract 59
3.2 Introduction 60
3.3 Methods 63
3.3.1 Acoustic data collection 64
3.3.2 Detector development 65
3.3.3 Sonobuoy received level calibrations 69
3.3.4 Detection range and area estimation 71
3.3.5 Call density estimation 72
3.3.6 Inter-call intervals 73
3.4 Results 74
3.4.1 Detector performance 74
3.4.2 Detection area estimates 76
3.4.3 Call density estimates 78
3.4.4 Inter-call intervals 79
3.5 Discussion 79
3.6 Acknowledgments 87
3.7 Figures and Tables 87
3.8 Data availability 87
3.9 Code availability 91

Bibliography 96
3.10 Supplementary Material 103

Chapter 4 Two decades of environmental change alter cetacean community composition in the southern California Current Ecosystem 118
4.1 Abstract 118
4.2 Introduction 119
4.3 Methods 122
4.3.1 Study area and survey design 122
4.3.2 Density estimation 123
4.3.3 Trend analysis and community composition 126
4.4 Results 129
4.4.1 Survey effort and sightings 129
4.4.2 Detection functions 130
4.4.3 Density and abundance estimation 130
4.4.4 Community composition and diversity 131
4.4.5 Relationships with sea surface temperature 133
4.5 Discussion 133

Bibliography 155
4.6 Supplementary Material 163
4.6.1 S1 Survey Metadata 163

4.7 S2 Detection functions 166
4.8 S3 Sea surface temperature regression results 180

Chapter 5 Integrating marine mammal visual and acoustic surveys through a shared latent density model 181
5.1 Abstract 181
5.2 Introduction 182
5.3 Methods 185
5.3.1 Multi-modal survey data 186
5.3.2 Model overview 188
5.3.3 Simulation and model fitting 191
5.4 Results 193
5.4.1 Model performance 193
5.4.2 Environmental drivers, species distributions, and seasonal cue rates . . . 195
5.5 Discussion 196

Bibliography 211
5.6 Supplementary Material 219

LIST OF FIGURES

Figure 2.1. PAM sites ranging across the Northeastern Pacific overlaid with geographic boundaries of the North Pacific and CA/OR/WA Pacific white-sided dolphin management stocks, and hypothesized boundaries of the cryptic Southern California/Baja population. 35

Figure 2.2. Bin-level examples for five odontocete categories: Risso's dolphin (Gg, row 1), Pacific white-sided dolphin (LoA, row 2), Pacific white-sided dolphin (LoB, row 3), unidentified dolphin (UD, row 4), and Cuvier's beaked whale (Zc, row 5). 36

Figure 2.3. Site-specific scaled diel activity. 37

Figure 2.4. Site-specific seasonal presence of LoA and LoB click types. 38

Figure 2.5. Climatic variations in NPGO and ONI three-month running means between 2009 and 2021. 39

Figure 2.6. Boxplots displaying the distribution of LoA (blue) and LoB (coral) presence before, during, and after the 2014–2016 marine heatwave (MHW) event at 3 long-term monitoring stations including CINMS, SCB_H, and SCB_N. 40

Figure 2.7. Site-specific GLMs from long-term monitoring SCB stations. 41

Figure 2.8. LoA hourly click-positive timeseries at CINMS. Gray sections represent nighttime hours and white sections represent daytime. Black lines denote click-positive hourly bins. Periods of no recording effort are highlighted in transparent blue. 54

Figure 2.9. LoA hourly click-positive timeseries at SCB_H. Gray sections represent nighttime hours and white sections represent daytime. Black lines denote click-positive hourly bins. Periods of no recording effort are highlighted in transparent blue. 55

Figure 2.10. LoB hourly click-positive timeseries at SCB_H. Gray sections represent nighttime hours and white sections represent daytime. Black lines denote click-positive hourly bins. Periods of no recording effort are highlighted in transparent blue. 56

Figure 2.11. LoA hourly click-positive timeseries at SCB_N. Gray sections represent nighttime hours and white sections represent daytime. Black lines denote click-positive hourly bins. Periods of no recording effort are highlighted in transparent blue. 57

Figure 2.12. LoB hourly click-positive timeseries at SCB_N. Gray sections represent nighttime hours and white sections represent daytime. Black lines denote click-positive hourly bins. Periods of no recording effort are highlighted in transparent blue. 58

Figure 3.1. Total CalCOFI sonobuoy acoustic recording effort across the Southern California Current Ecosystem, HARP deployment sites, and estimated blue whale D call detection areas at ten representative stations. 88

Figure 3.2. Iterative human-in-the-loop training pipeline for blue and fin whale call detection. 89

Figure 3.3. Performance statistics for the third model configuration across four evaluation datasets. 90

Figure 3.4. Received level distributions for blue whale D calls used for call density estimation. Left: Modeled received levels (dB re 1 µPa) across the southern California Current Ecosystem for representative offshore and inshore stations. 91

Figure 3.5. Annual inshore and offshore call density for blue and fin whale call types estimated from the 20-year CalCOFI sonobuoy archive (2004–2024). . . . 92

Figure 3.6. Intercall interval (ICI) distributions for blue and fin whale call types and call transitions. Histograms show the distribution of intercall intervals (ICIs; seconds) computed from long-term passive acoustic detections across all analyzed sonobuoy deployments. 93

Figure 3.7. True positive, false positive, and false negative rates for A calls across evaluation datasets. 107

Figure 3.8. Received level distributions for blue whale A calls used for density estimation. 108

Figure 3.9. True positive, false positive, and false negative rates for B calls across evaluation datasets. 111

Figure 3.10. Received level distributions for blue whale B calls used for density estimation. 112

Figure 3.11. True positive, false positive, and false negative rates for D calls across evaluation datasets. 113

Figure 3.12. True positive, false positive, and false negative rates for 20 Hz calls across evaluation datasets. 114

Figure 3.13. Received level distributions for fin whale 20 Hz calls used for density estimation. 115

Figure 3.14. True positive, false positive, and false negative rates for 40 Hz calls across evaluation datasets. 116

Figure 3.15. Received level distributions for fin whale 40 Hz calls used for density estimation. 117

Figure 4.1. Seasonal visual survey effort along CalCOFI transect lines in the SCCE, 2004–2025. Colors indicate the number of cruises during which each transect segment was surveyed. Black dots mark CalCOFI stations. 143

Figure 4.2. Annual density trends (animals per 1,000 km^2) for baleen whale species, 2004–2025. 144

Figure 4.3. Mean seasonal density (animals per 1,000 km^2) for baleen whale species averaged across 2004–2025. 145

Figure 4.4. Annual density trends (animals per 1,000 km^2) for toothed whale species, 2004–2025. 149

Figure 4.5. Mean seasonal density (animals per 1,000 km^2) for toothed whale species averaged across 2004–2025. 150

Figure 4.6. Annual Shannon–Wiener diversity index (H') for the ten-species community calculated from abundance and biomass-weighted community matrices, 2004–2025. 151

Figure 4.7. NMDS ordination of cetacean community composition based on Bray–Curtis dissimilarity, 2004–2025. 153

Figure 4.8. Annual density versus annual mean sea surface temperature anomaly for species with significant bootstrap slope confidence intervals. 154

Figure 4.9. Fitted detection functions for the ten cetacean species analyzed, with scaled histograms of observed perpendicular distances. 178

Figure 4.10. Quantile–quantile plots for the fitted detection functions. 179

Figure 5.1. Seasonal spatial distribution of blue whale segment-level density estimates and acoustic density estimates of blue whale B and D calls across the CalCOFI survey grid, 2004–2024. 204

Figure 5.2. Seasonal spatial distribution of fin whale segment-level density estimates and acoustic density estimates of fin whale 20 Hz and 40 Hz calls across the CalCOFI survey grid, 2004–2024. 205

Figure 5.3. Seasonal spatial distribution of humpback whale segment-level density estimates and acoustic presence density estimates of across the CalCOFI survey grid, 2004–2024. 206

Figure 5.4. Schematic of the joint Bayesian model linking visual line-transect and passive acoustic survey data through a shared latent log-density field. . . . 206

Figure 5.5. Posterior predictive checks comparing observed and model-predicted total counts (log-log scale), by species, call type or visual detection, season, and CalCOFI quadrant. 207

Figure 5.6. Posterior marginal response of species-specific log-density to sea surface temperature, sea surface height, salinity, and chlorophyll-*a*, with 95% credible intervals. 208

Figure 5.7. Posterior median seasonal density surfaces (animals/km^2) for blue, fin, and humpback whales across the CalCOFI study area. 209

Figure 5.8. Posterior seasonal cue and presence rates ($\beta_{\text{type}}[m]$) for blue, fin, and humpback whales. 210

Figure 5.9. Precision-recall curve for the Allen et al. (2021) humpback whale acoustic detector, in 0.01 score bins, evaluated against five manually reviewed CalCOFI cruises. A score threshold of 0.2 was selected, and precision and recall in each dataset at this threshold is denoted by the black stars. 219

Figure 5.10. Station-level modeled detection area estimates for humpback whales, computed from received-level thresholding at 100 dB. 220

Figure 5.11. Prior predictive check: blue whale. Overlaid observed vs. prior-predictive frequency distributions by season, for visual group counts and each acoustic call type. 221

Figure 5.12. Prior predictive check: fin whale. Overlaid observed vs. prior-predictive frequency distributions by season, for visual group counts and each acoustic call type. 222

Figure 5.13. Prior predictive check: humpback whale. Overlaid observed vs. prior-predictive frequency distributions by season, for visual group counts and acoustic presence minutes. 223

Figure 5.14. Posterior distributions of all recovered parameters across the $M = 10$ simulated replicates for the blue whale model. 224

Figure 5.15. Posterior distributions of all recovered parameters across the $M = 10$ simulated replicates for the fin whale model. 225

Figure 5.16. Posterior distributions of all recovered parameters across the $M = 10$ simulated replicates for the humpback whale model. 226

Figure 5.17. Prior vs. posterior comparison for blue whale seasonal call rates (β_B, β_D). 227

Figure 5.18. Prior vs. posterior comparison for fin whale seasonal call rates (β_{20}, β_{40}) 227

Figure 5.19. Prior vs. posterior comparison for the humpback whale seasonal presence-minute rate (β_{Mn}) 228

LIST OF TABLES

Table 2.1. Summary of recording locations, depths, recording effort, and number of days with Pacific white-sided dolphin LoA and LoB click presence at each site. 32

Table 2.2. Signal category, deployment number, and number of 5-minute bin-level training examples that were used as input for the deep neural network. . . . 33

Table 2.3. Confusion matrix for bin-level classifier on testing dataset with 500 examples from each category. Values indicate percentages of the total number of detections classified. 33

Table 2.4. Results of paired t-tests comparing diel activity patterns of the LoA and LoB click types across sites. Alternative hypothesis corresponds to true mean difference in normalized diel activity, compared across all sites. 33

Table 2.5. Summary of spatial-seasonal GAM model results for LoA and LoB presence. *Te* represents the tensor product smooth term. 34

Table 2.6. Summary of Kruskal-Wallis test results comparing LoA and LoB presence before, during, and after the 2014–2016 MHW event at long-term Southern California monitoring stations. 34

Table 2.7. Summary of environmental GLMs for LoA and LoB presence at sites CINMS, SCB_H, and SCB_N. 34

Table 2.8. Deployment metadata including deployment name, latitude and longitude, recorder depth, start of recording and end of recording for each deployment included in this study. 47

Table 2.9. Confusion table comparing automatically generated vs. manually generated bin-level labels for each category for a subset of detections from deployment SCB_H_29. 53

Table 2.10. Confusion table comparing automatically generated vs. manually generated bin-level labels for each category for a subset of detections from deployment SCB_P_35. 53

Table 2.11. Confusion table comparing automatically generated vs. manually generated bin-level labels for each category for a subset of detections from deployment CINMS_C_33. 53

Table 3.1. Platform and call-type composition of the training, validation, and test datasets. Each spectrogram represents a 60-second window of acoustic recordings from either HARP or CalCOFI sonobuoy deployments. 94

Table 3.2. Mean precision and recall by call type for the initial detector, the final detector after HITL refinement, and the final operational detector incorporating contextual call-characteristic filtering and received-level (RL) thresholding. 94

Table 3.3. Call-specific source levels (SL) and received-level (RL) detection thresholds used for propagation modeling and detection-area estimation. 95

Table 3.4. Summary of CalCOFI sonobuoy survey cruises included in analysis. Recording hours reflect the total duration of sonobuoy deployments within each cruise. 104

Table 3.5. CalCOFI sonobuoy cruises used for model training and testing. 109

Table 3.6. HARP deployments used for model training, validation, and testing. Recording hours reflect the total duration of 60-s spectrograms sampled from each deployment for training and validation, and the full annotated deployment duration for the CHNMS test dataset. 110

Table 3.7. Detection areas by call type at each modeled CalCOFI station. 110

Table 4.1. Truncation distance (w) in meters, number of on-effort, on-transect sightings (n), fitted detection function model, retained covariates, and mean effective strip width ($\hat{\mu}$) in meters for each species. 143

Table 4.2. Mean annual density and abundance estimates for the ten cetacean species, averaged across all years and seasons from the bootstrap GAM analysis. . 146

Table 4.3. Seasonal density estimates (animals per 1,000 km^2) by species, averaged across 2004–2025. Values are bootstrap means; 95% bootstrap confidence intervals are given in parentheses. 147

Table 4.4. Mean annual rate of density change and 95% bootstrap confidence interval for each species, estimated from the GAM temporal smooth evaluated at 2005 and 2025. 148

Table 4.5. Bootstrap PERMANOVA results for cetacean community composition comparisons based on Bray–Curtis dissimilarity matrices. 152

Table 4.6. Survey effort for each CalCOFI cruise in the study area. Trackline length is the total on-effort, on-transect distance surveyed within the southern CalCOFI grid. Observer height is the height of the observation platform above the waterline for the ship used during a given cruise. 163

Table 4.7. Summary of CalCOFI visual survey effort by season. 167

Table 4.8. Candidate detection function models evaluated for each species, ranked by AIC. 167

Table 4.9. Goodness-of-fit statistics for the selected detection function model for each species. 177

Table 4.10. Bootstrap mean regression slope and R^2 for the relationship between annual density (animals per 1,000 km^2) and annual mean SST anomaly (°C) for each species. 180

Table 5.1. All prior distributions used in the joint model. 208

Table 5.2. Posterior median seasonal cue/presence rates with 95% CI by species and call type. Units are calls/whale/hr for blue and fin whale, min/whale/hr for humpback whale. 208

Table 5.3. False negative (FN) and false positive (FP) rates used to correct acoustic call and presence counts for each species and call type, estimated from precision and recall from automated acoustic detection algorithms for each call type as described in the main text 229

Table 5.4. True parameter values assigned for the simulation-based validation (Table 5.5). β_{type} is a single values applied to all four seasons. 229

Table 5.5. Simulation-based recovery of the density intercept (μ), seasonal cue/presence rates (β_{type}), and environmental spline coefficients, across $M = 10$ simulated replicates per species. 230

Table 5.6. Posterior predictive check for the proportion-of-zeros statistic, pooled across seasons. 231

Table 5.7. Posterior predictive check for the total-count statistic, stratified jointly by season and CalCOFI quadrant (North/South $\times$ Inshore/Offshore). 232

ACKNOWLEDGEMENTS

I am deeply grateful for the support from my academic mentors, colleagues, friends, and family who have supported me through my PhD. First, I would like to acknowledge and thank my thesis advisor, Simone Baumann-Pickering. Thank you for believing in me and always pushing me to do my best work. I feel lucky to have developed into a scientist, marine ecologist, oceanographer, and teacher through your mentorship. Thank you to my committee member Kaitlin Frasier for your kindness, creative thinking, and ability to effortlessly explain even the most complex topics. Thank you to my committee member Marie Roch for inspiring me to think like a scientist. You ask the best questions, and I will always appreciate the extra time you took to sit down with me. From neural networks to Python code, to the meaning of whale songs, it has been an honor to work with you and learn from you. Thank you to my committee member John Hildebrand for always letting me walk into your office unannounced, paper and pencil in hand. You helped broaden my perspective and interpret my results, all while deriving underwater sound propagation equations from memory and making me laugh. Thank you to my committee members Duncan Watson-Parris and Carolyn Kurle for your mentorship, wisdom, and expertise in machine learning and ecosystem processes, your guidance has improved the science in this dissertation.

Thank you to the National Defense Science and Engineering Graduate (NDSEG) Fellowship for supporting my PhD. I am grateful to have been paired with Regina Guazzo as my NDSEG mentor, I don't think I could have asked for a pairing. Thank you Regina for encouraging me to keep going, always taking the time to provide thoughtful feedback, and graciously providing examples and templates. From gray whale calls to Latex formatting, I have learned so much from you.

Thank you to the many, many researchers, engineers, students, and staff that make up the Scripps Marine Bioacoustics Research Collaborative. Our lab is so special and I am grateful to have been a part of it. Thank you to all the students I mentored during my time at Scripps:

Angeles Rios, Shane Andres, Dolapo Adesanya, Kaya Cohen, Anika Agarwal, Isabelle Jeuris, and Anna Mothersole, you taught me how to be a mentor and educator, which was the most fulfilling part of my PhD. Thank you to the broader Scripps community which I have been a part of since 2018, when I started as an undergraduate student myself. A huge thank you to Dovi Kacev and Peter Franks, whose teaching styles were engaging and creative, your lessons will always stick with me.

Lastly, thank you to my friends and family for helping me stick with this, for being excited for me when I was excited, and for being support pillars when I was frustrated. To my dear friend and Cliffridge sister, Eva Hidalgo Pla, thank you for always making me feel worthy and proud of myself, I am so grateful for you. Thank you to my best friend and fellow Scripps PhD graduate, Natalie Grayson, for always encouraging me to go surfing and making me feel seen and heard. Getting to start and finish our PhD's together has been one of the joys of my life. Thank you to my best friend and twin soul sister, Grace Barioni. When I think of who I want to be as a person, it's always you that comes to mind. Thank you to my big sister Juliana, you have been my inspiration since day one and I am so proud of you, and proud of us. I wouldn't have gotten here without you. Thank you to my best friend and fiancé Cole DeNormandie, you light up my life, make me laugh, and always know how to cheer me up, I am so glad I found you. Thank you to my stepmom Marji for being exactly who I've always needed. And lastly, thank you to my mom, Monica, for everything you've done to support me. Without your fierce, and sometimes tough love, and most of all your unwavering support, this PhD would never have been possible. You taught me that loving ourselves means loving our planet, and that we must care for it and respect it. Your perspective on environmental justice is what drives me to be a compassionate scientist, an inspiring educator, and a steward of the ocean and all it's inhabitants.

Chapter 2, in full, is a reprint of the material as it appears in Diversity and Distributions. Alksne, Michaela N., Kok, Annebelle C.M., Agarwal, Anika, Frasier, Kaitlin E., Baumann-Pickering, Simone. Wiley, 2024. The dissertation author was the primary investigator and author of this paper.

Chapter 3, in full, is currently in review for publication in Scientific Reports. Alksne, Michaela N., Roch, Marie A., Frasier, Kaitlin E., Hildebrand, John A., Andres, Shane, Adesanya, Dolapo, Baggett, Lauren M., Jones, Joshua M., Širović, Ana, Baumann-Pickering, Simone. Springer Nature, 2026. The dissertation author was the primary investigator and author of this paper.

VITA

2020	Bachelor of Science in Marine Biology, University of California San Diego
2024	Masters of Science in Oceanography, University of California San Diego
2026	Doctor of Philosophy in Oceanography, University of California San Diego

PUBLICATIONS

Alksne, M. N., Kok, A.C., Agarwal, A., Frasier, K.E., Baumann-Pickering, S. (2024). Biogeographic patterns of Pacific white-sided dolphins based on long-term passive acoustic records. *Diversity and Distributions*, 30(9), e13903.
https://doi.org/10.1111/ddi.13903

Alksne, M. N., Roch, M.A., Frasier, K.E., Hildebrand, J.A., Andres, S., Adesanya, D., Baggett, L. M., Jones, M. J., Širović, A., Baumann-Pickering, S. Application of deep learning to estimate blue and fin whale call density in the southern California Current Ecosystem. *in review, Scientific Reports*.
https://doi.org/10.21203/rs.3.rs-9203950/v1

ABSTRACT OF THE DISSERTATION

Characterizing Cetacean Distribution and Density across Two Decades of Environmental Change in the Southern California Current Ecosystem

by

Michaela Noel Alksne

Doctor of Philosophy in Oceanography

University of California San Diego, 2026

Professor Simone Baumann-Pickering, Chair

The southern California Current Ecosystem has experienced extreme marine heatwaves and El Niño events over the last two decades, causing mass die-offs and species range shifts. The region is also one of the most well-monitored marine ecosystems, through the California Cooperative Oceanic Fisheries Investigations (CalCOFI) program, which has conducted marine mammal visual and passive acoustic monitoring (PAM) since 2004. This dissertation applies deep learning and statistical methods to CalCOFI visual and acoustic data and to long-term High Frequency Acoustic Recording Package (HARP) data to characterize cetacean distribution and density across this period of change. Chapter 1 trains a deep neural network to classify

two echolocation click types produced by Pacific white-sided dolphins and applies it to 57 years of HARP recordings from 14 sites between the Gulf of California and the Gulf of Alaska. Spatial, seasonal, and diel patterns are consistent with two acoustically distinct populations that experienced possible range shifts after the 2014-2016 marine heatwave. Chapter 2 trains a deep-learning object detection algorithm to classify five blue and fin whale call types from two decades of CalCOFI PAM recordings and combines these detections with acoustic propagation modeling to produce 20-year call density estimates, showing inshore-offshore differences and interannual variability linked to ocean conditions. Chapter 3 estimates long-term density trends for ten cetacean species from CalCOFI visual surveys conducted between 2004 and 2025, finding declines in Dall's porpoise and Pacific white-sided dolphin and increases in long-beaked common dolphin and humpback whale, consistent with range contractions, expansions, and recovery. Community composition shifted between pre- and post-heatwave periods, driven by species turnover rather than a change in diversity. Chapter 4 develops a joint Bayesian model integrating CalCOFI visual and acoustic data through a shared latent density field to estimate spatial-seasonal density surfaces and acoustic cue rates for blue, fin, and humpback whales. We find species-specific habitat associations, spatial-seasonal partitioning, and seasonally offset peak singing periods between the three migratory baleen whale species. These chapters document biogeographic change linked to ocean warming and provide methods for estimating cetacean density from long-term survey data to inform conservation and management as the region continues to change.

Chapter 1

Introduction

In the last two decades, the southern California Current Ecosystem (SCCE) has experienced extreme marine heatwaves and El Niño events, which have had major consequences on its diverse marine food webs (Cavole et al., 2016; Suryan et al., 2021; Bond et al., 2015). During the 2014-2016 marine heatwave, krill and forage fish declined, harmful algal blooms spread, and mass strandings of seabirds and marine mammals followed (Cavole et al., 2016). Juvenile white sharks appeared in central California in large numbers (Tanaka et al., 2021), two tropical booby species established new breeding colonies in the Channel Islands (Russell et al., 2025), and humpback whale entanglements increased as their habitat compressed towards shore (Santora et al., 2020). The SCCE is a thermal transition zone, where warm, salty, oligotrophic water from the North Pacific Subtropical Gyre meets cold, nutrient-rich California Current water flowing south from Alaska (Bograd et al., 2019), and is influenced by the California Undercurrent which transports warm, salty, oligotrophic, low-oxygen water poleward (Checkley Jr and Barth, 2009) and intensifies during marine heatwave events, further warming the region (Zaba and Rudnick, 2016). As the SCCE continues to warm, cool-water species are contracting and warm-water species are expanding (Koslow et al., 2015; McClatchie et al., 2016; Russell et al., 2025).

This dissertation investigates long-term biogeographic trends of sentinel cetacean species in the SCCE throughout two decades of environmental change. Cetaceans are long-lived, highly mobile top predators, and their distribution and abundance reflect the ecosystem conditions

around them (Hazen et al., 2019). The SCCE sits at the warm range limit of cool-water species such as Dall's porpoise (Fleming et al., 2018) and Pacific white-sided dolphin (Salvadeo et al., 2010), and at the cool range limit of warm-water species such as long-beaked common dolphin (Becker et al., 2014; Barlow, 2016), making it a useful place to track how the balance between these species is shifting. It is also an important foraging ground for blue, fin, and humpback whales, all of which were depleted by commercial whaling in the twentieth century and have since recovered to varying degrees (Rocha et al., 2014; Clapham et al., 1999), so any climate signal in their distribution is layered on top of ongoing recovery.

Detecting long-term biogeographic change needs monitoring data collected at spatial and temporal resolutions large enough to capture gradual and acute effects. The CalCOFI program has conducted quarterly ecosystem surveys since 1949, with visual line-transect marine mammal surveys and PAM since 2004. This dissertation uses those two decades of CalCOFI visual and acoustic data, as well as long-term High-Frequency Acoustic Recording Package (HARP) data, to ask how cetacean distribution and density in the SCCE have changed over this period. Answering that question required building on existing tools and developing new ones, because most methods were not built for datasets this large or this mixed. Passive acoustic recordings are collected faster than they can be manually reviewed, and converting them into animal density requires accounting for monitoring area and cue production rates, which are often unknown. Over four chapters, this dissertation produces timeseries of decadal acoustic presence, acoustic density, and visual density, and a method to jointly estimate animal density and acoustic cue rates by integrating CalCOFI's acoustic and visual timeseries, in order to characterize cetacean long-term distribution and density in the SCCE.

Chapter 1 builds on Soldevilla et al. (2008, 2010) asking whether two populations of Pacific white-sided dolphin can be distinguished acoustically across their range, and builds on that work by investigating whether their presence has shifted in the SCCE since the 2014-2016 marine heatwave. To answer this, I combined automated click detection, unsupervised clustering,

and train a deep neural network, built using custom software from (Frasier, 2021), to detect and classify two echolocation click types produced by Pacific white-sided dolphins. I applied this method, combined with manual review, to 57 years of PAM recordings across 14 sites between the Gulf of California and the Gulf of Alaska. The two click types show distinct spatial, seasonal, and diel patterns consistent with the two populations, and their relative presence shifted after the 2014–2016 marine heatwave, suggesting a range shift of the northern population out of and the southern population into the SCCE.

Chapter 2 asks how blue and fin whale calling behavior, both song (Oleson et al., 2007b; Thompson et al., 1996; Croll et al., 2002) and non-song calls associated with social behavior and foraging (McDonald et al., 2001; Oleson et al., 2007a; Romagosa et al., 2021; Širović et al., 2013), has varied over space and time across two decades of CalCOFI sonobuoy recordings. Existing detection and classification methods for these call types do not produce reliable call-level detections without extensive tuning and manual review (Rasmussen and Širović, 2021; Szesciorka et al., 2020). Our goal was to leverage new deep-learning tools to develop a single detector for all five of these principal calls that would work with CalCOFI sonobuoy and HARP data from the SCCE. This chapter takes advantage of previously manually labeled calls and trains a Faster R-CNN object detector, combined with an active learning pipeline to more quickly generate additional labels and build a robust, generalizable algorithm. We evaluate the algorithm on four held-out test datasets spanning CalCOFI and HARP data and different seasons, and find that it is mostly reliable across call types, but performs poorly in the presence of humpback whale singing activity, which was often mistaken for blue and fin whale downsweeps. We estimated call-level acoustic density from the resulting 20-year call-level detection timeseries by accounting for station-specific detection area estimates through range-dependent parabolic equation modeling (ZoBell et al., 2024) and for the false and missed detection rates from our evaluation dataset. The resulting call-level density timeseries has seasonal, spatial, and interannual variability matching known singing and calling phenology (Oleson et al., 2007b,a;

Romagosa et al., 2021; Širović et al., 2013; Szesciorka et al., 2020), and adds knowledge of how far the continental shelf blue and fin whales are detected, since most recording networks do not extend that far offshore. The density timeseries has been mostly stable interannually, with declines in foraging and song-assocaited calling during the 2014-2016 marine heatwave (ZoBell et al., 2025), and a reduction in offshore fin whale calling and singing activity in the years since. The detection workflow has since been expanded to additional datasets and low-frequency baleen whale call types in the region (Baggett et al., 2026).

Chapters 1 and 2 use only acoustic data. Chapter 3 turns to CalCOFI's visual surveys to ask how the broader cetacean community has changed since the 2014-2016 heatwave. Following Campbell et al. (2015) I use distance sampling to estimate long-term density trends and a bootstrap approach to estimate uncertainty, for ten species from CalCOFI surveys between 2004 and 2025. We find that Dall's porpoise and Pacific white-sided dolphin have declined while long-beaked common dolphin and humpback whale have increased, consistent with species range shifts for those at their range edges, and possible population recovery for humpback whales. This pattern matches predictions from MacLeod (2009) that species at their thermal range boundaries would show the largest responses to warming, while mid-range species would change little. We also investigate community-level change and find that community composition has shifted between pre- and post-heatwave periods but diversity has remained stable, suggesting change is occurring through turnover rather than a net gain or loss in diversity, at least across these ten species, as cool-water-affiliated odontocetes are replaced by their warm-water counterparts.

Chapter 2's call density, the number of calls detected per unit effort and area, is combined with Chapter 3's animal density, the number of animals per unit area, in Chapter 4 to produce estimates of seasonal call-specific cue rates, the average number of calls produced per whale per hour, as well as species-specific seasonal-spatial heatmaps based on the two datastreams and environmental covariates. I implement this in a joint Bayesian framework that links the two separate processes by informing the same underlying latent density state (Pacifici et al., 2017;

Miller et al., 2019; Fletcher et al., 2019). For humpback whales, whose acoustic detections were minute-level presence/absence rather than individual calls, I estimated a presence rate using the same joint structure. Existing approaches to combining acoustic and visual data usually estimate density surfaces separately and combine the estimates afterward (Frasier et al., 2021), which does not work here since the CalCOFI acoustic densities cannot be converted to animal density without a cue rate. Our model instead treats seasonal patterns in the acoustic data that are not explained by the shared density field as the cue rate, allowing it to be estimated directly from the data. We validated the joint model structure using simulated data with known densities and cue rates, and then applied it to the full CalCOFI record. The model recovered density and cue rate parameters across all three simulated species, and when applied to 20 years of concurrent CalCOFI visual and acoustic data, the model converged, and posterior predictive checks showed that it could recover the true range of values in most conditions tested. The average seasonal cue rates of foraging-associated blue and fin whale calls both peaked in the summer, while song-associated calls, peaked in the summer and fall for blue whales and the fall and winter for fin whales. Humpback presence rates peaked in the winter. The seasonal peaks are offset across species, which may suggest acoustic partitioning of a shared foraging ground driven by differences in breeding season timing. Two studies of blue, fin, and humpback whale song, one using CalCOFI data (Vu, 2015), and another in the Monterey Bay (Ryan et al., 2025), found similar seasonal structure across species. Our results convert the previously described seasonal acoustic patterns of these three species into seasonally varying regional-average cue rates, which can hopefully be used in future studies to convert acoustic density to animal density.

Across four chapters, this dissertation characterizes how two decades of environmental change have affected the SCCE cetacean community, showing species-specific range shifts, community turnover, and the impacts of an extreme marine heatwave. This dissertation also develops transferable tools, including an automated acoustic detection, classification, and active learning workflow, and a joint visual-acoustic density estimation method, that can be used

beyond this region and these species. These findings support fisheries and protected species management, inform conservation of baleen whale populations still recovering from historical whaling, and provide evidence that change in the SCCE's cetacean community is well underway.

Bibliography

Baggett, L. M., Posdaljian, N., ZoBell, V. M., Andres, J. F., Pickering, L. P., Schriber, N. E., Alksne, M. N., Lenssen, K. L., Thayre, B. J., and Baumann-Pickering, S. (2026). Baseline soundscapes and bioacoustic considerations relevant to floating offshore wind development along the U.S. West Coast. *Under Review*.

Barlow, J. (2016). Cetacean abundance in the California Current estimated from ship-based line-transect surveys in 1991–2014. *Administrative report lJ-12-01. Southwest Fisheries Science Center, National Marine Fisheries Service, la Jolla, California, uSA*.

Becker, E. A., Forney, K. A., Foley, D. G., Smith, R. C., Moore, T. J., and Barlow, J. (2014). Predicting seasonal density patterns of California cetaceans based on habitat models. *Endangered Species Research*, 23:1–22.

Bograd, S. J., Schroeder, I. D., and Jacox, M. G. (2019). A water mass history of the southern California current system. *Geophysical Research Letters*, 46(12):6690–6698.

Bond, N. A., Cronin, M. F., Freeland, H., and Mantua, N. (2015). Causes and impacts of the 2014 warm anomaly in the NE Pacific. *Geophysical Research Letters*, 42(9):3414–3420.

Campbell, G. S., Thomas, L., Whitaker, K., Douglas, A. B., Calambokidis, J., and Hildebrand, J. A. (2015). Inter-annual and seasonal trends in cetacean distribution, density and abundance off southern California. *Deep Sea Research Part II: Topical Studies in Oceanography*, 112:143–157.

Cavole, L. M., Demko, A. M., Diner, R. E., Giddings, A., Koester, I., Pagniello, C. M. L. S., Paulsen, M.-L., Ramirez-Valdez, A., Schwenck, S. M., Yen, N. K., Zill, M. E., and Franks, P. J. S. (2016). Biological impacts of the 2013-2015 warm-water anomaly in the Northeast Pacific winners, losers, and the future. *Oceanography*, 29(2):273–285.

Checkley Jr, D. M. and Barth, J. A. (2009). Patterns and processes in the California Current System. *Progress in Oceanography*, 83(1-4):49–64.

Clapham, P. J., Young, S. B., and Brownell Jr, R. L. (1999). Baleen whales: conservation issues and the status of the most endangered populations. *Mammal Review*, 29(1):37–62.

Croll, D. A., Clark, C. W., Acevedo, A., Tershy, B., Flores, S., Gedamke, J., and Urban, J. (2002). Only male fin whales sing loud songs. *Nature*, 417(6891):809–809.

Fleming, A. H., Yack, T., Redfern, J. V., Becker, E. A., Moore, T. J., and Barlow, J. (2018). Combining acoustic and visual detections in habitat models of Dall's porpoise. *Ecological Modelling*, 384:198–208.

Fletcher, R. J. J., Hefley, T. J., Robertson, E. P., Zuckerberg, B., McCleery, R. A., and Dorazio, R. M. (2019). A practical guide for combining data to model species distributions. *Ecology*, 100(6):e02710.

Frasier, K. E. (2021). A machine learning pipeline for classification of cetacean echolocation clicks in large underwater acoustic datasets. *PLoS Computational Biology*, 17(12):e1009613.

Frasier, K. E., Garrison, L. P., Soldevilla, M. S., Wiggins, S. M., and Hildebrand, J. A. (2021). Cetacean distribution models based on visual and passive acoustic data. *Scientific Reports*, 11:8896.

Hazen, E. L., Abrahms, B., Brodie, S., Carroll, G., Jacox, M. G., Savoca, M. S., Scales, K. L., Sydeman, W. J., and Bograd, S. J. (2019). Marine top predators as climate and ecosystem sentinels. *Frontiers in Ecology and the Environment*, 17(10):565–574.

Koslow, J. A., Miller, E. F., and McGowan, J. A. (2015). Dramatic declines in coastal and oceanic fish communities off California. *Marine Ecology Progress Series*, 538:221–227.

MacLeod, C. (2009). Global climate change, range changes and potential implications for the conservation of marine cetaceans: A review and synthesis. *Endangered Species Research*, 7:125–136.

McClatchie, S., Thompson, A. R., Alin, S. R., Siedlecki, S., Watson, W., and Bograd, S. J. (2016). The influence of Pacific equatorial water on fish diversity in the southern California Current System. *Journal of Geophysical Research: Oceans*, 121(8):6121–6136.

McDonald, M. A., Calambokidis, J., Teranishi, A. M., and Hildebrand, J. A. (2001). The acoustic calls of blue whales off California with gender data. *Journal of the Acoustical Society of America*, 109(4):1728–1735.

Miller, D. A. W., Pacifici, K., Sanderlin, J. S., and Reich, B. J. (2019). The recent past and promising future for data integration methods to estimate species' distributions. *Methods in Ecology and Evolution*, 10(1):22–37.

Oleson, E., Calambokidis, J., Burgess, W., McDonald, M., LeDuc, C. A., and Hildebrand, J. A. (2007a). Behavioral context of Northeast Pacific blue whale call production. *Marine*

Ecology-progress Series, 330:269–284.

Oleson, E. M., Wiggins, S. M., and Hildebrand, J. A. (2007b). Temporal separation of blue whale call types on a southern California feeding ground. *Animal Behaviour*, 74(4):881–894.

Pacifici, K., Reich, B. J., Miller, D. A. W., Gardner, B., Stauffer, G., Singh, S., McKerrow, A., and Collazo, J. A. (2017). Integrating multiple data sources in species distribution modeling: a framework for data fusion. *Ecology*, 98(3):840–850.

Rasmussen, J. H. and Širović, A. (2021). Automatic detection and classification of baleen whale social calls using convolutional neural networks. *Journal of the Acoustical Society of America*, 149(5):3635–3644.

Rocha, R. C., Clapham, P. J., and Ivashchenko, Y. V. (2014). Emptying the oceans: a summary of industrial whaling catches in the 20th century. *Marine Fisheries Review*, 76(4):37–48.

Romagosa, M., Perez-Jorge, S., Cascao, I., Mourino, H., Lehodey, P., Pereira, A., Marques, T. A., Matias, L., and Silva, M. A. (2021). Food talk: 40-Hz fin whale calls are associated with prey biomass. *Proceedings of the Royal Society B*, 288(1954):20211156.

Russell, T. M., Pereksta, D. M., Tietz, J. R., Vernet, M., Jahncke, J., and Ballance, L. T. (2025). Increase of tropical seabirds (Sula) in the California Current Ecosystem with warmer ocean conditions. *Frontiers in Marine Science*, 12:1561438.

Ryan, J. P., Oestreich, W. K., Benoit-Bird, K. J., Waluk, C. M., Rueda, C. A., Cline, D. E., Zhang, Y., Cheeseman, T., Calambokidis, J., and Fahlbusch, J. A. (2025). Audible changes in marine trophic ecology: Baleen whale song tracks foraging conditions in the eastern North Pacific. *Plos one*, 20(2):e0318624.

Salvadeo, C. J., Lluch-Belda, D., Gomez-Gallardo, A., Urban-Ramirez, J., and MacLeod, C. D. (2010). Climate change and a poleward shift in the distribution of the Pacific white-sided dolphin in the northeastern Pacific. *Endangered Species Research*, 11(1):13–19.

Santora, J. A., Mantua, N. J., Schroeder, I. D., Field, J. C., Hazen, E. L., Bograd, S. J., Sydeman, W. J., Wells, B. K., Calambokidis, J., and Saez, L. (2020). Habitat compression and ecosystem shifts as potential links between marine heatwave and record whale entanglements. *Nature communications*, 11(1):536.

Širović, A., Williams, L. N., Kerosky, S. M., Wiggins, S. M., and Hildebrand, J. A. (2013). Temporal separation of two fin whale call types across the eastern North Pacific. *Marine Biology*, 160(1):47–57.

Soldevilla, M. S., Henderson, E. E., Campbell, G. S., Wiggins, S. M., Hildebrand, J. A.,

and Roch, M. A. (2008). Classification of Risso's and Pacific white-sided dolphins using spectral properties of echolocation clicks. *The Journal of the Acoustical Society of America*, 124(1):609–624.

Soldevilla, M. S., Wiggins, S. M., and Hildebrand, J. A. (2010). Spatio-temporal comparison of Pacific white-sided dolphin echolocation click types. *Aquatic Biology*, 9(1):49–62.

Suryan, R. M., Arimitsu, M. L., Coletti, H. A., Hopcroft, R. R., Lindeberg, M. R., Barbeaux, S. J., Batten, S. D., Burt, W. J., Bishop, M. A., and Bodkin, J. L. (2021). Ecosystem response persists after a prolonged marine heatwave. *Scientific reports*, 11(1):6235.

Szesciorka, A. R., Ballance, L. T., Širović, A., Rice, A., Ohman, M. D., Hildebrand, J. A., and Franks, P. J. S. (2020). Timing is everything: Drivers of interannual variability in blue whale migration. *Scientific Reports*, 10(1):7710.

Tanaka, K. R., Van Houtan, K. S., Mailander, E., Dias, B. S., Galginaitis, C., O'Sullivan, J., Lowe, C. G., and Jorgensen, S. J. (2021). North Pacific warming shifts the juvenile range of a marine apex predator. *Scientific reports*, 11(1):3373.

Thompson, P. O., Findley, L. T., Vidal, O., and Cummings, W. C. (1996). Underwater sounds of blue whales, *Balaenoptera musculus*, in the Gulf of California, Mexico. *Marine Mammal Science*, 12(2):288–293.

Vu, E. T. A. (2015). *Habitat use of calling baleen whales in the southern California Current Ecosystem*. Thesis, UC San Diego.

Zaba, K. D. and Rudnick, D. L. (2016). The 2014–2015 warming anomaly in the Southern California Current System observed by underwater gliders. *Geophysical Research Letters*, 43(3):1241–1248.

ZoBell, V. M., Hildebrand, J. A., and Frasier, K. E. (2024). Comparing pre-industrial and modern ocean noise levels in the Santa Barbara Channel. *Marine Pollution Bulletin*, 202:116379.

ZoBell, V. M., Posdaljian, N., Lenssen, K. L., Wiggins, S. M., Hildebrand, J. A., Baumann-Pickering, S., and Frasier, K. E. (2025). Climatic and economic fluctuations revealed by decadal ocean soundscapes. *Journal of the Acoustical Society of America*, 157(6):4233–4251.

Chapter 2

Biogeographic patterns of Pacific white-sided dolphins based on long-term passive acoustic records

2.1 Abstract

This study investigates the biogeographic patterns of Pacific white-sided dolphins *(Lagenorhynchus obliquidens)* in the Eastern North Pacific based on long-term passive acoustic records spanning 2005 to 2021. We aim to elucidate the ecological and behavioral significance of distinct echolocation click types and their implications for population delineation, geographic distribution, environmental adaptation, and management. Over 50 cumulative years of Passive Acoustic Monitoring (PAM) data from 14 locations in the Eastern North Pacific were analyzed using a deep neural network to classify two distinct Pacific white-sided dolphin echolocation click types. We assessed spatial, diel, seasonal, and interannual patterns of the two click types, correlating them with major environmental drivers such as the El Niño Southern Oscillation and the North Pacific Gyre Oscillation, and modeled long-term spatial-seasonal patterns. Distinct spatial, seasonal, and diel patterns were observed for each click type. Significant biogeographical shifts in presence were observed following the 2014-2016 marine heatwave event. Distinct spatial distributions of the two click types support the hypothesis that Pacific white-sided dolphins produce population-specific echolocation clicks. Seasonal and diel patterns suggest

spatio-temporal niche partitioning between the populations in Southern California. Interannual changes, notably initiated during the 2014-2016 marine heatwave, indicate climate-driven range expansions and contractions related to gradual tropicalization of the Southern California Bight.

2.2 Introduction

Pacific white-sided dolphins (*Lagenorhynchus obliquidens*) are small pelagic delphinids endemic to the eastern and western North Pacific Ocean (Walker et al., 1986). From east to west their distribution ranges as far south as the Gulf of California, up to the Gulf of Alaska, across to the Sea of Okhotsk, and down into the East China Sea (Hayano et al., 2004; Leatherwood and Walker, 1982; Walker et al., 1986). Multiple genetically and morphologically-distinct populations exist throughout the Pacific white-sided dolphins' geographic range (Hayano et al., 2004; Lux et al., 1997; Walker et al., 1986). However, as is true for many cetacean populations, understanding of gene flow, population dynamics, and geographic overlap has been limited by survey effort and data processing capacity and technology.

In the Eastern North Pacific, at least two Pacific white-sided dolphin populations occur along the west coast of North America (Walker et al., 1986). Walker et al. (1986) observed that animal crania recovered off the coast of Baja California (below 32° N) were markedly different in shape and size than those recovered north of 37° N. In the Southern California Bight, between 32°3' N and 34°3' N, they observed significant variability in cranial morphometrics. Taken together, Walker et al. (1986) interpreted these results to be evidence of two morphometrically distinct populations: with a southern form occupying Southern California and Baja, and a northern form occupying central and northern California, Oregon, and Washington (CA/OR/WA population), with the Southern California Bight being a region of overlap between the two. Additionally, Lux et al. (1997) examined genetic samples from four regions including Baja California, the U.S. West Coast, British Columbia and Alaska, and offshore waters of the North Pacific. Their findings revealed genotypic distinctions between each region, suggesting that four

populations may exist across the eastern North Pacific (Lux et al., 1997). Lastly, Soldevilla et al. (2008) hypothesized that the Southern California/Baja form and California/Oregon/Washington form described by Walker et al. (1986) could be distinguished acoustically.

Soldevilla et al. (2008) identified two distinct echolocation click types produced by Pacific white-sided dolphins off Southern California: Type A with spectral peaks at 22, 27, and 39.5 kHz, and Type B at 22, 26, and 36 kHz. Further investigation (Soldevilla et al., 2010) revealed these types had unique spatial and diel patterns in the Southern California Bight, with Type A present at six passive acoustic monitoring (PAM) stations, mainly at night, and Type B at two southern inshore stations, mainly during the day. The diel activity patterns, combined with differences in spatial presence, lead to multiple hypotheses regarding the biological significance of each click type: the two click types might represent different behaviors within a single dolphin population or distinct populations with unique acoustic signatures. Combining these findings with morphometric and genetic data **?**Walker et al. (1986) suggests two overlapping, morphologically and acoustically-distinct Pacific white-sided dolphin populations occupying the region. However, since these seminal studies, no study has compared Soldevilla's type A (LoA) and type B (LoB) click usage patterns throughout the Eastern North Pacific. Here, we use an automated classification method combined with expert review to compare the distribution of LoA and LoB click presence. Pacific white-sided dolphin detections were compared from 57 cumulative years of PAM data from 14 long term monitoring stations distributed between the Gulf of California and the Gulf of Alaska to further delineate the spatial and temporal distribution of the two click types.

Our study aimed to assess whether the spatio-temporal distribution of the two click types aligns with proposed population geographic ranges in the Eastern North Pacific (Lux et al., 1997; Walker et al., 1986), therefore illuminating possible population-specific biogeographic patterns. Conflicting hypotheses regarding the migration patterns of Pacific white-sided dolphins (Brown and Norris, 1956; Forney and Barlow, 1998) prompted our investigation of spatial-seasonal

trends to identify the potential influence of latitude and season on Pacific white-sided dolphin acoustic presence.

Hypotheses suggesting a poleward range shift of Pacific white-sided dolphins out of the Gulf of California, potentially linked to warming sea surface temperatures (Salvadeo et al., 2010) further guided our examination of long-term changes in acoustic presence in the Southern California Bight. The decade from 2010-2020 witnessed extreme climatic events in the North Pacific Ocean, including a coupled marine heatwave and El Niño from 2014-2016 leading to persistent positive temperature anomalies (Leising et al., 2015; Wells et al., 2017), biogeographic range shifts (Cavole et al., 2016), and widespread die offs of marine mammals and seabirds (McClatchie et al., 2016; Piatt et al., 2020). Our study period, spanning 2008-2021, coincides with these events at three long-term monitoring sites in Southern California. Nearly continuous recording effort and frequent Pacific white-sided dolphin detections at each of these sites allowed us to examine the relationship between click type presence and environmental drivers including the North Pacific Gyre Oscillation (NPGO) index (Di Lorenzo et al., 2008) and Ocean Niño index (ONI), and to compare relative presence before, during, and after the marine heatwave of 2014-2016.

As our rapidly changing climate continues to affect the distribution of marine foraging habitats, it is important that researchers can predict the shifting movement patterns (MacLeod, 2009) of protected species such as Pacific white-sided dolphins who are known to interact with fisheries (Carretta et al., 2022). The two cryptic populations are currently managed as a single stock by the National Marine Fisheries Service (NMFS) as they are visually indistinguishable (Carretta et al., 2022). By investigating potential acoustic delineation, we aim to address the knowledge gap regarding population-specific biogeographic patterns of Pacific white-sided dolphins with the goal that this information can be used to support future policy and management directives (Martien et al., 2019).

2.3 Methods

2.3.1 Data Collection

We selected 14 long-term Passive Acoustic Monitoring (PAM) stations across the Eastern North Pacific (Table 2.1, Table 2.8, Figure 2.1). These included a southernmost station at the mouth of the Gulf of California (GofCA_P1), two further north in the Gulf (GofCA_P2, GofCA_P3), a station west of Guadalupe Island (Baja_GI), six in the Southern California Bight (SCB: H, M, N, P, T, U), one off Point Conception near the Channel Islands National Marine Sanctuary (CINMS), and three northern stations at Point Sur (PS), in the Olympic Coast National Marine Sanctuary (OCNMS), and in the Gulf of Alaska (GofAK). The temporal coverage varied from 2005 to 2021, with nearly continuous recording at two SCB stations (H and N) and the CINMS station. High-Frequency Acoustic Recording Packages (HARPs) were deployed at depths of 500-1200 meters, continuously recording 16-bit audio at a 200 kHz sampling rate, with an effective recording bandwidth of 10 Hz to 100 kHz for up to one year Wiggins and Hildebrand (2007). Some sites (PS, GofCA_P1, P2, P3) operated on a duty cycle of 5 minutes on and 10, 20, or 25 minutes off to extend deployment durations. HARP hydrophones were suspended 10-20 meters above the seafloor.

2.3.2 Data Processing

Click Detection: For each HARP deployment, echolocation clicks were detected using customized routines in the MATLAB-based software program *Triton* (Wiggins and Hildebrand, 2007). A two-step detection approach was implemented in *Triton* following methods outlined in Soldevilla et al. (2008) and Roch et al. (2011), with the objective that all acoustic signals within an expected frequency range and duration of odontocete echolocation clicks and with an 8 dB signal-to-noise ratio would be returned.

Unsupervised clustering phase I: Outputs from the detector were passed through an unsupervised clustering algorithm developed in *Triton* used to categorize consistent signal types

into 5-minute bin level averages Frasier et al. (2017). We applied a 120 dB peak-to-peak (pp) re: 1 μPa threshold to filter out low-quality detections before clustering them based on spectral and waveform similarity scores. Similarity scores were computed between all clicks detected in a five minute time period (bin), up to a maximum of 5,000 clicks for computational efficiency. For each bin, a network was formed in which clicks represented nodes connected by "edges", or linkages based on inter-click similarity scores. The weakest 95% of edges in the network were pruned to facilitate clustering, and the Chinese Whispers algorithm (Biemann, 2006) was used to identify clusters of similar clicks within the network. This algorithm iteratively assigns nodes into common clusters, seeking to maximize within-cluster similarity and minimize between-cluster similarity. A maximum of 15 clustering iterations was allowed, however reassignments typically cease after 5-10 iterations. Clusters consisting of a minimum of 50 clicks were retained, and multiple clusters could form per time bin. If fewer than 50 clicks were detected in a five minute bin, they were treated as a single cluster for classification purposes. If more than 5,000 clicks were detected in a five minute bin, a subsample of 5,000 clicks was randomly selected for clustering and classification purposes. Each cluster's normalized mean spectrum and waveform envelope were calculated, along with the inter-click interval (ICI) between clicks, binned in 10 msec increments from 0.1 to 1 sec. ICI distributions were plotted as histograms to define modal ICI for each type within a 5-minute bin.

Unsupervised clustering phase II: Dominant signal types within a subset of four deployments were identified to form a training dataset for development of a deep neural network for classification using a second phase of clustering. The bin level clusters were grouped using one large network (maximum size 20,000 bins) based on similarity to identify the dominant signal types (typically 5 to 15 types) observed across a particular deployment. Types were considered dominant if they consisted of at least 50 bins. Up to 30 iterations of the Chinese Whispers algorithm (Biemann, 2006) were allowed in this case. This step aggregated examples of the dominant signal types found in each deployment into distinct clusters (Frasier et al., 2017).

Expert review of dominant types: An expert analyst (MA) merged the aggregated clusters of six dominant signal types across deployments to develop a robust classifier training set. Five oceanic dolphins are commonly observed in Southern California, including long-beaked common dolphins (*Delphinus capensis*), short-beaked common dolphins (*Delphinus delphis*), bottlenose dolphins (*Tursiops truncatus*), Risso's dolphins (*Grampus griseus*), and Pacific white-sided dolphins (Bearzi, 2005; Becker et al., 2022; Campbell et al., 2015; Soldevilla et al., 2008). Soldevilla et al. (2008) determined that Risso's and Pacific white-sided dolphin echolocation clicks are acoustically distinguishable by their unique spectral banding patterns, whereas bottlenose and common dolphins are not. Here, we use the characteristic spectral peak and notch features described by Soldevilla et al. (2008) to identify Risso's dolphin (Gg) and Pacific white-sided dolphin's LoA and LoB clusters present in the phase II clustering output (Figure 2.2). Clusters resembling common dolphin and bottlenose dolphin clicks were categorized as unidentified dolphin (UD). Additionally, clusters for Cuvier's beaked whale (*Ziphius cavirostris*) (Zc) (Baumann-Pickering et al., 2013; Zimmer et al., 2005) and boat noise were identified and incorporated into the training dataset as non-target classes to improve classifier performance.

Deep neural network training and testing: Aggregated examples of Risso's and Pacific white-sided dolphin categories were pooled across four deployments: three in the Southern California Bight (SCB_H_61, SCB_H_66, SCB_E_65, Table 2.2), and one in the Olympic Coast National Marine Sanctuary (OCNMS_QC_12). For the background UD, Boat, and Zc categories, examples were pulled only from the SCB_H_61 deployment, which had the best representation of all six categories. Some types are more common than others (e.g., UD), therefore, to balance the dataset we drew 500 examples from each category to form the training set. The Boat and Zc categories, and the combined LoB category, contained fewer than 500 bin-level examples (Table 2.2). Therefore, those categories were randomly resampled to reach the 500 sample target size. The 3,000 bin level examples (500 x 6 categories) were split into

66% training and 33% testing.

The deep neural network ran as an add-on package in *Triton* using MATLAB's *Deep Learning Toolbox* and was trained on spectral averages, mean waveform envelope and ICI distributions of the 5-minute-level clusters representing the six signal categories. Labels were numerically encoded for the network, which comprised four 512-node fully connected layers, featuring 50% dropout, leaky ReLU activations, and a Softmax output layer, limited to 15 training epochs. Performance using this architecture, further detailed in Frasier (2021), was evaluated based on accuracy, precision, and recall on the testing dataset. Additionally, we tested model performance on novel data by comparing its labels with an expert analyst's (MA) manual annotations for three deployments (SCB_P_35, SCB_H_29, and CINMS_C_33) (Tables 2.9–2.11). We selected this wide range of test deployments to investigate the potential for domain shift, or cases when differences between the training data and target (novel) data results in reduced performance (Ben-David et al., 2010).

2.3.3 Data analysis

Signal review and timeseries generation: The data processing workflow for each deployment included signal detection, Phase I clustering, and classification of bin-level averages using the trained network. LoA, LoB, and Gg labels were evaluated by three expert analysts, including co-authors MA and AA, using the *DetEdit* interface Solsona-Berga et al. (2020), enabling review and re-classification of mislabeled clusters.

We implemented a final received level threshold of 123 dB_{pp} re:1 µPa to maintain consistency in detection thresholds across recording sites. The initial 8 dB SNR threshold may have excluded high-amplitude low-SNR clicks, resulting in non-linear detection curves. If no clicks are missed, a theoretical detection curve would scale linearly with dB amplitude as more clicks are detected further away from the hydrophone (Hildebrand et al., 2019). By thresholding above 123 dB_{pp} re:1 µPa, we retained only the highest quality detections and effectively restricted our detection range at each site.

Detections were binned into hourly intervals, with 'click-positive' bins indicating any number of detected clicks in a bin. This binning facilitated initial visualization of diel and long-term patterns. Timeseries were generated at each site using the *Tethys* (Roch et al., 2016) package in MATLAB. Detections were then grouped into ‘click-positive days’ indicating that at least one click-positive hour was present during that day, to analyze the spatial biogeographic patterns of the LoA and LoB click types. We illustrated the percentage of recording days with Pacific white-sided dolphins present at each site as scaled circles and overlaid current stock boundaries defined by NMFS (Carretta et al., 2022).

Analysis of diel patterns: To test whether LoA clicks occurred more frequently at night and LoB clicks during the day, we binned detections into minutes per hour, labeling each hour as 'day' or 'night' using RStudio's (team, 2016) *suncalc* package. Day and night hourly detections were summed and divided by recording effort, being the total number of day or night recording hours. We applied one-sided t-tests to the scaled diel activity values to test whether the mean difference in LoA activity was greater during the night than day, and whether the mean difference in LoB activity was less during the night than day, as was observed by (Soldevilla et al., 2010).

Analysis of seasonal and spatial patterns: We analyzed the seasonal patterns of Pacific white-sided dolphins by converting daily detections into the number of days with presence per season. Seasons were categorized into Winter (December-February), Spring (March-May), Summer (June-August), and Fall (September-November), focusing on sites with at least 25% recording effort for a given season. To investigate the relationship between click type presence, season, and latitude, we built Generalized Additive Models (GAMs) for both LoA and LoB clicks using the *mgcv* package (Wood, 2011) in RStudio. These models, designed to handle nonlinear seasonal interactions and latitudinal influences, used the number of click-positive days per season as the response variable, applying a Tweedie distribution (Wood et al., 2016) for zero-inflation adjustment. The GAMs were constructed using a tensor product smooth term to capture the interaction between season and latitude, allowing us to investigate variation

in seasonality with latitude. Model diagnostics were performed to assess the quality of the fits and the significance of each term. Contour plots were generated to visually represent the spatial-seasonal interactions and display large-scale biogeographic patterns.

Analysis of interannual and environmentally driven patterns: We examined interannual variations in Pacific white-sided dolphin acoustic presence at three long-term monitoring sites in Southern California. Using the ONI and NPGO as covariates, we applied Generalized Linear Models (GLMs) at sites CINMS, SCB_H, and SCB_N to test the null hypothesis of no correlation between climate drivers and Pacific white-sided dolphin presence. The ONI and NPGO data, indicative of sea-surface temperature deviations and biological productivity in the California Current, were sourced from NOAA's National Weather Service Climate Prediction Center and http://www.o3d.org/npgo/, respectively (Di Lorenzo et al., 2008). We calculated a three-month running average of the NPGO variable to match the resolution of the ONI and seasonal dolphin presence. Each GLM, fitted with a Tweedie distribution to handle zero-inflation, included linear coefficients for both ONI and NPGO, with diagnostic assessments to evaluate model fits. Additionally, we examined the relationship between Pacific white-sided dolphin acoustic presence and the extreme marine heatwave event of 2014-2016 (Leising et al., 2015). We used Kruskal-Wallis and Dunn's post-hoc tests to assess the null hypothesis that Pacific white-sided dolphin presence was the same before, during, and after the 2014-2016 marine heatwave event at the aforementioned long-term monitoring sites.

2.4 Results

We analyzed 163 HARP deployments between the Gulf of California and the Gulf of Alaska, representing 57 cumulative years of recording effort. The majority of effort occurred in Southern California at sites CINMS, SCB_H, and SCB_N, where recording was nearly continuous between 2009-2021.

2.4.1 Classifier Performance

The classification accuracy of the deep neural network was 99.6% on the test dataset and testing recall and precision was above 98% for each category (Table 2.3). However, these metrics overestimate the model's performance because they are estimated using the highest quality examples aggregated from a subset of sites by the phase II clustering process. On truly novel and minimally-curated bin-level clusters consisting of one or more clicks, the model's precision ranged from 22% to 75% for the LoA category, and 0.67% to 67% for the LoB category reflecting a relatively high false positive rate (Tables 2.9–2.11). Recall ranged from 83% to 92% for the LoA category and was 100% for the rare LoB category. Given these results, all LoA and LoB labels were manually reviewed to remove false positives.

2.4.2 Biogeographic Patterns

Geographic Distribution: The Pacific white-sided dolphin LoA click type was detected at 11 of the 14 study sites (Figure 2.1), including the northern locations (GofAK, OCNMS, PS), CINMS, all SCB sites, and Guadalupe Island (Baja_GI), but not at the Gulf of California sites (GofCA P1, P2, P3). Daily detection frequencies varied, with the highest at OCNMS (29.3% of days) and PS (29.5%). LoA clicks were detected at the CINMS station on 24.7% of days, and in the Southern California Bight, detections ranged from 1% to 16.5% with greater values trending towards offshore sites (Figure 2.1). The southernmost LoA detection was at Baja_GI, present on less than 1% of recording days. Conversely, LoB clicks were observed at 8 sites, predominantly in the SCB, with isolated detections at CINMS and GofCA_P1. The highest presence of LoB clicks was observed at the inshore site SCB_T (9.3% of days). LoB clicks were not detected at GofAK, PS, OCNMS, Baja_GI, GofCA_P2, or GofCA_P3.

Diel patterns: Analysis of diel patterns in Pacific white-sided dolphins showed significant differences in day and night acoustic activities. The one-sided t-test suggested that LoA clicks occurred significantly more frequently at nighttime (mean difference = 64.16, p = 0.0029)

(Table 2.4). Conversely, LoB clicks occurred significantly more frequently during the daytime (mean difference = -15.30, p = 0.034) (Table 2.4). The scaled site-specific patterns in Figure 2.3 indicate that LoA clicks are detected more often during nighttime at northern and central California sites OCNMS, PS, and CINMS (Figure 2.3). In the Southern California Bight, a slight preference for nighttime activity was evident at SCB_H. As suggested by the one-sided t-test, the scaled activity of the LoB click type was greater during the daytime, indicating an inverse relationship to LoA clicks, especially evident at SCB_T (Figure 2.3).

Seasonal-spatial patterns: Pacific white-sided dolphin LoA and LoB click presence exhibited seasonal site-specific spatial variability (Figure 2.4, a1-a4). LoA presence was greater off the coast of Central California and Southern California during winter and spring, with minimal presence detected at Baja_GI during spring. Seasonal presence increased at OCNMS and GofAK during the summer and fall, suggesting a north-south seasonal migration. The GAM revealed a significant nonlinear relationship between LoA presence and the interaction between season and latitude (Table 2.5), and predicted greatest LoA presence during summer at mid to higher latitudes, ranging from 35° to 45°N (Figure 2.4, a5). The model's smooth term captured 19.8% of the variance, suggesting that additional ecological dynamics play a role shaping the biogeographic distribution of LoA's presence.

LoB click presence peaked at inshore stations in the Southern California Bight during fall and winter, with minimal detections in the Gulf of California during winter and spring (Figure 2.4, b1-b4). The GAM model results for LoB indicated a significant nonlinear relationship between seasonal presence and latitude (Table 2.5), with predictions concentrated in the southern half of the species geographic range during winter, spring, and extending into fall (Figure 2.4, b5). However, the lack of temporal overlap between Southern California and Gulf of California stations makes it challenging to resolve LoB seasonal patterns across the region, especially when considering interannual variability. The LoB model accounted for 22.4% of the variance in presence, indicating that while the model captures some of the ecological dynamics, others

may play a significant role in determining LoB presence across the region.

Interannual patterns and environmental drivers: Biogeographic patterns at three long-term monitoring sites in Southern California showed significant changes in LoA and LoB acoustic presence, particularly during and following the 2014-2016 marine heatwave and El Niño (Figure 2.5). Notably, LoB presence was detected for the first time at site CINMS during the fall of 2018, and again in the fall of 2019 (Figure 2.5). There were marked differences in dolphin presence before, during, and after the heatwave at all sites (Figure 2.6, Table 2.6). Post hoc analyses further detailed these shifts. At site CINMS, LoA presence decreased during the heatwave, with no significant differences detected in periods before and after the event (Figure 2.6a). At SCB_H, LoA presence decreased significantly during and post-heatwave, while LoB presence significantly increased post-heatwave, marking a notable shift in dominance between click types (Figure 2.6b). At SCB_N, LoA presence was significantly higher before the heatwave compared to during and after, whereas LoB presence showed no significant changes across these periods (Figure 2.6c).

The shifts in presence coincided with inflection points of the ONI and NPGO indices Leising et al. (2015); Wells et al. (2017), suggesting that interannual changes in Pacific white-sided dolphin presence are driven by large-scale climate phenomena. Our GLMs further substantiated this link (Figure 2.7, Table 2.7). At site CINMS, LoA was slightly negatively correlated with the NPGO and ONI. At site SCB_H, LoA was positively correlated with the NPGO, while LoB was negatively correlated, highlighting different environmental conditions favoring the two click types. LoA presence showed a negative correlation with the ONI and a positive correlation with the NPGO at SCB_N, indicating a preference for cooler, nutrient-rich conditions typically found during La Niña phases in Southern California. LoB, however, was not significantly correlated with either environmental driver at site SCB_N. These findings may highlight how Pacific white-sided dolphins navigate climate phases in the Eastern North Pacific, shifting their distribution in response to dynamic ocean conditions.

2.5 Discussion

Results from this study support the hypothesis that Pacific white-sided dolphins produce population-specific echolocation clicks. LoA clicks were detected throughout the study region, with seasonally specific peak occurrences off Point Conception, Point Sur, and Washington. LoB clicks were detected seasonally throughout the Southern California Bight and at the southernmost tip of the Gulf of California. Soldevilla et al. (2010) put forward multiple hypotheses to explain significance of the two distinct click types, and our results most consistently match the population-specific click hypothesis, stating that LoA clicks are produced by the CA/OR/WA population, and LoB clicks are produced by the Southern California/Baja population. It is possible that anatomical differences in cranial shape (Walker et al., 1986) between the populations result in the unique spectral content of each click type (Cranford et al., 1996; Soldevilla et al., 2008, 2010). Here we address the results of each of our hypotheses and put into context the ecological relevance of our findings.

The geographic distribution of the LoA click type associates with the geographic distribution of the CA/OR/WA population laid out by (Walker et al., 1986) cranial morphometric comparisons and (Lux et al., 1997) genetic distinctions. The majority of LoA presence was detected within the CA/OR/WA stock boundaries. LoA clicks were also detected during summer and fall in the Gulf of Alaska, indicating that the CA/OR/WA population may move northward during warmer months, potentially exploiting dense aggregations of prey that are present during that time of year. Lux et al. (1997) found evidence of another genetically distinct population off the coast of British Columbia and Alaska. However, spectral and temporal properties of echolocation clicks at our GofAK site matched the LoA echolocation click type found throughout the Eastern North Pacific. It is possible that only the CA/OR/WA population frequents this location in summer and fall months, and another distinct click type, represented by the North Pacific population, could exist in a different spatial-temporal region not covered by our study. Alternatively, it is possible that the CA/OR/WA and the North Pacific population are

not acoustically distinct. One LoA encounter was detected at the Baja_GI site, although no LoB clicks were detected there throughout the three year recording period. The Baja_GI LoA detection occurred during the spring, corresponding to a time of year when LoA presence peaked in the Southern California Bight, suggesting that the CA/OR/WA Pacific white-sided dolphin population may migrate further south than originally hypothesized.

Comparing their spatial distributions, the Southern California/Baja population appears to produce the LoB click type as hypothesized by Soldevilla et al. (2010). Our results suggest that the Southern California/Baja population prefers coastal inshore habitats as demonstrated by the peak in LoB acoustic presence at sites SCB_T and SCB_P, in the San Diego Trough and off of Point La Jolla. Species distribution models of Pacific white-sided dolphins in Baja California waters predict highest densities near shore, with increasing density further offshore in Southern California Bight waters (Becker et al., 2022). Relative abundance estimates from Becker et al. (2022) were less accurate in the Southern California Bight region, possibly due to the differing habitat preferences between the two overlapping populations (Becker et al., 2022). Together, these findings suggest that animals observed nearshore off San Diego and Baja California are more likely from the Southern California/Baja population, whereas animals observed offshore in the Southern California Bight are more likely from the CA/OR/WA population.

In a recent study by Kanes et al. (2023) Pacific white-sided dolphin pulsed calls (Henderson et al., 2011) were detected year-round throughout a two-year study period (2013-2015) near Barkley Canyon offshore of Vancouver Island, British Columbia. Kanes et al. (2023) findings demonstrated that Pacific white-sided dolphin pulsed call presence was greatest during summer months, with a majority of activity during nighttime and dawn periods. Our analysis of diel and seasonal patterns of echolocation clicks corroborates and extends these findings across different geographic locations. Expanding upon the notion that echolocation click rate can serve as an indicator of behavioral state in odontocetes (Madsen et al., 2005), our study employed a methodology that assumes higher echolocation rates to infer increased foraging potential

(Nowacek, 2005; Van Parijs and Corkeron, 2001). The significant nocturnal bias in echolocation activity, especially at sites OCNMS, PS, and CINMS, implies that foraging activities are more intense at night in these habitats and suggests that the animals may be consuming vertically migrating mesopelagic fish and squid when they are accessible at the surface, which has been proposed for other delphinid species (Caruso et al., 2017; Rice et al., 2021).

In the Southern California Bight, our findings illustrate distinct diel patterns of echolocation activity between the click types. Our results align with Soldevilla et al. (2010) findings that LoA clicks were detected more frequently at night and LoB more frequently during the day. By expanding our analysis geographically and temporally, we hypothesize that differences in diel activity may be evidence of habitat-based niche partitioning between the populations. The CA/OR/WA population appears to favor offshore, nocturnal foraging locations such as site SCB_H, whereas the Southern California/Baja population appears to favor inshore, diurnal foraging locations such as SCB_T. Consistent with our findings, Henderson et al. (2011) observed that animals producing LoA clicks in Southern California were traveling slowly and milling, and exhibited little daytime foraging activity, whereas animals producing LoB clicks were observed traveling and foraging. Coupling the observed behavioral patterns with the diurnal activity of the click types suggests that during daytime hours when the CA/OR/WA population is present in Southern California, they may be seen exhibiting resting or social behaviors, whereas the Southern California/Baja population may be seen foraging.

Furthermore, Pacific white-sided dolphin clicks detected in Southern California consistently separated into two distinct clusters: LoA and LoB. Previous studies have documented odontocete species exhibiting adaptive control over the source-level, inter-click-interval, and frequency content of their echolocation clicks (Au et al., 1985, 1995; Houser et al., 1999; Ladegaard et al., 2019; Simon et al., 2007). During object detection and discrimination tasks in captive settings, Au et al. (1985, 1995) and Houser et al. (1999) documented multiple click types varying in frequency content produced by individual animals. If the two Pacific white-sided

dolphin echolocation click types were purely indicative of adaptive control in a single population, more intermediate click types would likely have been observed during the clustering step. The absence of such intermediate click types lends further support to the hypothesis that Pacific white-sided dolphin LoA and LoB click types are representative of two distinct populations whose echolocation frequency spectra are shaped by their distinct skull and melon morphology (Soldevilla et al., 2008, 2010; Walker et al., 1986).

Our seasonal-spatial GAM models display how Pacific white-sided dolphin acoustic presence varies seasonally with latitude (Figure 2.4). We demonstrate that the CA/OR/WA population's presence increases off Central and Southern California during winter and spring and shifts northward during summer and fall (Figure 2.4). Previous studies observed similar seasonal patterns in the region (Becker et al., 2019; Forney and Barlow, 1998; Rice et al., 2021), yet ours is the first to delineate these patterns at the population level. Presence of the LoB click type, likely produced by the Southern California/Baja population, increases at coastal inshore sites in Southern California during fall and winter, suggesting that while there may be sympatry in terms of shared geographical space, it is likely structured temporally, with each population favoring different habitats during different times of the year. The Southern California/Baja population seems to prefer inshore habitats during the winter and fall, while the CA/OR/WA population is more frequently found offshore during winter and spring. However, it remains unclear whether the Southern California/Baja Population moves further offshore of Southern California, or further south into Baja California during summer months. The peak in coastal inshore presence of the southern population in fall and winter may be influenced by the dynamics of the Southern California Counter-current. This inshore current transports warm water from Baja California and is linked to distinct community assemblages (Lavenberg and Ebeling, 1967), with increased strength during fall and winter seasons (Collins et al., 2000; Lynn and Simpson, 1987).

In the past decade, the Eastern North Pacific has experienced extreme climatic events,

including a severe marine heatwave starting in late 2013, followed by the strongest El Niño on record in 2015-2016 (Jacox et al., 2016). Following these heatwaves, coupled with steadily rising temperatures, range-expansions have been documented for zooplankton and sub-tropical fishes (Cavole et al., 2016; Leising et al., 2015; Wells et al., 2017), as well as oceanic dolphins including short-beaked common dolphins and striped dolphins (Becker et al., 2019). Our findings suggest that a range expansion may be occurring for the Southern California/Baja Pacific white-sided dolphin population, while a range contraction out of the Southern California Bight may be occurring for the CA/OR/WA population. Notably, the detection of LoB clicks at site CINMS in the fall of 2018 and 2019 - beyond the known range of the Southern California/Baja population - lends further support to the possibility of a northward range expansion in response to changing oceanographic conditions. The inverse relationships between both click types and environmental drivers supports the hypothesis that the click types represent distinct populations, and that those populations favor opposing oceanographic conditions in the Southern California Bight (Figure 2.7). Our findings indicate that the LoA click type, associated with the CA/OR/WA population, shows a preference for cooler, nutrient-rich waters typically found during La Niña conditions, as evidenced by their negative correlation with the ONI and positive correlation with the NPGO in the Southern California Bight. This suggests a reliance on the upwelling-driven productivity that characterizes such periods. Alternatively, at site CINMS, the CA/OR/WA LoA was weakly negatively correlated with both the ONI and NPGO. The timeseries in Figure 2.5 indicates that LoA presence has increased at site CINMS in recent years. We hypothesize that this may be further evidence of a range contraction, meaning, the CA/OR/WA population may be staying further north to remain within their preferred cool-temperate habitat rather than entering the warmer waters of the Southern California Bight, thus resulting in the weak negative correlation with the ONI and NPGO during this timeframe. Conversely, the LoB click type, associated with the Southern California/Baja population, exhibits a positive correlation with the ONI and a negative correlation with the NPGO in the Southern California Bight, suggesting a

preference for warmer, less productive conditions that prevail during El Niño phases or positive phases of the NPGO. Finally, the significant differences in LoA and LoB presence before, during, and after the 2014-2016 marine heatwave highlights the profound effect this extreme event may have had on the geographic distribution of the two populations.

The CA/OR/WA and Southern California/Baja Pacific white-sided dolphin populations remain visually indistinguishable; however, our work demonstrates that they may be acoustically distinguishable by the two click types described in Soldevilla et al. (2008, 2010). Here we have provided evidence to resolve the geographic boundaries of each stock, as well as elucidating biogeographic range shifts throughout a decade of environmental change in Southern California. Passive acoustic monitoring is used in this context as a valuable tool for population-level cetacean assessments and we encourage future policy and management directives to integrate our findings when developing tailored management approaches for each stock. Additionally, integrating environmental DNA sampling (Suarez-Bregua et al., 2022) alongside PAM and visual surveys offers a promising avenue for future research. Such a multidisciplinary approach would not only enrich the lines of evidence (Martien et al., 2019) available across sampling platforms but also provide a deeper insight into stock structure and geographic boundaries. This comprehensive understanding is critical, particularly in light of potential climate-driven range shifts, as it will inform and refine population-level management and conservation strategies, ensuring they are adaptable and effective in the face of new environmental challenges.

2.5.1 Limitations

Our study relied on automated detection and classification of echolocation clicks and manual removal of false positives. This technique, while greatly increasing the efficiency of our data processing pipeline, resulted in some missed detections. We assessed missed detection rates by comparing analyst labels with automatically generated labels in three test deployments outside of the source domain, spanning multiple years and locations not included in the training data. Recall, or the true positive rate, ranged from 83% to 92% for the LoA category and was

100% for the LoB category (Tables 2.9–2.11). These findings suggest an expected recall of over 83% for LoA and 100% for LoB categories across our study, acknowledging possible fluctuations in other untested datasets. By removing all false positives, our study achieved 100% precision. While potential biases between analysts were not explicitly addressed, they are presumed to be minimal due to the consistent training and methodology imparted to all three analysts. Despite potential limitations, the amalgamation of automated detection and manual validation was an efficient, consistent, and robust methodology for examining the spatio-temporal distribution of Pacific white-sided dolphins across diverse biogeographic regions, encompassing over 50 cumulative years of data.

Our findings suggest that Pacific white-sided dolphins produce population level echolocation clicks and partition the Southern California Bight habitat in time and space. Nonetheless, alternative hypothesis cannot be completely rejected. The differences in spatial distribution in the Southern California Bight could reflect specific acoustic signals being used by the same animals in different habitats based on prey composition. Detection of the LoA click type at Baja_GI presents confounding evidence for the hypothesis that the clicks are population-specific. It is possible that the Southern California/Baja population could produce the LoA click type in certain regions, or when hunting certain prey items. Although, with only one encounter of Pacific white-sided dolphins at this site during three continuous years of recording effort, the most parsimonious explanation is that the species is rare in this region and environmental conditions were favorable for the CA/OR/WA animals to venture further south resulting in detection at Baja_GI.

2.5.2 Conclusions

Here we demonstrate how long-term PAM can be used to study population-level species dynamics. The biogeographic patterns of Pacific white-sided dolphins described in this study support the hypothesis that the CA/OR/WA and Southern California/Baja populations are acoustically distinct, and exhibit spatial and temporal niche partitioning in the Southern California

Bight. The implications of this research are especially important in the context of extreme climatic events witnessed in the Eastern North Pacific over the past decade. Our results suggest a potential range expansion of the southern population and a range contraction of the northern population in response to warming ocean conditions. As the marine environment continues to change rapidly, dynamic and innovative management strategies will be increasingly called upon to protect species and their ecosystems. Long-term passive acoustic monitoring is a valuable tool for establishing baselines and should be further integrated into protected species management as we navigate this period of unprecedented environmental change.

2.6 Acknowledgments

Chapter 2, in full, is a reprint of the material as it appears in Diversity and Distributions. Alksne, Michaela N., Kok, Annebelle C.M., Agarwal, Anika, Frasier, Kaitlin E., Baumann-Pickering, Simone. Wiley, 2024. The dissertation author was the primary investigator and author of this paper.

2.7 Data Availability Statement

Binned hourly detections and deployment metadata from each recording site are privately available for review on Dryad. Binned hourly detections contain counts of click positive minutes per hour for each click type at each site where they were detected.

Link: https://doi.org/10.5061/dryad.95x69p8rj

Table 2.1. Summary of recording locations, depths, recording effort, and number of days with Pacific white-sided dolphin LoA and LoB click presence at each site.

Site	Coordinates	Instrument depth (m)	Recording effort (# days)	LoA present (# days, % days)	LoB present (# days, % days)
GofAK	56.243' N, −142.757' W	990	679	39 (5.7%)	0 (0%)
OCNMS	47.501' N, −125.353' W	650	1,056	310 (29.3%)	0 (0%)
PS	36.299' N, −122.393' W	1,220	1,645	486 (29.5%)	0 (0%)
CINMS	34.316' N, −120.805' W	770	2,794	689 (24.7%)	2 (0.0007%)
SCB_M	33.509' N, −119.254' W	940	2,008	107 (5.3%)	35 (1.7%)
SCB_H	32.847' N, −119.176' W	1,100	3,800	627 (16.5%)	191 (5.1%)
SCB_T	32.886' N, −117.556' W	850	397	6 (1.5%)	37 (9.3%)
SCB_P	32.523' N, −117.163' W	520	1,645	14 (0.85%)	50 (3.0%)
SCB_N	32.369' N, −118.565' W	1,230	3,756	436 (11.6%)	57 (1.5%)
SCB_U	31.851' N, −118.484' W	1,200	466	8 (1.7%)	1 (0.21%)
Baja_GI	29.085' N, 118.155' W	1,180	706	0 (0%)	0 (0%)
GofCA_P1	23.498' N, 109.378' W	660	743	0 (0%)	2 (0.26%)
GofCA_P2	28.364' N, 112.303' W	400	430	0 (0%)	0 (0%)
GofCA_P3	29.016' N, 113.225' W	600	433	0 (0%)	0 (0%)

Table 2.2. Signal category, deployment number, and number of 5-minute bin-level training examples that were used as input for the deep neural network. Each category contained less than or equal to 500 examples, where 66% were used for training and 33% were used for testing. For the Gg, LoA, and LoB categories, examples from multiple deployments were included to increase variability.

Signal category	Deployment number	# bin-level training examples
Boat	SCB_H61	18
Gg	SCB_H61	392
	OCNMS12QC	108
LoA	SCB_H61	78
	SCB_H66	54
	SCB_E65	83
	OCNMS12QC	285
LoB	SCB_H61	77
	SCB_H66	73
UD	SCB_H61	500
Zc	SCB_H61	377

Table 2.3. Confusion matrix for bin-level classifier on testing dataset with 500 examples from each category. Values indicate percentages of the total number of detections classified.

		True class						
	Category	**Boat**	**Gg**	**LoA**	**LoB**	**UD**	**Zc**	**Precision**
Predicted class	Boat	**16.70%**	0.10%	0.00%	0.00%	0.00%	0.00%	99.60%
	Gg	0.00%	**16.40%**	0.00%	0.00%	0.10%	0.00%	99.80%
	LoA	0.00%	0.00%	**16.60%**	0.00%	0.00%	0.00%	100%
	LoB	0.00%	0.00%	0.10%	**16.40%**	0.00%	0.00%	99.80%
	UD	0.00%	0.20%	0.10%	0.00%	**16.60%**	0.00%	98.40%
	Zc	0.00%	0.00%	0.00%	0.00%	0.00%	**16.70%**	100%
	Recall	100%	98.40%	99.40%	100%	99.80%	100%	**99.60%**

Table 2.4. Results of paired t-tests comparing diel activity patterns of the LoA and LoB click types across sites. Alternative hypothesis corresponds to true mean difference in normalized diel activity, compared across all sites.

Paired t-test	Alternative hypothesis	Mean difference	t	df	p-value
LoA	true mean difference is greater than 0	64.16	3.41	11	**0.0029**
LoB	true mean difference is less than 0	−15.30	2.02	11	**0.034**

Table 2.5. Summary of spatial-seasonal GAM model results for LoA and LoB presence. *Te* represents the tensor product smooth term.

Model	Smooth term	EDF	Ref. df	F	p-value	Deviance explained
LoA	te(Season, Latitude)	5.8	8	9.3	**<2E-16**	19.8%
LoB	te(Season, Latitude)	4.8	8	3.8	**5.93E-06**	22.4%

Table 2.6. Summary of Kruskal-Wallis test results comparing LoA and LoB presence before, during, and after the 2014–2016 MHW event at long-term Southern California monitoring stations.

Site	Chi-squared	df	p-value
CINMS	42.6	5	**4.49E-08**
SCB_H	42.5	5	**4.65E-08**
SCB_N	45.7	5	**1.03E-08**

Table 2.7. Summary of environmental GLMs for LoA and LoB presence at sites CINMS, SCB_H, and SCB_N.

Model	Coefficient	Estimate	SE	t-value	p-value
LoA ~ ONI + NPGO @ CINMS	ONI	−0.58	0.17	−2.66	**0.012**
	NPGO	−0.29	0.14	−2.05	**0.048**
LoA ~ ONI + NPGO @ SCB_H	ONI	−0.32	0.16	−1.97	0.055
	NPGO	0.41	0.11	3.69	**0.001**
LoA ~ ONI + NPGO @ SCB_N	ONI	−0.55	0.19	−2.91	**0.006**
	NPGO	0.82	0.13	6.29	**1.16E-07**
LoB ~ ONI + NPGO @ SCB_H	ONI	0.23	0.22	1.06	0.293
	NPGO	−0.84	0.18	−4.71	**2.49E-05**
LoB ~ ONI + NPGO @ SCB_N	ONI	−0.01	0.28	−0.037	0.971
	NPGO	0.35	0.19	1.82	0.076

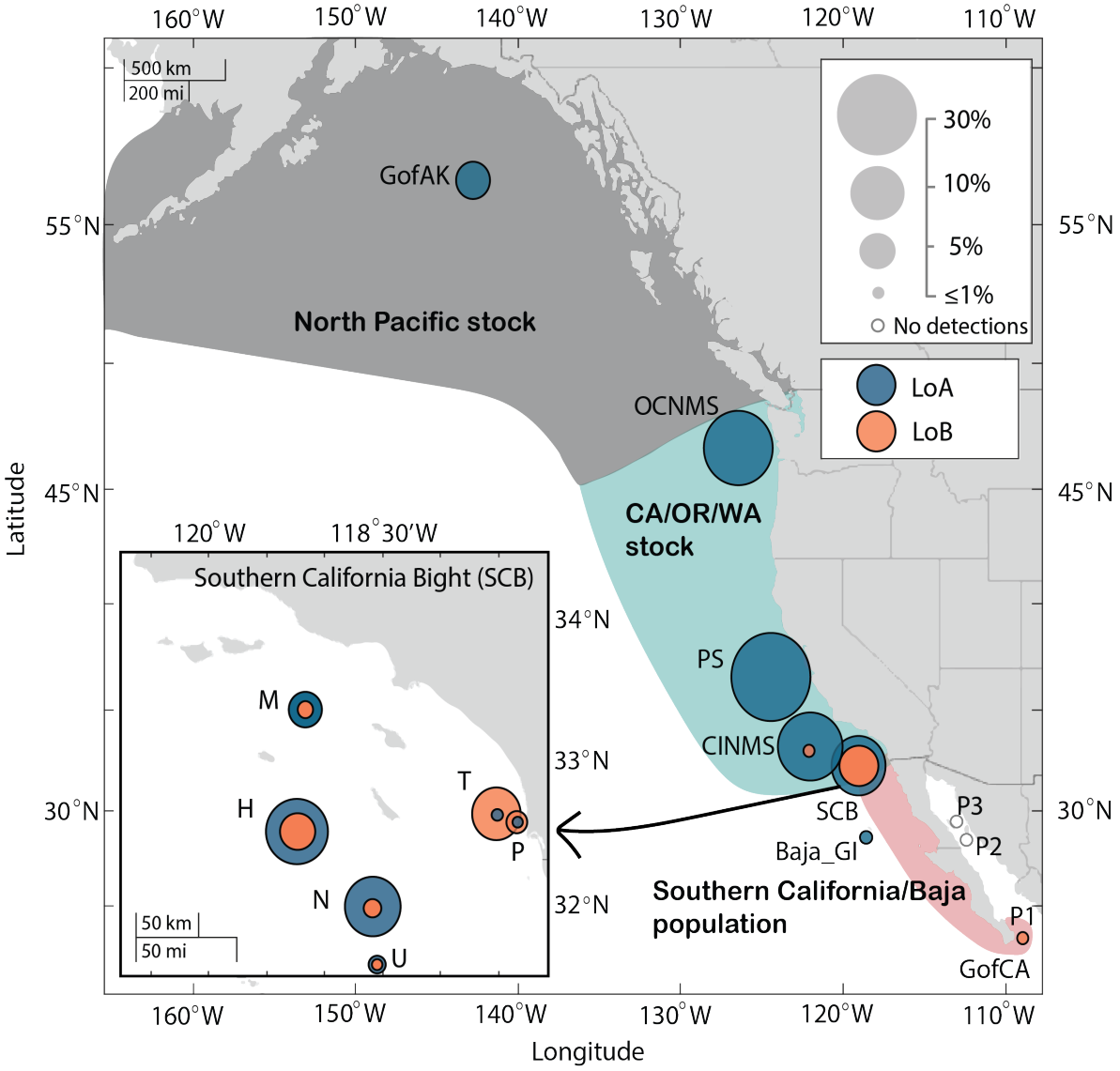


Figure 2.1. PAM sites ranging across the Northeastern Pacific overlaid with geographic boundaries of the North Pacific and CA/OR/WA Pacific white-sided dolphin management stocks, and hypothesized boundaries of the cryptic Southern California/Baja population. The North Pacific stock boundaries are outlined in gray, CA/OR/WA stock boundaries are outlined in blue, and Southern California/Baja stock boundaries are outlined in pink. HARP locations are presented as circles scaled by percentage of recording days with Pacific white-sided dolphin clicks present, with blue circles representing LoA clicks and coral representing LoB clicks. The percentage of recording days with presence are summed for all sites in the Southern California Bight (SCB). The black arrow points from the summed SCB values to the inset box which displays percentages at six Southern California recording sites. LoA clicks were detected between 56.2433' N and 31.8515' N, with the highest percentage of click positive recording days at PS (36.2993' N, −122.3930' W). LoB clicks were detected between 34.3168' N and 23.4983' N, with the highest percentage of click positive recording days at SCB_T (32.8868' N, −117.5560' W).

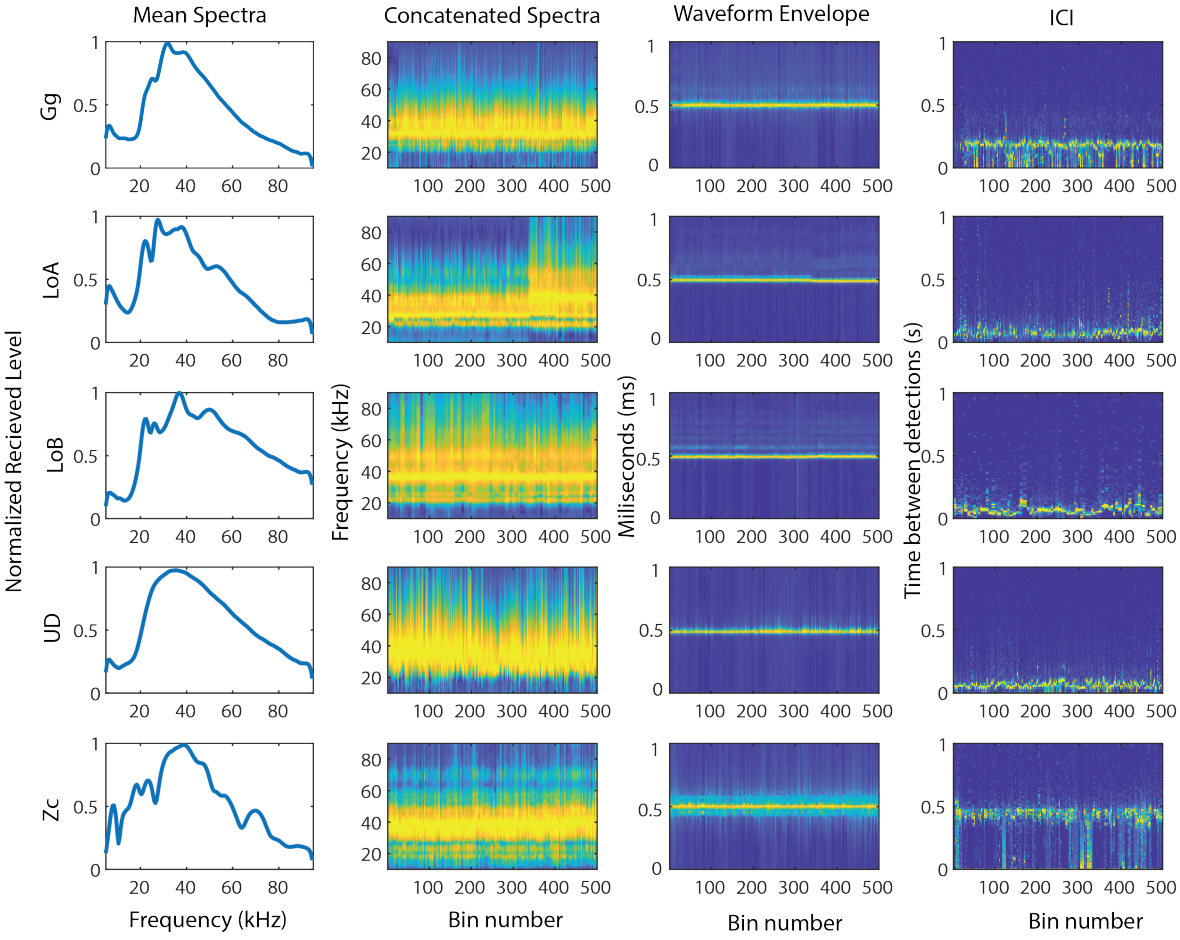


Figure 2.2. Bin-level examples for five odontocete categories: Risso's dolphin (Gg, row 1), Pacific white-sided dolphin (LoA, row 2), Pacific white-sided dolphin (LoB, row 3), unidentified dolphin (UD, row 4), and Cuvier's beaked whale (Zc, row 5). Columns display unique spectral and temporal properties of each signal category. Species specific spectral banding patterns evident in Gg, LoA, LoB, and Zc categories concatenated spectrum plots. Gg peaks at 30 and 40 kHz, LoA peaks at 22, 27.5, and 39 kHz, LoB peaks at 22, 26, and 37 kHz, and Zc peaks at 18, 22, and 40 kHz.

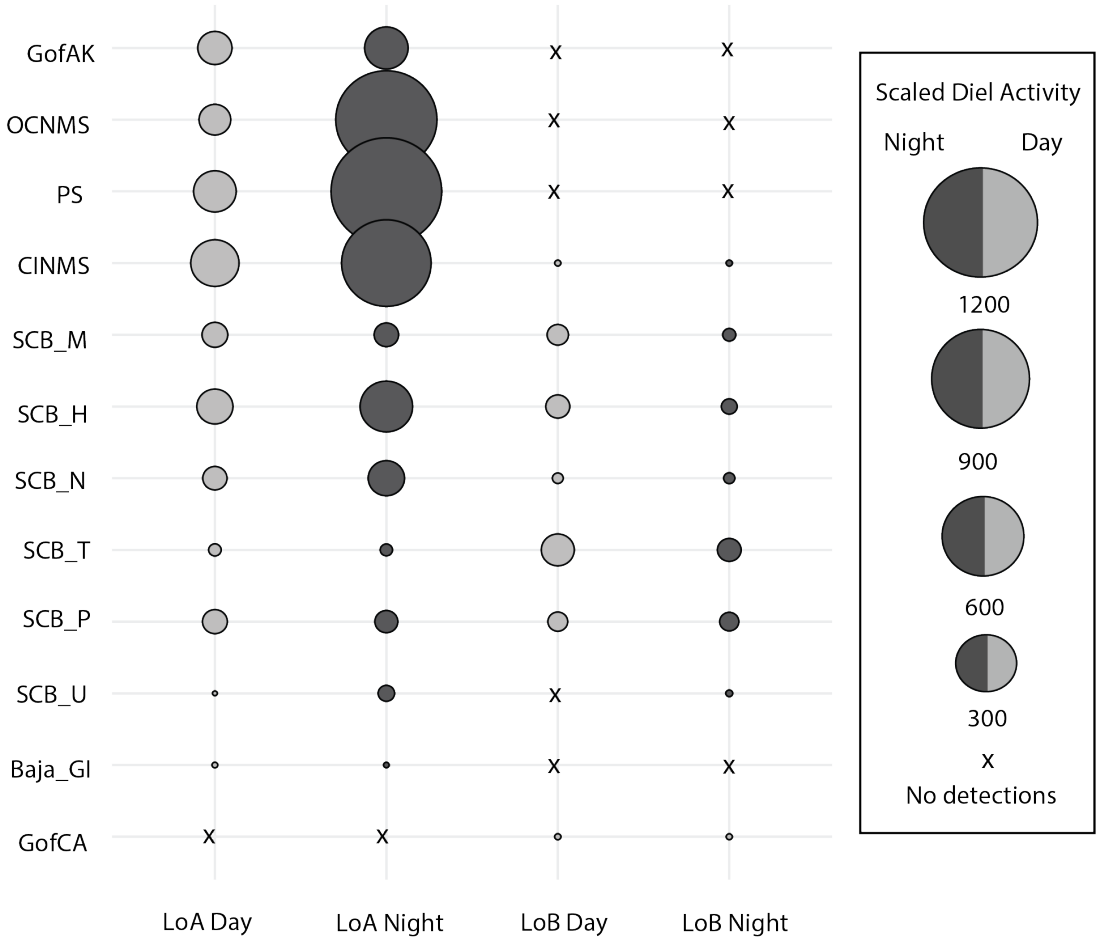


Figure 2.3. Site-specific scaled diel activity. Each recording site is represented on the y-axis, and diel activity of each click type represented on the x-axis. Dark gray circles represent nighttime and light gray circles represent daytime, with circle size representing scaled presence throughout the diel recording periods. Scaled diel presence is the total number of click positive minutes per hour divided by the total number of recording hours.

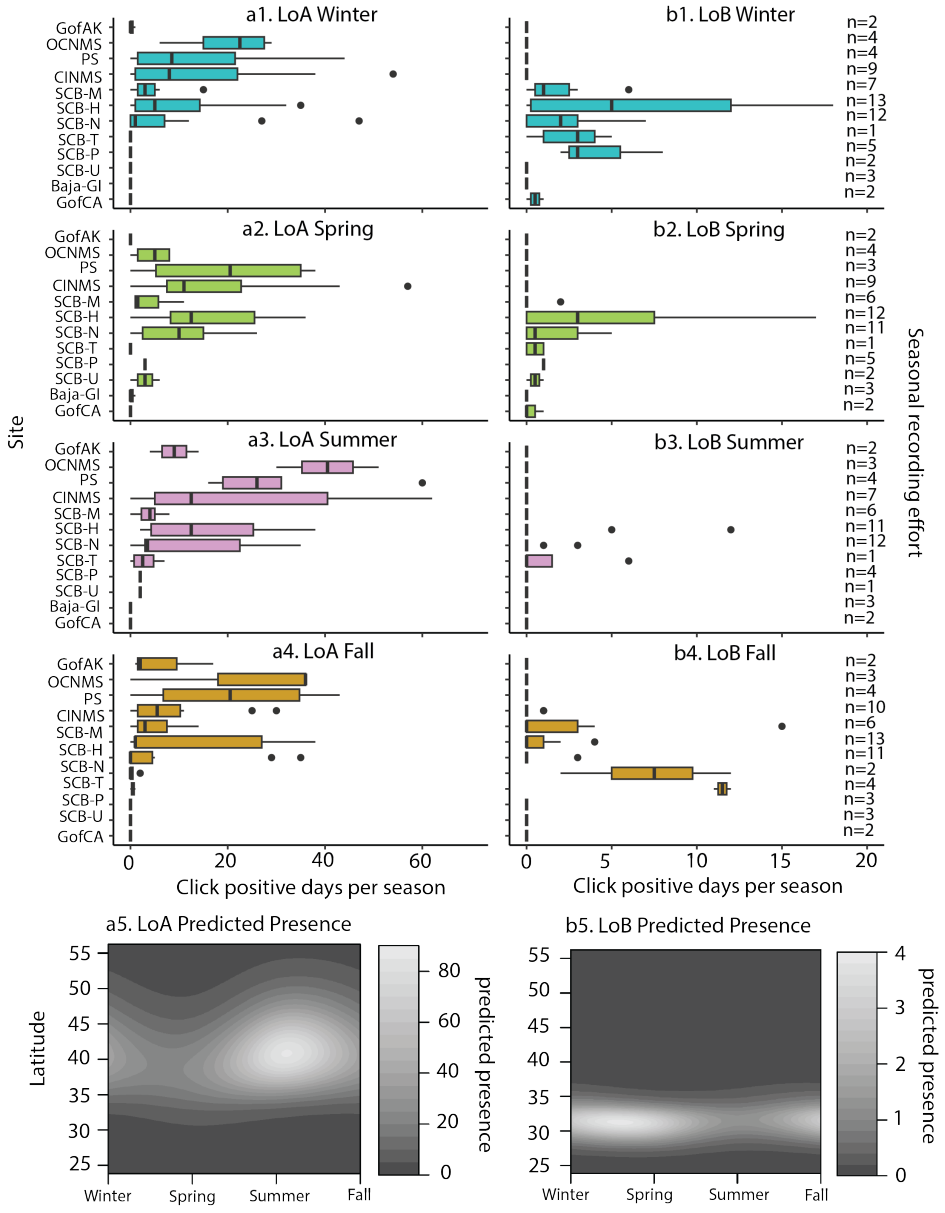


Figure 2.4. Site-specific seasonal presence of LoA and LoB click types. (**a1–a4**) Site-specific boxplots of LoA click positive days for winter, spring, summer, and fall. (**a5**) Contour surface map displaying predicted LoA presence as a function of season and latitude, based on a Poisson GAM. Seasonal changes are represented cyclically, latitude ranges from site GofCA to GofAK, and the grey scale represents predicted number of click positive days. (**b1–b4**) Site-specific boxplots of LoB click positive days for winter, spring, summer, and fall. (**b5**) Contour surface map displaying predicted LoB presence as a function of season and latitude, based on a Tweedie GAM. Seasonal changes are represented cyclically, latitude ranges from site GofCA to GofAK, and the grey scale represents predicted number of click positive days.

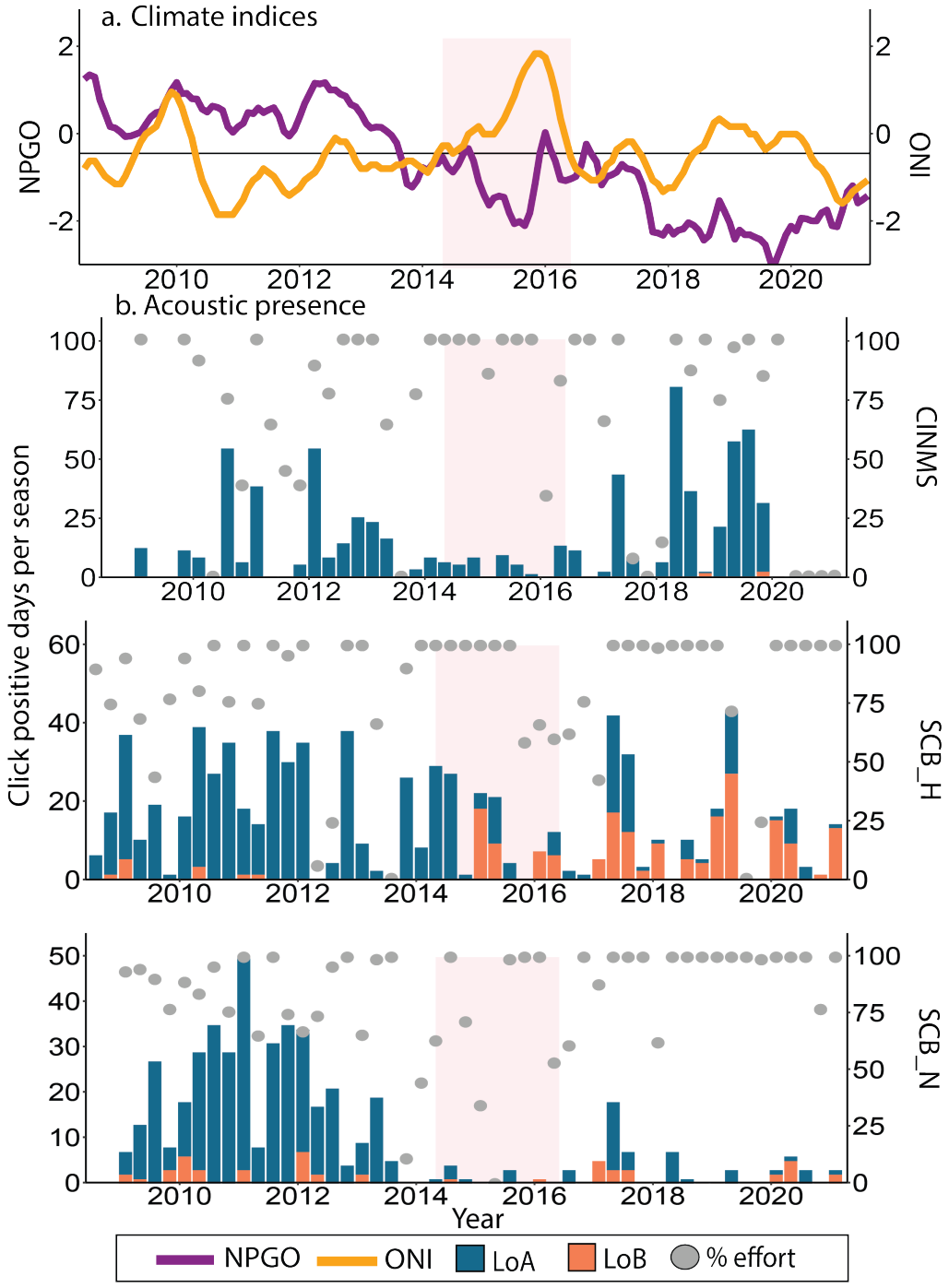


Figure 2.5. (**a**) Climatic variations in NPGO and ONI three-month running means between 2009 and 2021. Purple line denoting NPGO and orange denoting ONI, with light pink box highlighting the time period of the 2014–2016 marine heatwave. (**b**) Pacific white-sided dolphin acoustic presence at three long-term monitoring stations in the SCB. Number of LoA and LoB click positive days per season are represented as stacked blue and coral bars, respectively. Percent of recording effort for that season represented by gray circles.

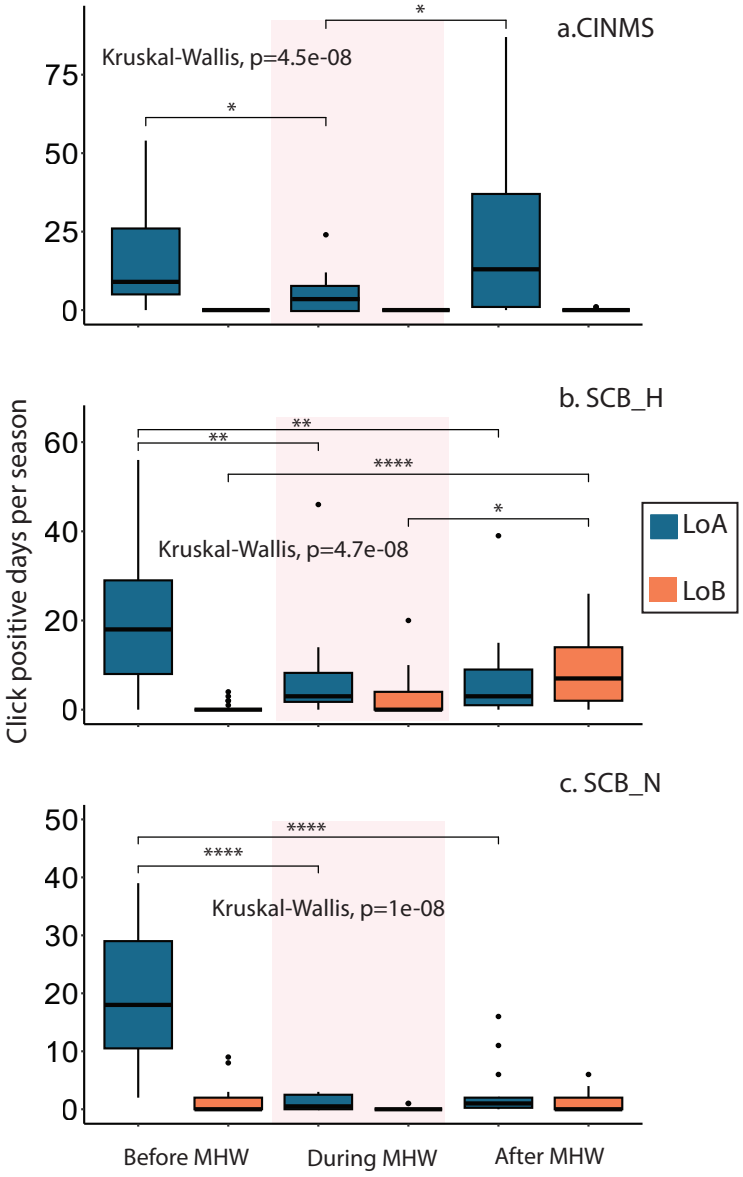


Figure 2.6. Boxplots displaying the distribution of LoA (blue) and LoB (coral) presence before, during, and after the 2014–2016 marine heatwave (MHW) event at 3 long-term monitoring stations including CINMS, SCB_H, and SCB_N. Results of Kruskal-Wallis test displayed for each site and significant Dunn's Post Hoc Test pairwise comparisons displayed as asterisks ($p<0.05$ *; $p<0.01$**, $p<0.001$***). Time period before the MHW event spans recording effort at each site between 07/01/2008–12/31/2013, during the MHW event spans recording effort at each site between 01/01/2014–12/31/2016, and after the MHW event spans recording effort at each site between 01/01/2017–09/30/2021. LoA boxplots in blue and LoB in coral, with the MHW event time period highlighted in light pink.

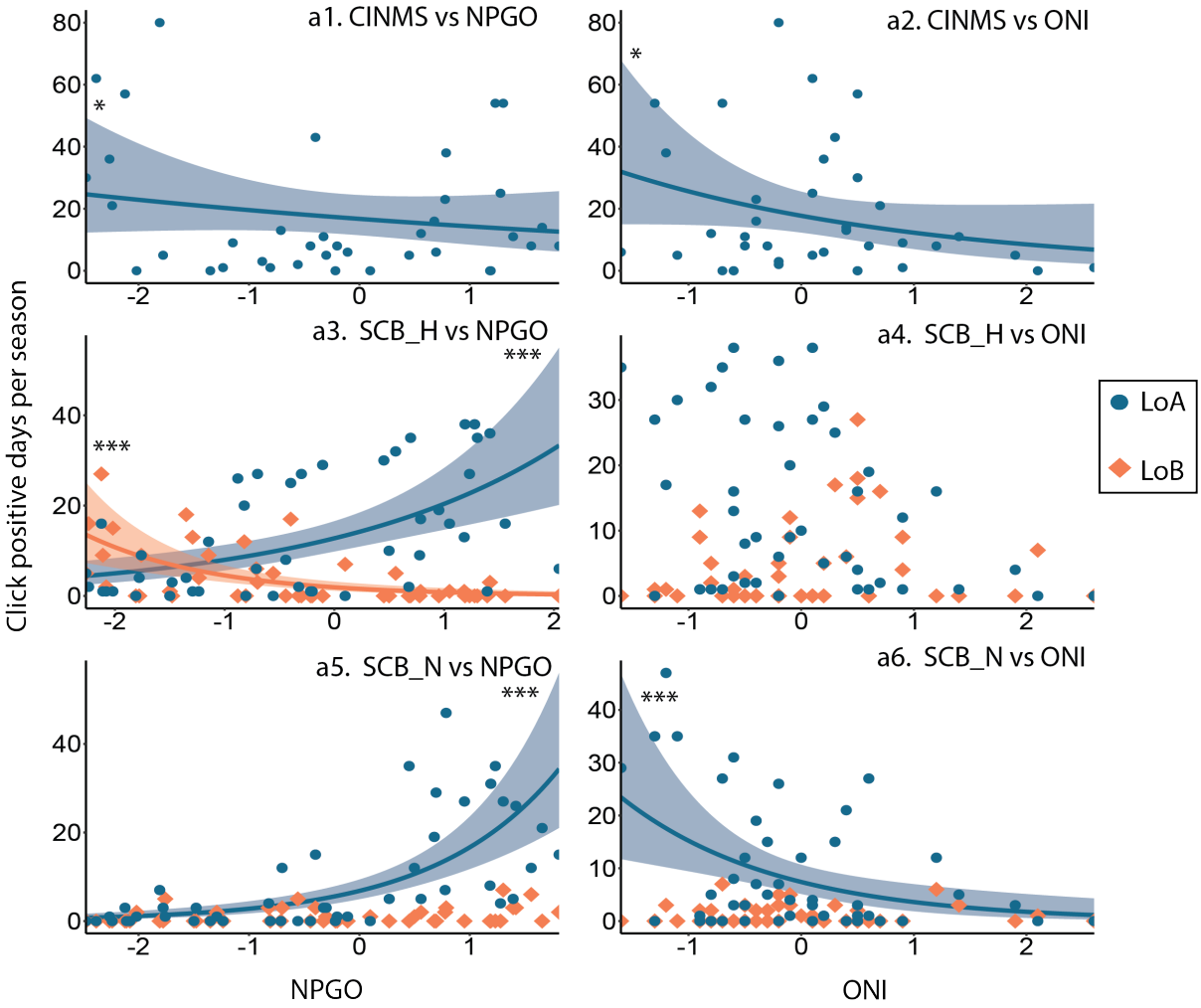


Figure 2.7. Site-specific GLMs from long-term monitoring SCB stations. The models are overlaid with Pacific white-sided dolphin acoustic presence in seasonal bins, plotted against corresponding climate index indices as blue circles and coral diamonds. Only significant linear relationships ($p<0.05$) are plotted for each click type, station, and per index, with significance codes displayed as asterisks ($p<0.05$ *; $p<0.01$**, $p<0.001$***) for each fit.

Bibliography

Au, W. W., Carder, D. A., Penner, R. H., and Scronce, B. L. (1985). Demonstration of adaptation in beluga whale echolocation signals. *The Journal of the Acoustical Society of America*, 77(2):726–730.

Au, W. W., Pawloski, J. L., Nachtigall, P. E., Blonz, M., and Gisner, R. C. (1995). Echolocation signals and transmission beam pattern of a false killer whale (Pseudorca crassidens). *The Journal of the Acoustical Society of America*, 98(1):51–59.

Baumann-Pickering, S., McDonald, M. A., Simonis, A. E., Solsona Berga, A., Merkens, K. P., Oleson, E. M., Roch, M. A., Wiggins, S. M., Rankin, S., and Yack, T. M. (2013). Species-specific beaked whale echolocation signals. *The Journal of the Acoustical Society of America*, 134(3):2293–2301.

Bearzi, M. (2005). Habitat partitioning by three species of dolphins in Santa Monica Bay, California. *Bulletin, Southern California Academy of Sciences*, 104(3):113–124.

Becker, E. A., Forney, K. A., Miller, D. L., Barlow, J., Rojas-Bracho, L., Urban R, J., and Moore, J. E. (2022). Dynamic habitat models reflect interannual movement of cetaceans within the California current ecosystem. *Frontiers in Marine Science*, 9:829523.

Becker, E. A., Forney, K. A., Redfern, J. V., Barlow, J., Jacox, M. G., Roberts, J. J., and Palacios, D. M. (2019). Predicting cetacean abundance and distribution in a changing climate. *Diversity and Distributions*, 25(4):626–643.

Ben-David, S., Blitzer, J., Crammer, K., Kulesza, A., Pereira, F., and Vaughan, J. W. (2010). A theory of learning from different domains. *Machine learning*, 79:151–175.

Biemann, C. (2006). Chinese whispers-an efficient graph clustering algorithm and its application to natural language processing problems. In *Proceedings of TextGraphs: the first workshop on graph based methods for natural language processing*, pages 73–80.

Brown, D. H. and Norris, K. S. (1956). Observations of captive and wild cetaceans. *Journal of Mammalogy*, 37(3):311–326.

Campbell, G. S., Thomas, L., Whitaker, K., Douglas, A. B., Calambokidis, J., and Hildebrand, J. A. (2015). Inter-annual and seasonal trends in cetacean distribution, density and abundance off southern California. *Deep Sea Research Part II: Topical Studies in Oceanography*, 112:143–157.

Carretta, J. V., Oleson, E. M., Forney, K. A., Muto, M. M., Weller, D. W., Lang, A. R., Baker, J., Hanson, B., Orr, A. J., and Barlow, J. (2022). US Pacific marine mammal stock assessments: 2021. *Revista Latinoamericana de Psicopatologia Fundamental*, 25(2):A–389.

Caruso, F., Alonge, G., Bellia, G., De Domenico, E., Grammauta, R., Larosa, G., Mazzola, S., Riccobene, G., Pavan, G., and Papale, E. (2017). Long-term monitoring of dolphin biosonar activity in deep pelagic waters of the Mediterranean Sea. *Scientific Reports*, 7(1):4321.

Cavole, L. M., Demko, A. M., Diner, R. E., Giddings, A., Koester, I., Pagniello, C. M. L. S., Paulsen, M.-L., Ramirez-Valdez, A., Schwenck, S. M., Yen, N. K., Zill, M. E., and Franks, P. J. S. (2016). Biological impacts of the 2013-2015 warm-water anomaly in the Northeast Pacific winners, losers, and the future. *Oceanography*, 29(2):273–285.

Collins, C., Garfield, N., Rago, T., Rischmiller, F., and Carter, E. (2000). Mean structure of the inshore countercurrent and California undercurrent off Point Sur, California. *Deep Sea Research Part II: Topical Studies in Oceanography*, 47(5-6):765–782.

Cranford, T. W., Amundin, M., and Norris, K. S. (1996). Functional morphology and homology in the odontocete nasal complex: implications for sound generation. *Journal of morphology*, 228(3):223–285.

Di Lorenzo, E., Schneider, N., Cobb, K. M., Franks, P., Chhak, K., Miller, A. J., McWilliams, J. C., Bograd, S. J., Arango, H., and Curchitser, E. (2008). North Pacific Gyre Oscillation links ocean climate and ecosystem change. *Geophysical research letters*, 35(8).

Forney, K. A. and Barlow, J. (1998). Seasonal patterns in the abundance and distribution of CALIFORNIA cetaceans, 1991-1992. *Marine Mammal Science*, 14(3):460–489.

Frasier, K. E. (2021). A machine learning pipeline for classification of cetacean echolocation clicks in large underwater acoustic datasets. *PLoS Computational Biology*, 17(12):e1009613.

Frasier, K. E., Roch, M. A., Soldevilla, M. S., Wiggins, S. M., Garrison, L. P., and Hildebrand, J. A. (2017). Automated classification of dolphin echolocation click types from the Gulf of Mexico. *PLoS computational biology*, 13(12):e1005823.

Hayano, A., Yoshioka, M., Tanaka, M., and Amano, M. (2004). Population differentiation in the Pacific white-sided dolphin *Lagenorhynchus obliquidens* inferred from mitochondrial DNA and microsatellite analyses. *Zoological Science*, 21(9):989–999.

Henderson, E. E., Hildebrand, J. A., and Smith, M. H. (2011). Classification of behavior using vocalizations of Pacific white-sided dolphins *Lagenorhynchus obliquidens*. *The Journal of the Acoustical Society of America*, 130(1):557–567.

Hildebrand, J. A., Frasier, K. E., Baumann-Pickering, S., Wiggins, S. M., Merkens, K. P., Garrison, L. P., Soldevilla, M. S., and McDonald, M. A. (2019). Assessing seasonality and density from passive acoustic monitoring of signals presumed to be from pygmy and dwarf sperm whales in the Gulf of Mexico. *Frontiers in Marine Science*, 6:66.

Houser, D., Helweg, D., and Moore, P. (1999). Classification of dolphin echolocation clicks by energy and frequency distributions. *The Journal of the Acoustical Society of America*, 106(3):1579–1585.

Jacox, M. G., Hazen, E. L., Zaba, K. D., Rudnick, D. L., Edwards, C. A., Moore, A. M., and Bograd, S. J. (2016). Impacts of the 2015-2016 El Nino on the California Current System: Early assessment and comparison to past events. *Geophysical Research Letters*, 43(13):7072–7080.

Kanes, K. J., Dosso, S. E., Insua, T. L., Mouy, X., and Bateman, A. (2023). Seasonal and diel patterns in Pacific white-sided dolphin *Lagenorhynchus obliquidens* pulsed calls near Barkley Canyon. *Marine Mammal Science*.

Ladegaard, M., Mulsow, J., Houser, D. S., Jensen, F. H., Johnson, M., Madsen, P. T., and Finneran, J. J. (2019). Dolphin echolocation behaviour during active long-range target approaches. *Journal of Experimental Biology*, 222(2).

Lavenberg, R. J. and Ebeling, A. W. (1967). Distribution of midwater fishes among deep-water basins of the southern California shelf. In Philbrick, R. N., editor, *Proceedings of the Symposium on the Biology of the California Islands*, pages 185–201. Santa Barbara Botanic Garden, Santa Barbara, California.

Leatherwood, S. and Walker, W. A. (1982). Population biology and ecology of the Pacific white-sided dolphin Lagenorhynchus obliquidens in the Northeastern Pacific: Part I: Distribution, seasonal movements and abundance with a bibliography and summary of specimen material. Noaa administrative report, NOAA, NMFS, Southwest Fisheries Center.

Leising, A. W., Schroeder, I. D., Bograd, S. J., Abell, J., Durazo, R., Gaxiola-Castro, G., Bjorkstedt, E. P., Field, J., Sakuma, K., Robertson, R. R., Goericke, R., Peterson, W. T., Brodeur, R., Barcelo, C., Auth, T. D., Daly, E. A., Suryan, R. M., Gladics, A. J., Porquez, J. M., McClatchie, S., Weber, E. D., Watson, W., Santora, J. A., Sydeman, W. J., Melin, S. R., Chavez, F. P., Golightly, R. T., Schneider, S. R., Fisher, J., Morgan, C., Bradley, R., and Warybok, P. (2015). *State of the California Current 2014-15: Impacts of the Warm-Water "Blob"*. Scripps Institution of Oceanography.

Lux, C., Costa, A., and Dizon, A. (1997). Mitochondrial DNA population structure of the Pacific white-sided dolphin.

Lynn, R. J. and Simpson, J. J. (1987). The California Current System: The seasonal variability of its physical characteristics. *Journal of Geophysical Research: Oceans*, 92(C12):12947–12966.

MacLeod, C. (2009). Global climate change, range changes and potential implications for the conservation of marine cetaceans: A review and synthesis. *Endangered Species Research*, 7:125–136.

Madsen, P., Johnson, M., De Soto, N. A., Zimmer, W., and Tyack, P. (2005). Biosonar performance of foraging beaked whales (Mesoplodon densirostris). *Journal of Experimental Biology*, 208(2):181–194.

Martien, K. K., Lang, A. R., Taylor, B. L., Rosel, P. E., Simmons, S. E., Oleson, E. M., Boveng, P. L., and Hanson, M. B. (2019). The DIP delineation handbook: a guide to using multiple lines of evidence to delineate demographically independent populations of marine mammals. Noaa technical memorandum, NOAA Technical Memorandum NMFS-SWFSC-622.

McClatchie, S., Field, J., Thompson, A. R., Gerrodette, T., Lowry, M., Fiedler, P. C., Watson, W., Nieto, K. M., and Vetter, R. D. (2016). Food limitation of sea lion pups and the decline of forage off central and southern California. *Royal Society Open Science*, 3(3):150628.

Nowacek, D. P. (2005). Acoustic ecology of foraging bottlenose dolphins (Tursiops truncatus), habitat-specific use of three sound types. *Marine mammal science*, 21(4):587–602.

Piatt, J. F., Parrish, J. K., Renner, H. M., Schoen, S. K., Jones, T. T., Arimitsu, M. L., Kuletz, K. J., Bodenstein, B., Garcia-Reyes, M., Duerr, R. S., Corcoran, R. M., Kaler, R. S. A., McChesney, G. J., Golightly, R. T., Coletti, H. A., Suryan, R. M., Burgess, H. K., Lindsey, J., Lindquist, K., Warzybok, P. M., Jahncke, J., Roletto, J., and Sydeman, W. J. (2020). Extreme mortality and reproductive failure of common murres resulting from the northeast Pacific marine heatwave of 2014-2016. *PLOS ONE*, 15(1):e0226087.

Rice, A., Debich, A. J., Širović, A., Oleson, E. M., Trickey, J. S., Varga, L. M., Wiggins, S. M., Hildebrand, J. A., and Baumann-Pickering, S. (2021). Cetacean occurrence offshore of Washington from long-term passive acoustic monitoring. *Marine Biology*, 168:1–22.

Roch, M. A., Batchelor, H., Baumann-Pickering, S., Berchok, C. L., Cholewiak, D., Fujioka, E., Garland, E. C., Herbert, S., Hildebrand, J. A., and Oleson, E. M. (2016). Management of acoustic metadata for bioacoustics. *Ecological informatics*, 31:122–136.

Roch, M. A., Klinck, H., Baumann-Pickering, S., Mellinger, D. K., Qui, S., Soldevilla, M. S.,

and Hildebrand, J. A. (2011). Classification of echolocation clicks from odontocetes in the Southern California Bight. *The Journal of the Acoustical Society of America*, 129(1):467–475.

Salvadeo, C. J., Lluch-Belda, D., Gomez-Gallardo, A., Urban-Ramirez, J., and MacLeod, C. D. (2010). Climate change and a poleward shift in the distribution of the Pacific white-sided dolphin in the northeastern Pacific. *Endangered Species Research*, 11(1):13–19.

Simon, M., Wahlberg, M., and Miller, L. A. (2007). Echolocation clicks from killer whales (Orcinus orca) feeding on herring (Clupea harengus). *The Journal of the Acoustical Society of America*, 121(2):749–752.

Soldevilla, M. S., Henderson, E. E., Campbell, G. S., Wiggins, S. M., Hildebrand, J. A., and Roch, M. A. (2008). Classification of Risso's and Pacific white-sided dolphins using spectral properties of echolocation clicks. *The Journal of the Acoustical Society of America*, 124(1):609–624.

Soldevilla, M. S., Wiggins, S. M., and Hildebrand, J. A. (2010). Spatio-temporal comparison of Pacific white-sided dolphin echolocation click types. *Aquatic Biology*, 9(1):49–62.

Solsona-Berga, A., Frasier, K. E., Baumann-Pickering, S., Wiggins, S. M., and Hildebrand, J. A. (2020). DetEdit: A graphical user interface for annotating and editing events detected in long-term acoustic monitoring data. *PLOS Computational Biology*, 16(1):e1007598.

Suarez-Bregua, P., Alvarez-Gonzalez, M., Parsons, K. M., Rotllant, J., Pierce, G. J., and Saavedra, C. (2022). Environmental DNA (eDNA) for monitoring marine mammals: Challenges and opportunities. *Frontiers in Marine Science*, page 1886.

team, R. (2016). Integrated development environment for R. RStudio. *Inc.: Boston, USA*.

Van Parijs, S. M. and Corkeron, P. J. (2001). Vocalizations and behaviour of Pacific humpback dolphins Sousa chinensis. *Ethology*, 107(8):701–716.

Walker, W. A., Leatherwood, S., Goodrich, K., Perrin, W., and Stroud, R. (1986). Geographical variation and biology of the Pacific white-sided dolphin, Lagenorhynchus obliquidens, in the north-eastern Pacific. *Research on dolphins*, 441:465.

Wells, B., Schroeder, I., Bograd, S., Hazen, E., Jacox, M., Leising, A., Mantua, N., Santora, J., Fisher, J., Peterson, W. T., Bjorkstedt, E., Robertson, R., Chavez, F., Goericke, R., Kudela, R., Anderson, C., Lavaniegos, B., Gomez-Valdes, J., Brodeur, R., and Thayre, B. (2017). State of the California Current 2016-17: still anything but "normal" in the north. *California Cooperative Oceanic Fisheries Investigations Report*, 58.

Wiggins, S. M. and Hildebrand, J. A. (2007). High-frequency acoustic recording package

(HARP) for broad-band, long-term marine mammal monitoring. In *2007 symposium on underwater technology and workshop on scientific use of submarine cables and related technologies*, pages 551–557. IEEE.

Wood, S. N. (2011). Fast stable restricted maximum likelihood and marginal likelihood estimation of semiparametric generalized linear models. *Journal of the Royal Statistical Society Series B: Statistical Methodology*, 73(1):3–36.

Wood, S. N., Pya, N., and Safken, B. (2016). Smoothing parameter and model selection for general smooth models. *Journal of the American Statistical Association*, 111(516):1548–1563.

Zimmer, W. M., Johnson, M. P., Madsen, P. T., and Tyack, P. L. (2005). Echolocation clicks of free-ranging Cuvier's beaked whales (Ziphius cavirostris). *The Journal of the Acoustical Society of America*, 117(6):3919–3927.

2.8 Supplementary Material

2.8.1 Deployment Metadata

Table 2.8. Deployment metadata including deployment name, latitude and longitude, recorder depth, start of recording and end of recording for each deployment included in this study.

Deployment	Latitude (N)	Longitude (W)	Depth (m)	Start effort	End effort
GofAK_PT_01	56.243	-142.757	989	9/9/2012 0:00	6/10/2013 15:05
GofAK_PT_02	56.243	-142.757	987	6/11/2013 2:00	8/20/2013 2:30
GofAK_PT_03	56.242	-142.756	988	9/3/2013 5:00	3/21/2014 3:53
GofAK_PT_04	56.243	-142.757	998	4/30/2014 0:00	9/10/2014 20:00
OCNMS_QC_12	47.500	-125.353	650	1/27/2011 6:00	10/7/2011 7:23
OCNMS_QC_14	47.500	-125.353	1394	12/7/2011 6:00	7/15/2012 7:00
OCNMS_QC_15	47.500	-125.353	1394	9/14/2012 0:00	6/30/2013 9:22
OCNMS_QC_16	47.500	-125.354	1384	7/17/2013 0:00	5/2/2014 9:32
PS02	36.299	-122.393	1390	1/25/2007 0:00	6/4/2007 21:20
PS03	36.298	-122.393	1386	7/19/2007 0:00	10/29/2007 13:45
PS05	36.390	-122.305	833	8/4/2008 0:00	1/6/2009 4:04
PS06	36.298	-122.393	1386	2/1/2009 0:00	5/7/2009 8:50
PS11	36.298	-122.393	850	6/21/2011 0:00	4/7/2012
PS13	36.299	-122.393	845	7/3/2012 0:00	8/26/2012

(continued on next page)

(Table 2.8 continued)

Deployment	Latitude (N)	Longitude (W)	Depth (m)	Start effort	End effort
PS14	36.299	-122.393	858	11/14/2018 0:00	6/10/2019
PS15	36.299	-122.393	858	6/11/2019 0:00	1/25/2020 21:00
CINMS_C_10	34.318	-120.807	780	11/4/2009 0:00	2/20/2010 12:32
CINMS_C_13	34.316	-120.806	915	6/24/2010 23:00	9/21/2010 3:45
CINMS_C_15	34.333	-120.806	850	11/16/2010 0:00	3/2/2011 3:30
CINMS_C_16	34.333	-120.806	850	4/5/2011 21:00	7/11/2011 23:12
CINMS_C_17	34.316	-120.805	825	10/27/2011 0:00	3/3/2012 12:28
CINMS_C_18	34.316	-120.805	758	3/25/2012 0:00	8/2/2012 17:20
CINMS_C_19	34.325	-120.806	800	8/2/2012 18:00	12/7/2012 20:19
CINMS_C_20	34.323	-120.806	800	12/18/2012 0:00	4/28/2013 15:16
CINMS_C_22	34.317	-120.805	823	9/22/2013 0:00	1/14/2014 19:35
CINMS_C_23	34.316	-120.805	828	1/14/2014 21:00	4/9/2014 17:41
CINMS_C_24	34.316	-120.804	754	4/9/2014 20:00	7/29/2014 7:22
CINMS_C_25	34.324	-120.806	800	7/29/2014 12:00	11/4/2014 9:38
CINMS_C_26	34.324	-120.806	800	11/4/2014 14:00	2/5/2015 14:53
CINMS_C_27	34.326	-120.806	770	2/6/2015 0:00	6/10/2015 22:17
CINMS_C_28	34.326	-120.806	755	6/11/2015 0:00	10/4/2015 21:06
CINMS_C_29	34.321	-120.804	754	10/5/2015 0:00	12/18/2015 2:35
CINMS_C_30	34.323	-120.806	755	3/17/2016 0:00	7/27/2016 20:21
CINMS_C_31	34.324	-120.806	756	7/28/2016 0:00	11/9/2016 21:19
CINMS_C_32	34.324	-120.807	760	11/10/2016 0:00	2/22/2017 8:36
CINMS_C_33	34.324	-120.805	755	2/22/2017 18:00	6/8/2017 2:26
CINMS_C_36	34.323	-120.805	758	2/17/2018 0:00	6/29/2018 18:54
CINMS_C_37	34.32275	-120.809	766	7/12/2018 0:00	12/1/2018 13:22
CINMS_C_38	34.322	-120.809	765	1/24/2019 0:00	4/12/2019 19:31
CINMS_C_39	34.323	-120.808	765	4/16/2019 0:00	9/5/2019 20:51
CINMS_C_40	34.320	-120.805	726	9/20/2019 20:00	1/3/2020 17:41
SCB_M_31	33.509	-119.254	895	1/13/2009 0:00	3/8/2009 12:18
SCB_M_32	33.509	-119.254	1123	3/11/2009 0:00	5/4/2009 6:17
SCB_M_33	33.509	-119.254	1120	5/17/2009 0:00	7/8/2009 14:55
SCB_M_34	33.515	-119.246	902	7/27/2009 0:00	9/16/2009 13:35
SCB_M_35	33.515	-119.246	912	9/25/2009 0:00	11/17/2009 17:08
SCB_M_36	33.515	-119.246	912	12/5/2009 0:00	1/24/2010 20:54
SCB_M_37	33.515	-119.238	891	1/30/2010 0:00	3/25/2010 6:18
SCB_M_38	33.514	-119.248	917	4/10/2010 0:00	7/12/2010 17:45
SCB_M_40	33.514	-119.247	909	7/22/2010 0:00	11/7/2010 8:49
SCB_M_41	33.514	-119.248	919	12/5/2010 0:00	4/24/2011 8:52

(continued on next page)

(Table 2.8 continued)

Deployment	Latitude (N)	Longitude (W)	Depth (m)	Start effort	End effort
SCB_M_44	33.514	-119.247	928	5/11/2011 0:00	10/2/2011 10:06
SCB_M_45	33.514	-119.248	927	10/27/2011 0:00	3/18/2012 0:00
SCB_M_46	33.513	-119.248	926	3/24/2012 0:00	7/22/2012 15:40
SCB_M_47	33.509	-119.240	660	8/10/2012 0:00	12/19/2012 23:30
SCB_M_48	33.509	-119.255	907	12/20/2012 2:00	4/25/2013 18:41
SCB_M_49	33.510	-119.255	882	4/30/2013 0:00	9/5/2013 6:17
SCB_M_50	33.509	-119.254	940	9/10/2013 0:00	1/6/2014 20:43
SCB_M_51	33.509	-119.254	877	1/6/2014 22:00	4/4/2014 19:08
SCB_M_52	33.509	-119.255	890	4/4/2014 20:00	7/6/2014 8:34
SCB_M_53	33.514	-119.248	900	7/30/2014 2:00	11/3/2014 17:35
SCB_M_54	33.513	-119.249	900	11/4/2014 0:00	2/5/2015 1:53
SCB_H_26	32.847	-119.176	1012	6/5/2008 0:00	7/25/2008 20:58
SCB_H_27	32.847	-119.174	1018	8/4/2008 12:00	9/27/2008 18:18
SCB_H_29	32.847	-119.177	1015	10/21/2008 0:00	12/14/2008 6:15
SCB_H_30	32.845	-119.173	1010	12/21/2008 11:00	1/12/2009 19:10
SCB_H_31	32.843	-119.169	1004	1/13/2009 0:00	3/8/2009 6:18
SCB_H_32	32.843	-119.169	935	3/14/2009 0:00	5/7/2009 6:18
SCB_H_34	32.842	-119.171	992	7/23/2009 12:00	9/15/2009 18:17
SCB_H_35	32.842	-119.171	995	9/25/2009 15:00	11/18/2009 21:17
SCB_H_36	32.842	-119.171	997	12/6/2009 0:00	1/29/2010 6:17
SCB_H_37	32.842	-119.171	992	1/30/2010 18:00	3/22/2010 23:16
SCB_H_38	32.842	-119.170	989	4/10/2010 15:00	7/22/2010 23:31
SCB_H_40	32.842	-119.170	1004	7/23/2010 0:00	11/8/2010 9:26
SCB_H_41	32.842	-119.170	1002	12/6/2010 20:00	4/17/2011 20:57
SCB_H_44	32.842	-119.171	989	5/11/2011 17:00	10/12/2011 15:57
SCB_H_45	32.842	-119.170	1008	10/16/2011 0:00	3/5/2012 11:48
SCB_H_47	32.846	-119.176	1006	8/10/2012 2:00	12/20/2012 23:51
SCB_H_48	32.842	-119.170	1000	12/21/2012 2:00	4/30/2013 22:29
SCB_H_50	32.838	-119.166	995	9/10/2013 12:00	1/7/2014 0:18
SCB_H_51	32.838	-119.166	960	1/7/2014 2:00	4/3/2014 20:01
SCB_H_52	32.846	-119.176	986	4/4/2014 0:00	7/30/2014 6:25
SCB_H_53	32.844	-119.176	1005	7/30/2014 12:00	11/5/2014 0:47
SCB_H_54	32.846	-119.175	1000	11/5/2014 6:00	2/4/2015 20:33
SCB_H_55	32.846	-119.176	1000	2/5/2015 0:00	6/1/2015 16:16
SCB_H_56	32.846	-119.176	1000	6/2/2015 0:00	10/13/2015 0:27
SCB_H_58	32.845	-119.177	1000	11/21/2015 18:00	4/25/2016 8:51
SCB_H_59	32.845	-119.176	1000	7/6/2016 18:00	11/9/2016 5:16

(continued on next page)

(Table 2.8 continued)

Deployment	Latitude (N)	Longitude (W)	Depth (m)	Start effort	End effort
SCB_H_61	32.845	-119.175	1000	2/22/2017 0:00	6/6/2017 22:33
SCB_H_62	32.845	-119.175	1000	6/7/2017 0:00	10/4/2017 23:45
SCB_H_63	32.845	-119.174	1000	10/5/2017 4:00	2/2/2018 22:55
SCB_H_64	32.845	-119.174	1078	2/4/2018 0:00	7/9/2018 12:31
SCB_H_65	32.842	-119.170	1000	7/9/2018 18:00	11/29/2018 0:33
SCB_H_66	32.841	-119.167	1013	11/29/2018 1:00	5/5/2019 18:01
SCB_H_68	32.854	-119.148	1131	11/9/2019 20:00	5/8/2020 21:12
SCB_H_69	32.841	-119.167	1134	5/9/2020 0:00	10/29/2020 20:56
SCB_H_70	32.841	-119.167	1130	10/30/2020 0:00	4/24/2021 23:26
SCB_N_31	32.370	-118.565	1369	1/14/2009 0:00	3/9/2009 6:18
SCB_N_32	32.370	-118.565	1295	3/14/2009 0:00	5/7/2009 12:18
SCB_N_33	32.369	-118.564	1295	5/9/2009 0:00	7/12/2009 21:17
SCB_N_34	32.369	-118.564	1287	7/22/2009 0:00	9/15/2009 2:18
SCB_N_35	32.369	-118.564	1295	9/26/2009 0:00	11/19/2009 9:17
SCB_N_36	32.369	-118.562	1282	12/6/2009 0:00	1/26/2010 8:53
SCB_N_37	32.369	-118.562	1280	1/31/2010 0:00	3/26/2010 6:17
SCB_N_38	32.369	-118.563	1284	4/11/2010 0:00	7/18/2010 21:41
SCB_N_40	32.369	-118.563	1288	7/23/2010 14:00	11/8/2010 23:26
SCB_N_41	32.369	-118.563	1271	12/7/2010 0:00	4/9/2011 22:02
SCB_N_44	32.369	-118.563	1282	5/12/2011 16:00	9/23/2011 7:00
SCB_N_45	32.369	-118.564	1295	10/16/2011 0:00	2/13/2012 18:40
SCB_N_46	32.370	-118.565	1292	3/25/2012 0:00	8/5/2012 20:10
SCB_N_47	32.369	-118.565	1285	8/10/2012 12:00	12/6/2012 11:38
SCB_N_48	32.369	-118.565	1300	12/20/2012 20:00	5/1/2013 6:13
SCB_N_49	32.369	-118.564	1292	5/2/2013 18:00	9/11/2013 7:32
SCB_N_51	32.3699	-118.564	1230	1/7/2014 20:00	2/16/2014 15:15
SCB_N_52	32.369	-118.565	1154	4/4/2014 3:59	7/30/2014 13:23
SCB_N_53	32.369	-118.563	1235	7/30/2014 18:00	11/5/2014 8:02
SCB_N_56	32.369	-118.564	1230	6/2/2015 0:00	10/3/2015 14:36
SCB_N_57	32.370	-118.564	1260	10/3/2015 18:00	11/21/2015 10:17
SCB_N_58	32.369	-118.564	1200	11/21/2015 12:00	4/18/2016 14:16
SCB_N_59	32.370	-118.564	1200	7/7/2016 0:00	11/8/2016 23:57
SCB_N_60	32.369	-118.564	1200	11/9/2016 6:00	2/21/2017 15:00
SCB_N_61	32.370	-118.564	1300	2/21/2017 18:00	6/7/2017 1:58
SCB_N_62	32.370	-118.564	1300	6/7/2017 2:00	12/21/2017 1:02
SCB_N_63	32.370	-118.564	1296	2/4/2018 0:00	7/9/2018 2:45
SCB_N_64	32.368	-118.564	1290	7/9/2018 3:00	11/28/2018 16:06

(continued on next page)

(Table 2.8 continued)

Deployment	Latitude (N)	Longitude (W)	Depth (m)	Start effort	End effort
SCB_N_65	32.369	-118.565	1240	11/29/2018 0:00	5/5/2019 2:43
SCB_N_66	32.369	-118.565	1285	5/5/2019 4:00	11/6/2019 21:46
SCB_N_67	32.369	-118.565	1292	11/8/2019 20:00	4/29/2020 16:42
SCB_N_68	32.369	-118.565	1293	4/29/2020 17:00	10/15/2020 19:37
SCB_N_69	32.36945	-118.565	1300	11/6/2020 0:00	4/15/2021 22:30
SCB_T_01	32.898	-117.061	900	9/29/2016 0:00	12/15/2016 20:50
SCB_T_02	32.886	-117.556	825	3/5/2017 0:00	7/6/2017 22:20
SCB_T_03	32.886	-117.558	814	7/8/2017 17:00	1/18/2018 19:37
SCB_P_19	32.896	-117.374	600	2/12/2013 0:00	3/13/2013 22:46
SCB_P_23	32.891	-117.400	422	1/25/2014 0:00	3/5/2014 1:53
SCB_P_26	32.890	-117.400	500	3/6/2014 20:00	6/27/2014 21:12
SCB_P_27	32.889	-117.401	500	6/28/2014 0:00	10/1/2014 20:46
SCB_P_28	32.890	-117.400	530	11/16/2014 0:00	1/12/2015 18:15
SCB_P_31	32.890	-117.400	500	11/20/2015 21:00	3/1/2016 0:00
SCB_P_34	32.868	-117.391	470	6/2/2015 0:00	9/18/2015 0:00
SCB_P_35	32.868	-117.374	380	4/9/2016 0:00	8/10/2016 19:45
SCB_P_36	32.884	-117.393	504	8/12/2016 18:00	10/26/2016 0:00
SCB_P_39	32.882	-117.397	490	2/14/2017 0:00	5/24/2017 0:00
SCB_P_42	32.882	-117.397	510	1/23/2018 0:00	6/15/2018 21:11
SCB_P_44	32.881	-117.398	500	8/18/2018 0:00	11/8/2018 19:17
SCB_U_01	31.851	-118.484	1200	11/17/2018 0:00	6/11/2019 16:52
SCB_U_02	31.851	-118.484	1193	11/6/2019 0:00	1/16/2020 20:10
SCB_U_03	31.851	-118.484	1197	4/29/2020 0:00	11/2/2020 19:55
Baja_GI_01	29.141	-118.260	1113	11/19/2018 3:00	10/22/2019 15:58
Baja_GI_02	29.142	-118.258	1187	10/23/2019 18:00	10/3/2020 13:51
Baja_GI_03	29.141	-118.260	1074	9/29/2021 1:00	9/13/2022 22:00
GofCA_PP_01	23.830	-109.631	659	3/10/2004 14:00	11/12/2004 20:43
GofCA_PP_03	23.830	-109.630	659	5/16/2005 5:00	9/30/2005 20:21
GofCA_PP_05	23.923	-109.666	846	2/7/2006 12:00	8/5/2006 0:15
GofCA_PP_06	23.910	-109.669	805	12/10/2006 0:00	6/5/2007 0:34
GofCA_TT_07	28.607	-112.505	400	6/20/2007 0:00	12/7/2007 11:25
GofCA_TT_08	28.606	-112.507	400	1/27/2008 0:00	3/17/2008 7:03
GofCA_CB_09	29.0269	-113.375	690	8/8/2008 0:00	12/25/2008 5:00
GofCA_CB_10	29.0273	-113.375	650	4/26/2009 0:00	9/12/2009 20:06
GofCA_CB_11	29.027	-113.375	600	12/7/2009 0:00	5/18/2010 18:47
GofCA_CB_09	29.026	-113.375	690	8/8/2008 0:00	12/25/2008 5:00
GofCA_CB_10	29.027	-113.375	650	4/26/2009 20:00	9/12/2009 20:06

(continued on next page)

(Table 2.8 continued)

Deployment	Latitude (N)	Longitude (W)	Depth (m)	Start effort	End effort
GofCA_CB_11	29.0275	-113.375	600	12/7/2009 0:00	5/18/2010 18:47

2.8.2 Automatic vs. Manual Label Comparison

Table 2.9. Confusion table comparing automatically generated vs. manually generated bin-level labels for each category for a subset of detections from deployment SCB_H_29.

Label	True negative	False negative	False positive	True positive	Precision	Recall
Boat	570	0	0	32	100	100
Gg	600	0	2	0	0	NaN
LoA	536	4	16	46	74.19	92
LoB	599	0	1	2	66.66	100
UD	152	14	5	431	98.85	96.85
Zc	513	0	5	84	94.38	100

Table 2.10. Confusion table comparing automatically generated vs. manually generated bin-level labels for each category for a subset of detections from deployment SCB_P_35.

Label	True negative	False negative	False positive	True positive	Precision	Recall
Boat	8,619	2	68	944	93.28	99.78
Gg	9,396	2	219	16	6.80	88.88
LoA	9,586	2	35	10	22.22	83.33
LoB	9,471	0	161	1	0.61	100
UD	968	354	76	8,235	99.08	95.87
Zc	9,408	0	220	5	2.22	100

Table 2.11. Confusion table comparing automatically generated vs. manually generated bin-level labels for each category for a subset of detections from deployment CINMS_C_33.

Label	True negative	False negative	False positive	True positive	Precision	Recall
Boat	768	0	23	123	84.24	100
Gg	814	3	35	62	63.91	95.38
LoA	903	1	3	7	70	87.50
LoB	880	0	34	0	0	NaN
UD	259	30	3	622	99.52	95.39
Zc	878	0	35	1	2.77	100

2.8.3 Diel Trends

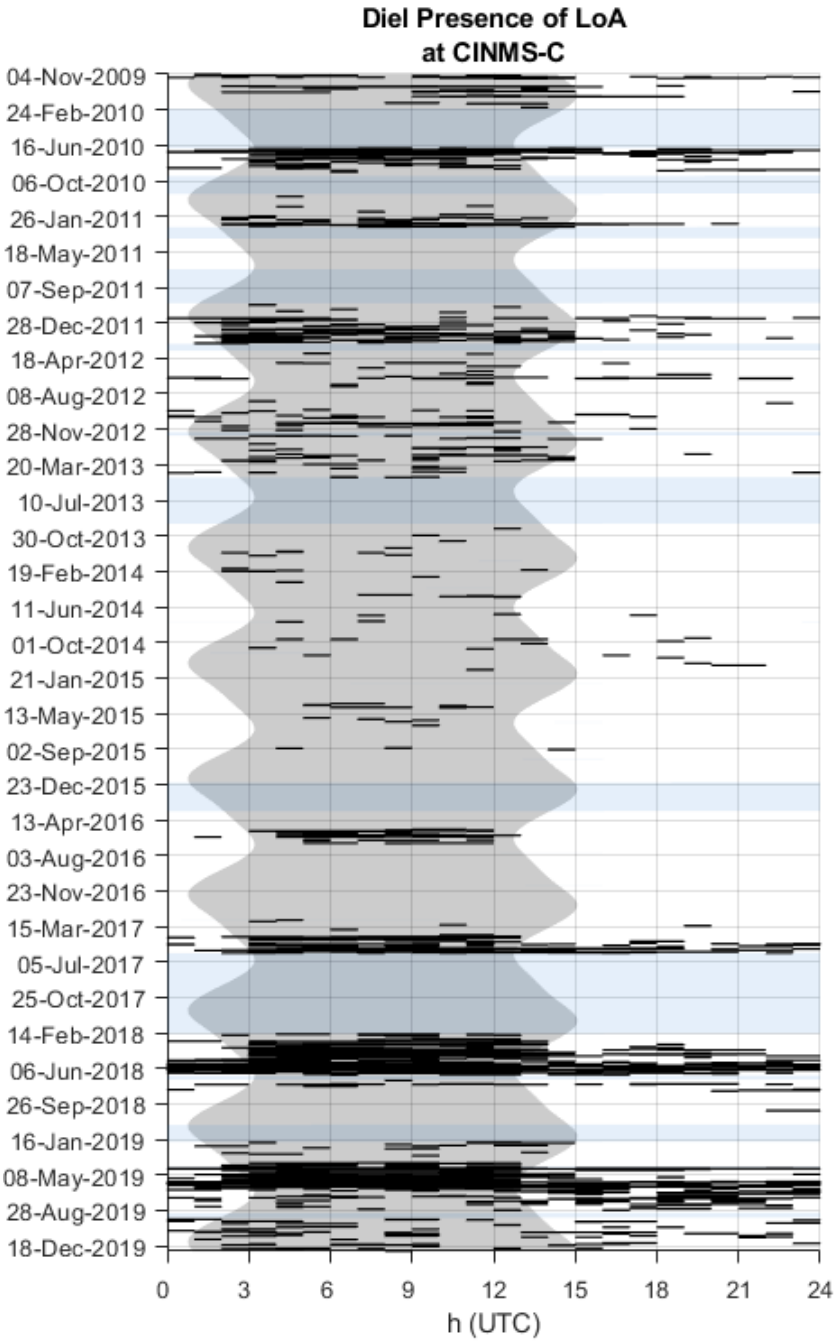


Figure 2.8. LoA hourly click-positive timeseries at CINMS. Gray sections represent nighttime hours and white sections represent daytime. Black lines denote click-positive hourly bins. Periods of no recording effort are highlighted in transparent blue.

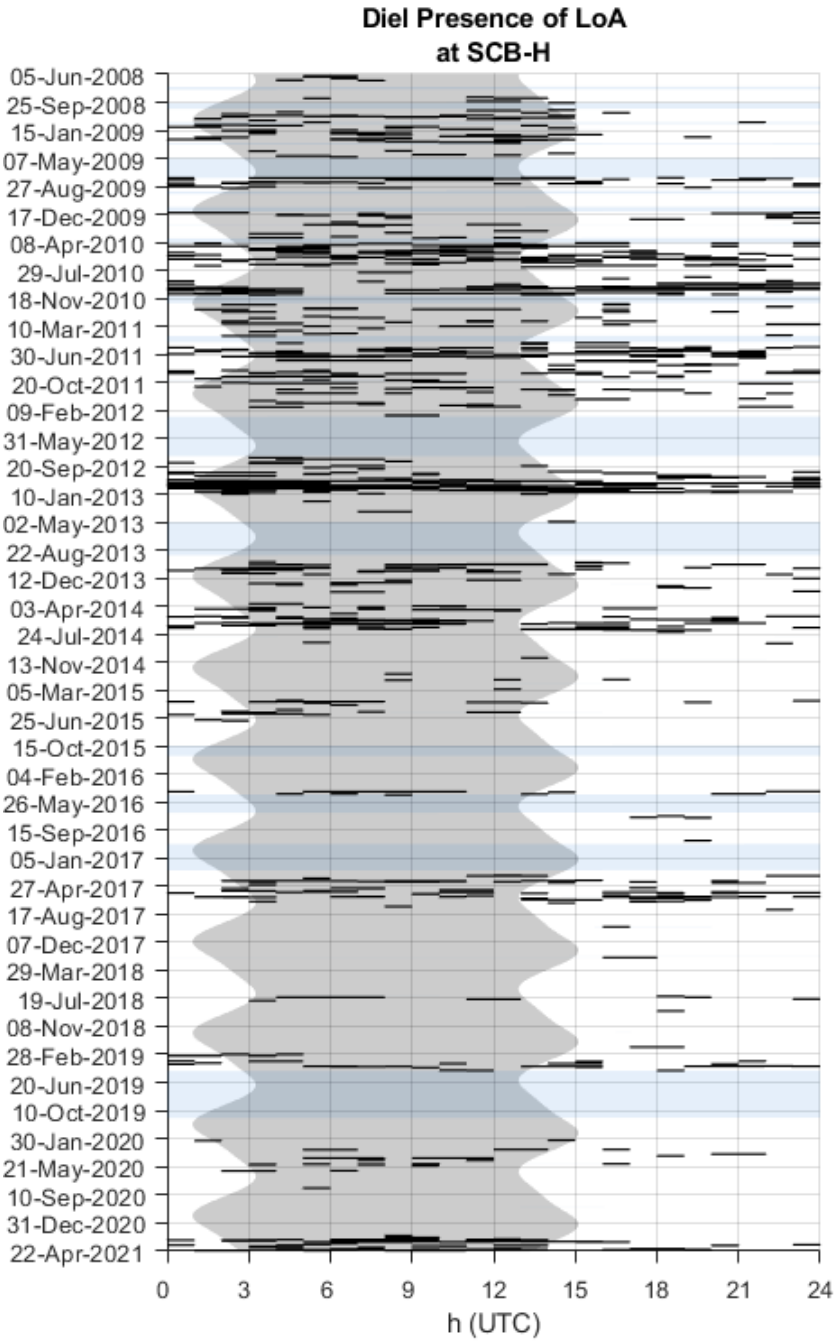


Figure 2.9. LoA hourly click-positive timeseries at SCB_H. Gray sections represent nighttime hours and white sections represent daytime. Black lines denote click-positive hourly bins. Periods of no recording effort are highlighted in transparent blue.

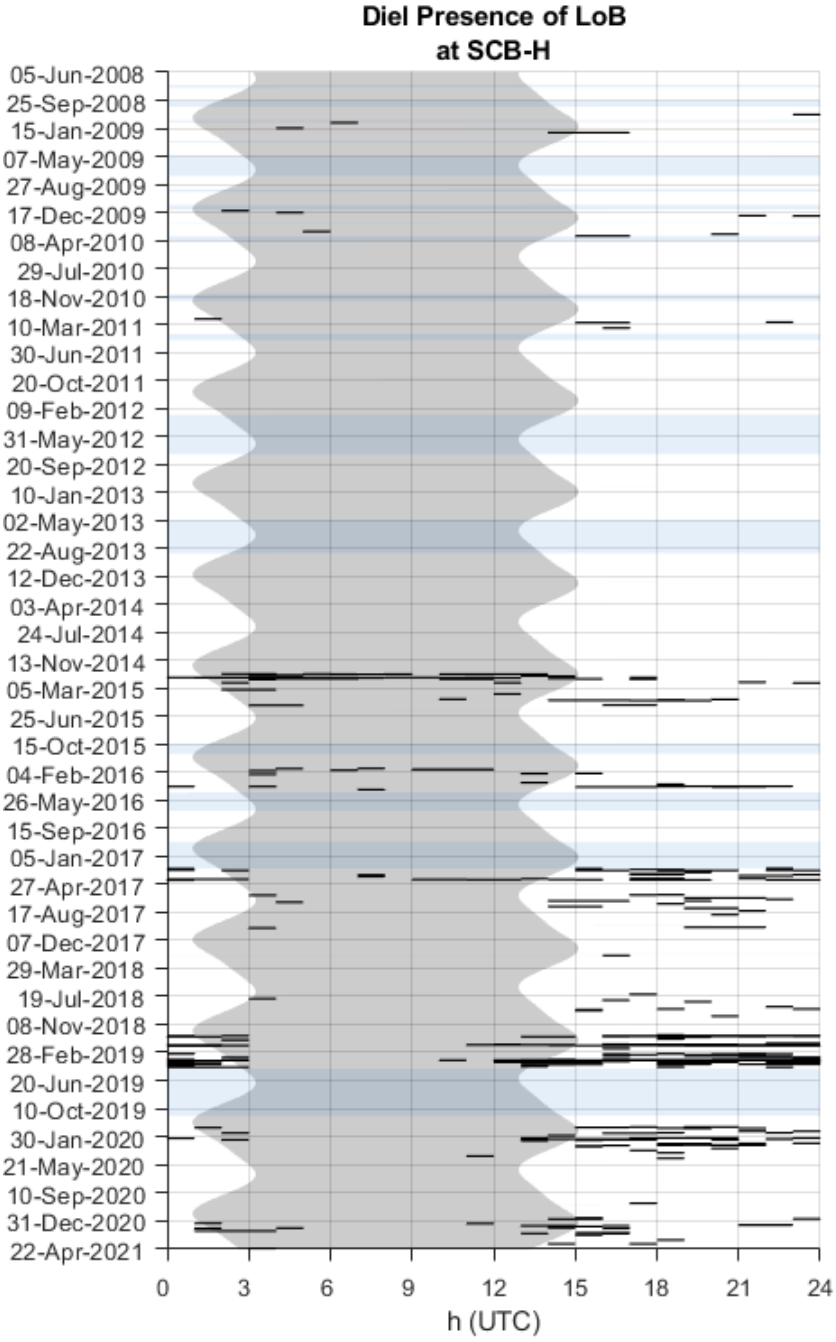


Figure 2.10. LoB hourly click-positive timeseries at SCB_H. Gray sections represent nighttime hours and white sections represent daytime. Black lines denote click-positive hourly bins. Periods of no recording effort are highlighted in transparent blue.

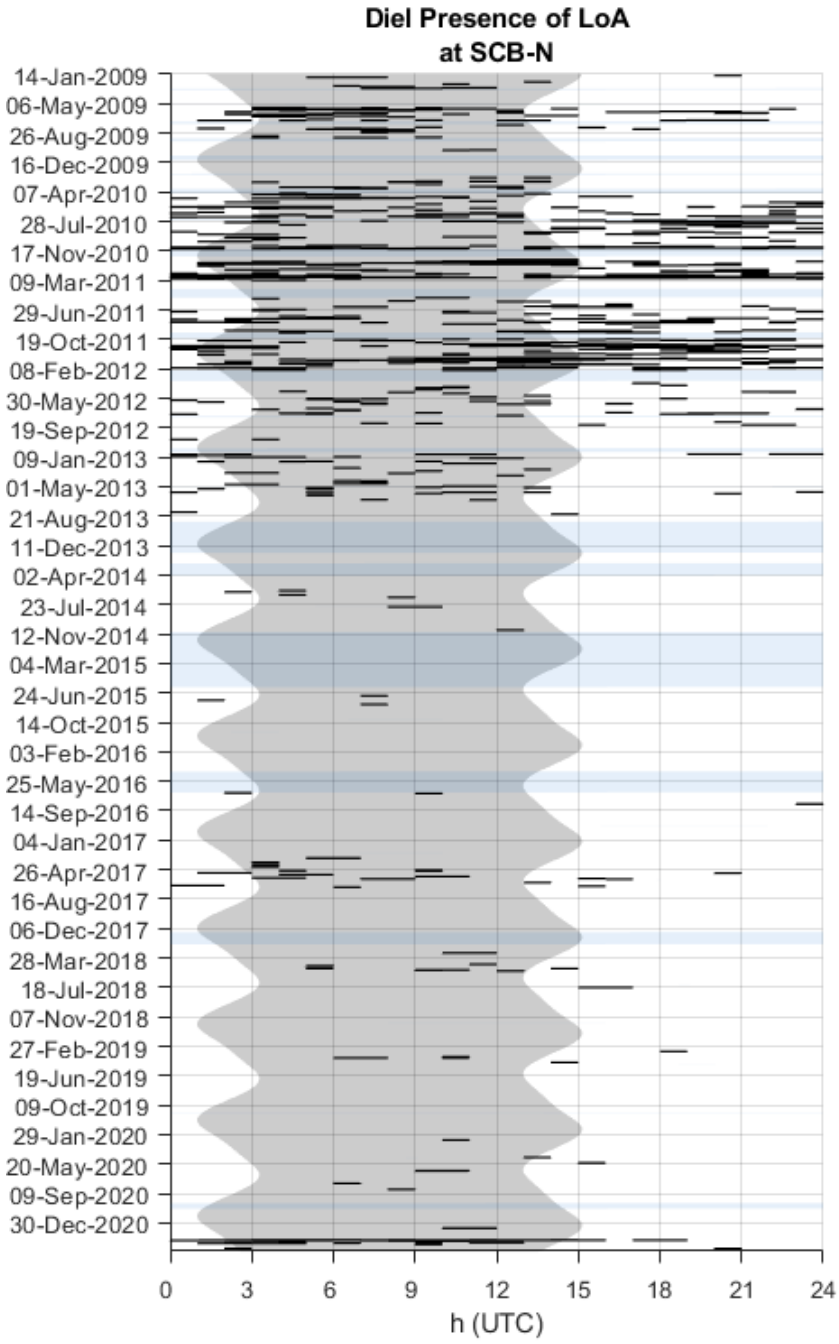


Figure 2.11. LoA hourly click-positive timeseries at SCB_N. Gray sections represent nighttime hours and white sections represent daytime. Black lines denote click-positive hourly bins. Periods of no recording effort are highlighted in transparent blue.

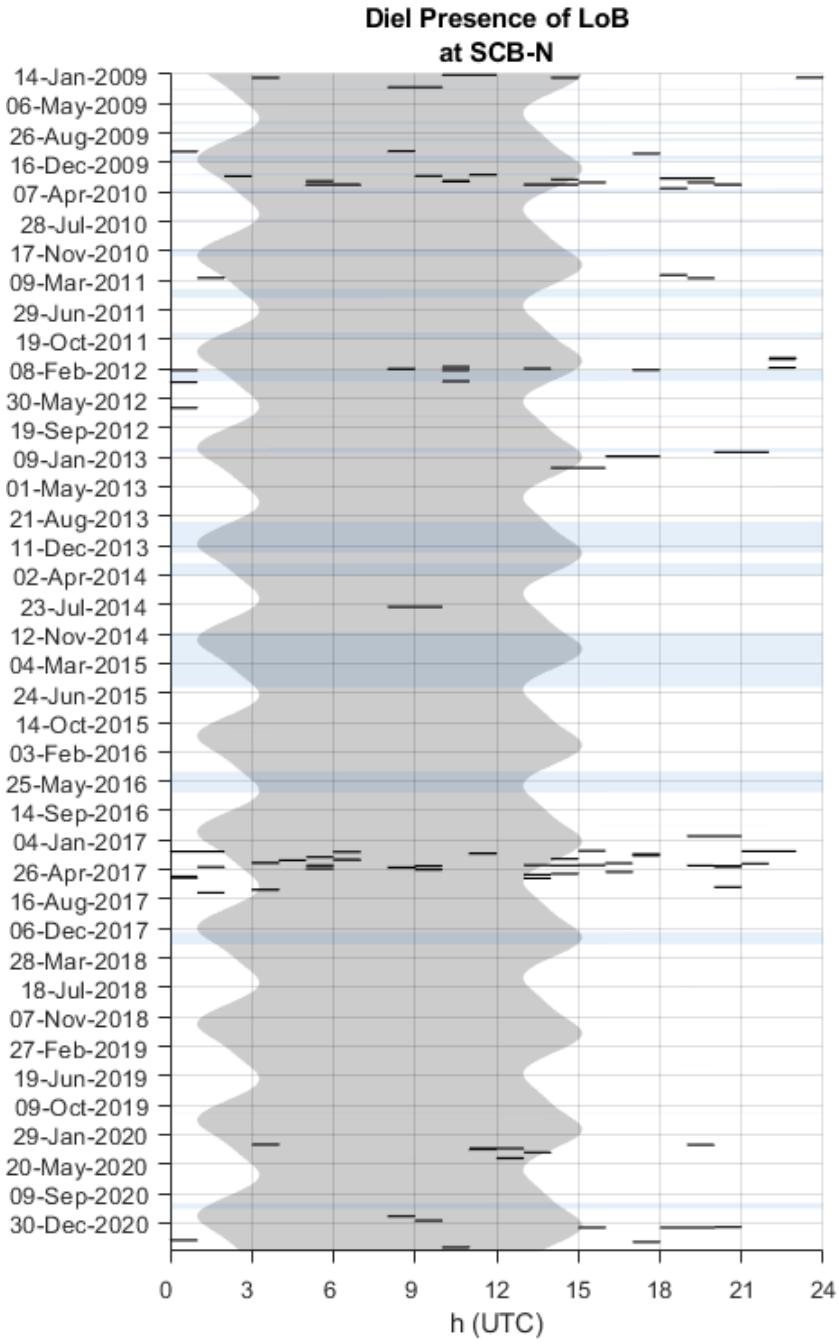


Figure 2.12. LoB hourly click-positive timeseries at SCB_N. Gray sections represent nighttime hours and white sections represent daytime. Black lines denote click-positive hourly bins. Periods of no recording effort are highlighted in transparent blue.

Chapter 3

Application of deep learning to estimate blue and fin whale call density in the southern California Current Ecosystem

3.1 Abstract

Blue (*Balaenoptera musculus*) and fin whales (*Balaenoptera physalus*) are dominant contributors to low-frequency ocean soundscapes, yet reliably extracting their calls from long-term passive acoustic recordings is methodologically challenging. Here, we train a multi-class deep-learning detector to identify five principal blue and fin whale call types (A, B, D, 20 Hz, and 40 Hz) from low-frequency spectrograms using a Faster R-CNN architecture combined with iterative human review, hard-negative mining, and multi-platform training on California Cooperative Oceanic Fisheries (henceforth, CalCOFI) sonobuoy and High-frequency Acoustic Recording Package recordings from the southern California Current Ecosystem. The detector was evaluated on four independent test datasets spanning multiple years, seasons, and recording platforms and then deployed on CalCOFI sonobuoy recordings collected quarterly over two decades (2004–2024). The final model achieved consistently high mean precision and recall for most call types (e.g., A: 0.71/0.71; B: 0.83/0.59; D: 0.79/0.84; 20 Hz: 0.87/0.74), while 40 Hz calls remained challenging (0.42/0.69), primarily due to confusion with spectrally overlapping humpback whale downsweeps. Detections were post-processed using call-specific characteristics

and received-level thresholds and normalized by recording effort and detection area to derive standardized indices of call density $\left(\frac{\text{calls}}{\text{h}\cdot 1000\ \text{km}^2}\right)$ with uncertainty estimates. Densities were aggregated annually and show call-specific differences between inshore and offshore habitats and interannual variability associated with periods of anomalous oceanographic conditions. Inter-call interval analyses suggested seasonal stability in blue whale song, high variability in blue and fin whale social calls, and seasonal and interannual variability in fin whale song repetition rates. This study is among the first to use deep-learning to estimate baleen whale call density from decades of passive acoustic recordings in a complex soundscape.

3.2 Introduction

Blue and fin whale calls occur within complex low-frequency soundscapes where biophony, geophony, and anthropophony overlap, and many of them are challenging to detect automatically. As passive acoustic monitoring (PAM) efforts expand globally, the volume of acoustic data collected has created a "big data" challenge in which analysis capacity, rather than data availability, has become the primary bottleneck (Stowell, 2022). This challenge is particularly acute in regions such as the southern California Current Ecosystem (SCCE), where long-term monitoring of low-frequency soundscapes has occurred since the early 2000s (Wiggins and Hildebrand, 2007). The SCCE is an important foraging ground for blue and fin whales (Calambokidis et al., 2015) with seasonally high levels of acoustic activity (Oleson et al., 2007b; Širović et al., 2015), making automated detection and classification necessary for estimating call density in the region. Knowledge of population density is necessary for sustainable management, particularly for blue and fin whales which are listed as endangered and vulnerable, respectively, on the IUCN Red List of Threatened Species (Cooke, 2018b,a). However, translating acoustic detections into population density requires knowledge of cue rates Marques et al. (2009, 2013), which remain poorly constrained and may vary with behavioral state for baleen whales (Lewis et al., 2018; Marques et al., 2011; Garcia et al., 2025). Call density, or the estimated number of

calls produced in a given search area over time (Hilmo et al., 2025; Harris et al., 2018, 2025) provides a standardized intermediate metric that enables comparison of acoustic activity across space and time without requiring cue rate estimates. Estimating call density from long-term recordings therefore represents an intermediate step toward estimating population density from passive acoustics.

Northeastern Pacific blue whales migrate annually to the SCCE, and their calls vary in spectral-temporal properties and seasonal occurrence (Oleson et al., 2007b). Blue whale A and B calls form the components of blue whale song, which has only been recorded from males and is hypothesized to serve a reproductive function (Oleson et al., 2007a; Lewis et al., 2018; McDonald et al., 2001). Singing activity peaks in early fall as animals transition from foraging to breeding-associated behavioral states (Širović et al., 2015; Szesciorka et al., 2020). B calls, which are long-duration tonal signals (Thompson et al., 1996), have been widely used as indices of blue whale presence because their stereotyped spectral-temporal structure makes them easier to detect automatically (Širović, 2015). In contrast, A calls, which are pulsed tonal signals (Thompson et al., 1996) produced less frequently, are more difficult to detect using traditional automated methods, and have received less attention in long-term acoustic analyses despite being a consistent component of blue whale calling and singing behavior (Szesciorka et al., 2020). Blue whales also produce highly variable D calls (Thompson et al., 1996), which are associated with foraging and social contexts (Oleson et al., 2007a), produced by both sexes (Oleson et al., 2007a; McDonald et al., 2001), and peak during summer months (Oleson et al., 2007b; Szesciorka et al., 2020) when foraging conditions are optimal (Bloom et al., 2025). Fin whales, which are present year-round in the SCCE (Campbell et al., 2015), similarly produce both stereotyped song components and more variable non-song calls. Fin whale 20 Hz calls (Watkins et al., 1987) form rhythmic song sequences associated with male reproductive behavior (Croll et al., 2002) and peak in late fall and winter (Širović et al., 2015, 2013), whereas, 40 Hz calls (Watkins, 1981), similar to blue whale D calls, are highly variable and linked to foraging

(Romagosa et al., 2021) and social contexts and peak in spring and summer (Širović et al., 2013). Notably, fin whale 40 Hz calls overlap in spectral characteristics with blue whale D calls, complicating their automated separation in PAM recordings (Rasmussen and Širović, 2021). Because of this spectral variability, much of the existing literature has focused on blue and fin whale song, biasing estimates of spatiotemporal trends toward reproductive signals produced by males rather than foraging-associated calls produced by both sexes. Therefore, accurate estimates of blue and fin whale spatiotemporal distribution and call density in the SCCE would benefit from including both song and non-song activity, particularly given that these calls are produced at different levels throughout the year (Širović et al., 2013; Oleson et al., 2007b; Szesciorka et al., 2020).

Reliably extracting this diversity of signals from long-term acoustic recordings requires automated methods that are robust to variable call structure, ambient noise conditions, and shifts across years (McDonald et al., 2009; Rice et al., 2022), seasons (Širović, 2015; Oleson et al., 2014), and recording platforms (Roch et al., 2015). Recent studies have shown the promise of convolutional neural networks (CNNs) for detecting baleen whale calls directly from spectrograms without reliance on predefined templates Allen et al. (2021); Rasmussen and Širović (2021); Darias-O'Hara et al. (2026). However, CNN performance is dependent on the diversity and representativeness of training data relative to testing data (Stowell, 2022). In long-term PAM applications, domain shift across regions, recording platforms, years, seasons, and soundscapes leads to overfitting and poor generalization, limiting the reliability of automated predictions when models are applied beyond their training domain (Kather et al., 2024; Schall et al., 2024). Consequently, few studies have deployed CNN-based detectors across long-term PAM datasets (Best et al., 2022; Lammers et al., 2023). In addition to detection challenges, variation in sound propagation and the long-range transmission of low-frequency baleen whale calls lead to substantial differences in detection range and effective sampling area across space and time (Helble et al., 2013). These effects must be accounted for when comparing acoustic

detection rates, particularly in long-term and spatially extensive datasets (Širović et al., 2015).

Here, we address the challenges described above by combining deep learning with human review and sound propagation modeling to estimate blue and fin whale call density in long-term (2004–2024) CalCOFI sonobuoy recordings. The CalCOFI dataset is unique in its experimental design, spanning inshore and offshore habitats of the SCCE and quarterly sampling for more than two decades. This long-term and spatially extensive sampling creates a heterogeneous and challenging acoustic scene, but also offers unprecedented resolution to investigate seasonal and spatial-temporal variability in blue and fin whale acoustic activity. To process this dataset, we fine-tuned a Faster R-CNN model (Ren et al., 2015) using both sonobuoy and high-frequency acoustic recording package (HARP)(Wiggins and Hildebrand, 2007) data, iteratively refining a single detector for the five principal blue and fin whale call types through hard-negative mining (HNM) and human-in-the-loop (HITL) labeling. This training strategy was designed to improve generalization across years, seasons, soundscapes, and recording platforms without requiring extensive additional manual labeling. Detected calls were subsequently post-processed and normalized by detection area and recording effort to generate standardized indices of call density with uncertainty, enabling investigation of long-term and inshore-offshore trends. In addition to estimating call density, we examined seasonal variability in inter-call intervals, which may be useful for future estimates of cue rates. Together, this approach provides a quantitative, long-term perspective on blue and fin whale call density within a key eastern North Pacific foraging region and describes an automated approach for processing multi-decadal, multi-platform PAM data.

3.3 Methods

We built an automated detection and classification pipeline to identify blue whale A, B, and D calls and fin whale 20 Hz and 40 Hz calls in long-term CalCOFI sonobuoy recordings. Model performance was iteratively improved through human-in-the-loop (HITL) labeling and

hard negative mining (Sung and Poggio, 1995) (HNM) refinement, and evaluated on four held-out datasets spanning multiple years, seasons, and deployment platforms (Table 3.1). We deployed the final model on CalCOFI sonobuoy recordings collected over quarterly twenty years (2004-2024) and we filtered detections using call-characteristic parameters, including frequency, repetition rate, and received levels above call-specific detection range thresholds. Detection ranges were estimated using range-dependent acoustic propagation models (RAMGEO) (ZoBell et al., 2024) and calibrated against empirical received-level distributions. These detection ranges were used to standardize detections by monitored area and recording effort, enabling estimation of call-level density $\left(\frac{\text{calls}}{\text{h}\cdot 1000\ \text{km}^2}\right)$ for blue and fin whales. Uncertainty in density estimates arising from variability in detection area and detector performance were propagated into annual density estimates.

3.3.1 Acoustic data collection

Sonobuoys have been deployed as part of CalCOFI's marine mammal monitoring program since 2004 across the core CalCOFI grid, which consists of transect lines extending up to 600 km offshore between San Diego and Avila Beach, California (Fig. 4.1). The transect lines numbered are 93.3 to 76.7, with stations numbered 28 to 120 increasing with distance from shore (Fig. 4.1) and stations are referred to throughout by their line and station number (e.g., 93.3-35, 90.0-37, 83.3-110). Sonobuoys were deployed during quarterly CalCOFI surveys during daylight hours at fixed sampling stations, typically 1 km prior to arrival at a given station, and recorded continuously while the ship remained on station (1–8 h). When available, both omnidirectional (OMNI) and directional frequency analysis and recording (DIFAR) sonobuoys were deployed. OMNI sonobuoys recorded acoustic signals in the 10 Hz–20/24 kHz range, while DIFAR sonobuoys record between 10–2,400 Hz. Following deployment, hydrophones were released to approximately 300 m depth and transmitted acoustic signals via VHF radio to ship-mounted receivers, where data were digitized and recorded as audio files using Ishmael Mellinger (2002) or PAMGuard Gillespie et al. (2026). In total, we processed 1,743 sonobuoy

deployments from 68 surveys between 2004-2024, totaling 5,104 h of acoustic recordings (Supplementary Table S3.4). Of these, small subsets of sonobuoy recordings from 17 surveys were used for model training (57 h total), and data from three surveys (Summer 2008, Spring 2013, Fall 2023) were reserved for testing (201 h total; Table 3.5).

HARP recordings (Wiggins and Hildebrand, 2007) collected throughout Central and Southern California were used as additional data for model training and testing (Fig. 4.1). HARPs were deployed at depths of 65–1,012 m and continuously recorded 16-bit audio, with an effective bandwidth of 10 Hz–100 or 160 kHz for up to one year. HARP hydrophones were suspended 10–20 m above the seafloor. Recordings from five HARP deployments across four stations were included in this study (Supplementary Table S3.6): data from three deployments in the Channel Islands National Marine Sanctuary (CINMS01-03), one from the Southern California Bight (SOCAL), and one near Diablo Canyon (DC) (109.3 h) were used for model training and validation using a 90/10 split, and one deployment in the Chumash Heritage National Marine Sanctuary (CHNMS; 269 h) was reserved for testing.

3.3.2 Detector development

The initial annotations were from the Detection, Classification, Localization, and Density Estimation 2015 (DCLDE, 2015) dataset and additional A and B calls in this dataset were labeled by expert analysts (MNA, DA) using the LoggerPro Remora in *Triton*. Spectrograms were visualized in 60-s windows spanning 10–150 Hz with 1 Hz frequency resolution and 90% overlap. Normalization settings were adjusted per deployment to account for variability in signal-to-noise ratios across HARP and sonobuoy platforms. Annotations were converted into bounding boxes [x, y, width, height] corresponding to pixel-level call locations within 60-s spectrograms. The detector was designed to operate on 60-s spectrograms computed with a 1-s Hamming window and 90% overlap, band-limited to 10–150 Hz, and restricted to an 80 dB dynamic range. Audio data were partitioned into non-overlapping 60-s clips, spectrograms were normalized individually between 0–1, and mapped to an 8-bit integer tensor. Annotations in

each spectrogram were retained if they met minimum duration thresholds (5 s for A/B calls, 3 s for D calls, and 1 s for 20/40 Hz calls), and spectrograms without valid calls were retained as negative examples.

The initial training dataset consisted of 3,058 spectrograms with 5,159 labeled calls, most of which were blue whale calls from HARP data (Table 3.1). A Faster R-CNN object detection model (Ren et al., 2015) with a 50 layer residual network backbone and feature pyramid network was fine-tuned on our initial, intermediate, and final training datasets. Faster R-CNN was selected as it was previously applied to blue whale D call and fin whale 40 Hz call detection in spectrograms (Rasmussen and Širović, 2021), and its two-stage architecture is known for having better precision than one-stage architectures in complex scenes (Ahmed and Das, 2025; Aboyomi and Daniel, 2023). The model proposes candidate regions using a region proposal network and applies non-maximum suppression (IoU > 0.3) to reduce redundant overlapping detections before classification and bounding box refinement. All models were trained for 15 epochs using stochastic gradient descent (learning rate = 0.001, momentum = 0.9, weight decay = 0.0005, batch size = 32) on a single NVIDIA (Santa Clara, CA, USA) GeForce RTX 4070 GPU. The final classification head was reconfigured to output five whale call classes plus background.

Performance was reported by computing precision and recall at different thresholds. For each threshold $\tau \in \{0.1, 0.2, \ldots, 0.9\}$ the following were counted:

- **True Positives (TP)**: Prediction associated with a ground-truth label of the same call type and sufficient overlap (score $\geq \tau$, IoU ≥ 0.5, matched class).
- **False Positives (FP)**: Prediction does not sufficiently coincide with a ground-truth label or the ground-truth label is of a different call type (score $\geq \tau$ with IoU < 0.5 or mismatched class).
- **False Negatives (FN)**: Ground-truth labels that are not matched by any prediction.

and used to compute precision and recall:

$$\text{Precision} = \frac{\text{TP}}{\text{TP} + \text{FP}}, \quad \text{Recall} = \frac{\text{TP}}{\text{TP} + \text{FN}}. \tag{3.1}$$

Fixed threshold results (Table 3.2) are reported at threshold $\tau = 0.2$ and IoU $= 0.5$.

A held-out 10% subset of HARP recordings was used as a validation set throughout training to monitor model performance and prevent overfitting; precision and recall were computed after each epoch and training was stopped at 15 epochs. The validation set was never used to update model weights or incorporated into subsequent training rounds. Three rounds of HITL auditing were conducted to iteratively expand and refine the training dataset (Table 3.1, Fig. 3.2). In the first round, the initial model was applied to the DC HARP and CalCOFI winter 2015 (CC1501) deployments. DC was selected for a high-level of call activity across most call types. CC1501 contained a large number of fin-whale 20 Hz calls. Revised labels were added back into training along with background spectrograms from non-target species (including humpback whale calls) as hard negatives, which were absent from the initial training set. In the second round, the retrained model was applied to the SOCAL26H HARP deployment to recover additional 20 Hz and 40 Hz calls, and to early CalCOFI cruises (2006–2015) to assess generalization across the sonobuoy platform. Performance on CalCOFI data was poor initially, and so verified detections from cruises CC0603, CC0706, CC1107, CC1110, CC1301, CC1307, CC1311, CC1407, and CC1507 were added to the training set. In the third round, the model was applied to more recent CalCOFI cruises (2016–2024) and, following analyst auditing, data from CC1601, CC1604, CC1611, CC1701, CC1806, CC1907, and CC2411 were incorporated to the training data. Training was stopped after this round because performance improved across most call categories on the held-out CalCOFI 2008 dataset and to limit the potential for the training data to bias the downstream call density estimates, though the majority of CalCOFI examples incorporated into training were verified hard negatives that didn't contain calls (Table 3.1), which likely minimized such bias. In all rounds, detections were audited by expert analysts (MNA, DA)

using a custom interactive annotation tool (https://github.com/m1alksne/WhaleMoanViz) built within the *Triton* PAM software package. In total, 6,517 annotations were added, resulting in 11,676 total calls and substantial rebalancing of the recording platform representation (Table 3.1, Fig. 3.2).

Detector performance was evaluated on four held-out datasets not used during training: three CalCOFI sonobuoy datasets spanning different seasons and years (Summer 2008, Spring 2013, and Fall 2023) and one year-long HARP dataset (CHNMS 2023; Table 3.1; Supplementary Tables S3.5 and S3.6). Ground-truth annotations for all test datasets were generated by applying the final trained model to each dataset and having expert analysts (MNA, LB) audit all detections and manually label missed calls using the same interactive annotation tool. For CalCOFI Summer 2008 (CC0808), pre-existing analyst labels generated independently prior to model development served as a reference for assessing model generalization during training; following the final training round, these labels were re-audited using the model-assisted approach to ensure completeness. The audited labels for all test datasets were used exclusively for evaluation and were never incorporated into the training data. For the CalCOFI test sets, evaluation units were individual sonobuoy deployments, and ground-truth annotations covered the full deployment duration. For the year-long CHNMS HARP dataset, annotations were reviewed in weekly 5-h bins; within each bin, analysts audited all detections and manually labeled missed calls as in the CalCOFI test sets, as auditing the complete year-long recording was not feasible.

Before deploying the model on the full CalCOFI archive, we developed a set of post-processing filters to reduce spurious detections based on the patterns we saw during HITL refinement and based on known call characteristics from the literature. First, detections had to pass a confidence score of threshold ($\tau \geq 0.2$) and each of those detections was retained only if 3 or more detections existed within a sliding $\pm$1-h window and at least one of them had a high confidence score ($\tau \geq 0.7$). This filtering step removed low confidence detections and isolated detections while retaining detections occurring during sustained calling periods. We then applied

call-type frequency constraints based on call bandwidths. A and B calls were retained only if their bounding boxes were completely within 70–90 Hz and 10–60 Hz (Thompson et al., 1996; McDonald et al., 2001), respectively. D calls, 20 Hz, and 40 Hz calls were retained if bounding boxes were completely within 20–100 Hz, 10–30 Hz, and 30–100 Hz, respectively (Thompson et al., 1996; McDonald et al., 2001; Watkins, 1981; Širović et al., 2013). We also developed a RL thresholding criterion which is described below. To evaluate how HITL refinement and post-processing affected detector performance, we compared three configurations using the held-out evaluation datasets:

1. **Initial model**: Faster R-CNN trained on the original training dataset (5,159 annotations), evaluated by comparing raw model predictions with ground-truth evaluation labels.

2. **Final model**: Faster R-CNN trained on the HITL refined dataset (11,676 annotations), evaluated by comparing raw model predictions with ground-truth evaluation labels.

3. **Final + Context + RL**: Final model predictions post-processed using contextual call-characteristic filters and received-level (RL) thresholding, compared with ground-truth evaluation labels.

3.3.3 Sonobuoy received level calibrations

To calculate calibrated root mean square (RMS) received levels for automatically detected blue and fin whale calls, we extracted waveform segments corresponding to bounding-box derived start and end times and computed power spectral density (PSD) using Welch's method (Hamming window, 90% overlap). The PSD ($\text{counts}^2/\text{Hz}$) was corrected using the frequency-dependent gain response of the deployed sonobuoy model (AN/SSQ-53D, 53G, or 57A), returned to linear units, and integrated over the bounding-box derived call bandwidth. Hydrophone sensitivity, radio telemetry gain, and A/D conversion scaling factors were then applied to compute calibrated spectral received levels (SPL_{rms} dB re 1 μPa).

$$\mathrm{SPL_{rms}} = 10\log_{10}\left(\int_{f_1}^{f_2} P(f)\,df\right) + V + S + \mathrm{ICOM}. \tag{3.2}$$

where:

V : A/D conversion term $\left(20\log_{10}\left(\frac{V}{2^n}\right);\ V = 5 \text{ volts},\ n = 16 \text{ bits}\right)$

S : Hydrophone sensitivity (90 dB re 1 V/μPa for DIFAR; 94 dB re 1 V/μPa for OMNI)

ICOM : Radio telemetry gain (46 dB re kHz/V)

f_1, f_2 : Lower and upper frequencies of integration, respectively

$P(f)$: Power spectral density (counts^2/Hz)

Because the dataset spanned twenty years of CalCOFI sonobuoy deployments, recorded with changing operational protocols and hardware, such as selectable gain tuning on the VHF radio receiver, the calibrated spectra still exhibited survey-specific gain offsets after applying the sonobuoy transfer functions. To account for these offsets, we normalized measured spectra using each deployment's timestamp and location together with the empirical relationship between ambient noise and wind speed described in Hildebrand et al. (2021). Per-deployment ambient noise levels were computed at 500 Hz (PSD estimated with a Hamming window and 0% overlap over $\sim$2-h deployment segments). We selected 500 Hz because this band is primarily dominated by wind-driven surface noise and lies outside the strongest contributions from baleen whales or commercial shipping. Expected noise levels were predicted from coincident Cross-Calibrated Multi-Platform (CCMP) (Wentz et al., 2016) wind speeds using the wind-generated ocean noise model from Hildebrand et al. (2021), and the dB difference between wind-predicted and hardware-calibrated levels was applied as an additive offset to generate the final wind-normalized received levels.

3.3.4 Detection range and area estimation

We estimated the detection range and area at ten stations for each call type to account for differences in location and bathymetry, which affect the range over which a whale call can be detected. Following methods described by (ZoBell et al., 2024), we used the range-dependent parabolic equation method (RAMGEO) (Collins, 1995) to estimate sound propagation loss along radials spaced 10 degrees apart cast 200 km out from positions of ten CalCOFI stations (Fig. 4.1, Supplementary Table S3.7). The ten stations were chosen to represent a range of bathymetric characteristics which resulted in different detection ranges inside and outside of the Southern California Bight and all had greater than 60 h of recording effort. Bathymetric data were obtained from the General Bathymetry Chart of the Oceans (GEBCO) with 15-arc second spatial resolution (ZoBell et al., 2024). We chose three stations offshore of the continental slope and seven stations along or inshore of the slope (Fig. 4.1). Of the seven inshore stations, one was along the continental slope (86.7-60), one between the southern Channel Islands (90.0-37), one on the southern most CalCOFI line (93.3-35), one nearshore station (86.7-35), one in the Santa Barbara Channel (81.8-46.9), one between the slope and northern Channel Islands (83.3-55) and one near the slope north of Point Conception (76.7-55). We used sound speed profiles averaged over fall months (Sept, Oct, Nov), as that is the peak calling season for blue and fin whales (Širović et al., 2015), and sediment properties as outlined in ZoBell et al. (2024). Transmission loss was calculated at 43 Hz for all call types, with source depths of 15 m for D calls, 20 Hz and 40 Hz calls, and 23 m for A and B calls, based on known calling and singing depths (Lewis et al., 2018; Stimpert et al., 2015), and receiver depth was set to 300 m. We assumed reciprocity between source and receiver positions, and computed received levels by subtracting modeled transmission loss from call-type specific source levels (Table 3.3).

For each call type, simulated received levels (RL; dB re 1 μPa) at each modeled station were compared to wind-normalized received levels from sonobuoy detections matched by habitat class (inshore vs offshore). Stations were classified as inshore (CalCOFI station number ≤ 60;

within/landward of the continental slope) or offshore (station number > 60; seaward of the slope). We aggregated modeled RLs from the seven inshore/slope/island-associated modeled stations and compared them with detected call RLs from deployments occurring at CalCOFI stations ≤ 60. We compared modeled RLs from the offshore modeled stations with detected call RLs from CalCOFI stations > 60.

For each call type and habitat class, we examined histograms of modeled and detected RL distributions to identify the RL at which detections began to drop off more rapidly than predicted by the simulated distribution (i.e., the lower-tail indicating reduced detectability at low RL). This RL was selected as the operational RL detection threshold for that call type, representing a conservative lower bound above which calls were assumed to be reliably detectable. For each modeled station, all range–bearing points along 10°-spaced radials with received levels exceeding the calibrated RL threshold were extracted, converted to Cartesian coordinates, and used to compute detection areas (km^2) for each call type at each modeled station. The detection area was computed as the area of the tightest enclosing polygon around these points, with a maximum gap tolerance equal to the radial spacing (10 km) to prevent bridging across areas where received levels fell below the detection threshold. Detection areas for inshore environments were averaged across the seven inshore/slope/island-associated modeled stations to obtain a representative inshore detection area per call type and the associated variance across stations was retained for uncertainty propagation. Offshore detection area for each call type was based on the average of the offshore modeled stations with uncertainty. These areas (Table 3.3, Supplementary Table S3.7) were used to normalize detection rates to calls per hour per 1000 km^2.

3.3.5 Call density estimation

We estimated call density for blue and fin whale call types as the number of calls per unit time and unit area, expressed as calls per hour per 1000 km^2. Density estimates were calculated from automatically detected calls after post-processing and received-level filtering. Stations

were classified as inshore (station number ≤ 60) or offshore (> 60), and density was estimated separately for each habitat class. Density was computed independently for each call type at every station and then aggregated annually over the year.

For a given year, acoustic call density was estimated as:

$$\hat{D} = \frac{\sum_i N_i (1 - \hat{p}_{\mathrm{FP}})}{(1 - \hat{p}_{\mathrm{FN}}) \sum_i A_i T_i}, \tag{3.3}$$

where N_i is the number of detected calls in deployment i after post-processing and RL thresholding, A_i is the estimated detection area (km^2) assigned to deployment i based on habitat class (inshore vs offshore) and call type, and T_i is the recording duration (hours). The denominator represents the total acoustic exposure in units of hours km^2. The terms $\hat{p}_{\mathrm{FP}}$ and $\hat{p}_{\mathrm{FN}}$ represent the estimated proportions of false detections and missed detections, respectively, for each call type following post-processing. These proportions were based on the four independent test datasets and were assumed constant across space and time for a given call type.

Uncertainty in annual density estimates was quantified using the delta method approximation (Marques et al., 2009, 2011), propagating variance associated with detection counts, detection area, and classification error. Specifically, uncertainty in detection area (A) for inshore stations was represented by the variance across the four modeled inshore/slope/island-associated stations for each call type; offshore detection area was treated as fixed. Uncertainty in $\hat{p}_{\mathrm{FP}}$ and $\hat{p}_{\mathrm{FN}}$ was represented by variability in precision/recall across the four held-out evaluation datasets for each call type and configuration, converted to FP and FN proportions. Density estimates are reported as annual means with ± 1 standard error.

3.3.6 Inter-call intervals

For each call type, ICIs were computed as the time difference between the start times of consecutive detections within the same recording deployment. Only detections that passed call-characteristic filtering and received-level thresholding were included. ICIs were restricted

to intervals less than 180 s for blue whale A and B calls and 60 s for blue whale D calls and fin whale 20 Hz and 40 Hz calls (Oleson et al., 2007b; Lewis and Širović, 2018; Širović et al., 2013, 2017). ICIs were calculated separately for each call type and aggregated seasonally across the entire dataset to investigate seasonal call structure.

3.4 Results

The CalCOFI dataset comprised 5,104 hours of spatially and temporally distributed recordings collected under a standardized seasonal survey design (Fig. 4.1). Samples were taken across fixed stations, seasons, and habitats over two decades (Supplementary Table S3.4).

Our HITL–HNM approach was designed around the available data and leveraged additional annotations from moored HARP recorders. The continuous HARP recordings span peak calling seasons (Širović et al., 2015) and many have annotation effort (Rasmussen and Širović, 2021). Consequently, our initial training dataset consisted mostly of HARP data (Table 3.1). CalCOFI sonobuoy recordings, by contrast, had no time-frequency annotations, were of short duration (~2 h), collected across seasons, and include regions where whale acoustic activity is often low. We therefore deployed the HARP-trained model on CalCOFI recordings to generate initial labels, then used HITL rounds to correct substantial false positives generated across noisy, empty recordings by incorporating 2,792 background spectrograms (spectrograms that did not contain blue or fin whale calls) as hard negatives and adding 1,513 targeted positive examples to the final training set (Table 3.1). Post-processing filters based on call characteristics were then applied to further reduce false positives in the final time series.

3.4.1 Detector performance

The final Faster R-CNN model was trained on 11,676 labeled calls drawn from the two recording platforms: HARP and CalCOFI sonobuoys (Table 3.1). Call annotations from CalCOFI sonobuoy recordings grew from 765 to 1,513 in the final training set, though the majority of CalCOFI additions were background spectrograms. Model performance was eval-

uated by comparing three configurations: (1) the original model trained on the initial dataset, (2) the final model trained on the HITL–HNM refined dataset, and (3) the final model with call-characteristic filters and received-level thresholds applied. All configurations were evaluated on four independent datasets for which analysts labeled all calls: three CalCOFI test datasets spanning different seasons and years (Spring 2013, Summer 2008, and Fall 2023) and one year-long HARP dataset collected in the Chumash Heritage National Marine Sanctuary in 2023 (CHNMS 2023). Across all four test datasets, detector performance improved substantially from the initial to the final configuration, and precision improved further with post-processing applied (Table 3.2). These metrics were calculated at a minimum confidence score ($\tau \geq 0.2$), with detections considered true positives if they overlapped the ground truth box by at least 50%, or at an intersection over union (IoU) threshold of ≥ 0.5. False positive, true positive, and false negative rates were calculated for each sonobuoy deployment in the CalCOFI test data. For the CHNMS test data, the analyst went through one 5-h bin per week of the year, and false detection rates were calculated for each 5-h bin. Performance varied by call type, season, and recording platform, with 20 Hz calls detected most reliably and 40 Hz calls showing the greatest variability across datasets.

Blue whale A-call performance was best for the final model with post-processing applied (precision 0.71; recall 0.71; Table 3.2). A-call performance varied across test datasets (Fig. 3.3, Supplementary Fig. S3.7); precision was generally higher in the CalCOFI test sets than in CHNMS, while recall was more variable. Confusion between A and B calls was rare, with only one isolated case observed in the CalCOFI Summer 2008 test set during periods of call overlap. Blue whale B-call performance improved markedly relative to the initial configuration, particularly in precision (Table 3.2). Mean precision was highest for the post-processed configuration (0.83), while recall was highest for the unfiltered final model (0.59), reflecting a precision–recall tradeoff after filtering. Across evaluation datasets, B-call false positive rates were more variable than A-call false positive rates (Fig. 3.3) and were concentrated

during periods of elevated calling activity (Supplementary Fig. S3.9). Blue whale D-call recall was highest for the unfiltered final model (0.84) and precision was highest after post-processing (0.79; Table 3.2). D calls were detected in the CalCOFI summer 2008 and CHNMS 2023 test datasets with high recall, although the CalCOFI summer 2008 dataset had lower precision (Fig. 3.3; Supplementary Fig. S3.11) and some confusion with fin whale 20 Hz and 40 Hz calls. Fin whale 20 Hz call performance was highest overall and was stable across CalCOFI test datasets (precision 0.86; recall 0.74 for the final model; Table 3.2). This call type also increased the most in training representation during HITL refinement (Table 3.1). False-positive rates were generally low relative to other call types (Fig. 3.3), and cross-category confusion was limited. Fin whale 40 Hz calls remained the most challenging category, with performance varying substantially across evaluation datasets (Fig. 3.3). Precision and recall were high in the CalCOFI Spring 2013 test set but lower in the CalCOFI Summer 2008 test set, where confusion with fin whale 20 Hz and blue whale D calls was observed. In the CHNMS dataset, 40 Hz recall was high while precision was reduced by frequent confusion with humpback whale downsweeps. Throughout CHNMS, false-positive rates were relatively consistent through time despite a large cumulative number of false detections (Fig. 3.3; Supplementary Fig. S3.14).

3.4.2 Detection area estimates

To identify consistent received-level (RL) detection thresholds, calibrated RLs were compared with modeled RL distributions derived from range-dependent acoustic (RAMGEO) propagation models (ZoBell et al., 2024) built using call-specific parameters (Table 3.3) for eight representative monitoring stations in the SCCE. Of the eight stations, seven were categorized as inshore and one as offshore, based on their position relative to the continental slope, which approximately tracks CalCOFI station 60 across all six transect lines (Fig. 4.1). Stations at or closer to shore than station 60 were classified as inshore, and the single modeled station beyond station 60 was classified as offshore. Across call types, received levels of calls detected inshore were generally concentrated at higher received levels, with a larger proportion between

approximately 100–110 dB re 1 µPa, whereas calls detected offshore were shifted toward lower received levels, typically between 95–100 dB re 1 µPa. This pattern indicates that offshore deployments captured a greater fraction of lower-RL, more distant calls, while inshore detections more often reflected higher-amplitude calls. Similar patterns were evident in the simulated RL distributions; however, modeled inshore distributions were more strongly skewed toward high received levels than the received levels of detected calls.

For most call types, detectability declined at received levels near 90–95 dB re 1 µPa, marking a consistent lower bound for reliable detection. While detection counts are expected to increase as fainter, more distant calls are included, histogram comparisons between the modeled and empirical distributions identified the RL at which the detector begins to miss calls, above which detection probability is be assumed to be one. For blue whale A calls, offshore detected call RLs were sparse and restricted to lower received levels, whereas inshore detected call RLs tracked the simulated inshore distribution, although fewer high amplitude calls were detected than were predicted by the model (Supplementary Fig. S3.8). Based on this, a RL detection threshold of 90 dB re 1 µPa was selected for A calls (Table 3.3; Supplementary Fig. S3.8). For blue whale B calls, inshore detected call RLs exhibited higher mid-range received levels than predicted by the model, while offshore detected call RLs were consistently higher in amplitude than simulated values, and a detection threshold of 96 dB re 1 µPa was selected (Supplementary Fig. S3.10). For blue whale D calls, detected call RLs and modeled RLs had similar distributions in inshore and offshore environments, although the model predicted more high amplitude detections at inshore environments than were observed, and detection threshold of 95 dB re 1 µPa was selected (Fig. 3.4). Fin whale 20 Hz calls exhibited similar distribution shapes between detected call RLs and simulated RLs in both habitats, though detected call RLs were consistently shifted toward higher received levels (Supplementary Fig. S3.13). A detection threshold of 96 dB re 1 µPa was selected. Fin whale 40 Hz detected and modeled RL distributions were similar in both environments, and a threshold of 94 dB re 1 µPa was selected

(Supplementary Fig. S3.15).

Across all call types, the offshore mean had a detection area roughly twice that of the inshore mean area (Table 3.3). Inshore detection areas varied among stations, ranging from 4,629 km^2 at station 81.8–46.9 to 21,646 km^2 at the slope station 86.7–60 for blue whale A calls, with similar patterns across all call types (Supplementary Table S3.7), reflecting the complex bathymetry of the Southern California Bight. Among call types, detection areas were largest for blue whale D calls and fin whale 40 Hz calls, and smallest for blue whale A calls, driven by differences in modeled source levels and selected received-level thresholds.

3.4.3 Call density estimates

Annual blue and fin whale acoustic density estimates were visualized on a logarithmic scale to account for the wide dynamic range of call density observed across years and to show order-of-magnitude differences between inshore (station ≤ 60) and offshore (station > 60) recording stations (Fig. 3.5). For all call types, densities were higher inshore than offshore. Blue whale A calls were detected at the lowest densities overall, and offshore A calls were only detected in four recording years (2004, 2005, 2008, and 2010). Inshore A-call densities were highest in 2008 and 2019, and lowest in 2014 and 2016. No A calls were detected in 2009, 2013, 2015, 2017, or 2018. Blue whale B call densities were generally an order of magnitude higher than A-call densities and showed interannual variability, with consistently higher values inshore than offshore, although three out of four years with offshore A calls did not have offshore B calls. B-call densities were highest in 2008 and 2022 and lowest in 2005, 2007, 2014, and 2018. Unlike A calls, B calls were detected in every year with recording effort. Blue whale D calls were detected at similar magnitudes to A calls but were more consistently detected offshore than A calls. D-call densities were highest in summer 2024. The deployment with the highest number of D calls in the summer 2024 survey was reviewed and the calling pattern was consistent with the recently described D-call sequencing phenomenon (Arrieta, 2023). Elevated D-call densities were also observed in 2005 and 2006, while in 2010 and 2014 densities were low and

detections only occurred offshore. D calls were not detected in 2015 or 2021. Fin whale 20 Hz calls occurred at the highest densities of all call types and were detected in every year with recording effort, except 2018 which had no fall or winter effort. Densities were generally higher inshore than offshore, and after 2016 offshore densities were lower than years prior. The highest densities occurred in 2004, and densities were relatively stable across years although there was a decrease in inshore annual density in 2015. Fin whale 40 Hz calls were the most variable call type. Densities were higher inshore than offshore, and the highest densities occurred in 2007 and 2024. Between 2015–2023, call densities were low inshore and absent offshore.

3.4.4 Inter-call intervals

Inter-call intervals (ICIs) were computed on post-processed detections to investigate seasonal variability in calling rates. The ICI of A calls (number of seconds between one A call to the next) had a mode of 128 s, with a slight increase in fall relative to summer. The A-to-B ICI was the most stereotyped, with a mode of 49 s and nearly identical summer and fall distributions despite higher overall call counts in summer. The B-to-A ICI mode of 73 s was less stereotyped than the A-to-B transition but showed similar modal structure across summer and fall. The B-to-B ICI had a primary mode at 49 s with secondary modes at approximately 25 and 125 s, predominantly in summer. D call ICIs were highly variable with a mode of 6 s and were concentrated in summer. The dominant mode of fin whale 20-Hz call ICIs was 12 s in fall, with secondary modes at approximately 18 and 22 s, and winter distributions were slightly shorter and with lower counts (Fig. 3.6). Fin whale 40-Hz ICIs were highly variable and followed a similar distribution to D call ICIs, with a mode of 10 s in spring and secondary modes around 14 and 20 s in spring and summer.

3.5 Discussion

Despite their widespread adoption and emphasis on future potential, few studies have applied CNN-based detectors to long-term passive acoustic datasets where model generalization

across years, seasons, and background conditions is necessary (Best et al., 2022; Lammers et al., 2023; Shiu et al., 2020; Allen et al., 2021). Most CNN applications for baleen whale acoustic detection and classification focus on optimizing testing performance and do not operationally deploy models for ecological inference (Kirsebom et al., 2020; Madhusudhana et al., 2021; Zhong et al., 2021). Here, we developed a framework for constructing generalizable detectors from unlabeled data by using a combination of analyst labeling and detector-guided analyst auditing of labels. We show that by combining this framework with domain-specific knowledge of call characteristics and sound propagation modeling, we can generate ecologically meaningful measurements of call density.

We evaluated the Faster-R-CNN detector on labeled data from two independent platforms: a bottom-moored HARP and sonobuoy deployments from three CalCOFI surveys. The HARP mooring provided a continuous year-long recording from a single nearshore location, capturing seasonal peaks in calling activity, while CalCOFI sonobuoys provided short and discrete recordings across a broad spatial grid of inshore and offshore habitats. After three rounds of analyst refinement, the detector generalized across acoustic environments, with performance varying by call type for reasons discussed below.

The final model trained on the HITL-HNM refined dataset performed best on fin whale 20 Hz calls, which made up 25.4% of the training data. Fin whale 20 Hz calls are acoustically stereotyped, occur in high densities, and occupy a narrow frequency band with minimal overlap from other baleen whale downsweeps (Širović et al., 2013; Watkins et al., 1987; Watkins, 1981). These characteristics make them a comparatively straightforward target for deep-learning-based object detection (Best et al., 2022). In addition, their high abundance in our evaluation data stabilized precision–recall estimates and reduced sensitivity to individual misclassifications.

Blue whale D calls were present at high densities in the CHNMS evaluation dataset, where the final model's precision and recall exceeded 90% at low score thresholds, reflecting the model's ability to capture seasonal patterns in D call activity with high sensitivity and specificity.

In contrast, D calls were present in lower numbers in the CalCOFI summer 2008 test dataset. False positive rates were comparable to CHNMS; however, the reduced number of true positive events, likely due to seasonal timing outside peak calling periods and spatially limited occurrence across stations, resulted in fewer detections that could be evaluated. Although false positive rates were low, their persistence across low-density deployments contributed more false positives than true positives, reducing the proportional number of true detections available for performance estimation. Application of call-characteristic filters and received-level thresholds improved D call precision from 0.71 to 0.79 with minimal loss of recall, suggesting that domain-specific filtering was effective at removing isolated false detections in low-density recordings. A similar pattern can occur in continuous recordings from long-term mooring deployments when they fall outside high-density calling seasons. However, continuous long-term recordings also capture the most acoustically active months of the year, resulting in higher true positive calling rates that reduce the proportional influence of false detections, resulting in better statistical performance. A similar pattern was evident for blue whale A and B call performance across the CalCOFI and CHNMS test datasets. The CHNMS deployment captured the seasonal peak in blue whale singing, characterized by high call rates of A and B calls in late September. The CalCOFI summer 2008 and fall 2023 evaluation datasets also contained deployments with high call rates, but false detection rates carried more weight in the precision-recall estimates because there were fewer total true positive detections available for evaluation.

Fin whale 40 Hz calls were the most challenging category for the final model trained on the HITL-HNM refined dataset. These calls are produced irregularly with large spectral variability (Širović et al., 2013; Watkins, 1981) and constituted only 9% of the final training annotations (1430 calls). This data sparsity likely contributed to lower classifier performance. Additional factors affecting performance included confusion with humpback whale downsweeps and the tendency for the performance of infrequent call categories to be more severely impacted by false positives. Early iterations of the HITL review resulted in the inclusion of humpback

whale calling bouts as hard negatives. The review was also responsible for a seven fold increase in the number of labeled calls used in training. These refinements improved 40 Hz call precision by an average of 26%, substantially reducing the number of humpback whale downsweeps mislabeled as fin whale 40 Hz calls. Despite these improvements, persistent humpback whale singing in the CHNMS dataset continued to contribute to false positives. Humpback whale songs span wide spectral and temporal ranges (Payne and McVay, 1971) and represent a major source of interference when detecting spectrally similar calls from other baleen whale species (Darias-O'Hara et al., 2026; Baumgartner et al., 2013). Future work could explore focal loss or class-balanced sampling to improve performance on 40 Hz calls, as well as transformer-based architectures capable of learning the temporal contextual space (Hagiwara, 2023; Zhang et al., 2025; Schafer-Zimmermann et al., 2024; Robinson et al., 2024) to better discriminate humpback downsweeps from those of rarer baleen whales in acoustically complex environments.

The CHNMS mooring recorded at a shallow nearshore location off Point Conception recognized as a biologically important area (BIA) for humpback whales (Calambokidis et al., 2015, 2024), a pattern reflected acoustically by persistent singing activity. Because the majority of CalCOFI recordings were collected within fin whale BIAs and outside humpback BIAs Calambokidis et al. (2015, 2024), humpback false positives are expected to be substantially lower in the CalCOFI 40 Hz time series than in the CHNMS evaluation data. Furthermore, the present detector consistently separated blue whale D calls from fin whale 40 Hz calls, with little confusion between the two, which has been difficult in the past (Rasmussen and Širović, 2021). We therefore interpret the call-characteristic filtered and received-level–thresholded 40 Hz time series as being dominated by true fin whale 40 Hz calling, while acknowledging that residual errors remain that were incorporated into our call density uncertainty estimates.

Translating detections from the operational detector into standardized call density estimates required accounting for variation in detection area across the inshore-offshore gradient sampled by CalCOFI. Simulation-based studies have shown that detection area can vary greatly

due to environmental conditions and call characteristics (Harris et al., 2025; Helble et al., 2013; Miotto, 2025). Using our empirical data, we adopted a similar, yet simplified approach to capture the dominant inshore–offshore contrasts in detectability, comparing detected RLs with simulated RLs from propagation models and applying a conservative detectability threshold above which detection probability was assumed to be one. We report average annual call densities for inshore and offshore habitats. Because the inshore propagation models were produced across a representative range of bathymetric complexity within the Southern California Bight, the resulting mean inshore detection area likely provided an unbiased metric for estimating mean inshore call density. Uncertainty in detection area was propagated into the density estimates, capturing inshore variability and likely some seasonal and interannual variability in propagation conditions, though not explicitly modeled (Harris et al., 2025; Helble et al., 2013; Miotto, 2025). Miotto (2025) showed that detection area variability for blue whale D calls in the Southern California Bight is approximately $\pm 15\%$ at received level thresholds ≥ 95 dB due to seasonal and interannual changes in upper-ocean conditions, and that this variability is greater at basin and shelf-break stations than at offshore recording stations. The $\pm 15\%$ detection area variability reported by Miotto (2025) at the ≥ 95 dB threshold suggests that temporal changes in ocean conditions introduced minimal bias into our density estimates, significantly smaller than the uncertainty already included by the range of inshore detection areas within the Southern California Bight. Additionally, sonobuoy drift during deployments may have introduced minor positional uncertainty, with the greatest potential influence in inshore environments where detection ranges are smallest.

After standardizing detections by recording effort and detection area, the call density time series showed patterns consistent with prior observations from bottom-mounted recorders inshore of the continental shelf (Lewis and Širović, 2018; Širović et al., 2015) and new findings extending those observations further offshore and across a longer time period. Across call types, densities were generally higher inshore than offshore. This is consistent with ship-based

visual sightings (Campbell et al., 2015) and reflects the Southern California Bight's role as a biologically important foraging region for blue and fin whales (Calambokidis et al., 2015, 2024). Blue whale A and B call densities were higher inshore, in agreement with prior observations of greater singing activity at nearshore sites (Lewis and Širović, 2018). Our results show that B calls were detected offshore in most years, while A calls were detected in offshore habitats only occasionally. Lewis and Širović (2018) documented inshore dominance of AB-type songs and offshore dominance of ABB-type songs. Combined with our finding that A calls are mostly absent past the continental slope, this may suggest a gradient in song type proportions with increasing distance from shore, potentially driven by the greater propagation range of B calls in deep water favoring their production for long-range mate attraction (Lewis and Širović, 2018; Širović et al., 2015). Blue whale D calls were also detected beyond the continental slope in most years, suggesting some feeding or social behaviors occur offshore (Oleson et al., 2007a), consistent with tag-based observations of blue whales foraging on dispersed prey patches beyond the continental shelf (Irvine et al., 2019). Similar to blue whales, fin whale call densities were generally higher inshore than offshore. Širović et al. (2015) found that fin whale 20 Hz calls were detected in higher densities at southern, offshore sites than blue whale B calls, which were detected in higher densities at northern, inshore sites. Fin whale 20 Hz calls were detected in the highest densities beyond the continental shelf of any call type, supporting the habitat separation hypothesis proposed by Širović et al. (2015) Fin whale 40 Hz calls were detected in similar inshore-offshore magnitudes to blue whale D calls, suggesting that both species extend their foraging effort into offshore waters where prey is more dispersed (Irvine et al., 2019). While offshore occurrence of both species has been documented through tagging studies (Irvine et al., 2019; Hazen et al., 2017; Palacios et al., 2025), the consistency of acoustic detections across most years provides the first long-term passive acoustic evidence of regular blue and fin whale acoustic activity beyond the continental shelf.

Interannual variability appeared associated with anomalous oceanographic conditions,

with reduced blue whale call density during El Niño and/or marine heatwave periods in 2009–2010 and 2014–2016 (Ryan et al., 2025; ZoBell et al., 2025). Fin whale 20 Hz and 40 Hz call densities also declined in offshore habitats following the 2014–2016 marine heatwave, while inshore 20 Hz densities were stable, suggesting a potential shoreward contraction of fin whale singing and foraging activity in recent years. The period from 2019 to 2021 was also anomalously warm (Weber et al., 2021; Thompson et al., 2022), and blue whale D calls were detected in lower densities, similar to fin whale 40 Hz calls which were detected in 2019 but not in 2021, suggesting that the warm, stratified conditions may provide reduced foraging opportunities in the region, which has been proposed elsewhere (Barlow et al., 2023). In 2024, however, fin whale 40 Hz calls were detected in high densities, concurrent with the spike in blue whale D call densities due to D-call sequencing (Arrieta, 2023), suggesting that both species may have responded to a common change in prey availability that year. The observed interannual patterns likely reflect species-specific prey preferences, with each species tracking and responding to shifts in the distribution and abundance of their preferred prey (Nickels et al., 2019, 2018; Irvine et al., 2019), warranting further investigation.

We hypothesize that much of the variability in our time series arises from fine-scale changes in acoustic behavioral states intermittently captured by the CalCOFI sampling design. Blue whale D-call sequencing events during summer 2024, for example, increased inshore call densities by an order of magnitude relative to other years, highlighting the difficulty of estimating baleen whale acoustic cue rates, which are strongly dependent on behavioral state and sex (Lewis et al., 2018; Guazzo et al., 2024). The close agreement between our reported ICI modes and those from manually verified annotations (Lewis and Širović, 2018; Arrieta, 2023; Širović et al., 2017; Oleson et al., 2007a) supports the reliability of our approach and its feasibility for investigating fine-scale calling and singing behavior. Although we did not classify A and B calls into categorical song types, the observed ICI patterns were consistent with those of Lewis and Širović (2018), who performed such classification. The highly stereotyped A–B ICI

of 49 s exactly matches the value of 49 $\pm$ 7 s reported by Lewis and Širović (2018) and is close to the 47.8 $\pm$ 3.7 s value reported by Oleson et al. (2007a). The more variable B–A ICI mode of 73 s falls between the inter-phrase interval of 70 $\pm$ 29 s of Lewis and Širović (2018) and the 83 $\pm$ 21.1 s B–A ICI of Oleson et al. (2007a). The multimodal B–B ICI distribution, with a primary mode at 49 s near Lewis and Širović (2018) reported 51 s interval and secondary modes at approximately 25 and 125 s, is consistent with the presence of AB and ABB song types: the shortest mode may reflect overlapping singers or singular call bouts (Oleson et al., 2007a; Lewis and Širović, 2018), while the 49 s mode likely reflects the consecutive B calls of ABB phrases, and the longest mode likely reflects the ICI between two B calls separated by an intervening A call. The close agreement in A–B ICIs among these three datasets and the seasonally stable 49 s mode in our recordings suggests that the primary component of eastern North Pacific blue whale song has not undergone change of the magnitude documented elsewhere; Miller et al. (2014) reported ICIs approximately 15 s longer in 2013 than in 1997 for New Zealand blue whales. Whether subtler long-term change is occurring in the eastern North Pacific remains an open question.

Fin whale 20-Hz ICI modes broadly matched literature values, with a dominant mode of 12 s in fall and secondary modes at approximately 18 and 22 s, consistent with the short doublet song pattern reported in Southern California from 2006–2012 by Širović et al. (2017), which showed ICIs increasing gradually from approximately 10/15 s to 15/20 s over that period. The co-occurrence of multiple distinct modes may reflect continued long-term lengthening of fin whale song ICIs in the SCCE, consistent with trends documented in the Southern California Bight (Širović et al., 2017), off Oregon and Washington (Weirathmueller et al., 2017), and in the Central Pacific (Helble et al., 2020, 2025). Fin whale 40-Hz ICIs were shorter than previously reported values in Southern California (Wiggins and Hildebrand, 2020) and highly variable, though the consistency of multiple seasonal modes warrants further investigation.

Our ecological findings are consistent with prior observations and apply deep learning

to extend them over a longer time period and across a wider spatial range. Prior studies characterizing blue and fin whale call and song structure provided the foundation for validating our automated outputs, and the close agreement between our ICI estimates and manually inspected values speaks to the reliability of our approach and the value of prior work. By iteratively refining training data through human-assisted auditing, we show that deep-learning detectors can generalize across diverse acoustic environments without requiring large pre-labeled datasets. Paired with propagation modeling and domain knowledge of call characteristics, this approach yielded standardized call density estimates that captured patterns of habitat use and interannual variability for the two largest baleen whales, whose far-reaching calls and songs dominate low-frequency soundscapes of the eastern North Pacific.

3.6 Acknowledgments

We thank the many Scripps Whale Acoustics Lab students and collaborators who deployed sonobuoys over the last twenty years and we especially thank Katherine Whittaker, Greg Campbell, Lauren Roche, Melissa Soldevilla, Regina Guazzo, Bruce Thayre, and Jack Ewing for their contributions to the broader CalCOFI marine mammal monitoring program.
Chapter 3, in full, is currently in review for publication in Scientific Reports. Alksne, Michaela N., Roch, Marie A., Frasier, Kaitlin E., Hildebrand, John A., Andres, Shane, Adesanya, Dolapo, Baggett, Lauren M., Jones, Joshua M., Širović, Ana, Baumann-Pickering, Simone. Springer Nature, 2026. The dissertation author was the primary investigator and author of this paper.

3.7 Figures and Tables

3.8 Data availability

The blue and fin whale annual call density estimates generated and analyzed in this study are available in the Dryad repository, DOI:10.5061/dryad.dbrv15fh1.

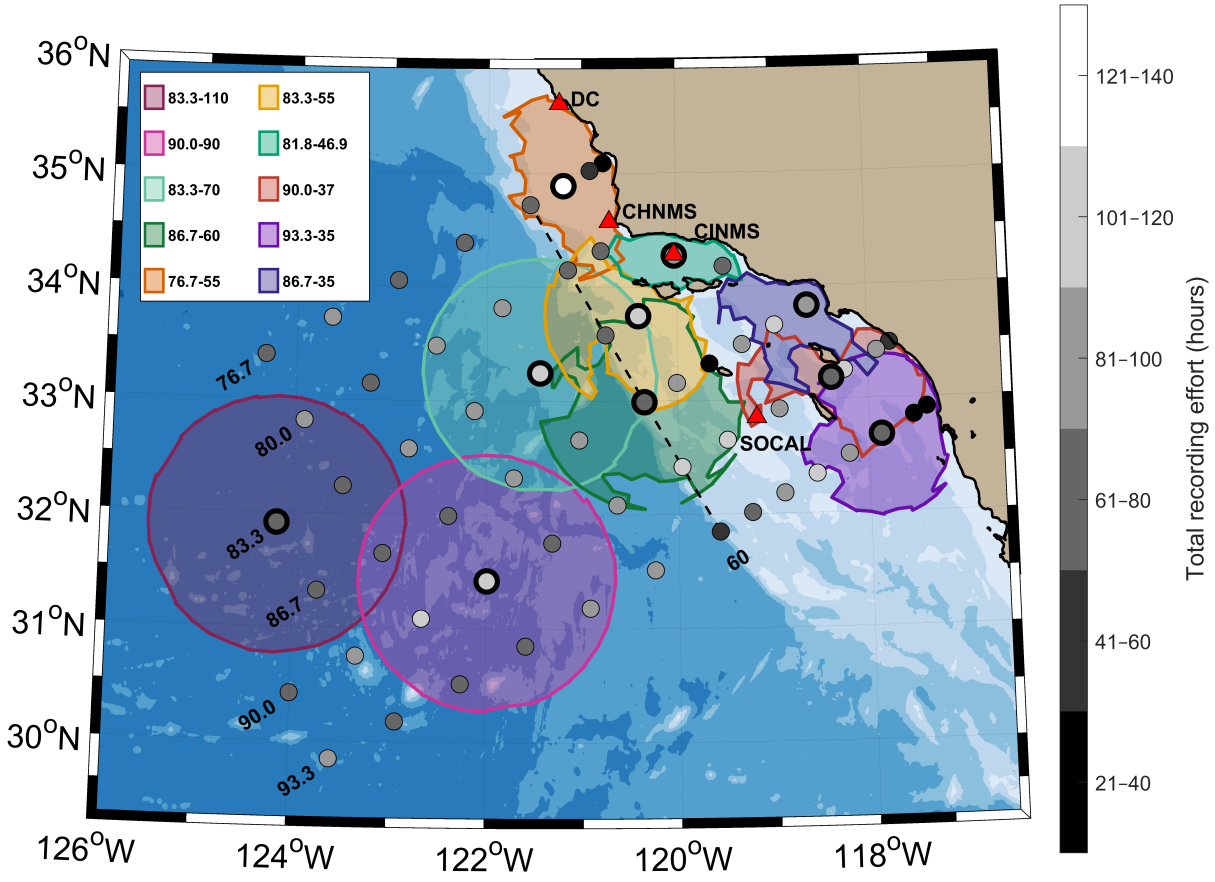


Figure 3.1. Total CalCOFI sonobuoy acoustic recording effort across the Southern California Current Ecosystem, HARP deployment sites, and estimated blue whale D call detection areas at ten representative stations. Cumulative recording effort (hours) at each CalCOFI station is summed across all deployments from that station, with the grayscale shading of each station marker indicating binned recording effort as shown in the colorbar. Numbers on the western edge of the map refer to CalCOFI survey lines which run from southwest to northeast. A dashed line connects station 60 across all survey lines, delineating inshore (station number ≤ 60) from offshore (station number > 60) recording stations. HARP stations are indicated by red triangles with respective station names. Colored polygons indicate the estimated acoustic detection area for blue whale D calls (received level ≥ 95 dB re 1 µPa) at ten representative CalCOFI stations, based on range-dependent acoustic propagation modeling with assumptions outlined in the methods (e.g., fixed source level). Thick black open circles identify the sonobuoy deployment location at each modeled station.

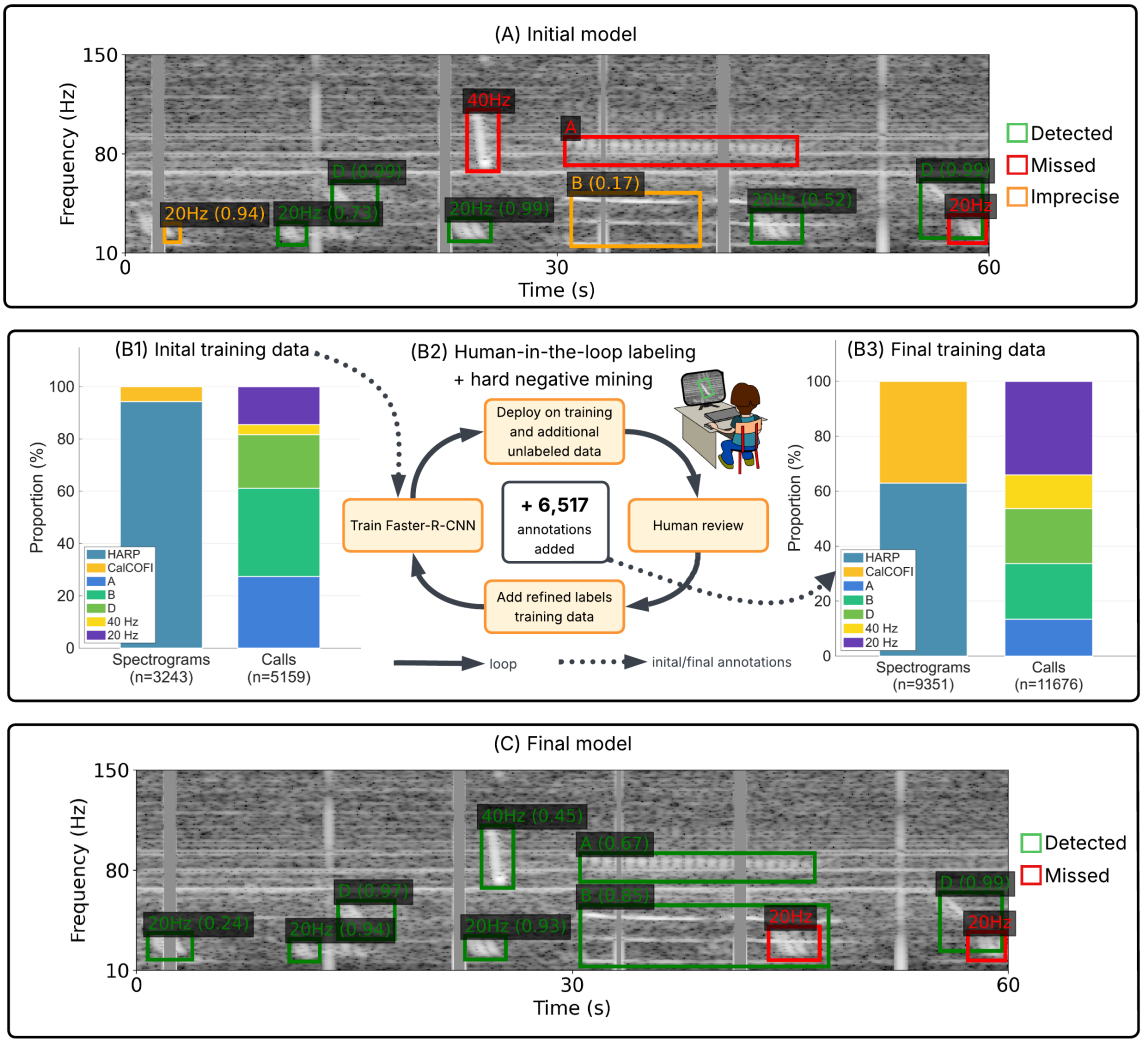


Figure 3.2. Iterative human-in-the-loop training pipeline for blue and fin whale call detection. (A) Example 60-second spectrogram from a CalCOFI sonobuoy deployment (Summer 2008) with detections from the initial model. Bounding boxes indicate detected calls (green), missed calls (red), and imprecise detections (orange), with call type and confidence score labeled. (B1) Training data composition prior to iterative refinement, showing the proportion of unique spectrograms and labeled calls by recording platform (HARP vs. CalCOFI) and call type. (B2) The iterative human-in-the-loop labeling and hard negative mining workflow. Over three rounds, the current model was deployed on unlabeled HARP and CalCOFI sonobuoy data, predictions were reviewed by a human analyst, and confirmed detections, missed calls, and hard negatives were added to the training set, adding 6,517 annotations in total. (B3) Training data composition after three rounds of iterative refinement, showing increased representation of CalCOFI sonobuoy spectrograms and a more balanced call type distribution relative to the initial training data. (C) The same example spectrogram as in (A) with predictions from the final model, showing improved detection of previously missed call types and more precise call localization relative to the initial model.

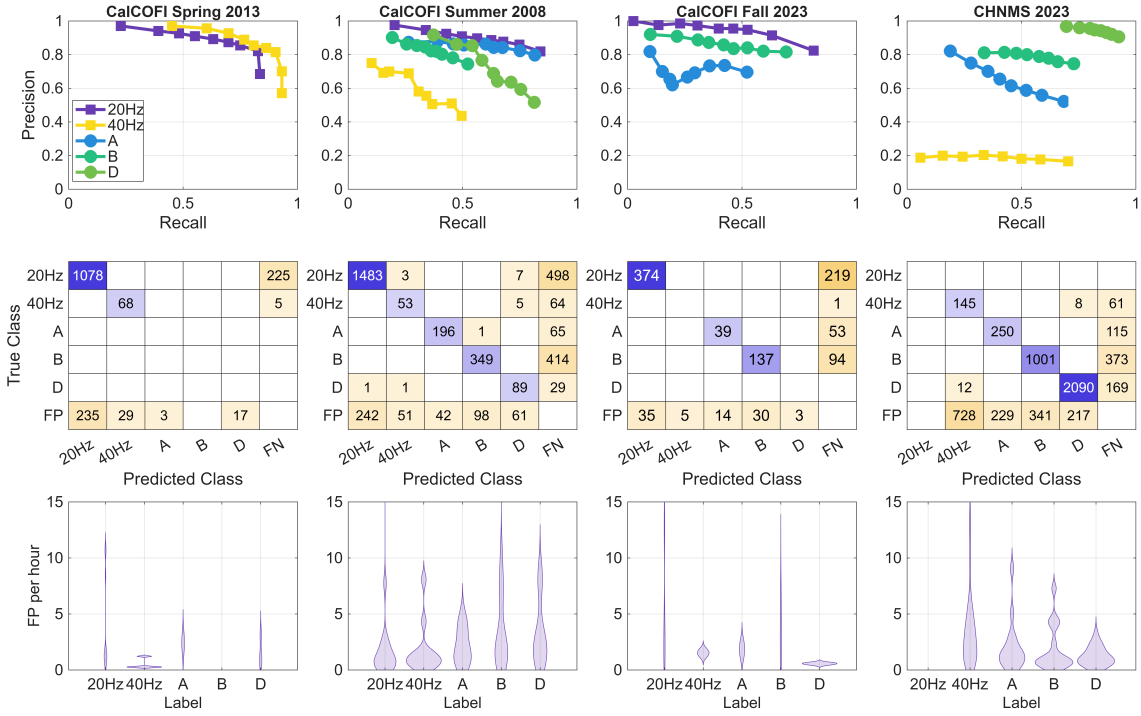


Figure 3.3. Performance statistics for the third model configuration across four evaluation datasets. Top: precision–recall curves for each call type across CalCOFI Spring 2013, CalCOFI Summer 2008, CalCOFI Fall 2023, and CHNMS 2023 (IoU $\geq$ 0.5; points reflect increasing score thresholds from 0.1 to 0.9). Middle: confusion matrices at the operating score threshold (0.2) and IoU $\geq$ 0.5. FP-false positive; FN-false negative. Bottom: false-positive rates (FP h^{-1}) by call type across sonobuoy deployments or 5-h bins, shown as violin plots.

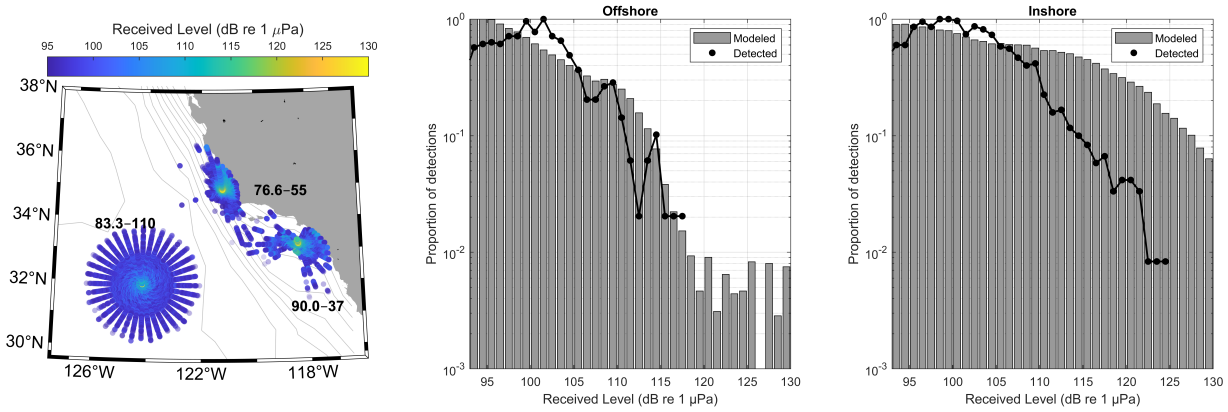


Figure 3.4. Received level distributions for blue whale D calls used for call density estimation. Left: Modeled received levels (dB re 1 µPa) across the southern California Current Ecosystem for representative offshore and inshore stations. Center and right: Distributions of received levels for detected calls in offshore (center) and inshore (right) environments. Gray bars show modeled received level distributions from propagation modeling, while black points show received levels of detected calls.

3.9 Code availability

The fine-tuned Faster R-CNN model weights used in this study are available in the Zenodo repository, DOI:10.5281/zenodo.19164290. The code to run inference or retrain the model is available on GitHub: https://github.com/m1alksne/WhaleMoanDetector and the code for human-in-the-loop auditing of model predictions is also on GitHub: https://github.com/m1alksne/WhaleMoanViz.

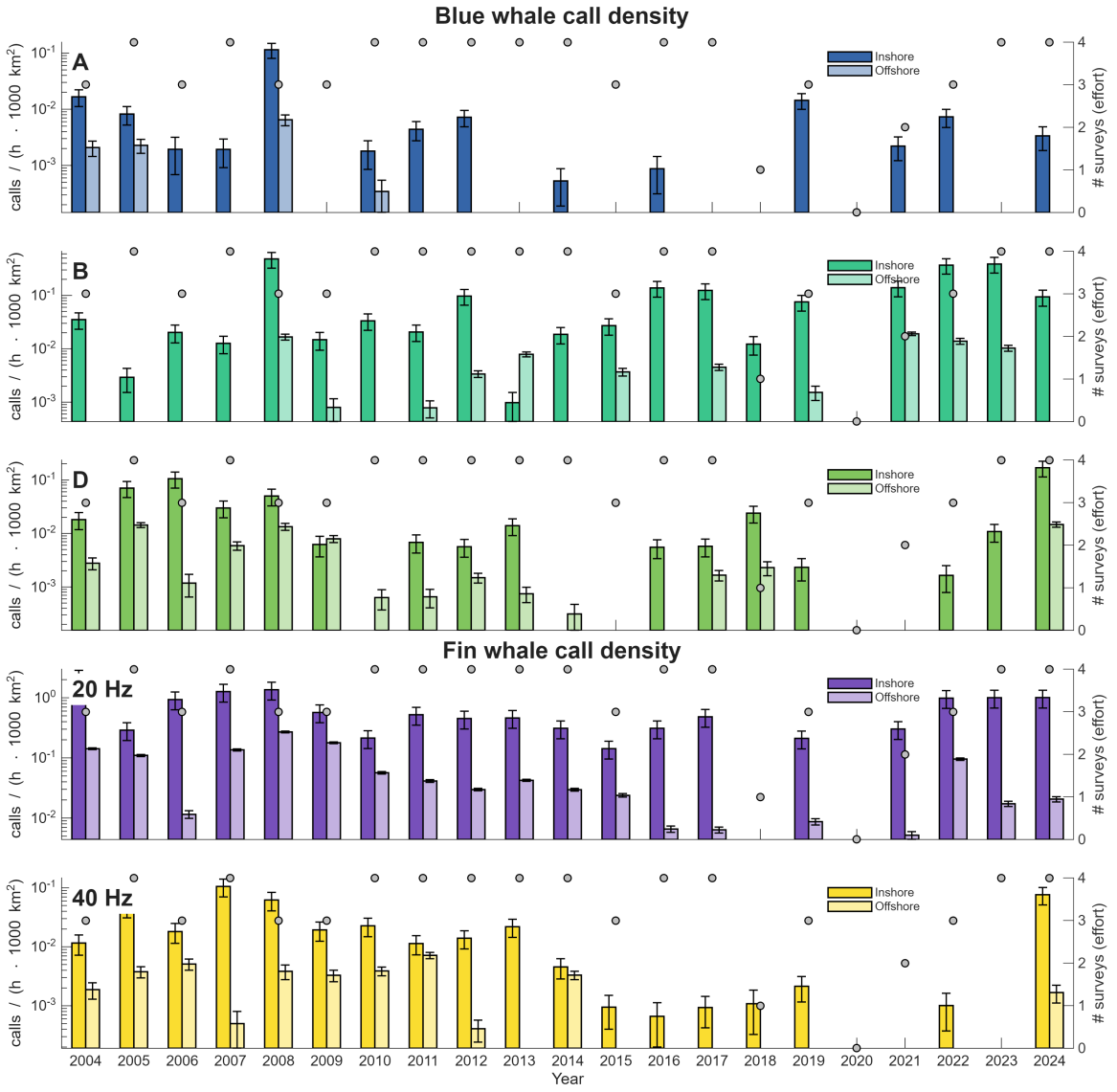


Figure 3.5. Annual inshore and offshore call density for blue and fin whale call types estimated from the 20-year CalCOFI sonobuoy archive (2004–2024). Bars show annual call density $\left(\frac{\text{calls}}{\text{h}\cdot 1000\ \text{km}^2}\right)$ computed from post-processed Faster R-CNN detections and normalized by recording effort and call-type–specific detection area. Densities are shown on a logarithmic scale to visualize order-of-magnitude variability and to compare inshore (darker colors; station number ≤ 60) and offshore (lighter colors; station number > 60) habitats. Error bars represent ± 1 standard error. Note that error bars appear asymmetric due to the logarithmic scale. Gray points (secondary axis) show number of acoustic surveys contributing to each estimate.

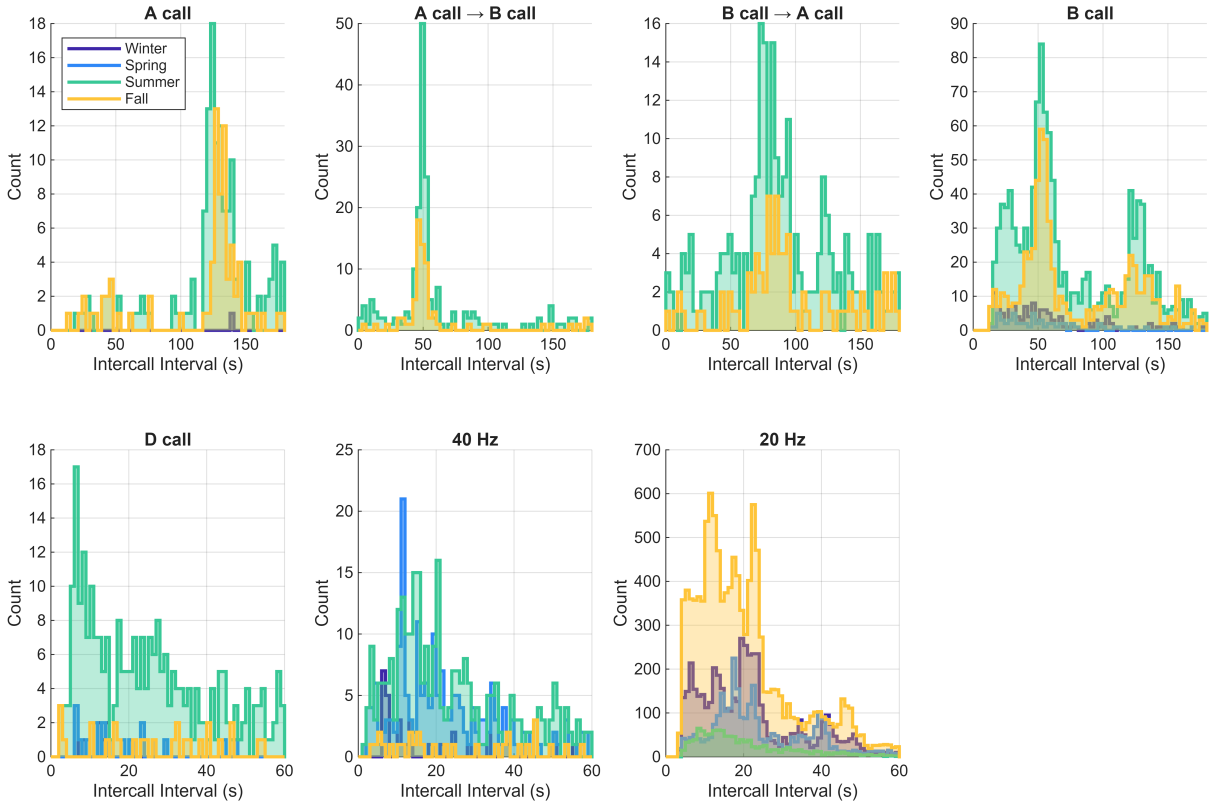


Figure 3.6. Intercall interval (ICI) distributions for blue and fin whale call types and call transitions. Histograms show the distribution of intercall intervals (ICIs; seconds) computed from long-term passive acoustic detections across all analyzed sonobuoy deployments. Panels correspond to blue whale A calls, A→B call transitions, B→A call transitions, B calls, D calls, and fin whale 20 Hz and 40 Hz calls. ICIs were calculated as the elapsed time between the start of consecutive detections of the same call type within a given sonobuoy deployment, after applying call-specific filters and thresholds; A→B or B→A ICIs represent the time from an A or B call to the immediately following B or A call, respectively.

Table 3.1. Platform and call-type composition of the training, validation, and test datasets. Each spectrogram represents a 60-second window of acoustic recordings from either HARP or CalCOFI sonobuoy deployments. Initial training labels reflect analyst annotations prior to HITL auditing; final training labels reflect three rounds of HITL auditing in which model predictions were reviewed and corrected by analysts. Background spectrograms, being those that did not contain blue or fin whale calls, were incorporated as hard negatives during HITL auditing to improve model specificity on recordings with no blue or fin whale acoustic activity. Zeros in the training and testing column indicates that a given call or spectrogram type was not present in that dataset. Dash in the test column indicates no evaluation effort for a given call type in that dataset (i.e., 20 Hz calls were not evaluated in the HARP test set).

	Training				**Validation**	**Test**			
	Initial		**Final**			**Sum. 2008**	**Spr. 2013**	**Fall 2023**	**CHNMS**
	HARP	*CalCOFI*	*HARP*	*CalCOFI*	*HARP*	*CalCOFI*	*CalCOFI*	*CalCOFI*	*HARP*
60-s spectrograms									
With calls	3,058	185	5,602	672	634	1,265	655	338	2,457
Background	0	0	285	2,792	37	2,904	6,286	628	13,693
Total	**3,058**	**185**	**5,887**	**3,464**	**671**	**4,169**	**6,941**	**966**	**16,150**
Combined total	**3,243**		**9,351**		**671**	**28,226**			
Call annotations									
A	1,413	0	1,520	47	162	261	0	92	365
B	1,741	0	2,047	318	202	763	0	231	1,374
D	1,058	0	2,282	55	246	118	0	0	2,259
20 Hz	0	749	2,974	1,003	348	1,981	1,302	593	—
40 Hz	182	16	1,340	90	169	117	73	1	206
Total	**4,394**	**765**	**10,163**	**1,513**	**1,127**	**3,240**	**1,375**	**917**	**4,204**
Combined total	**5,159**		**11,676**		**1,127**	**9,736**			

Table 3.2. Mean precision and recall by call type for the initial detector, the final detector after HITL refinement, and the final operational detector incorporating contextual call-characteristic filtering and received-level (RL) thresholding. Metrics are averaged across independent CalCOFI and CHNMS test datasets at a detection score threshold of 0.2 and an IoU threshold of 0.5. Bold values indicate the highest precision and recall achieved for each call type.

	Initial		Final		Final + Context + RL	
Call type	Precision	Recall	Precision	Recall	Precision	Recall
A	0.69	0.30	0.70	0.62	**0.71**	**0.71**
B	0.35	0.10	0.78	**0.59**	**0.83**	0.51
D	0.76	0.58	0.71	**0.84**	**0.79**	0.81
20 Hz	0.59	0.32	**0.86**	**0.74**	0.84	0.73
40 Hz	0.29	0.35	0.39	**0.69**	**0.42**	0.65

Table 3.3. Call-specific source levels (SL) and received-level (RL) detection thresholds used for propagation modeling and detection-area estimation. Inshore areas represent the mean across seven modeled stations located inshore of the continental slope; offshore areas represent the mean across three offshore stations.

Species / Call type	SL (dB re 1 μPa)	SL Bandwidth (Hz)	SL Reference	RL (dB re 1 μPa)	Inshore Area (km^2)	Offshore Area (km^2)
Blue whale A call	178	10–110	McDonald et al. McDonald et al. (2001)	90	13,567	37,340
Blue whale B call	186	10–110	McDonald et al. McDonald et al. (2001)	96	15,284	39,071
Blue whale D call	190	43–88	Miller et al. Miller et al. (2021)	95	16,168	39,900
Fin whale 20-Hz call	189	15–25	Weirathmuller et al. Weirathmueller et al. (2013)	96	15,171	39,355
Fin whale 40-Hz call	188	41–60	Wiggins & Hildebrand Wiggins and Hildebrand (2020)	94	15,671	39,676

Bibliography

Aboyomi, D. D. and Daniel, C. (2023). A comparative analysis of modern object detection algorithms: YOLO vs. SSD vs. faster R-CNN. *ITEJ (Information Technology Engineering Journals)*, 8(2):96–106.

Ahmed, I. and Das, R. (2025). Comparative Analysis of YOLO and Faster R-CNN Models for Detecting Traffic Object. *International Journal of Advanced Computer Science & Applications*, 16(3).

Allen, A. N., Harvey, M., Harrell, L., Jansen, A., Merkens, K. P., Wall, C. C., Cattiau, J., and Oleson, E. M. (2021). A Convolutional Neural Network for Automated Detection of Humpback Whale Song in a Diverse, Long-Term Passive Acoustic Dataset. *Frontiers in Marine Science*, 8(607321).

Arrieta, G. M. (2023). *Calling Behavior and Localization of Blue Whales in Southern California*. Thesis, University of California, San Diego.

Barlow, D. R., Klinck, H., Ponirakis, D., Branch, T. A., and Torres, L. G. (2023). Environmental conditions and marine heatwaves influence blue whale foraging and reproductive effort. *Ecology and Evolution*, 13(2):e9770.

Baumgartner, M. F., Fratantoni, D. M., Hurst, T. P., Brown, M. W., Cole, T. V., Van Parijs, S. M., and Johnson, M. (2013). Real-time reporting of baleen whale passive acoustic detections from ocean gliders. *Journal of the Acoustical Society of America*, 134(3):1814–1823.

Best, P., Marxer, R., Paris, S., and Glotin, H. (2022). Temporal evolution of the Mediterranean fin whale song. *Scientific reports*, 12(1):13565.

Bloom, S., Alksne, M., Rice, A., Lankhorst, M., Širović, A., Warren, J., and Baumann-Pickering, S. (2025). Seasonal changes in physical oceanography modulate cetacean predator-prey dynamics in the San Diego Trough. *Marine Ecology Progress Series*, 762:111–133.

Calambokidis, J., Kratofil, M. A., Palacios, D. M., Lagerquist, B. A., Schorr, G. S., Hanson, M. B., Baird, R. W., Forney, K. A., Becker, E. A., and Rockwood, R. C. (2024). Biologically important areas II for cetaceans within US and adjacent waters-West Coast Region. *Frontiers*

in Marine Science, 11:1283231.

Calambokidis, J., Steiger, G. H., Curtice, C., Harrison, J., Ferguson, M. C., Becker, E., DeAngelis, M., and Van Parijs, S. M. (2015). Biologically important areas for selected cetaceans within US waters-west coast region. *Aquatic Mammals*, 41(1):39.

Campbell, G. S., Thomas, L., Whitaker, K., Douglas, A. B., Calambokidis, J., and Hildebrand, J. A. (2015). Inter-annual and seasonal trends in cetacean distribution, density and abundance off southern California. *Deep Sea Research Part II: Topical Studies in Oceanography*, 112:143–157.

Collins, M. D. (1995). User's Guide for RAM Versions 1.0 and 1.0 p. *Naval Research Lab, Washington, DC*, 20375:14.

Cooke, J. (2018a). *Balaenoptera musculus*. *The IUCN red list of threatened species*, pages 2018–2.

Cooke, J. (2018b). *Balaenoptera physalus*. *The IUCN red list of threatened species*, pages 2018–2.

Croll, D. A., Clark, C. W., Acevedo, A., Tershy, B., Flores, S., Gedamke, J., and Urban, J. (2002). Only male fin whales sing loud songs. *Nature*, 417(6891):809–809.

Darias-O'Hara, A. K., Nguyen Hong Duc, P., Madhusudhana, S., McCauley, R., Tollefsen, C., Erbe, C., and Miller, B. S. (2026). Machine Learning Methods for the Detection of Antarctic Minke Whales (*Balaenoptera bonaerensis*) in East Antarctica and Western Australia. *Marine Mammal Science*, 42(1):e70118.

Garcia, M. L., Tolkova, I., Madhusudhana, S., Rahaman, A., Baker, C. S., Mayo, C. A., Hudak, C. A., and Klinck, H. (2025). Acoustic abundance estimation for Critically Endangered North Atlantic Right whales in Cape Cod bay, Massachusetts, USA. *Endangered Species Research*, 56:101–115.

Gillespie, D., Macaulay, J., Oswald, M., and Roch, M. (2026). PAMGuard: Application software for passive acoustic detection, classification, and localisation of animal sounds. *Journal of the Acoustical Society of America*, 159(1):437–443.

Guazzo, R. A., Stevenson, D. L., Edell, M. K., Gagnon, G. J., and Helble, T. A. (2024). A decade of change and stability for fin whale song in the North Atlantic. *Frontiers in Marine Science*, 11:1278068.

Hagiwara, M. (2023). Aves: Animal vocalization encoder based on self-supervision. In *ICASSP 2023-2023 IEEE International Conference on Acoustics, Speech and Signal Processing*

(ICASSP), pages 1–5. IEEE.

Harris, D. V., Mellinger, D. K., Heaney, K. D., Clarke, T., Miles, D., and Thomas, L. (2025). Estimating the detection probability of long-ranging baleen whale song using a single sensor: Towards density estimation. *Journal of the Acoustical Society of America*, 158(6):4582–4593.

Harris, D. V., Miksis-Olds, J. L., Vernon, J. A., and Thomas, L. (2018). Fin whale density and distribution estimation using acoustic bearings derived from sparse arrays. *Journal of the Acoustical Society of America*, 143(5):2980–2993.

Hazen, E. L., Palacios, D. M., Forney, K. A., Howell, E. A., Becker, E., Hoover, A. L., Irvine, L., DeAngelis, M., Bograd, S. J., and Mate, B. R. (2017). WhaleWatch: a dynamic management tool for predicting blue whale density in the California Current. *Journal of Applied Ecology*, 54(5):1415–1428.

Helble, T. A., D'Spain, G. L., Hildebrand, J. A., Campbell, G. S., Campbell, R. L., and Heaney, K. D. (2013). Site specific probability of passive acoustic detection of humpback whale calls from single fixed hydrophones. *Journal of the Acoustical Society of America*, 134(3):2556–2570.

Helble, T. A., Guazzo, R. A., Alongi, G. C., Martin, C. R., Martin, S. W., and Henderson, E. E. (2020). Fin whale song patterns shift over time in the central North Pacific. *Frontiers in Marine Science*, 7:587110.

Helble, T. A., Guazzo, R. A., Dugan, P. J., Alongi, G. C., Martin, C. R., Martin, S. W., and Henderson, E. E. (2025). Twelve years of fin whale song evolution in the central North Pacific. *Frontiers in Marine Science*, 12:1642598.

Hildebrand, J. A., Frasier, K. E., Baumann-Pickering, S., and Wiggins, S. M. (2021). An empirical model for wind-generated ocean noise. *Journal of the Acoustical Society of America*, 149(6):4516–4533.

Hilmo, R., Harris, D., and Wilcock, W. (2025). Applying distance sampling to estimate densities of fin whale calls recorded by ocean bottom seismometers in the Marianas region. *Endangered Species Research*, 58:159–174.

Irvine, L. M., Palacios, D. M., Lagerquist, B. A., and Mate, B. R. (2019). Scales of blue and fin whale feeding behavior off California, USA, with implications for prey patchiness. *Frontiers in Ecology and Evolution*, 7:338.

Kather, V., Seipel, F., Berges, B., Davis, G., Gibson, C., Harvey, M., Henry, L.-A., Stevenson, A., and Risch, D. (2024). Development of a machine learning detector for North Atlantic humpback whale song. *Journal of the Acoustical Society of America*, 155(3):2050–2064.

Kirsebom, O. S., Frazao, F., Simard, Y., Roy, N., Matwin, S., and Giard, S. (2020). Performance of a deep neural network at detecting North Atlantic right whale upcalls. *Journal of the Acoustical Society of America*, 147(4):2636–2646.

Lammers, M. O., Goodwin, B., Kugler, A., Zang, E. J., Harvey, M., Margolina, T., Martinez, J. A., Merkens, K., and Hatch, L. T. (2023). The occurrence of humpback whales across the Hawaiian archipelago revealed by fixed and mobile acoustic monitoring. *Frontiers in Marine Science*, 10:1083583.

Lewis, L. A., Calambokidis, J., Stimpert, A. K., Fahlbusch, J., Friedlaender, A. S., McKenna, M. F., Mesnick, S. L., Oleson, E. M., Southall, B. L., Szesciorka, A. R., and Širović, A. (2018). Context-dependent variability in blue whale acoustic behaviour. *Royal Society Open Science*, 5(8):180241.

Lewis, L. A. and Širović, A. (2018). Variability in blue whale acoustic behavior off southern California. *Marine Mammal Science*, 34(2):311–329.

Madhusudhana, S., Shiu, Y., Klinck, H., Fleishman, E., Liu, X., Nosal, E.-M., Helble, T., Cholewiak, D., Gillespie, D., Širović, A., and Roch, M. A. (2021). Improve automatic detection of animal call sequences with temporal context. *Journal of the Royal Society Interface*, 18(180):20210297.

Marques, T. A., Munger, L., Thomas, L., Wiggins, S., and Hildebrand, J. A. (2011). Estimating North Pacific right whale *Eubalaena japonica* density using passive acoustic cue counting. *Endangered Species Research*, 13(3):163–172.

Marques, T. A., Thomas, L., Martin, S. W., Mellinger, D. K., Ward, J. A., Moretti, D. J., Harris, D., and Tyack, P. L. (2013). Estimating animal population density using passive acoustics. *Biological reviews*, 88(2):287–309.

Marques, T. A., Thomas, L., Ward, J., DiMarzio, N., and Tyack, P. L. (2009). Estimating cetacean population density using fixed passive acoustic sensors: An example with Blainville's beaked whales. *Journal of the Acoustical Society of America*, 125(4):1982–1994.

McDonald, M., Hildebrand, J. A., and Mesnick, S. (2009). Worldwide decline in tonal frequencies of blue whale songs. *Endangered Species Research*, 9:13–21.

McDonald, M. A., Calambokidis, J., Teranishi, A. M., and Hildebrand, J. A. (2001). The acoustic calls of blue whales off California with gender data. *Journal of the Acoustical Society of America*, 109(4):1728–1735.

Mellinger, D. (2002). Ishmael 1.0 User's Guide. Technical report, NOAA/PMEL.

Miller, B. S., Calderan, S., Leaper, R., Miller, E. J., Širović, A., Stafford, K. M., Bell, E., and Double, M. C. (2021). Source level of Antarctic blue and fin whale sounds recorded on sonobuoys deployed in the deep-ocean off Antarctica. *Frontiers in Marine Science*, 8:792651.

Miller, B. S., Collins, K., Barlow, J., Calderan, S., Leaper, R., McDonald, M., Ensor, P., Olson, P. A., Olavarria, C., and Double, M. C. (2014). Blue whale vocalizations recorded around New Zealand: 1964-2013. *Journal of the Acoustical Society of America*, 135(3):1616–1623.

Miotto, C. (2025). *Acoustic Detection Ranges of Blue Whale (Balaenoptera musculus) D Calls Under Changing Ocean Conditions*. Thesis, UC San Diego.

Nickels, C. F., Sala, L. M., and Ohman, M. D. (2018). The morphology of euphausiid mandibles used to assess selective predation by blue whales in the southern sector of the California Current System. *Journal of Crustacean Biology*, 38(5):563–573.

Nickels, C. F., Sala, L. M., and Ohman, M. D. (2019). The euphausiid prey field for blue whales around a steep bathymetric feature in the southern California current system. *Limnology and Oceanography*, 64(1):390–405.

Oleson, E., Calambokidis, J., Burgess, W., McDonald, M., LeDuc, C. A., and Hildebrand, J. A. (2007a). Behavioral context of Northeast Pacific blue whale call production. *Marine Ecology-progress Series*, 330:269–284.

Oleson, E. M., Širović, A., Bayless, A. R., and Hildebrand, J. A. (2014). Synchronous seasonal change in fin whale song in the North Pacific. *PloS one*, 9(12):e115678.

Oleson, E. M., Wiggins, S. M., and Hildebrand, J. A. (2007b). Temporal separation of blue whale call types on a southern California feeding ground. *Animal Behaviour*, 74(4):881–894.

Palacios, D. M., Irvine, L. M., Machette, T., Lagerquist, B. A., Falcone, E. A., Schorr, G. S., and Mate, B. R. (2025). Dispersal, revisitation, and residency of satellite-tagged blue and fin whales in the Eastern North Pacific Ocean. *Animal Biotelemetry*, 13(1):43.

Payne, R. S. and McVay, S. (1971). Songs of Humpback Whales. *Science*, 173(3997):585–597.

Rasmussen, J. H. and Širović, A. (2021). Automatic detection and classification of baleen whale social calls using convolutional neural networks. *Journal of the Acoustical Society of America*, 149(5):3635–3644.

Ren, S., He, K., Girshick, R., and Sun, J. (2015). Faster r-cnn: Towards real-time object detection with region proposal networks. *Advances in neural information processing systems*, 28.

Rice, A., Širović, A., Hildebrand, J. A., Wood, M., Carbaugh-Rutland, A., and Baumann-Pickering, S. (2022). Update on frequency decline of Northeast Pacific blue whale (*Balaenoptera musculus*) calls. *PloS one*, 17(4):e0266469.

Robinson, D., Miron, M., Hagiwara, M., Weck, B., Keen, S., Alizadeh, M., Narula, G., Geist, M., and Pietquin, O. (2024). NatureLM-audio: An audio-language foundation model for bioacoustics. *arXiv preprint arXiv:2411.07186*.

Roch, M. A., Stinner-Sloan, J., Baumann-Pickering, S., and Wiggins, S. M. (2015). Compensating for the effects of site and equipment variation on delphinid species identification from their echolocation clicks. *Journal of the Acoustical Society of America*, 137(1):22–29.

Romagosa, M., Perez-Jorge, S., Cascao, I., Mourino, H., Lehodey, P., Pereira, A., Marques, T. A., Matias, L., and Silva, M. A. (2021). Food talk: 40-Hz fin whale calls are associated with prey biomass. *Proceedings of the Royal Society B*, 288(1954):20211156.

Ryan, J. P., Oestreich, W. K., Benoit-Bird, K. J., Waluk, C. M., Rueda, C. A., Cline, D. E., Zhang, Y., Cheeseman, T., Calambokidis, J., and Fahlbusch, J. A. (2025). Audible changes in marine trophic ecology: Baleen whale song tracks foraging conditions in the eastern North Pacific. *Plos one*, 20(2):e0318624.

Schafer-Zimmermann, J. C., Demartsev, V., Averly, B., Dhanjal-Adams, K. L., Duteil, M., Gall, G., Faiss, M., Johnson-Ulrich, L., Stowell, D., and Manser, M. B. (2024). animal2vec and MeerKAT: A self-supervised transformer for rare-event raw audio input and a large-scale reference dataset for bioacoustics. *Methods in Ecology and Evolution*.

Schall, E., Kaya, I. I., Debusschere, E., Devos, P., and Parcerisas, C. (2024). Deep learning in marine bioacoustics: a benchmark for baleen whale detection. *Remote Sensing in Ecology and Conservation*, 10(5):642–654.

Shiu, Y., Palmer, K. J., Roch, M. A., Fleishman, E., Liu, X., Nosal, E.-M., Helble, T., Cholewiak, D., Gillespie, D., and Klinck, H. (2020). Deep neural networks for automated detection of marine mammal species. *Scientific reports*, 10(1):607.

Širović, A. (2015). Variability in the performance of the spectrogram correlation detector for North-east Pacific blue whale calls. *Bioacoustics*, 25:1–16.

Širović, A., Oleson, E. M., Buccowich, J., Rice, A., and Bayless, A. R. (2017). Fin whale song variability in southern California and the Gulf of California. *Scientific Reports*, 7(1):10126.

Širović, A., Rice, A., Chou, E., Hildebrand, J. A., Wiggins, S., and Roch, M. (2015). Seven years of blue and fin whale call abundance in the Southern California Bight. *Endangered Species Research*, 28.

Širović, A., Williams, L. N., Kerosky, S. M., Wiggins, S. M., and Hildebrand, J. A. (2013). Temporal separation of two fin whale call types across the eastern North Pacific. *Marine Biology*, 160(1):47–57.

Stimpert, A. K., DeRuiter, S. L., Falcone, E. A., Joseph, J., Douglas, A. B., Moretti, D. J., Friedlaender, A. S., Calambokidis, J., Gailey, G., and Tyack, P. L. (2015). Sound production and associated behavior of tagged fin whales (*Balaenoptera physalus*) in the Southern California Bight. *Animal Biotelemetry*, 3(1):23.

Stowell, D. (2022). Computational bioacoustics with deep learning: a review and roadmap. *PeerJ*, 10:e13152.

Sung, K.-K. and Poggio, T. (1995). Learning human face detection in cluttered scenes. In *International Conference on Computer Analysis of Images and Patterns*, pages 432–439. Springer.

Szesciorka, A. R., Ballance, L. T., Širović, A., Rice, A., Ohman, M. D., Hildebrand, J. A., and Franks, P. J. S. (2020). Timing is everything: Drivers of interannual variability in blue whale migration. *Scientific Reports*, 10(1):7710.

Thompson, A. R., Bjorkstedt, E. P., Bograd, S. J., Fisher, J. L., Hazen, E. L., Leising, A., Santora, J. A., Satterthwaite, E. V., Sydeman, W. J., and Alksne, M. (2022). State of the California Current Ecosystem in 2021: Winter is coming? *Frontiers in Marine Science*, 9:958727.

Thompson, P. O., Findley, L. T., Vidal, O., and Cummings, W. C. (1996). Underwater sounds of blue whales, *Balaenoptera musculus*, in the Gulf of California, Mexico. *Marine Mammal Science*, 12(2):288–293.

Watkins, W. A. (1981). Activities and underwater sounds of fin whales. *Sci. Rep. Whales Res. Inst*, 33:83–117.

Watkins, W. A., Tyack, P., Moore, K. E., and Bird, J. E. (1987). The 20-Hz signals of finback whales (*Balaenoptera physalus*). *Journal of the Acoustical Society of America*, 82(6):1901–1912.

Weber, E. D., Auth, T. D., Baumann-Pickering, S., Baumgartner, T. R., Bjorkstedt, E. P., Bograd, S. J., Burke, B. J., Cadena-Ramirez, J. L., Daly, E. A., and de la Cruz, M. (2021). State of the California Current 2019-2020: back to the future with marine heatwaves? *Frontiers in Marine Science*, 8:709454.

Weirathmueller, M. J., Stafford, K. M., Wilcock, W. S., Hilmo, R. S., Dziak, R. P., and Trehu, A. M. (2017). Spatial and temporal trends in fin whale vocalizations recorded in the NE Pacific Ocean between 2003-2013. *Plos one*, 12(10):e0186127.

Weirathmueller, M. J., Wilcock, W. S., and Soule, D. C. (2013). Source levels of fin whale 20 Hz pulses measured in the Northeast Pacific Ocean. *Journal of the Acoustical Society of America*, 133(2):741–749.

Wentz, F. J., Scott, J., Hoffman, R., Leidner, M., Atlas, R., and Ardizzone, J. (2016). Cross-Calibrated Multi-Platform Ocean Surface Wind Vector Analysis Product V2, 1987–ongoing. Research Data Archive at the National Center for Atmospheric Research, Computational and Information Systems Laboratory.

Wiggins, S. M. and Hildebrand, J. A. (2007). High-frequency Acoustic Recording Package (HARP) for broad-band, long-term marine mammal monitoring. In *2007 symposium on underwater technology and workshop on scientific use of submarine cables and related technologies*, pages 551–557. IEEE.

Wiggins, S. M. and Hildebrand, J. A. (2020). Fin whale 40-Hz calling behavior studied with an acoustic tracking array. *Marine Mammal Science*, 36(3):964–971.

Zhang, X., Liu, X., Alksne, M. N., and Roch, M. A. (2025). Automating time frequency annotations of delphinid whistles by adapting a foundational transformer neural network. *Scientific Reports*, 15(1):37809.

Zhong, M., Torterotot, M., Branch, T. A., Stafford, K. M., Royer, J.-Y., Dodhia, R., and Lavista Ferres, J. (2021). Detecting, classifying, and counting blue whale calls with Siamese neural networks. *Journal of the Acoustical Society of America*, 149(5):3086–3094.

ZoBell, V. M., Hildebrand, J. A., and Frasier, K. E. (2024). Comparing pre-industrial and modern ocean noise levels in the Santa Barbara Channel. *Marine Pollution Bulletin*, 202:116379.

ZoBell, V. M., Posdaljian, N., Lenssen, K. L., Wiggins, S. M., Hildebrand, J. A., Baumann-Pickering, S., and Frasier, K. E. (2025). Climatic and economic fluctuations revealed by decadal ocean soundscapes. *Journal of the Acoustical Society of America*, 157(6):4233–4251.

3.10 Supplementary Material

Table 3.4. Summary of CalCOFI sonobuoy survey cruises included in analysis. Recording hours reflect the total duration of sonobuoy deployments within each cruise.

Cruise ID	Year	Season	Start	End	No. Buoys	Recording (hrs)
CC0403	2004	Spring	23-Mar	08-Apr	24	61.7
CC0407	2004	Summer	13-Jul	24-Jul	22	54.2
CC0411	2004	Fall	03-Nov	18-Nov	38	128.1
CC0501	2005	Winter	04-Jan	18-Jan	27	61.1
CC0504	2005	Spring	15-Apr	30-Apr	31	83.8
CC0507	2005	Summer	02-Jul	16-Jul	32	79.8
CC0511	2005	Fall	05-Nov	20-Nov	26	39.8
CC0604	2006	Spring	02-Apr	16-Apr	29	62.2
CC0607	2006	Summer	09-Jul	24-Jul	36	73.6
CC0610	2006	Fall	22-Oct	04-Nov	27	58.2
CC0701	2007	Winter	13-Jan	30-Jan	24	105.2
CC0703	2007	Spring	28-Mar	14-Apr	27	56.1
CC0706	2007	Summer	29-Jun	13-Jul	27	57.5
CC0711	2007	Fall	03-Nov	18-Nov	23	49.5
CC0803	2008	Spring	25-Mar	05-Apr	18	35.6
CC0808	2008	Summer	15-Aug	29-Aug	31	67.7
CC0810	2008	Fall	15-Oct	29-Oct	19	29.8
CC0901	2009	Winter	22-Jan	21-Jan	30	68.9
CC0903	2009	Spring	08-Mar	22-Mar	28	56.3
CC0907	2009	Summer	15-Jul	30-Jul	36	155.5
CC1001	2010	Winter	13-Jan	31-Jan	20	55.9
CC1004	2010	Spring	12-Apr	16-Apr	12	28.6

Continued on next page

Table 3.4 continued

Cruise ID	Year	Season	Start	End	No. Buoys	Recording (hrs)
CC1007	2010	Summer	31-Jul	15-Aug	22	94.9
CC1010	2010	Fall	29-Oct	12-Nov	20	56.0
CC1101	2011	Winter	13-Jan	28-Jan	27	70.8
CC1104	2011	Spring	10-Apr	27-Apr	29	55.0
CC1107	2011	Summer	27-Jul	12-Aug	33	73.0
CC1110	2011	Fall	17-Oct	30-Oct	19	75.9
CC1201	2012	Winter	28-Jan	12-Feb	23	119.5
CC1203	2012	Spring	25-Mar	06-Apr	25	47.8
CC1207	2012	Summer	10-Jul	26-Jul	29	136.9
CC1210	2012	Fall	20-Oct	03-Nov	26	63.0
CC1301	2013	Winter	11-Jan	25-Jan	21	89.9
CC1304	2013	Spring	07-Apr	22-Apr	21	79.3
CC1307	2013	Summer	07-Jul	21-Jul	31	73.4
CC1311	2013	Fall	10-Nov	24-Nov	25	82.3
CC1401	2014	Winter	29-Jan	04-Feb	12	44.3
CC1404	2014	Spring	02-Apr	16-Apr	26	121.6
CC1407	2014	Summer	07-Jul	21-Jul	26	72.6
CC1411	2014	Fall	09-Nov	22-Nov	27	89.2
CC1501	2015	Winter	16-Jan	29-Jan	28	95.3
CC1507	2015	Spring	30-Jul	30-Jul	29	77.8
CC1510	2015	Fall	29-Oct	13-Nov	28	86.7
CC1601	2016	Winter	08-Jan	21-Jan	26	86.8
CC1604	2016	Spring	01-Apr	14-Apr	22	78.1

Continued on next page

Table 3.4 continued

Cruise ID	Year	Season	Start	End	No. Buoys	Recording (hrs)
CC1607	2016	Summer	10-Jul	26-Jul	28	82.0
CC1611	2016	Fall	07-Nov	21-Nov	26	92.0
CC1701	2017	Winter	06-Jan	20-Jan	30	103.2
CC1703	2017	Spring	29-Mar	12-Apr	29	62.0
CC1708	2017	Summer	02-Aug	15-Aug	31	88.4
CC1711	2017	Fall	09-Nov	23-Nov	25	57.0
CC1806	2018	Summer	09-Jun	24-Jun	30	126.8
CC1902	2019	Winter	07-Feb	12-Feb	12	46.3
CC1904	2019	Spring	03-Apr	16-Apr	23	73.6
CC1907	2019	Summer	12-Jul	26-Jul	30	114.7
CC2107	2021	Summer	19-Jul	01-Aug	33	115.2
CC2110	2021	Fall	31-Oct	14-Nov	28	100.0
CC2204	2022	Spring	07-Apr	16-Apr	17	57.7
CC2208	2022	Summer	16-Aug	29-Aug	25	42.9
CC2211	2022	Fall	06-Nov	19-Nov	17	53.2
CC2301	2023	Winter	07-Jan	25-Jan	36	89.7
CC2303	2023	Spring	26-Mar	15-Apr	27	83.7
CC2307	2023	Summer	03-Jul	17-Jul	28	62.7
CC2311	2023	Fall	04-Nov	18-Nov	27	53.0
CC2401	2024	Winter	11-Jan	31-Jan	22	63.1
CC2403	2024	Spring	29-Mar	07-Apr	4	17.9
CC2407	2024	Summer	28-Jul	11-Aug	40	150.5
CC2411	2024	Fall	16-Nov	23-Nov	13	29.4

Continued on next page

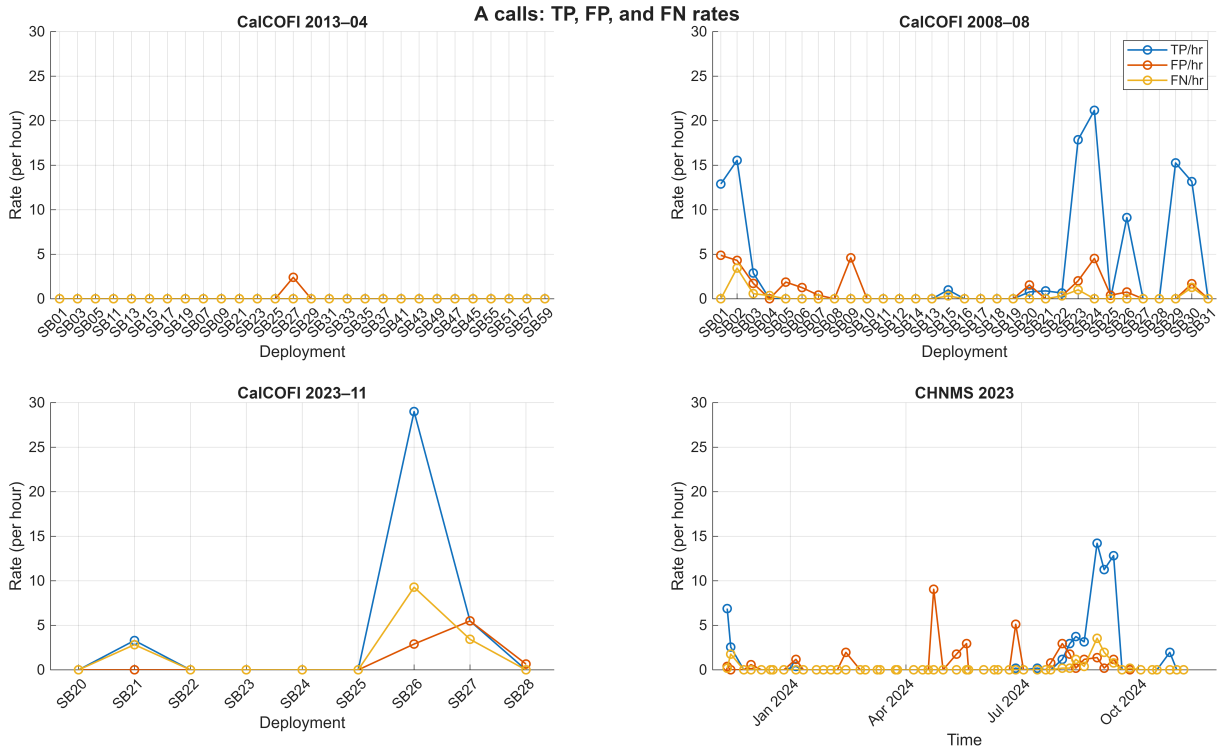


Figure 3.7. True positive, false positive, and false negative rates for A calls across evaluation datasets. Four panels show the rate of true positives (TP/hr), false positives (FP/hr), and false negatives (FN/hr) for A-call detections, standardized by recording effort (counts divided by effort duration in hours) at the deployment/encounter level. CalCOFI datasets (2013–04, 2008–08, 2023–11) are summarized by individual sonobuoy deployment (x-axis labeled by deployment ID), while CHNMS 2023 is summarized over verified encounter windows (5-hrs) through time. Rates are shown as lines with markers to highlight variability in detection outcomes among deployments/encounters and differences in error structure across datasets.

Table 3.4 continued

Cruise ID	Year	Season	Start	End	No. Buoys	Recording (hrs)
			Total (68 cruises)		**1743**	**5104.3**

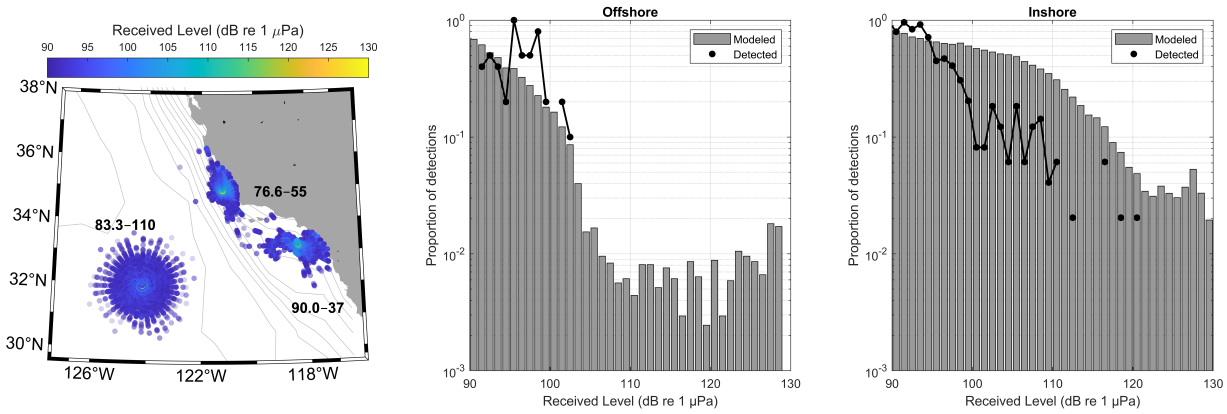


Figure 3.8. Received level distributions for blue whale A calls used for density estimation. Left: Modeled received levels (dB re 1 µPa) across the southern California Current Ecosystem for representative offshore and inshore stations. Center and right: Distributions of received levels for detected calls in offshore (center) and inshore (right) environments. Gray bars show modeled received level distributions from propagation modeling, while black points show received levels from detected calls.

Table 3.5. CalCOFI sonobuoy cruises used for model training and testing. For training, recording hours reflect the total duration of 60-s spectrograms sampled from each cruise (not full deployment durations). For testing, recording hours reflect the full duration of all annotated sonobuoy deployments.

Cruise ID	Year	Season	Sonobuoys	Recording (hrs)
Training				
CC0603	2006	Winter	1	2.00
CC0706	2007	Summer	12	5.37
CC1107	2011	Summer	1	0.32
CC1110	2011	Fall	1	4.43
CC1301	2013	Winter	1	0.03
CC1307	2013	Summer	9	0.80
CC1311	2013	Fall	5	0.48
CC1407	2014	Summer	9	6.13
CC1501	2015	Winter	6	14.93
CC1507	2015	Summer	8	3.22
CC1601	2016	Winter	3	4.28
CC1604	2016	Spring	1	1.07
CC1611	2016	Fall	1	0.02
CC1701	2017	Winter	2	0.13
CC1806	2018	Summer	5	0.15
CC1907	2019	Summer	3	9.97
CC2411	2024	Fall	1	4.40
		Train total		**57.73**
Testing				
CC0808	2008	Summer	32	69.50
CC1304	2013	Spring	28	115.68
CC2311	2023	Fall	9	16.11
		Test total		**201.29**

Table 3.6. HARP deployments used for model training, validation, and testing. Recording hours reflect the total duration of 60-s spectrograms sampled from each deployment for training and validation, and the full annotated deployment duration for the CHNMS test dataset.

Station	Latitude	Longitude	Depth (m)	Deployed	Recovered	Role	Recording (hrs)
CINMS01	34.28°N	120.03°W	580	2011-10-24	2012-03-21	Train/Val	0.38
CINMS02	34.29°N	120.03°W	580	2012-03-22	2012-08-01	Train/Val	11.92
CINMS03	34.29°N	120.02°W	900	2012-08-02	2012-12-03	Train/Val	0.57
SOCAL	32.85°N	119.18°W	1012	2008-06-04	2008-08-03	Train/Val	28.03
DC	35.61°N	121.24°W	65	2012-11-06	2013-03-19	Train/Val	68.40
CHNMS	34.57°N	120.71°W	73	2023-11-06	2024-11-06	Test	269.17
						Train/Val total	**109.30**
						Test total	**269.17**

Table 3.7. Detection areas by call type at each modeled CalCOFI station. Inshore stations (86.7–60, 93.3–35, 90.0–37, 76.7–55, 86.7–35, 81.8–46.9, and 83.3–55) are located inshore of the continental slope; offshore stations (83.3–110, 90.0–90, and 83.3–70) are located offshore of the continental slope.

Station	Latitude	Longitude	A (km^2)	B (km^2)	D (km^2)	20 Hz (km^2)	40 Hz (km^2)
Inshore stations							
86.7–60	32.99°N	120.35°W	21,646	24,954	26,418	24,915	25,617
93.3–35	32.68°N	117.87°W	18,484	21,746	22,480	21,431	22,196
90.0–37	33.18°N	118.39°W	13,349	13,842	14,507	13,855	14,253
76.7–55	34.89°N	121.20°W	11,619	12,848	13,638	12,564	12,986
86.7–35	33.82°N	118.63°W	8,006	8,661	9,402	8,494	8,802
81.8–46.9	34.27°N	120.03°W	4,629	4,813	4,916	4,824	4,874
83.3–55	33.75°N	120.41°W	17,238	20,127	21,819	20,115	20,971
Offshore stations							
83.3–110	31.91°N	124.17°W	38,427	40,095	40,798	40,267	40,576
90.0–90	31.42°N	122.00°W	37,712	39,644	40,389	39,703	40,283
83.3–70	33.25°N	121.44°W	35,880	37,475	38,512	38,096	38,168

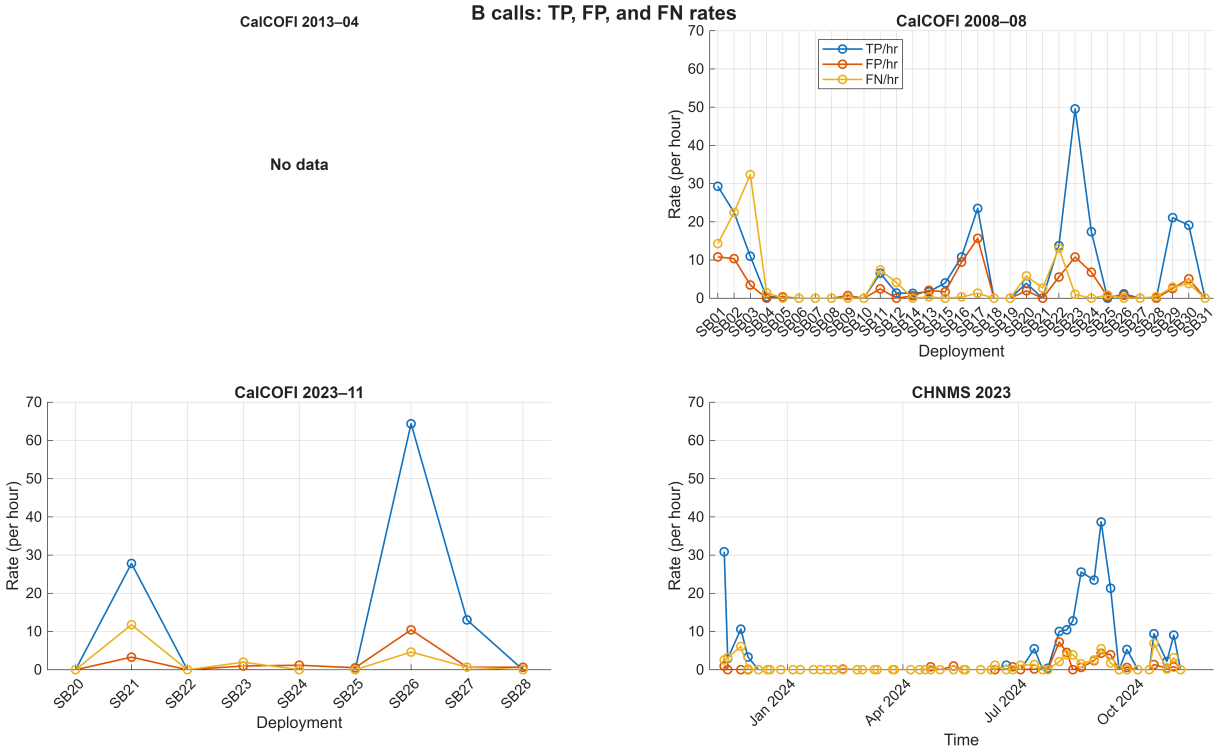


Figure 3.9. True positive, false positive, and false negative rates for B calls across evaluation datasets. Four panels show the rate of true positives (TP/hr), false positives (FP/hr), and false negatives (FN/hr) for B-call detections, standardized by recording effort (counts divided by effort duration in hours) at the deployment/encounter level. CalCOFI datasets (2013–04, 2008–08, 2023–11) are summarized by individual sonobuoy deployment (x-axis labeled by deployment ID), while CHNMS 2023 is summarized over verified encounter windows (5-hrs) through time. Rates are shown as lines with markers to highlight variability in detection outcomes among deployments/encounters and differences in error structure across datasets.

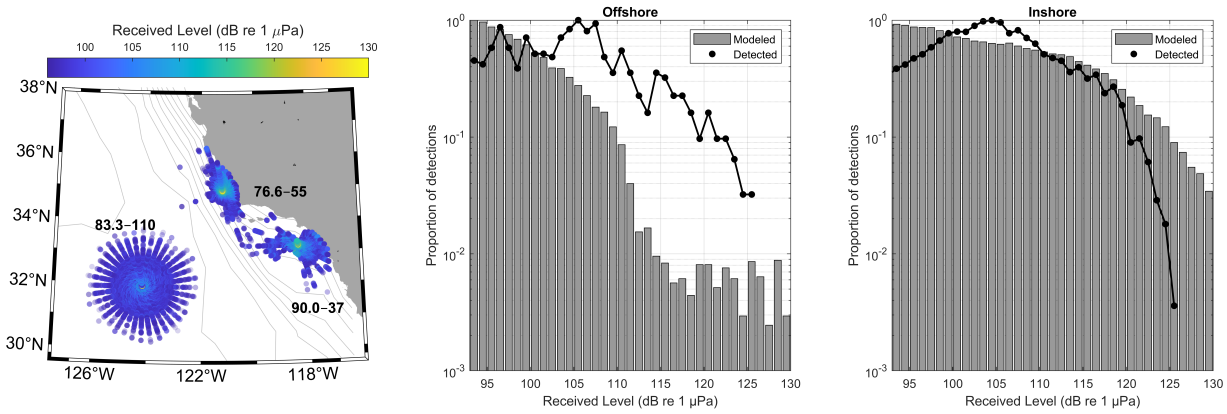


Figure 3.10. Received level distributions for blue whale B calls used for density estimation. Left: Modeled received levels (dB re 1 µPa) across the southern California Current Ecosystem for representative offshore and inshore stations. Center and right: Distributions of received levels for detected calls in offshore (center) and inshore (right) environments. Gray bars show modeled received level distributions from propagation modeling, while black points show received levels from detected calls.

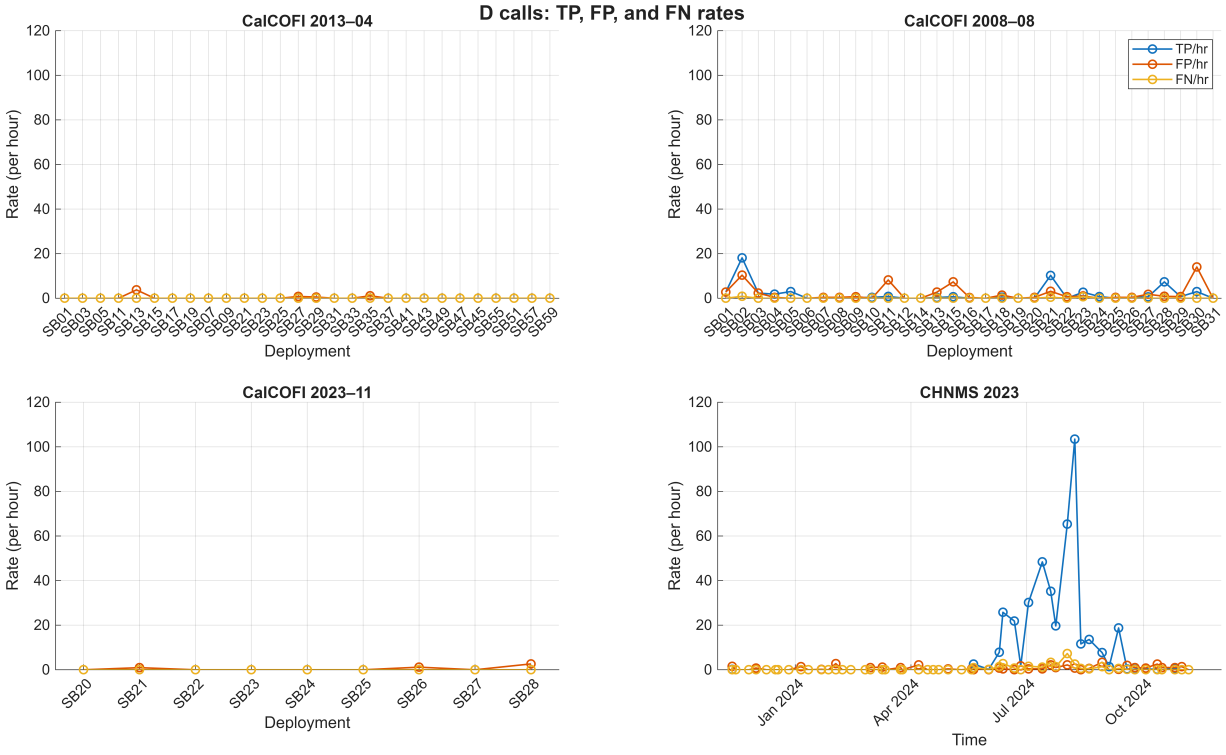


Figure 3.11. True positive, false positive, and false negative rates for D calls across evaluation datasets. Four panels show the rate of true positives (TP/hr), false positives (FP/hr), and false negatives (FN/hr) for D-call detections, standardized by recording effort (counts divided by effort duration in hours) at the deployment/encounter level. CalCOFI datasets (2013–04, 2008–08, 2023–11) are summarized by individual sonobuoy deployment (x-axis labeled by deployment ID), while CHNMS 2023 is summarized over verified encounter windows (5-hrs) through time. Rates are shown as lines with markers to highlight variability in detection outcomes among deployments/encounters and differences in error structure across datasets.

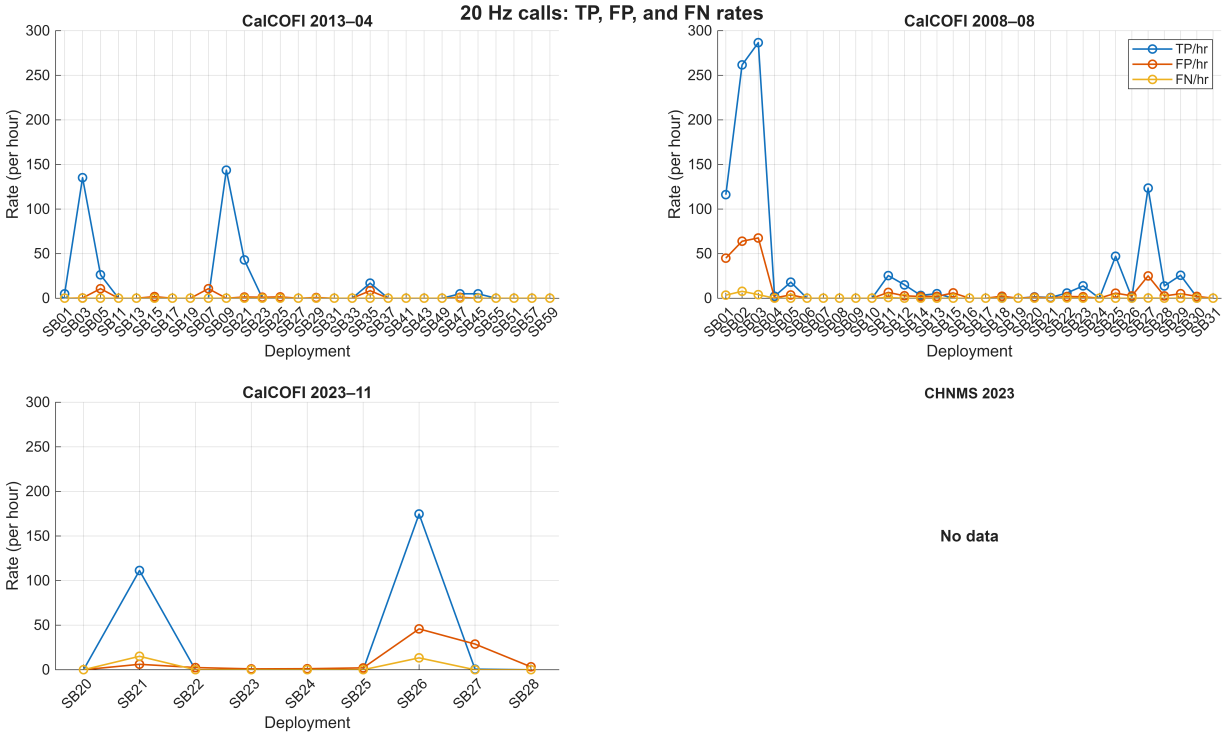


Figure 3.12. True positive, false positive, and false negative rates for 20 Hz calls across evaluation datasets. Four panels show the rate of true positives (TP/hr), false positives (FP/hr), and false negatives (FN/hr) for 20 Hz-call detections, standardized by recording effort (counts divided by effort duration in hours) at the deployment/encounter level. CalCOFI datasets (2013–04, 2008–08, 2023–11) are summarized by individual sonobuoy deployment (x-axis labeled by deployment ID), while CHNMS 2023 is summarized over verified encounter windows (5-hrs) through time. Rates are shown as lines with markers to highlight variability in detection outcomes among deployments/encounters and differences in error structure across datasets.

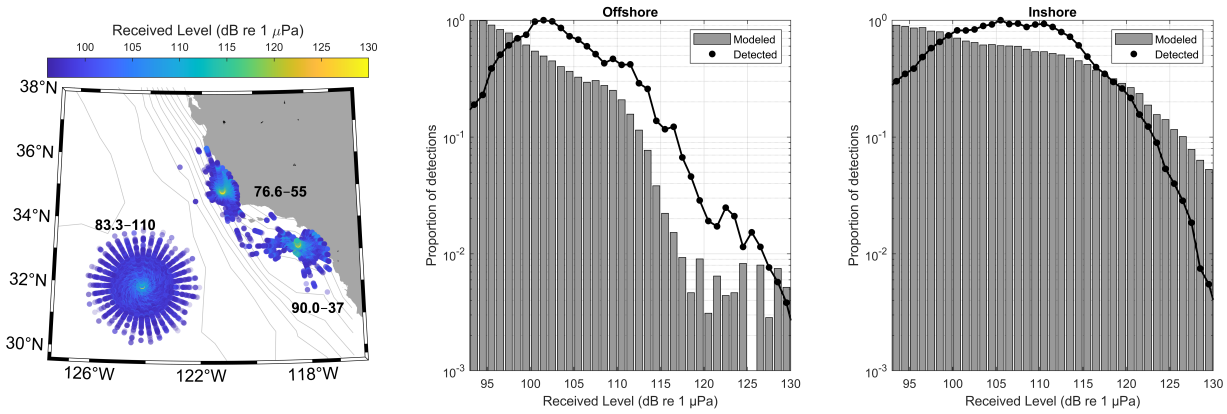


Figure 3.13. Received level distributions for fin whale 20 Hz calls used for density estimation. Left: Modeled received levels (dB re 1 µPa) across the southern California Current Ecosystem for representative offshore and inshore stations. Center and right: Distributions of received levels for detected calls in offshore (center) and inshore (right) environments. Gray bars show modeled received level distributions from propagation modeling, while black points show received levels from detected calls.

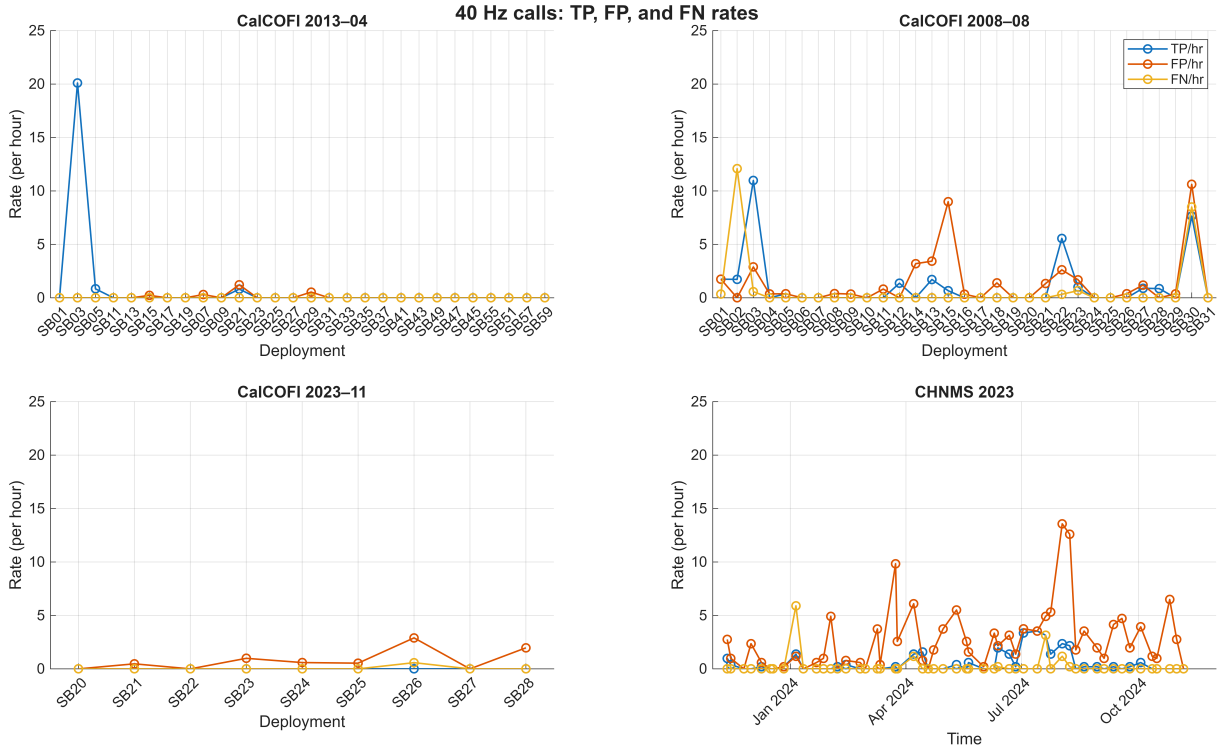


Figure 3.14. True positive, false positive, and false negative rates for 40 Hz calls across evaluation datasets. Four panels show the rate of true positives (TP/hr), false positives (FP/hr), and false negatives (FN/hr) for 40 Hz-call detections, standardized by recording effort (counts divided by effort duration in hours) at the deployment/encounter level. CalCOFI datasets (2013–04, 2008–08, 2023–11) are summarized by individual sonobuoy deployment (x-axis labeled by deployment ID), while CHNMS 2023 is summarized over verified encounter windows (5-hrs) through time. Rates are shown as lines with markers to highlight variability in detection outcomes among deployments/encounters and differences in error structure across datasets.

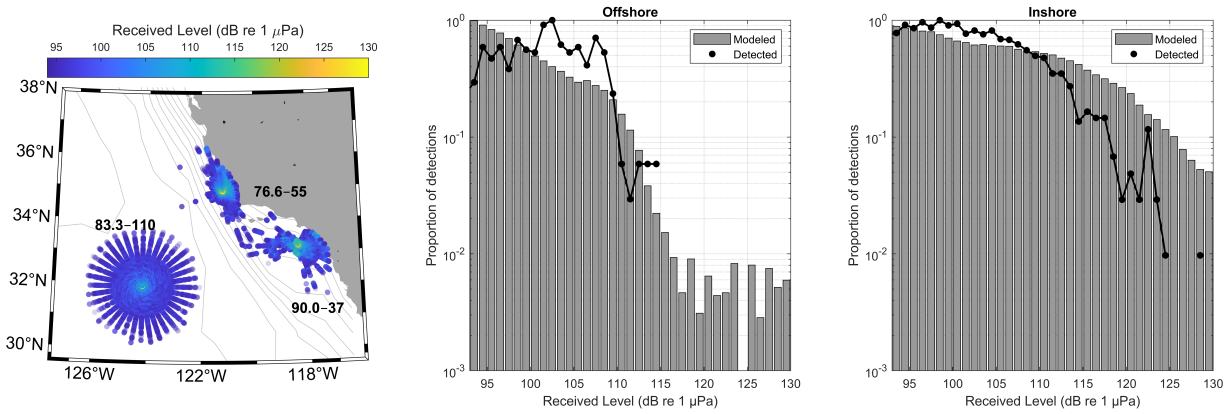


Figure 3.15. Received level distributions for fin whale 40 Hz calls used for density estimation. Left: Modeled received levels (dB re 1 µPa) across the southern California Current Ecosystem for representative offshore and inshore stations. Center and right: Distributions of received levels for detected calls in offshore (center) and inshore (right) environments. Gray bars show modeled received level distributions from propagation modeling, while black points show received levels from detected calls.

Chapter 4

Two decades of environmental change alter cetacean community composition in the southern California Current Ecosystem

4.1 Abstract

Rising ocean temperatures are having severe consequences for marine biodiversity. The eastern North Pacific has experienced multiple extreme marine heatwaves over the past two decades, including the 2014–2016 north Pacific marine heatwave, which caused mass die-offs and species redistributions as organisms tracked their shifting thermal niches. Cetaceans are top predators whose distribution, abundance, and community composition reflect environmental conditions, yet knowledge of their community-level responses to ocean warming is limited. We estimated density for ten cetacean species from 75 quarterly visual line-transect surveys conducted in the southern California Current Ecosystem during California Cooperative Oceanic Fisheries Investigations (CalCOFI) cruises from 2004 to 2025, using a bootstrap approach to propagate uncertainty through all analyses. Long-term trends were statistically significant for three species: Dall's porpoise declined by 19.2% per year, while long-beaked common dolphin and humpback whale increased by 11.2% and 11.5% per year, respectively. These same three species were also significantly related to sea surface temperature anomalies. Dall's porpoise,

at its warm range limit, had the strongest negative temperature relationship and long-beaked common dolphin, at its cool range limit, the strongest positive relationship, consistent with cool-water species contraction and warm-water species expansion in the region. Pacific white-sided dolphin densities followed a similar trajectory as Dall's porpoise, but their 9.2% per year decline was not statistically significant. The increased density of humpback whales in recent years aligns with their ongoing recovery from commercial whaling and increased nearshore prey availability. Cetacean community composition among the ten species differed significantly between seasons and between pre- and post-heatwave (2004–2013, 2014–2025) periods, while overall (alpha) diversity remained stable, suggesting community reorganization through species turnover rather than net loss or gain. Differences were more pronounced under biomass than abundance weighting, reflecting the disproportionate influence of large baleen whales on community structure. These findings provide quantitative estimates to support cetacean management and indicate that sustained ocean warming is altering top predator communities on rapid timescales.

4.2 Introduction

Climate-driven range shifts can alter community structure and ecosystem function (Doney et al., 2012; Pecl et al., 2017; Poloczanska et al., 2013). In the marine environment, species track their thermal niches and the pace of distributional change is accelerating (Jacox et al., 2020; Wernberg et al., 2025) as extreme marine heatwaves become more frequent, intense, and prolonged under anthropogenic climate change (Frölicher et al., 2018). Managing the ecological consequences of gradual or abrupt changes in species distribution and community composition requires sustained monitoring of multi-species communities across years to decades.

The California Current Ecosystem is an eastern boundary upwelling system and one of the most productive marine environments on Earth (Fréon et al., 2009). Coastal upwelling drives high primary productivity and supports diverse assemblages of top predators, including seabirds, sharks, pinnipeds, and cetaceans (Block et al., 2011). The southern California Current

Ecosystem (SCCE), ranging from Point Conception, California to Ensenada, Baja California, is also a thermal transition zone (Gelpi and Norris, 2008; Checkley Jr and Barth, 2009), where warm, salty, oligotrophic water from the North Pacific Subtropical Gyre meets cold, nutrient-rich California Current water flowing south from Alaska (Bograd et al., 2019). Along the coast, the California Undercurrent transports warm, saline, low-nutrient, and low-oxygen water poleward (Checkley Jr and Barth, 2009) and intensifies during marine heatwave events, further warming the region (Zaba and Rudnick, 2016). This warm-cool boundary makes the SCCE a biodiversity hot spot where cool- and warm-affiliated species overlap. As ocean temperatures rise, however, the SCCE is experiencing greater subtropical influence and its community composition is changing (Koslow et al., 2015; McClatchie et al., 2016; Russell et al., 2025).

The 2014–2016 northeast Pacific marine heatwave was among the most severe on record, and its biological impacts lasted for years after sea surface temperatures cooled (Suryan et al., 2021). Driven by an extreme warm-water anomaly and amplified by the 2015–2016 El Niño Jacox et al. (2016), it raised sea surface temperatures across the eastern North Pacific by 1–3°C for more than two years (Bond et al., 2015). The ecosystem consequences were severe. Krill and forage fish declined, harmful algal blooms spread, and mass strandings of seabirds and marine mammals followed Cavole et al. (2016). Juvenile white sharks appeared in central California in large numbers Tanaka et al. (2021), two tropical booby species established new breeding colonies in the Channel Islands (Russell et al., 2025), and humpback whale entanglements increased as their habitat compressed towards shore (Santora et al., 2020). Whether these changes are transient or permanent can only be resolved by sustained monitoring, and documenting how different species respond over long timescales will help predict the consequences of the next extreme event. The north Pacific saw another extreme marine heatwave in 2025 (NOAA Integrated Ecosystem Assessment, 2026), and a comparably strong El Niño is forecast for 2026 (NOAA Climate Prediction Center, 2026), making the comparison between the heatwave a decade ago and conditions today timely and relevant for ecosystem-based management.

As long-lived, highly mobile top predators, cetaceans are sensitive indicators, or sentinels, of change in marine ecosystems (Hazen et al., 2019). Yet most work on cetacean climate responses is limited to single species or short time series, and community-level responses across multiple species are rarely quantified (van Weelden et al., 2021). MacLeod (2009) predicted that cool-water cetaceans, especially shelf-associated porpoises and *Lagenorhynchus* dolphins, would contract poleward as waters warm, while warm-water species would expand and species with cosmopolitan or migratory ranges would show weaker directional responses. The SCCE is at the warm range limit of boreal odontocetes such as Dall's porpoise (Fleming et al., 2018) and Pacific white-sided dolphin, and at the cool range limit of warm-water species such as bottlenose and long-beaked common dolphin (Becker et al., 2014; Barlow, 2016). At these range edges, a small shift in temperature can be the difference between presence and absence, making the SCCE a region where the balance between warm- and cool-water species is sensitive to change.

The SCCE is also an important foraging ground and migratory corridor for large baleen whales, including blue, fin, humpback, and gray whales. Commercial whaling severely depleted these populations across the eastern North Pacific during the twentieth century (Rocha et al., 2014). Each has since recovered to varying degrees under legal protection, though recovery is incomplete and uneven across species (Clapham et al., 1999). While baleen whales may be redistributing in response to ocean warming, any climate signal is also layered on population recovery, and the two are difficult to separate. There is evidence for both. North Pacific humpback whales recovered until the 2014–2016 heatwave reduced their prey and drove a basin-wide decline (Cheeseman et al., 2024), and eastern North Pacific gray whales cycle through booms and busts tied to Arctic prey and sea-ice conditions (Stewart et al., 2023). Teasing apart recovery and climate signals for migratory baleen whales requires monitoring their distribution and abundance over many years, and such records are rare.

The California Cooperative Oceanic Fisheries Investigations (CalCOFI) program has conducted quarterly surveys of the SCCE since 1949, with visual line-transect cetacean surveys

since 2004 (Campbell et al., 2015). Campbell et al. (2015) used this dataset to characterize annual density and seasonal patterns for six cetacean species over 2004–2013, providing a density and abundance baseline for the region. Here we extend that analysis through fall 2025, adding twelve years that span the 2014–2016 marine heatwave and its aftermath, and four additional species. We estimate density for ten species (four baleen whales and six toothed whales), examine seasonal and long-term trends using generalized additive models, test for shifts in community composition between the pre- and post-heatwave periods and among seasons, and relate annual density to regional sea surface temperature anomalies to identify which species track ocean temperature most closely. These analyses document two decades of change in the SCCE cetacean community, and provide a baseline against which future change can be measured.

4.3 Methods

4.3.1 Study area and survey design

Visual monitoring for cetaceans was conducted during quarterly CalCOFI cruises from summer 2004 through fall 2025, spanning 75 surveys. Surveys followed the standard line-transect marine mammal survey protocol described by Campbell et al. (2015), with all effort conducted in passing mode. Two trained marine mammal observers searched with 7×50 Fujinon binoculars during daylight transits between CalCOFI stations. For each sighting, observers recorded species, group size estimates, binocular reticle distance, sighting bearing, ship heading, Beaufort sea state, swell height, and visibility. Survey effort was restricted to sea states of Beaufort 5 or lower and visibility beyond 1 km. Surveys were conducted aboard multiple Scripps Institution of Oceanography, UC San Diego, and National Oceanic and Atmospheric Administration (NOAA) research vessels (Supplemental Table 4.6.)

The study area is the southern CalCOFI grid, defined by a polygon encompassing six parallel transect lines running southwest to northeast from San Diego to north of Point Concep-

tion (Fig. 4.1), for a total area of 238,494 km^2 Campbell et al. (2015). Stations occur every 37 km inshore of the 2,000 m isobath and every 74 km offshore. CalCOFI cruises were conducted quarterly in most years. For our analyses, we defined seasons as: winter (December–February), spring (March–May), summer (June–August), and fall (September–November). Sightings were included in density analyses only when the vessel was both on-effort (two observers actively searching in Beaufort 0–5 with visibility $\geq$1 km and vessel speed $\geq$10 knots) and on-transect (transiting a primary CalCOFI line within the study area polygon).

4.3.2 Density estimation

Detection function estimation

Species-specific detection functions were estimated to account for differences in detectability due to variation in body size, surface behavior, and vessel response (Buckland et al., 2001). Ten cetacean species met the minimum of 60 on-effort, on-transect sightings required for robust detection function estimation (Buckland et al., 2001): blue whale (*Balaenoptera musculus*), fin whale (*Balaenoptera physalus*), humpback whale (*Megaptera novaeangliae*), gray whale (*Eschrichtius robustus*), Risso's dolphin (*Grampus griseus*), bottlenose dolphin (*Tursiops truncatus*), long-beaked common dolphin (*Delphinus bairdii*) (Jefferson et al., 2024), short-beaked common dolphin (*Delphinus delphis*), Pacific white-sided dolphin (*Lagenorhynchus obliquidens*), and Dall's porpoise (*Phocoenoides dalli*). Detection functions were estimated by pooling sightings across all surveys from 2004–2025 using the multiple covariate distance sampling (MCDS) framework Marques and Buckland (2003); Marques et al. (2007) implemented in the `Distance` package Thomas et al. (2010) in R.

Perpendicular distances were calculated from the measured binocular reticle position and sighting angle relative to bow, together with observer height above the water, using the formula of Lerczak and Hobbs (1998). Truncation distances were selected based on the upper quantiles of observed perpendicular distances, following (Buckland et al., 2001). A truncation of 2,400 m was applied to all large whale species (blue whale, fin whale, humpback whale, and gray whale),

consistent with Campbell et al. (2015). Truncation distances for smaller cetaceans were updated relative to that study to better reflect the full spread of observed distances in the larger dataset: 900 m for long-beaked common dolphin, short-beaked common dolphin, Dall's porpoise and Pacific white-sided dolphin; and 1,200 m for Risso's dolphin and bottlenose dolphin.

For each species, candidate detection functions were fit using forward selection, starting with a key function and adding terms if the resulting model had a lower AIC score (Akaike, 1974). Key functions considered were uniform with cosine adjustments, half-normal with cosine adjustments, and hazard-rate with polynomial adjustments. Covariates affecting the scale parameter of the key function were also considered for half-normal and hazard-rate models: Beaufort sea state (continuous), swell height (continuous), group size (continuous), and observer platform height (categorical). Observer platform height was grouped into three classes, $\leq$9 m (A), 9–12 m (B), and $>$12 m (C), to account for differences in detection probability arising from variation in eye height across the research vessels rotated through the survey program over the study period.

The final model chosen for inference was the one with the lowest AIC across all candidate models. Goodness-of-fit was assessed via Cramér–von Mises tests and visual inspection of detection function plots and quantile–quantile plots. For Pacific white-sided dolphin, Dall's porpoise, and bottlenose dolphin, the AIC-best model was not selected for inference because the fitted hazard-rate function produced an unrealistic spike in detection probability at small distances, consistent with vessel attraction documented in previous studies (Campbell et al., 2015; Williams and Thomas, 2007; Becker et al., 2014). The next-best model that did not use a hazard-rate key function was selected instead, which was a half-normal detection function for all three species (Table 4.1. For all remaining species, the AIC-best model was used for inference.

Bootstrap density and variance estimation

Density estimation, temporal trend modeling, and community-level analyses were conducted within a non-parametric bootstrap approach following Campbell et al. (2015), so that

uncertainty was propagated from the raw observations through to every derived quantity. One day of survey effort was used as the resampling unit. We generated 5,000 bootstrap replicates by resampling days within each cruise, keeping the sample size equal to the observed number of survey days for that cruise. Within each replicate, the detection function for each species was re-fitted to the resampled sightings using the model structure selected by AIC on the full dataset. Cruise-level density was estimated in each bootstrap replicate for each species using a Horvitz–Thompson estimator:

$$\hat{D}_c = \frac{1}{2 L_c g_0} \sum_{g=1}^{n_c} \frac{s_g}{\hat{\mu}(z_g)} \tag{4.1}$$

where $\hat{D}_c$ is estimated density (animals per km^2) for cruise c, L_c is total on-effort transect length (km) during cruise c, g_0 is the trackline detection probability (Barlow and Forney, 2007), n_c is the number of on-effort, on-transect sightings during cruise c, s_g is the observed group size of the gth detection, and $\hat{\mu}(z_g)$ is the effective strip width (ESW; km) for detection g predicted from the bootstrapped replicate-specific detection function given its covariate vector z_g. Because direct estimation of g_0 was not possible under the CalCOFI passing-mode protocol, species-specific values were used from (Barlow and Forney, 2007): $g_0 = 0.921$ for large whales (blue whale, fin whale, humpback whale, and gray whale), $g_0 = 0.856$ for delphinids (long-beaked common dolphin, short-beaked common dolphin, Risso's dolphin, Pacific white-sided dolphin, and bottlenose dolphin), and $g_0 = 0.822$ for Dall's porpoise. Abundance was estimated as density multiplied by the study area of 238,494 km^2.

Because the surveys were conducted in passing mode, there were a large percentage of unidentified animals in various taxonomic groupings: unidentified cetacean (UC), unidentified large whale (ULW), unidentified dolphin (UD), and unidentified common dolphin (UCD). ULW and UCD densities were pro-rated to identified large whales and common dolphins within each bootstrap replicate. For a given cruise, the adjusted density of identified species i belonging to unidentified group u is:

$$\hat{D}i^{*} = \hat{D}i + \hat{D}u \cdot \frac{\hat{D}i}{\sum_j \hat{D}_j}$$

where $\hat{D}i$ is the bootstrap density estimate for species i, $\hat{D}u$ is the density of the unidentified group, and the sum in the denominator is over all identified target species in that group. ULW density was pro-rated among blue, fin, humpback, and gray whales, and UCD density was pro-rated among long-beaked and short-beaked common dolphins. If all target species had zero estimated density in a given cruise, no pro-rating was applied. The UC and UD categories were not prorated as there were far fewer of them with large taxonomic uncertainty. Pro-rating was performed within each bootstrap replicate after refitting the detection function, so uncertainty in the pro-rated densities were propagated through to the final estimates. For each estimated quantity in the bootstrapped replicates, confidence intervals were retained around the 2.5th and 97.5th percentiles of the bootstrap distribution (Davison and Hinkley, 1997)

4.3.3 Trend analysis and community composition

Within each bootstrap replicate, species-specific and community-level seasonal and annual trends were estimated. To predict average species-specific seasonal and annual trends, a generalized additive model (GAM) was fit to the per-cruise density estimates for each species following the approach in Campbell et al. (2015). In cases where not all seasons were sampled in a year, the GAM estimates for the missing season(s) could then be used in the downstream annual trend analyses. The GAM used a quasi-Poisson error distribution with a log link, with season as a categorical fixed effect and year as a penalized thin-plate regression spline in the `mgcv` package in R).

The fitted model was then used to predict density in each year in every season. Seasonal mean densities were summarized by averaging GAM predictions across years and pairwise differences in density between seasons were evaluated by testing whether the 95% confidence interval of the paired bootstrap difference excluded zero. The average annual rate of change in

density was estimated from the GAM predictions as the mean change from 2005, the first year with complete seasonal survey effort, to 2025, and a trend was considered statistically significant when the 95% bootstrap confidence interval of r excluded zero.

$$r = \left(1 - \left[\left(\hat{D}_{2025} - \hat{D}_{2005}\right)/20\right]\right) \times 100\% \tag{4.2}$$

where $\hat{D}_y$ is the mean GAM-predicted density averaged over the four seasons for year y.

To characterize community-level change, we asked whether alpha diversity changed over time, whether community composition (beta diversity) shifted between the pre- and post-heatwave periods and among seasons, and how these patterns differed under abundance versus biomass weighting, the latter accounting for the large mass of baleen whales relative to the more abundant toothed whales. First, annual density estimates were calculated in the bootstrap replicates by averaging density across all four seasons in a year. For years with complete survey effort, the seasonal density estimates for each cruise were used. For years with incomplete survey effort, the GAM prediction for a missing season was substituted. This approach ensured that annual comparisons were not confounded by unequal seasonal coverage across years. Annual density was multiplied by the study area to obtain an annual abundance estimate, and abundance was multiplied by species-specific body mass (Barlow et al., 2008) to obtain an annual biomass estimate.

Alpha diversity was measured using the Shannon–Wiener diversity index (H') which was calculated annually for each bootstrap replicate using the annual abundance and biomass estimates:

$$H' = -\sum_{i=1}^{S} p_i \ln(p_i) \tag{4.3}$$

where $S = 10$ is the number of identified species and $p_i = N_i / \sum N$ is the proportional abundance (or biomass) of species i. Species absent in a given year contribute zero to H'. The theoretical

maximum is $H'_{\max} = \ln(10) \approx 2.30$ when all ten species are equally represented. Annual estimates of H' and 95% confidence intervals were summarized from the 5,000 bootstrap replicates using the percentile method. To test whether mean H' differed between the pre-heatwave (2004–2013) and post-heatwave (2014–2025) periods, within-replicate annual H' values were averaged separately over each period and the difference (post − pre) was retained for each of the 5,000 replicates. A difference was considered significant if the 95% CI of the resulting bootstrap distribution excluded zero.

Community-level changes in cetacean assemblage between the pre-heatwave and post-heatwave periods were examined using permutational multivariate analysis of variance (PERMANOVA; Anderson (2014)) and non-metric multidimensional scaling (NMDS) ordination, both using Bray–Curtis dissimilarity computed from the annual species abundance or biomass estimates as the distance measure. Within each bootstrap replicate, Bray-Curtis dissimilarities were computed between the annual species abundance or biomass estimates for all years, and PERMANOVA was applied to the resulting dissimilarity matrix to test whether assemblage structure differed significantly between pre- and post-heatwave periods using 999 permutations per replicate. Results were summarized across replicates as the median p-value, the proportion of replicates with $p < 0.05$, and the mean pseudo-F statistic with 95% bootstrap confidence interval. Community composition was visualized using NMDS ordination in two dimensions computed on the bootstrap-median annual species abundance matrix using Bray–Curtis dissimilarity. One point per year was plotted, and 95% confidence ellipses were drawn around the pre- and post-heatwave groups using the annual NMDS scores.

Seasonal differences in cetacean community composition were examined using the same PERMANOVA approach applied to a cruise-level community matrix. Within each bootstrap replicate, an $n_{\text{cruise}} \times S$ matrix was constructed in which each row was one cruise and each column was the bootstrapped abundance or biomass estimate for one of the ten identified species. Pairwise PERMANOVA tests between all six season pairs (winter–spring, winter–

summer, winter–fall, spring–summer, spring–fall, summer–fall) were conducted within the bootstraps. Results were summarized across replicates as the median p-value, the proportion of replicates with $p < 0.05$, and the mean pseudo-F statistic with 95% bootstrap confidence interval. Seasonal community composition was also visualized using NMDS ordination in two dimensions computed on the bootstrap-median year–season density matrix, with one point per year–season combination, 95% confidence ellipses drawn around each season.

Sea surface temperature anomaly analysis

To examine relationships between cetacean density and regional ocean temperature, we compared annual mean density estimates with sea surface temperature (SST) anomalies derived from the Hadley Centre Sea Ice and SST dataset (HadISST; Rayner et al. (2003)). Monthly anomalies were calculated over the CalCOFI survey domain (29.5–35.5°N, 117–125°W) relative to the 1991–2020 climatological baseline and averaged across all twelve months for a single annual value in each year. Within each bootstrap replicate, the annual density estimate for each species was regressed against the annual SST anomaly using ordinary least squares. The regression slope and R^2 were retained for each replicate and summarized as bootstrap means with 2.5th and 97.5th percentile confidence intervals. A species–SST relationship was considered significant where the 95% confidence interval of the slope excluded zero.

4.4 Results

4.4.1 Survey effort and sightings

Between summer 2004 and fall 2025, 75 CalCOFI cruises resulted in 68,532 km of on-effort on-transect line-transect sampling (Supplemental Table 4.7). Seasonal effort was greatest in summer, totaling 22,199 km over 19 cruises, followed by 15,603 km over 20 cruises in fall, 15,499 over 19 cruises in winter, and 15,231 km over 17 cruises in spring (Supplemental Table 4.7; Fig. 4.1).

4.4.2 Detection functions

Detection functions were estimated for ten species, with sample sizes, meaning the total number of sightings in the dataset, after truncation ranging from 58 (bottlenose dolphin) to 497 (short-beaked common dolphin). Half-normal and hazard-rate key functions were used depending on the species; for six species the detection function included covariates (Beaufort sea state, group size, swell height, or observer platform height) to account for variation in detectability with survey conditions. Model selection, truncation distances, and mean effective strip widths are summarized in Table 4.1. Full model selection tables and goodness-of-fit statistics are reported in Supplemental Table 4.8 and 4.9, respectively, and fitted detection functions and quantile-quantile plots are shown in Supplemental Fig. 4.9 and 4.10, respectively.

4.4.3 Density and abundance estimation

Humpback whales were the most abundant baleen whale in the study area with an average annual density of 4.01 animals per 1,000 km^2 (Table 4.2). Annual density estimates ranged from 0 in 2007 to a peak in 2025, with a significant increase of $+11.5\%$ per year over the study period (Table 4.4; Fig. 4.2). Seasonally, humpback whale density was significantly higher in spring and fall than in summer and winter (Table 4.3; Fig. 4.3). Fin whales had a mean annual density of 3.0 per 1,000 km^2 and annual estimates ranged from a low of 0.4 per 1,000 km^2 in 2019 to a peak of 7.6 per 1,000 km^2 in 2024, but the mean annual density change of $+2.3\%$ per year was not significant (Table 4.4; Fig. 4.2). Seasonally, fin whale density was significantly higher in summer than winter or spring (Table 4.3; Fig. 4.3). Blue whales had a mean annual density of 1.9 per 1,000 km^2 and their annual density change of $+4.0\%$ per year was not significant (Table 4.4; Fig. 4.2). Seasonally, blue whale density was significantly higher in summer than in all other seasons (Table 4.3; Fig. 4.3). Gray whales had the lowest mean annual density of the baleen whales at 1.3 per 1,000 km^2 and annual estimates ranged from 0 in 2005 and 2008 to a peak in 2015, though their mean annual density increased at $+9.7\%$ per year,

it was considered not significant because the 95% CI included zero (Table 4.4). Gray whale density was significantly higher during winter than in all other seasons (Table 4.3; Fig. 4.3).

Short-beaked common dolphins were the most abundant species in the study area, with a mean annual density of 773 per 1,000 km^2. The mean annual change of -0.2% per year was not significant (Table 4.4; Fig. 4.4). Seasonal short-beaked common dolphin density was significantly higher in winter and fall than in spring and summer (Table 4.3; Fig. 4.5). Long-beaked common dolphins had a mean annual density of 436 per 1,000 km^2. Density was variable across years, with no detections in 2006 and 2007, a noticeable but highly uncertain increase in 2015, and a maximum in 2025. Density increased significantly at $+11.2\%$ per year (Table 4.4) and was significantly higher in winter and fall than in spring (Table 4.3). Bottlenose dolphins had a mean annual density of 25.8 per 1,000 km^2. The mean annual change was not significant, and seasonal bottlenose dolphin density was highest in winter and fall (Table 4.4; Table 4.3; Fig. 4.5). Risso's dolphins had a mean annual density of 11.2 per 1,000 km^2. No significant long-term trend was detected and Risso's dolphin density was highest in spring and winter although the seasonal differences were not significant (Table 4.4; Table 4.3; Fig. 4.5). Pacific white-sided dolphins had a mean annual density of 16.7 per 1,000 km^2. Density declined at -9.2% per year although the trend was not considered significant because the 95% CI crossed zero (Table 4.4; Fig. 4.4). Pacific white-side dolphin density was significantly higher in spring than in all other seasons (Table 4.3; Fig. 4.5). Dall's porpoises had a mean annual density of 12.3 per 1,000 km^2. Annual estimates ranged from 0 in 2016 and 2025 to 41.4 per 1,000 km^2 in 2012 and density declined significantly at -19.2% per year (Table 4.4). Seasonal density was significantly higher in spring and winter compared to summer and fall, when the species was usually absent from the study area (Table 4.3; Fig. 4.5).

4.4.4 Community composition and diversity

Abundance-weighted Shannon–Wiener diversity (H') was variable from year to year, ranging from 0.39 in 2017 to 1.23 in 2011 (mean: 0.76; mean annual 95% CI: 0.26–1.30), and

no consistent directional trend was observed over the study period (Fig. 4.6). Biomass-weighted H' was consistently higher and with less interannual variablity, ranging from 1.17 in 2007 to 1.66 in 2004 (mean: 1.43; mean annual 95% CI: 1.04–1.71), reflecting the seasonally stable contributions of large baleen whales to community biomass. Mean H' did not differ significantly between the pre-heatwave (2004–2013) and post-heatwave (2014–2025) periods under either weighting (abundance: $\Delta H' = -0.10$, 95% CI -0.58 to $+0.15$; biomass: $\Delta H' = -0.004$, 95% CI -0.16 to $+0.15$; Table 4.5). Although abundance and biomass-weighted alpha diversity did not change directionally over time, the species contributing to it did, with a steady increase in the proportional contribution of long-beaked common dolphins and humpback whales and a decline in cold-water odontocetes including Dall's porpoises and Pacific white-sided dolphins (Fig. 4.6).

Cetacean community composition differed significantly between the pre-heatwave and post-heatwave periods under both biomass-weighted (pseudo-$F = 2.88$, significant in 77% of bootstrap replicates) and abundance-weighted (pseudo-$F = 3.51$, 64% of replicates) Bray–Curtis dissimilarity (Fig. 4.7). Composition also differed significantly among seasons under both weightings, more consistently under biomass weighting (pseudo-$F = 5.40$, significant in 100% of replicates) than abundance weighting (pseudo-$F = 2.01$, 81% of replicates; Table 4.5; Fig. 4.7). Pairwise biomass-weighted comparisons showed that winter assemblages differed significantly from all other seasons (winter–spring: $p < 0.05$ in 96% of replicates; winter–summer: 100%; winter–fall: 96%) and that spring and summer assemblages were consistently distinct from one another (100% of replicates). The summer–fall comparison was also significant under biomass weighting (98% of replicates). The spring–fall comparison was weak under both weightings (abundance: 41%, biomass: 46% of replicates). For the abundance-weighted community, the spring–summer contrast was the strongest pairwise signal (87% of replicates), followed by winter–spring (62%); all other season pairs were not consistently different (Table 4.5).

4.4.5 Relationships with sea surface temperature

Annual density was significantly associated with annual mean SST anomaly in three of the ten species (Supplemental Table S3; Fig. 4.8). Density increased with SST anomaly in long-beaked common dolphins ($R^2 = 0.20$) and humpback whale density showed a weakly positive association ($R^2 = 0.02$), with the bootstrap slope confidence interval just excluding zero. Density declined significantly with SST anomaly in Dall's porpoises ($R^2 = 0.23$) and Pacific white-sided dolphins showed a similar negative association, though the slope confidence interval included zero ($R^2 = 0.045$).

4.5 Discussion

This two-decade record of visual line-transect surveys documents shifts in cetacean density, trend, and community composition across a period of environmental change. Several methodological caveats should be considered in regard to the results discussed below. Day-level bootstrap resampling propagated encounter-rate and detection-function uncertainty, but for species seen on only one or two days per cruise, replicates alternated between zero detections and repeated draws of the same sighting day, which inflated uncertainty for those species. Because the passing-mode survey protocol does not allow trackline detection probability to be estimated, we used fixed values from Barlow and Forney (2007), so absolute densities depend on the assumption that these values hold across the vessels and conditions of our surveys. Survey effort was also uneven over time, most notably during the COVID-19 pandemic, when the program was reduced to one cruise in each of 2020 and 2021, leaving a gap in the middle of the post-heatwave period.

Over two decades, the cetacean community of the SCCE shifted in a direction consistent with ocean warming. Dall's porpoise, at the warm edge of a cool-water range, declined significantly, while long-beaked common dolphin, at the cool edge of a warm-water range, increased significantly. Humpback whales increased significantly, likely through a combination

of population recovery and climate-driven shifts in prey. None of the other migratory baleen whales or wide-ranging toothed whales showed a significant directional response, supporting MacLeod (2009) prediction that range-edge species track their thermal niches most strongly while wide-ranging species respond more weakly. At the community level, species-specific changes resulted in a significant shift in composition between the pre- and post-heatwave periods, even as alpha diversity remained stable, suggesting that the community reorganized through species turnover rather than net gain or loss of diversity.

A consistent feature of this community is its seasonal structure. Spring upwelling drives productivity along the California coast, drawing both warm- and cool-water species into the study area and supporting large aggregations of baleen whales (Croll et al., 2005; Palacios et al., 2019). Blue, humpback, and gray whales showed the clearest seasonal patterns. Blue whales were almost exclusively summer visitors, concentrated when krill aggregations are densest (Croll et al., 2005), while humpback whale density peaked in spring and fall, coinciding with their north- and southbound migration (Calambokidis et al., 2001), and gray whale density peaked in winter, coinciding with their southbound migration (Guazzo et al., 2019). Fin whale density was highest in summer and fall. These patterns match Campbell et al. (2015), who reported the same blue (summer), fin (summer, fall), humpback (spring, fall), and gray whale (winter) peaks over 2004–2013. Acoustic monitoring in the region aligns with these timings. Blue and fin whale foraging calls peak in summer and transition to singing in fall (Oleson et al., 2007; Širović et al., 2015, 2013; Szesciorka et al., 2020), humpback whale song peaks in fall (Baggett et al., 2026; Ryan et al., 2019), and gray whale singing tracks the winter–spring migration through the SCCE (Guazzo et al., 2019). The seasonal shift in baleen whale community composition reflects their migratory phenology and spatiotemporal partitioning of a critical foraging habitat. These distinct assemblages are evident in the biomass-weighted PERMANOVA, where the winter community differed significantly from all other seasons and the summer assemblage was the most distinct of any season. This summer signal likely reflects the summer dominance of blue

and fin whales, while winter separated through gray whale biomass and the low densities of other baleen whales. The spring–fall contrast was the lone weak pair in the community composition comparison under biomass weighting, which is likely driven by the high densities of humpback whales as they migrate to and from the region in those seasons. Weighting by biomass increased the effect sizes of every seasonal contrast, most pronounced for winter–summer (pseudo-F 2.2 to 11.3) and summer–fall (1.5 to 4.4). By biomass, the cetacean community is structured by the seasonal procession of large whales, while by abundance, it is a delphinid assemblage that turns over modestly with season.

Toothed whale seasonality had a similar pattern of species partitioning. Dall's porpoise and Pacific white-sided dolphins were concentrated in the cooler months and peaked in spring, consistent with their southward movement into the study area when the region is coldest (Barlow and Forney, 2007; Becker et al., 2014, 2022, 2019). The spring peak matches Campbell et al. (2015), suggesting that the seasonal phenology of these species has remained stable across two decades even as their regional abundance has declined. The spring Pacific white-sided dolphin peak matches the northern, acoustically distinct population at the northern edge of the SCCE (Soldevilla et al., 2010b), the same population that is thought to have shifted poleward in recent years (Alksne et al., 2024). Short-beaked common dolphins were present year-round with highest densities in winter and lowest in spring, similar to the findings of Campbell et al. (2015) and earlier studies suggesting the population concentrates in the SCCE during cool winter months and expands northward and offshore as the region warms (Dohl et al., 1986; Forney and Barlow, 1998; Barlow, 2016). Long-beaked common dolphins followed a similar winter and fall pattern. Short-beaked, long-beaked, and bottlenose dolphins cannot be distinguished acoustically in the SCCE, but Bloom et al. (2025) found that their aggregated echolocation signal dropped slightly in foraging activity over summer months, consistent with the lower common dolphin densities we observed in the summer. Risso's and bottlenose dolphins showed no significant seasonal differences, which may reflect their central range position or too few detections to detect

seasonal patterns. Risso's are known to be acoustically present year-round with a slight peak in fall (Soldevilla et al., 2010a). At the community level, the abundance-weighted PERMANOVA picked up the toothed whale seasonal partitioning. The spring–summer contrast was the strongest pairwise difference, reflecting the departure of cold-water species as the region warms into summer. The winter–spring contrast may have captured the tradeoff between groups moving in different directions. Common dolphins that packed into the SCCE in winter disperse through spring and summer, while Dall's porpoise and Pacific white-sided dolphins move in and peak in spring, shifting the community from a winter assemblage dominated by warm-affiliated common dolphins to a spring one dominated by cold-water species. Weighting by biomass increased the effect sizes of every seasonal contrast, most pronounced for winter–summer (pseudo-F 2.2 to 11.3) and summer–fall (1.5 to 4.4). By abundance, the cetacean community is a delphinid assemblage that turns over modestly with season, while by biomass, it is structured by the seasonal procession of large whales.

Dall's porpoise had the steepest annual decline of any species in the dataset. MacLeod (2009) predicted unfavorable range contraction for Dall's porpoise as a cool-water-limited shelf species, and our results support this prediction. Dall's had the only significant negative SST relationship in our dataset and the only significant negative trend in annual density at -19.2% per year. Campbell et al. (2015) found a negative but non-significant trend over 2004–2013, and our longer record suggests that this trajectory accelerated after the 2014–2016 heatwave and has not reversed in the decade since. The continued low densities since the heatwave suggests that conditions in the SCCE may have crossed a threshold that limits the population's use of the study area even when cooler La Niña conditions briefly returned in the early 2020's (Thompson et al., 2024). Recent acoustic evidence Andres et al. (2026) suggests that Dall's porpoise echolocation click presence was lower at an acoustic monitoring station off Point Conception during the 2014–2016 marine heatwave years, and has increased slightly in years since. However, this approach does not estimate density and the recording station is right at the boundary of the

SCCE, where conditions may still be favorable for this species.

Pacific white-sided dolphins showed a similar but non-significant decline, with densities highest in the early years of the study and declining in recent years. The mean annual rate of decline (-9.2% per year) had a confidence interval that touched zero, and the negative SST relationship was similarly just below significance. The direction is unambiguous, though, and it extends a decline already evident a decade earlier. Campbell et al. (2015) reported a significant decrease in Pacific white-sided dolphin density over 2004–2013, and our longer record shows that decline continuing. Like Dall's porpoise, this is a cold-water species negatively associated with warmer conditions across its California Current range (Becker et al., 2014, 2022, 2019). Salvadeo et al. (2010) documented its disappearance from the southwest Gulf of California, previously the southern boundary of its range, over three decades of warming, attributing the loss to a poleward range shift. The decline we observe in the SCCE extends that range contraction poleward. As additional evidence, passive acoustic monitoring across multiple SCCE stations found trends consistent with poleward redistribution during and after the 2014–2016 heatwave, with apparent declines in the acoustically distinguishable northern California/Oregon/Washington population and possible increases in a southern California/Baja population in the SCCE (Alksne et al., 2024). Acoustically, the southern population occurs less frequently in the region than the northern (Alksne et al., 2024; Henderson et al., 2011; Soldevilla et al., 2010b), so even if it is increasing, our visual estimates likely reflect the stronger signal of decline in the more abundant northern population, which is visually indistinguishable from the southern. Mixing of the visually cryptic populations may be the reason our annual trend and SST relationship are not significant (Becker et al., 2022), even if the northern is moving out while the southern population moves in.

Long-beaked common dolphins increased significantly over the study period ($+11.2\%$ per year) and showed the strongest positive SST relationship in the dataset. This warm-water coastal species, whose range spans from Baja California to central California (Barlow, 2016),

rose to a local maximum in 2015 and reached a study maximum in 2025. Where Dall's porpoise and Pacific white-sided dolphins sit at their warm range limit in the SCCE, long-beaked common dolphins sit at their cool limit, and they are responding in opposite directions to warming. A similar pattern has been documented in the rapidly warming Northeast US, where the relative abundance of warm-water toothed whales rose while cool-water species declined and shifted poleward (Thorne et al., 2022; Hirtle et al., 2026).

Short-beaked common dolphins were the most abundant species in the study area and showed no significant annual trend and their estimated mean annual abundance in the SCCE (184,356) was slightly higher than Campbell et al. (2015) estimates a decade ago (167,988). Risso's and bottlenose dolphins also had no significant annual trends. Interannual variability was evident in these species densities but the lack of a net trend may be due to the SCCE being within their thermal range preferences. Although, these species are documented shifting elsewhere. The northern limit of coastal bottlenose dolphins used to be the SCCE, but range expansions occurred during the 1983 El Nino and the population has been seen in central California ever since, and in recent years, has been documented moving even further north along the coast (Keener et al., 2023). Risso's dolphins have been acoustically detected expanding northward into the Bering and Chukchi Seas (Seger and Miksis-Olds, 2019), and while range expansions of short-beaked common dolphins have not yet been described in the eastern North Pacific, they have been observed in the north Atlantic (Thorne et al., 2022).

Unlike the toothed whales, no baleen whale in this dataset is range-limited by the SCCE, and the strongest long-term signal in this group is the recovery of humpback whales possibly coupled with nearshore habitat compression in recent years (Santora et al., 2020). Cheeseman et al. (2024) photo-ID record showed that at the scale of the entire eastern North Pacific, humpback whales were recovering until 2012, then declining between 2012 and 2021 as the 2014–2016 heatwave reduced prey at high-latitude feeding grounds. Humpback whales of the Mainland Mexican and Central American migratory herds (Martien et al., 2023) are

the primary ones seen feeding off the coast of California, and Cheeseman et al. (2024) point out that the Mainland Mexican herd did not decline. While our visual record cannot tell them apart, the increase in recent years suggests the Mainland Mexican and Central American herds continue to return in large numbers to the coast of Southern and Central California. Northern anchovy reached record highs in the California Current after the heatwave (Thompson et al., 2022), and humpbacks switch to anchovy when krill is scarce (Fleming et al., 2016; Santora et al., 2020). The same warming also compressed productive habitat into a narrow nearshore band (Santora et al., 2020), concentrating humpbacks closer to shore, which has likely raised their density in our study area while increasing their exposure to ship strikes and entanglement Santora et al. (2020, 2026). In Campbell et al. (2015), fin whales were the more abundant of the two over 2004–2013 (2.73 versus 1.17 per 1,000 km²), whereas in our record humpbacks now outnumber fin whales (4.01 versus 3.00 per 1,000 km²). While both species have increased in the last decade, the emerging dominance of humpback whales may reflect their regional success foraging on anchovy in recent warm years.

Blue and fin whales showed non-significant positive trends. Moore and Barlow (2011) estimated the California fin whale population grew from about 1,000 to nearly 3,000 whales between 1991 and 2008 and projected continued increase. The non-significant $+2.2\%$ per year is lower than the $+6.8\%$ increase Campbell et al. (2015) reported, and the CalCOFI acoustic record over the same period does not show an increase either (Alksne et al., 2026), suggesting that fin whale population growth may have slowed in recent years. Blue whale density appears to be slowly increasing in the SCCE. In our record, their trend was positive but not significant ($+4.0\%$ per year) and the mean annual abundance estimates were twice as high (472) as they were in Campbell et al. (2015) (217), who report a non-significant decline of -2.9% per year. Long-term trends for eastern North Pacific blue whales are debated. Monnahan et al. (2015) argued the population had plateaued at a density-dependent carrying capacity, and current stock assessment reports show that abundance estimates differ depending on method and don't have

any formal trend analysis (Carretta et al., 2024). A documented northward shift in blue whale distribution further complicates population abundance estimation, since animals moving out of a survey region can appear as a local decline or plateau (Barlow, 2016; Becker et al., 2022). The SCCE sits in the central-to-southern part of the blue whale summer foraging range, so a northward shift could register here as little or no change, as it may for the cosmopolitan toothed whales. The increased mean annual density since Campbell et al. (2015) suggests a local increase, and the higher densities in recent years match improved post-heatwave krill and productive early-2020s La Niña conditions Thompson et al. (2022, 2024).

Gray whales showed a positive but non-significant trend. They occur in the study area almost entirely in winter, during the southbound phase of their migration. Our surveys capture only a small portion of the population's migratory corridor, corresponding to an estimated few hundred individuals in any given year, so our density estimates represent only a small snapshot of the population's true density. We also rarely capture the northbound migration through California, since it occurs mainly between February-March (Poole, 1984) and our spring surveys run from March-April. The eastern North Pacific population has declined over our monitoring period, from about 27,000 in 2016 to roughly 13,000 by 2025 (Stewart et al., 2023), and the interannual variability in our record likely reflects this boom-and-bust population dynamic rather than local conditions. Our annual density estimates track these changes, rising until 2015, declining through 2023, and then increasing in 2024 and 2025. The short-term rebound is also visible in coast-wide surveys, which estimated a temporary increase in 2023/2024 (Eguchi et al., 2024) before the population fell again to its lowest level in 2025. Whether the rebound in our data continues or reverses will not be clear until additional surveys are completed. Even though we sample only a small portion of gray whale's migratory corridor, our local densities appear to track the annual shape of the population's ongoing boom-and-bust cycle.

The species-specific changes are reflected in the community level observations. By abundance, the community is dominated by common dolphins, while by biomass, the community

is dominated by large whales. Across the heatwave, both diversity metrics show the same result. Community composition shifted significantly between the pre- and post-heatwave periods, while mean alpha diversity remained stable. We interpret this as species compositional turnover that left the overall diversity of the community intact. The change in abundance-weighted community composition is likely driven by the influx of long-beaked common dolphins and the loss of cold-water toothed whales. The change in biomass-weighted community composition is likely driven by the increase in humpback whales occurring at the same time as a plateau in fin whales and a decline in gray whales. In both cases the species making up the community changed while its overall diversity did not, suggesting that gains and losses were balanced enough to hold evenness roughly constant. Stable aggregate diversity masking compositional turnover has been documented in other long-term marine studies Dornelas et al. (2014); Magurran and Henderson (2010). Whether the pre- and post-heatwave compositional shifts documented here have ecosystem-level consequences remains an open question. Barlow et al. (2008) estimated that cetaceans in the California Current Ecosystem consume 12% of net primary production, with baleen whales making up 70% of cetacean biomass, which has likely grown with their continued recovery. Blue, fin, and humpback whales have different prey preferences and have recently been associated with distinct microbial and planktonic communities in the SCCE (Satterthwaite et al., 2026), thus shifts in their relative abundance may alter how baleen whale consumption is distributed across trophic levels. Additional work estimating cetacean consumption and quantifying shifts in lower trophic level communities would help determine whether the compositional shifts documented here have altered the functional role the cetacean community plays in the California Current Ecosystem.

Lastly, the diversity metrics capture changes in the cetacean community composition across only these ten species. Other marine mammals and high tropic level consumers have similar functional roles in the SCCE ecosystem, as well as other cetacean species which were too rare in this dataset to estimate density. For instance, Bryde's whales have been acoustically

increasing in the SCCE (Kerosky et al., 2012) and striped dolphins have been as well (Becker et al., 2019), likely due to warming conditions, but our record does not reflect those trends because those species are uncommon in the 2004-2025 record.

The two-decade record compiled here shows that the main contributors to the SCCE cetacean community make up a different composition from what they did at the start of the study. Cold-water range-edge species have contracted, warm-water range-edge species have expanded, and humpback whales are altering the biomass composition through recovery. As marine heatwaves grow more frequent, intense, and long-lasting under continued warming (Frölicher et al., 2018), these episodic events will continue accelerating biogeographic range shifts, as has been shown here. This record gives a quantitative baseline for ten species and evidence that reorganization of the top predator community in the southern California Current Ecosystem is already well underway.

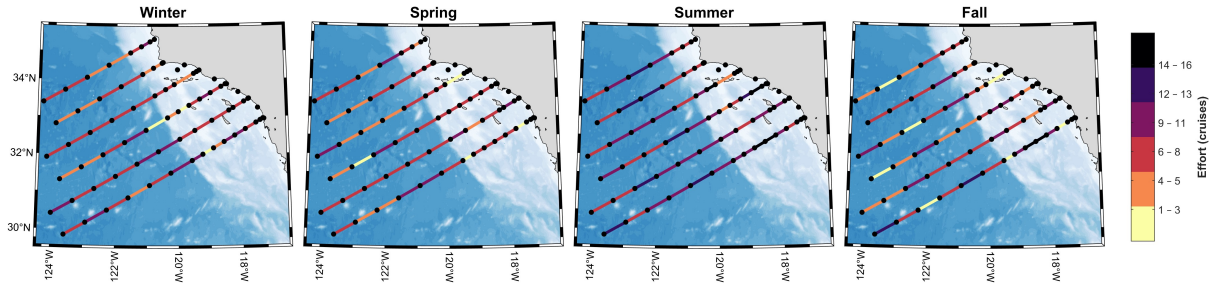


Figure 4.1. Seasonal visual survey effort along CalCOFI transect lines in the SCCE, 2004–2025. Colors indicate the number of cruises during which each transect segment was surveyed. Black dots mark CalCOFI stations.

Table 4.1. Truncation distance (w) in meters, number of on-effort, on-transect sightings (n), fitted detection function model, retained covariates, and mean effective strip width ($\hat{\mu}$) in meters for each species. Hn = half-normal; Unif = uniform; Hr = hazard-rate; Cos = cosine adjustment. Covariates: ss = Beaufort sea state; sz = group size; sw = swell height; oh = observer height.

Species	***w* (m)**	***n***	**Model**	**Covariates**	**$\hat{\mu}$ (m)**
Mysticetes					
Blue whale	2400	143	Unif + Cos	—	1320
Fin whale	2400	231	Hn	ss, sz, oh	1179
Gray whale	2400	62	Hn + Cos	—	1144
Humpback whale	2400	198	Hn	sw, oh, ss	1495
Odontocetes					
Dall's porpoise	900	71	Hn	ss	410
Pacific white-sided dolphin	900	76	Hn	ss	237
Risso's dolphin	1200	60	Hr	sz, ss	846
Bottlenose dolphin	1200	58	Hn + Cos	—	395
Long-beaked common dolphin	900	77	Hn	sz	499
Short-beaked common dolphin	900	497	Hr	ss, sz	171

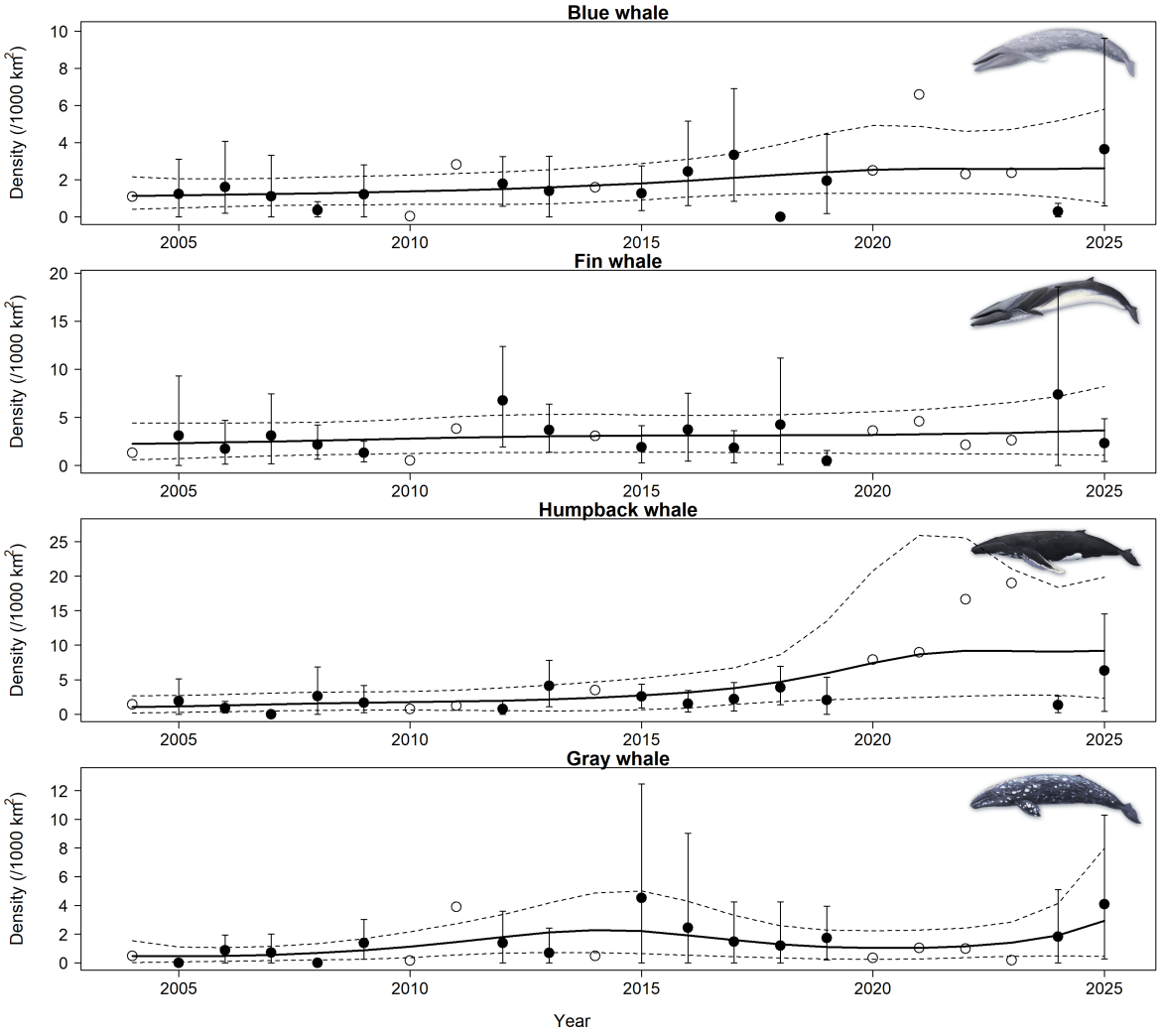


Figure 4.2. Annual density trends (animals per 1,000 km^2) for baleen whale species, 2004–2025. Solid line: bootstrap mean GAM prediction; dashed lines: 95% bootstrap confidence interval. Filled circles: years with all four seasons surveyed (error bars show 95% bootstrap CI on annual density); open circles: years with incomplete seasonal coverage.

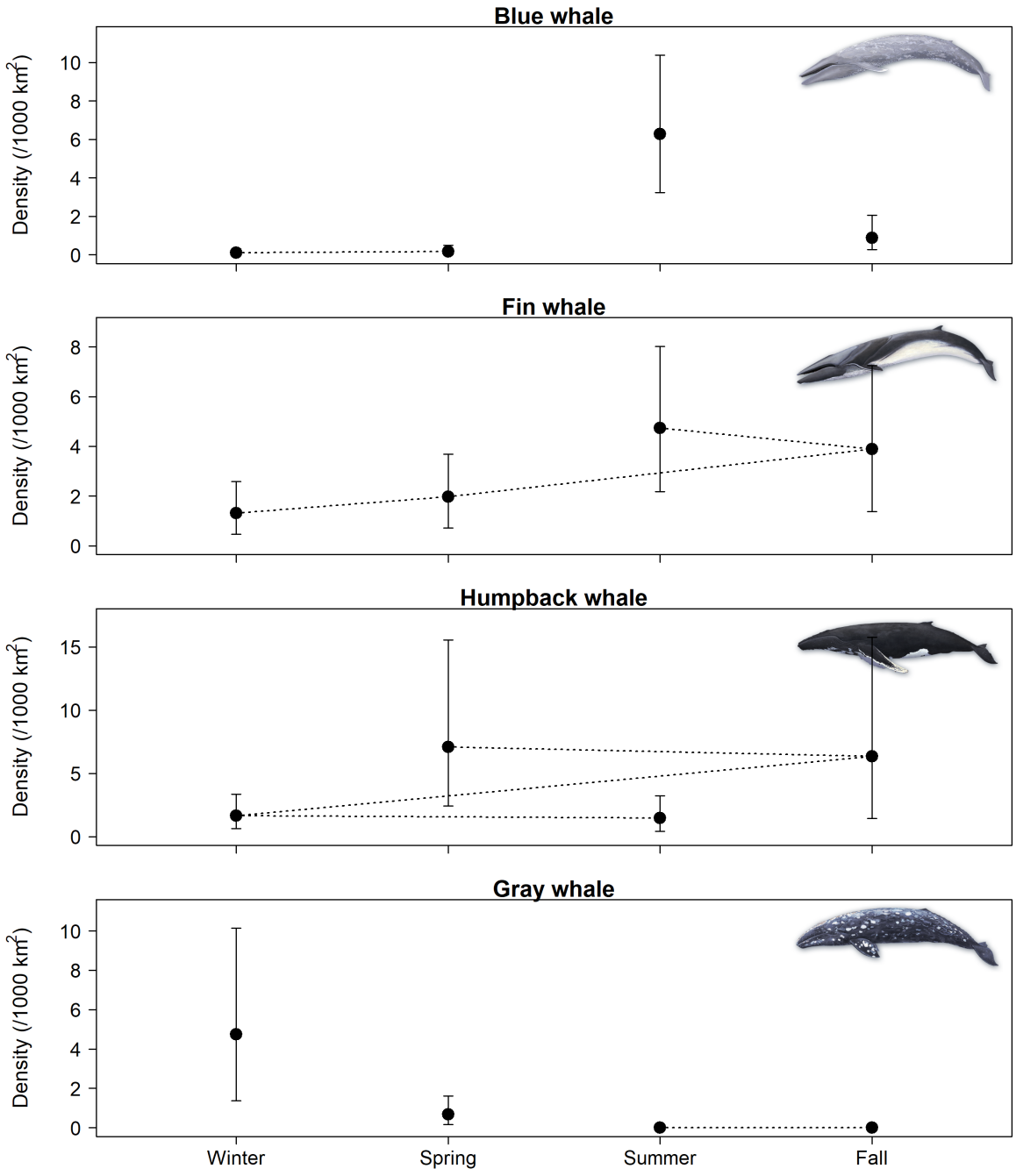


Figure 4.3. Mean seasonal density (animals per 1,000 km^2) for baleen whale species averaged across 2004–2025. Error bars show 95% bootstrap confidence intervals. Dotted lines connect season pairs whose 95% bootstrap confidence interval on the pairwise difference in mean density includes zero (i.e., not significantly different).

Table 4.2. Mean annual density and abundance estimates for the ten cetacean species, averaged across all years and seasons from the bootstrap GAM analysis. $\bar{D}$ = mean density (animals per 1,000 km^2); $\bar{N}$ = mean abundance (animals in study area of 238,494 km^2); 95% CI from the 2.5th and 97.5th percentiles of the bootstrap distribution.

Species	$\bar{D}$	**95% CI** (D)	$\bar{N}$	**95% CI** (N)
Mysticetes				
Blue whale	1.9	1.3–2.6	472	317–630
Fin whale	3.0	1.9–4.1	716	460–995
Gray whale	1.3	0.74–2.1	324	176–506
Humpback whale	4.0	2.3–6.3	956	553–1,514
Odontocetes				
Short-beaked common dolphin	773	488–1,099	184,356	116,400–262,200
Long-beaked common dolphin	436	215–820	103,983	51,300–195,600
Pacific white-sided dolphin	16.7	8.85–29.8	3,982	2,111–7,107
Risso's dolphin	11.2	4.92–23.6	2,671	1,173–5,629
Bottlenose dolphin	25.8	11.1–51.2	6,155	2,647–12,210
Dall's porpoise	12.3	7.12–19.1	2,934	1,698–4,555

Table 4.3. Seasonal density estimates (animals per 1,000 km^2) by species, averaged across 2004–2025. Values are bootstrap means; 95% bootstrap confidence intervals are given in parentheses.

Species	Winter	Spring	Summer	Fall
Mysticetes				
Blue whale	0.12 (0.00–0.31)	0.16 (0.00–0.51)	6.81 (3.42–11.4)	0.82 (0.25–1.91)
Fin whale	1.32 (0.46–2.58)	2.00 (0.75–3.73)	4.53 (2.15–7.44)	4.16 (1.47–7.81)
Gray whale	4.75 (1.40–10.1)	0.68 (0.16–1.59)	≈0	≈0
Humpback whale	1.66 (0.66–3.33)	7.03 (2.44–15.3)	1.33 (0.30–3.06)	6.02 (1.47–14.8)
Odontocetes				
Short-beaked common dolphin	1265 (559–2506)	427 (117–864)	478 (182–925)	920 (359–1654)
Long-beaked common dolphin	717 (109–2692)	86.3 (7.9–280)	206 (39.6–559)	733 (124–2188)
Pacific white-sided dolphin	9.73 (1.00–31.7)	39.7 (10.6–87.8)	10.4 (1.20–29.2)	7.17 (0.95–20.0)
Risso's dolphin	11.2 (2.30–26.3)	22.9 (1.43–87.7)	6.93 (0.69–20.9)	3.75 (0.42–10.9)
Bottlenose dolphin	31.7 (4.81–91.0)	14.2 (2.15–37.9)	26.4 (4.86–71.9)	31.2 (5.00–86.3)
Dall's porpoise	12.7 (4.11–26.9)	34.2 (11.7–73.2)	0.25 (0.00–0.76)	2.14 (0.00–6.36)

Table 4.4. Mean annual rate of density change and 95% bootstrap confidence interval for each species, estimated from the GAM temporal smooth evaluated at 2005 and 2025 (2004 excluded owing to incomplete seasonal coverage). Positive values indicate increasing density; negative values indicate decline. Species whose 95% CI excludes zero are indicated with an asterisk.

Species	**Mean change (% yr^{-1})**	**95% CI**
Mysticetes		
Blue whale	+4.0	−1.6 to +9.9
Fin whale	+2.2	−2.7 to +8.7
Gray whale	+9.7	0.0 to +21.7
Humpback whale*	+11.5	+3.5 to +18.4
Odontocetes		
Short-beaked common dolphin	−0.2	−6.4 to +4.3
Long-beaked common dolphin*	+11.2	+1.8 to +23.4
Risso's dolphin	+0.7	−8.6 to +13.1
Bottlenose dolphin	+4.0	−4.7 to +13.8
Pacific white-sided dolphin	−9.2	−25.6 to 0.0
Dall's porpoise*	−19.2	−48.0 to −4.9

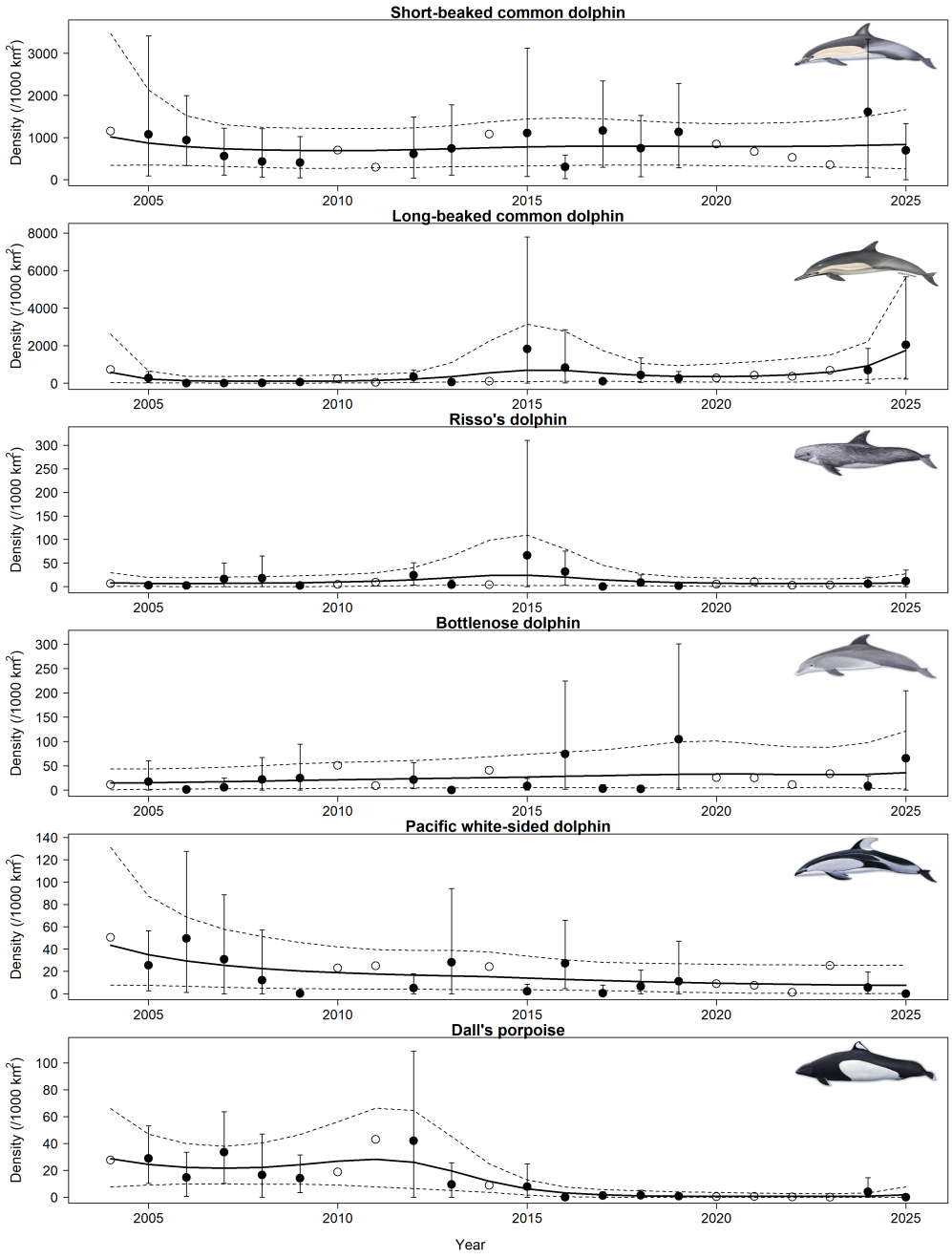


Figure 4.4. Annual density trends (animals per 1,000 km^2) for toothed whale species, 2004–2025. Solid line: bootstrap mean GAM prediction; dashed lines: 95% bootstrap confidence interval. Filled circles: years with all four seasons surveyed (error bars show 95% bootstrap CI on annual density); open circles: years with incomplete seasonal coverage

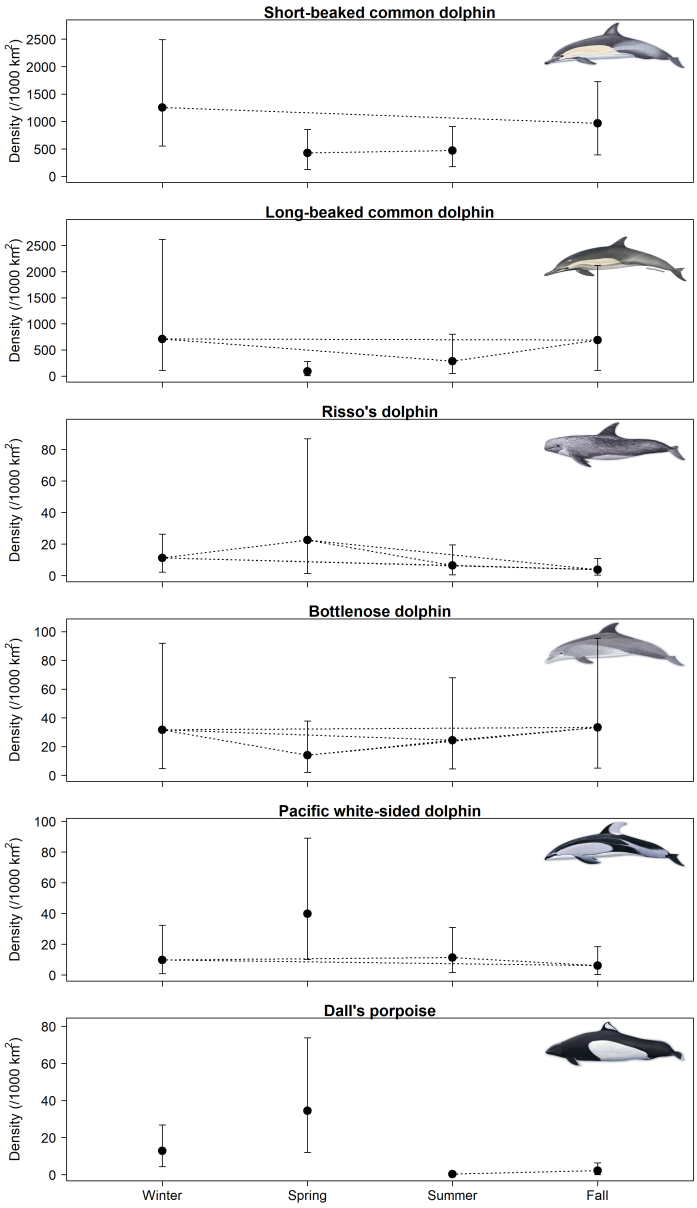


Figure 4.5. Mean seasonal density (animals per 1,000 km^2) for toothed whale species averaged across 2004–2025. Error bars show 95% bootstrap confidence intervals. Dotted lines connect season pairs whose 95% bootstrap confidence interval on the pairwise difference in mean density includes zero (i.e., not significantly different).

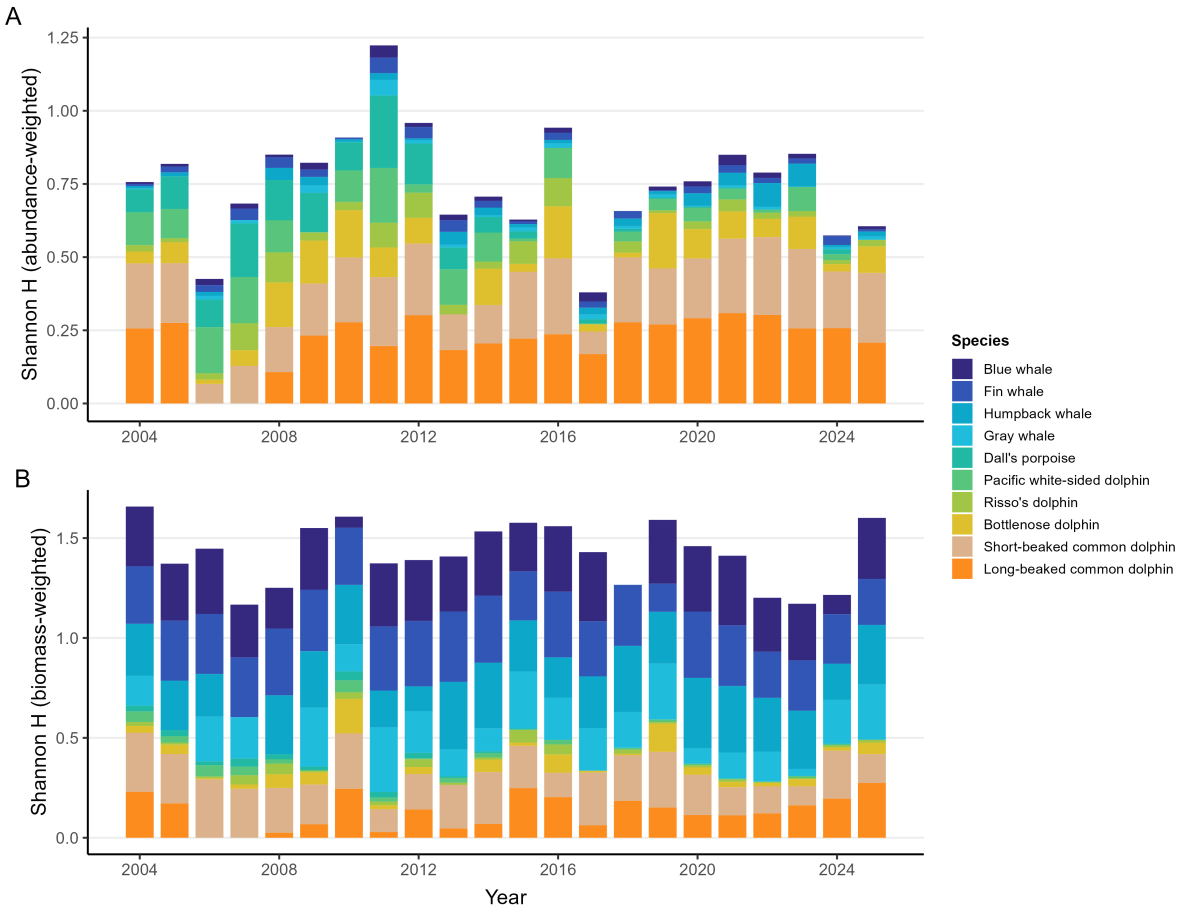


Figure 4.6. Annual Shannon–Wiener diversity index (H') for the ten-species community calculated from abundance and biomass-weighted community matrices, 2004–2025. Top panel shows annual abundance-weighted H' and bottom shows biomass-weighted. Colored bars show each species relative contribution to total H'.

Table 4.5. Bootstrap PERMANOVA results for cetacean community composition comparisons based on Bray–Curtis dissimilarity matrices. Values are bootstrap means and 95% bootstrap confidence intervals (2.5th–97.5th percentiles) from 5,000 replicates, each run with 999 permutations. p: median p-value across replicates; % sig.: proportion of replicates where $p < 0.05$.

	Abundance-weighted			**Biomass-weighted**		
Comparison	**Pseudo-*F* [95% CI]**	***p***	**% sig.**	**Pseudo-*F* [95% CI]**	***p***	**% sig.**
Period comparison						
Pre- vs. post-heatwave	3.51 [1.06–8.13]	0.03	64	2.88 [1.24–4.99]	0.02	77
Seasonal comparison						
All seasons	2.01 [1.29–2.89]	≤0.01	81	5.40 [3.94–7.04]	≤0.01	100
Winter–Spring	2.55 [1.11–4.60]	0.03	62	3.88 [2.02–6.08]	≤0.01	96
Winter–Summer	2.21 [0.93–4.18]	0.06	41	11.28 [7.68–15.66]	≤0.01	100
Winter–Fall	0.99 [0.28–2.17]	0.50	4	3.74 [1.79–5.78]	≤0.01	96
Spring–Summer	3.04 [1.73–5.20]	≤0.01	87	9.06 [5.82–13.28]	≤0.01	100
Spring–Fall	1.97 [1.05–3.38]	0.06	41	2.09 [1.03–3.58]	0.05	46
Summer–Fall	1.45 [0.59–2.84]	0.21	10	4.44 [2.42–6.91]	≤0.01	98

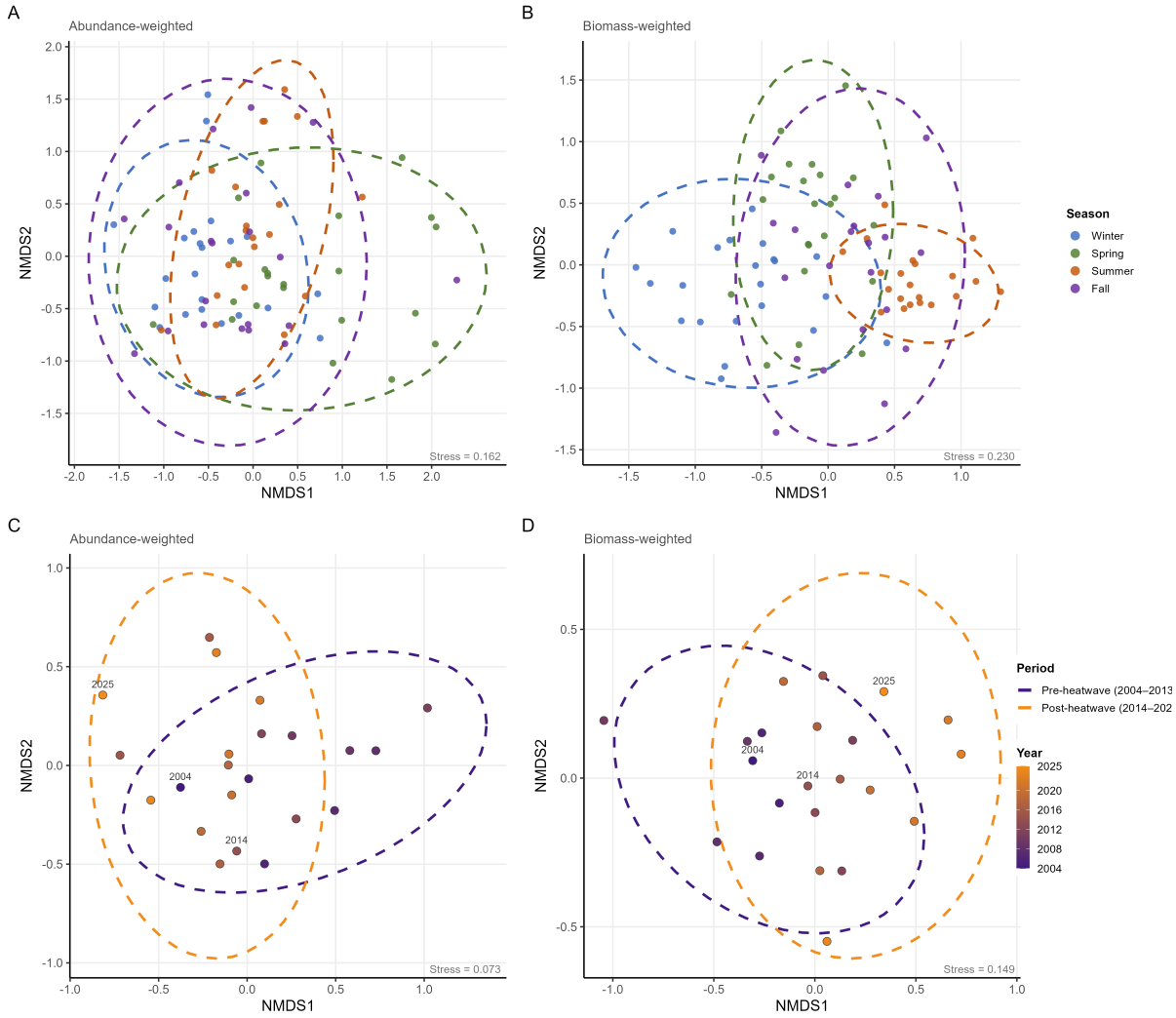


Figure 4.7. NMDS ordination of cetacean community composition based on Bray–Curtis dissimilarity, 2004–2025. Top row: seasonal ordination (A, abundance-weighted; B, biomass-weighted). Each point represents one year–season combination; colors indicate season and 95% confidence ellipses are drawn around each season group. Bottom row: annual ordination (C, abundance-weighted; D, biomass-weighted). Each point represents one year, filled by year (purple: 2004, orange: 2025), with 95% confidence ellipses drawn around the pre-heatwave and post-heatwave periods.

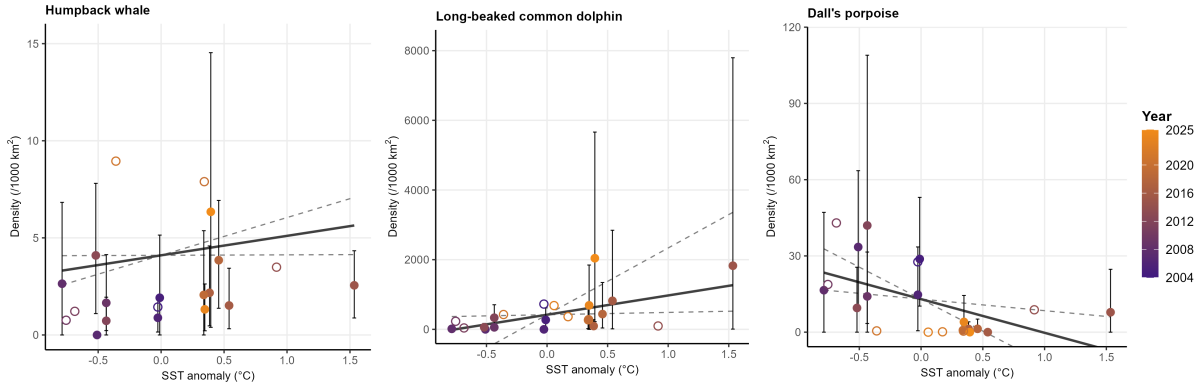


Figure 4.8. Annual density versus annual mean sea surface temperature anomaly for species with significant bootstrap slope confidence intervals. Points are colored by year (purple: 2004, orange: 2025). The solid line is the bootstrap mean regression; the shaded band is the 95% bootstrap prediction envelope. Error bars show 95% bootstrap confidence intervals on annual density estimates.

Bibliography

Akaike, H. (1974). A new look at the statistical model identification. *IEEE transactions on automatic control*, 19(6):716–723.

Alksne, M. N., Kok, A. C., Agarwal, A., Frasier, K. E., and Baumann-Pickering, S. (2024). Biogeographic patterns of Pacific white-sided dolphins based on long-term passive acoustic records. *Diversity and Distributions*, 30(9):e13903.

Alksne, M. N., Roch, M. A., Frasier, K. E., Hildebrand, J. A., Andres, S., Adesanya, D., Baggett, L. M., Jones, J. M., Liu, X., Širović, A., Zhang, X., Zingale, J., and Baumann-Pickering, S. (2026). Application of deep learning to estimate blue and fin whale call density in the southern California Current Ecosystem. *Under Review*.

Anderson, M. J. (2014). Permutational multivariate analysis of variance (PERMANOVA). *Wiley statsref*, pages 1–15.

Andres, J., Baggett, L., and Baumann-Pickering, S. (2026). Spatial and temporal distributions of odontocetes who emit narrow-band high frequency echolocation clicks in the North Pacific. Unpublished manuscript.

Baggett, L. M., Posdaljian, N., ZoBell, V. M., Andres, J. F., Pickering, L. P., Schriber, N. E., Alksne, M. N., Lenssen, K. L., Thayre, B. J., and Baumann-Pickering, S. (2026). Baseline soundscapes and bioacoustic considerations relevant to floating offshore wind development along the U.S. West Coast. *Under Review*.

Barlow, J. (2016). Cetacean abundance in the California Current estimated from ship-based line-transect surveys in 1991–2014. *Administrative report lJ-12-01. Southwest Fisheries Science Center, National Marine Fisheries Service, la Jolla, California, uSA*.

Barlow, J. and Forney, K. A. (2007). Abundance and population density of cetaceans in the California Current ecosystem. *Fishery Bulletin*, 105:509–526.

Barlow, J., Kahru, M., and Mitchell, B. (2008). Cetacean biomass, prey consumption, and primary production requirements in the California Current ecosystem. *Marine Ecology Progress Series*, 371:285–295.

Becker, E. A., Forney, K. A., Foley, D. G., Smith, R. C., Moore, T. J., and Barlow, J. (2014). Predicting seasonal density patterns of California cetaceans based on habitat models. *Endangered Species Research*, 23:1–22.

Becker, E. A., Forney, K. A., Miller, D. L., Barlow, J., Rojas-Bracho, L., Urban R, J., and Moore, J. E. (2022). Dynamic habitat models reflect interannual movement of cetaceans within the California current ecosystem. *Frontiers in Marine Science*, 9:829523.

Becker, E. A., Forney, K. A., Redfern, J. V., Barlow, J., Jacox, M. G., Roberts, J. J., and Palacios, D. M. (2019). Predicting cetacean abundance and distribution in a changing climate. *Diversity and Distributions*, 25(4):626–643.

Block, B. A., Jonsen, I. D., Jorgensen, S. J., Winship, A. J., Shaffer, S. A., Bograd, S. J., Hazen, E. L., Foley, D. G., Breed, G., and Harrison, A.-L. (2011). Tracking apex marine predator movements in a dynamic ocean. *Nature*, 475(7354):86–90.

Bloom, S., Alksne, M., Rice, A., Lankhorst, M., Širović, A., Warren, J., and Baumann-Pickering, S. (2025). Seasonal changes in physical oceanography modulate cetacean predator-prey dynamics in the San Diego Trough. *Marine Ecology Progress Series*, 762:111–133.

Bograd, S. J., Schroeder, I. D., and Jacox, M. G. (2019). A water mass history of the southern California current system. *Geophysical Research Letters*, 46(12):6690–6698.

Bond, N. A., Cronin, M. F., Freeland, H., and Mantua, N. (2015). Causes and impacts of the 2014 warm anomaly in the NE Pacific. *Geophysical Research Letters*, 42(9):3414–3420.

Buckland, S. T., Anderson, D. R., Burnham, K. P., Laake, J. L., Borchers, D. L., and Thomas, L. (2001). *Introduction to Distance Sampling: Estimating Abundance of Biological Populations*. Oxford University Press.

Calambokidis, J., Steiger, G. H., Straley, J. M., Herman, L. M., Cerchio, S., Salden, D. R., Urban R., J., Jacobsen, J. K., von Ziegesar, O., Balcomb, K. C., Gabriele, C. M., Dahlheim, M. E., Uchida, S., Ellis, G., Miyamura, Y., Ladron de Guevara P., P., Yamaguchi, M., Sato, F., Mizroch, S. A., Schlender, L., Rasmussen, K., Barlow, J., and Quinn II, T. J. (2001). Movements and population structure of humpback whales in the North Pacific. *Marine Mammal Science*, 17(4):769–794.

Campbell, G. S., Thomas, L., Whitaker, K., Douglas, A. B., Calambokidis, J., and Hildebrand, J. A. (2015). Inter-annual and seasonal trends in cetacean distribution, density and abundance off southern California. *Deep Sea Research Part II: Topical Studies in Oceanography*, 112:143–157.

Carretta, J. V., Oleson, E. M., Forney, K. A., Bradford, A. L., Yano, K. M., Weller, D. W.,

Lang, A. R., Baker, J., Orr, A. J., Hanson, B., Moore, J. E., Wallen, M., and Brownell, Robert L., J. (2024). U.s. Pacific marine mammal stock assessments: 2023. NOAA Technical Memorandum NMFS-SWFSC-704, NOAA Southwest Fisheries Science Center.

Cavole, L. M., Demko, A. M., Diner, R. E., Giddings, A., Koester, I., Pagniello, C. M. L. S., Paulsen, M.-L., Ramirez-Valdez, A., Schwenck, S. M., Yen, N. K., Zill, M. E., and Franks, P. J. S. (2016). Biological impacts of the 2013-2015 warm-water anomaly in the Northeast Pacific winners, losers, and the future. *Oceanography*, 29(2):273–285.

Checkley Jr, D. M. and Barth, J. A. (2009). Patterns and processes in the California Current System. *Progress in Oceanography*, 83(1-4):49–64.

Cheeseman, T., Barlow, J., Acebes, J. M., Audley, K., Bejder, L., Birdsall, C., Bracamontes, O. S., Bradford, A. L., Byington, J., and Calambokidis, J. (2024). Bellwethers of change: population modelling of North Pacific humpback whales from 2002 through 2021 reveals shift from recovery to climate response. *Royal Society Open Science*, 11(2):231462.

Clapham, P. J., Young, S. B., and Brownell Jr, R. L. (1999). Baleen whales: conservation issues and the status of the most endangered populations. *Mammal Review*, 29(1):37–62.

Croll, D. A., Marinovic, B., Benson, S., Chavez, F. P., Black, N., Ternullo, R., and Tershy, B. R. (2005). From wind to whales: trophic links in a coastal upwelling system. *Marine Ecology Progress Series*, 289:117–130.

Davison, A. C. and Hinkley, D. V. (1997). *Bootstrap methods and their application*. Cambridge university press.

Dohl, T. P., Bonnell, M. L., and Ford, R. G. (1986). Distribution and abundance of common dolphin, Delphinus delphis, in the Southern California Bight: A quantitative assessment based upon aerial transect data. *Fishery Bulletin*, 84(2):333–343.

Doney, S. C., Ruckelshaus, M., Duffy, J. E., Barry, J. P., Chan, F., English, C. A., Galindo, H. M., Grebmeier, J. M., Hollowed, A. B., and Knowlton, N. (2012). Climate change impacts on marine ecosystems. *Annual review of marine science*, 4(2012):11–37.

Dornelas, M., Gotelli, N. J., McGill, B., Shimadzu, H., Moyes, F., Sievers, C., and Magurran, A. E. (2014). Assemblage time series reveal biodiversity change but not systematic loss. *Science*, 344(6181):296–299.

Eguchi, T., Lang, A., and Weller, D. (2024). Abundance of eastern North Pacific gray whales 2023/2024. Noaa technical memorandum, NOAA Technical Memorandum NMFS-SWFSC-695.

Fleming, A. H., Clark, C. T., Calambokidis, J., and Barlow, J. (2016). Humpback whale diets respond to variance in ocean climate and ecosystem conditions in the California Current. *Global Change Biology*, 22(3):1214–1224.

Fleming, A. H., Yack, T., Redfern, J. V., Becker, E. A., Moore, T. J., and Barlow, J. (2018). Combining acoustic and visual detections in habitat models of Dall's porpoise. *Ecological Modelling*, 384:198–208.

Forney, K. A. and Barlow, J. (1998). Seasonal patterns in the abundance and distribution of CALIFORNIA cetaceans, 1991-1992. *Marine Mammal Science*, 14(3):460–489.

Fréon, P., Barange, M., and Arístegui, J. (2009). Eastern boundary upwelling ecosystems: integrative and comparative approaches.

Frölicher, T. L., Fischer, E. M., and Gruber, N. (2018). Marine heatwaves under global warming. *Nature*, 560(7718):360–364.

Gelpi, C. G. and Norris, K. E. (2008). Seasonal temperature dynamics of the upper ocean in the Southern California Bight. *Journal of Geophysical Research: Oceans*, 113(C4).

Guazzo, R. A., Schulman-Janiger, A., Smith, M. H., Barlow, J., Spain, G. L., Rimington, D. B., and Hildebrand, J. A. (2019). Gray whale migration patterns through the Southern California Bight from multi-year visual and acoustic monitoring. *Marine Ecology Progress Series*, 625:181–203.

Hazen, E. L., Abrahms, B., Brodie, S., Carroll, G., Jacox, M. G., Savoca, M. S., Scales, K. L., Sydeman, W. J., and Bograd, S. J. (2019). Marine top predators as climate and ecosystem sentinels. *Frontiers in Ecology and the Environment*, 17(10):565–574.

Henderson, E. E., Hildebrand, J. A., and Smith, M. H. (2011). Classification of behavior using vocalizations of Pacific white-sided dolphins (Lagenorhynchus obliquidens). *The Journal of the Acoustical Society of America*, 130(1):557–567.

Hirtle, N., Roberts, J. J., Redfern, J. V., Hazen, E. L., Palka, D., McLellan, W., Garrison, L., Barco, S., O'brien, O., and Quintana-Rizzo, E. (2026). Models incorporating non-stationarity improve detection of climate-driven range shifts in odontocetes. *Diversity and Distributions*, 32(2):e70154.

Jacox, M. G., Alexander, M. A., Bograd, S. J., and Scott, J. D. (2020). Thermal displacement by marine heatwaves. *Nature*, 584(7819):82–86.

Jacox, M. G., Hazen, E. L., Zaba, K. D., Rudnick, D. L., Edwards, C. A., Moore, A. M., and Bograd, S. J. (2016). Impacts of the 2015–2016 El Niño on the California Current

System: Early assessment and comparison to past events. *Geophysical Research Letters*, 43(13):7072–7080.

Jefferson, T. A., Archer, F. I., and Robertson, K. M. (2024). The long-beaked common dolphin of the eastern Pacific Ocean: Taxonomic status and redescription of *Delphinus bairdii*. *Marine Mammal Science*, 40(4):e13133.

Keener, W., Webber, M. A., Markowitz, T. M., Cotter, M. P., Maldini, D., Defran, R., Rice, M., Debich, A. J., Lang, A. R., and Kelly, D. L. (2023). Northern range expansion of California coastal bottlenose dolphins (Tursiops truncatus). *Aquatic Mammals*, 49(1):29–43.

Kerosky, S. M., Širović, A., Roche, L. K., Baumann-Pickering, S., Wiggins, S. M., and Hildebrand, J. A. (2012). Bryde's whale seasonal range expansion and increasing presence in the Southern California Bight from 2000 to 2010. *Deep Sea Research Part I: Oceanographic Research Papers*, 65:125–132.

Koslow, J. A., Miller, E. F., and McGowan, J. A. (2015). Dramatic declines in coastal and oceanic fish communities off California. *Marine Ecology Progress Series*, 538:221–227.

Lerczak, J. A. and Hobbs, R. C. (1998). Calculating sighting distances from angular readings during shipboard, aerial, and shore-based marine mammal surveys. *Marine Mammal Science*, 14(3):590–598.

MacLeod, C. (2009). Global climate change, range changes and potential implications for the conservation of marine cetaceans: A review and synthesis. *Endangered Species Research*, 7:125–136.

Magurran, A. E. and Henderson, P. A. (2010). Temporal turnover and the maintenance of diversity in ecological assemblages. *Philosophical Transactions of the Royal Society B: Biological Sciences*, 365(1558):3611.

Marques, F. F. and Buckland, S. T. (2003). Incorporating covariates into standard line transect analyses. *Biometrics*, 59(4):924–935.

Marques, T. A., Thomas, L., Fancy, S. G., and Buckland, S. T. (2007). Improving estimates of bird density using multiple-covariate distance sampling. *The Auk*, 124(4):1229–1243.

Martien, K. K., Taylor, B. L., Lang, A. R., Clapham, P. J., Weller, D. W., Archer, F. I., and Calambokidis, J. (2023). The migratory whale herd concept: A novel unit to conserve under the ecological paradigm. *Marine Mammal Science*, 39(4):1267–1292.

McClatchie, S., Thompson, A. R., Alin, S. R., Siedlecki, S., Watson, W., and Bograd, S. J. (2016). The influence of Pacific equatorial water on fish diversity in the southern California

Current System. *Journal of Geophysical Research: Oceans*, 121(8):6121–6136.

Monnahan, C. C., Branch, T. A., and Punt, A. E. (2015). Do ship strikes threaten the recovery of endangered eastern North Pacific blue whales? *Marine Mammal Science*, 31(1):279–297.

Moore, J. E. and Barlow, J. (2011). Bayesian state-space model of fin whale abundance trends from a 1991–2008 time series of line-transect surveys in the California Current. *Journal of Applied Ecology*, 48(5):1195–1205.

NOAA Climate Prediction Center (2026). El niño/la niña advisory. Accessed June 2026.

NOAA Integrated Ecosystem Assessment (2026). 2025 North Pacific marine heatwave report. Accessed June 2026.

Oleson, E. M., Wiggins, S. M., and Hildebrand, J. A. (2007). Temporal separation of blue whale call types on a southern California feeding ground. *Animal Behaviour*, 74(4):881–894.

Palacios, D. M., Bailey, H., Becker, E. A., Bograd, S. J., DeAngelis, M. L., Forney, K. A., Hazen, E. L., Irvine, L. M., and Mate, B. R. (2019). Ecological correlates of blue whale movement behavior and its predictability in the California Current Ecosystem during the summer-fall feeding season. *Movement Ecology*, 7(1):26.

Pecl, G. T., Araújo, M. B., Bell, J. D., Blanchard, J., Bonebrake, T. C., Chen, I.-C., Clark, T. D., Colwell, R. K., Danielsen, F., and Evengård, B. (2017). Biodiversity redistribution under climate change: Impacts on ecosystems and human well-being. *Science*, 355(6332):eaai9214.

Poloczanska, E. S., Brown, C. J., Sydeman, W. J., Kiessling, W., Schoeman, D. S., Moore, P. J., Brander, K., Bruno, J. F., Buckley, L. B., and Burrows, M. T. (2013). Global imprint of climate change on marine life. *Nature climate change*, 3(10):919–925.

Poole, M. M. (1984). Migration corridors of gray whales along the central California coast, 1980–1982. In Jones, M. L., Swartz, S. L., and Leatherwood, S., editors, *The Gray Whale, Eschrichtius robustus*. Academic Press, Orlando, FL.

Rayner, N. A., Parker, D. E., Horton, E., Folland, C. K., Alexander, L. V., Rowell, D., Kent, E. C., and Kaplan, A. (2003). Global analyses of sea surface temperature, sea ice, and night marine air temperature since the late nineteenth century. *Journal of Geophysical Research: Atmospheres*, 108(D14).

Rocha, R. C., Clapham, P. J., and Ivashchenko, Y. V. (2014). Emptying the oceans: a summary of industrial whaling catches in the 20th century. *Marine Fisheries Review*, 76(4):37–48.

Russell, T. M., Pereksta, D. M., Tietz, J. R., Vernet, M., Jahncke, J., and Ballance, L. T. (2025).

Increase of tropical seabirds (Sula) in the California Current Ecosystem with warmer ocean conditions. *Frontiers in Marine Science*, 12:1561438.

Ryan, J. P., Cline, D. E., Joseph, J. E., Margolina, T., Santora, J. A., Kudela, R. M., Chavez, F. P., Pennington, J. T., Wahl, C., Michisaki, R., Benoit-Bird, K., Forney, K. A., Stimpert, A. K., DeVogelaere, A., Black, N., and Fischer, M. (2019). Humpback whale song occurrence reflects ecosystem variability in feeding and migratory habitat of the northeast Pacific. *PLoS ONE*, 14(9):e0222456.

Salvadeo, C. J., Lluch-Belda, D., Gomez-Gallardo, A., Urban-Ramirez, J., and MacLeod, C. D. (2010). Climate change and a poleward shift in the distribution of the Pacific white-sided dolphin in the northeastern Pacific. *Endangered Species Research*, 11(1):13–19.

Santora, J. A., Mantua, N. J., Schroeder, I. D., Field, J. C., Hazen, E. L., Bograd, S. J., Sydeman, W. J., Wells, B. K., Calambokidis, J., and Saez, L. (2020). Habitat compression and ecosystem shifts as potential links between marine heatwave and record whale entanglements. *Nature communications*, 11(1):536.

Santora, J. A., Schroeder, I. D., Hazen, E. L., Field, J. C., and Forney, K. A. (2026). Whale entanglements disentangled through the lens of cumulative habitat compression. *PLOS Climate*.

Satterthwaite, E. V., Ruiz, T. D., Patin, N. V., Alksne, M. N., Thomas, L., Dinasquet, J., Lampe, R. H., Chan, K. G., Patrick, N. A., Allen, A. E., Baumann-Pickering, S., and Semmens, B. X. (2026). Microbial and small zooplankton communities predict density of baleen whales in the southern California Current Ecosystem. *PLOS ONE*, 21(5):e0334209.

Seger, K. D. and Miksis-Olds, J. L. (2019). Acoustic documentation of temperate odontocetes in the Bering and Chukchi seas. *Marine Mammal Science*.

Širović, A., Rice, A., Chou, E., Hildebrand, J. A., Wiggins, S., and Roch, M. (2015). Seven years of blue and fin whale call abundance in the Southern California Bight. *Endangered Species Research*, 28.

Širović, A., Williams, L. N., Kerosky, S. M., Wiggins, S. M., and Hildebrand, J. A. (2013). Temporal separation of two fin whale call types across the eastern North Pacific. *Marine Biology*, 160(1):47–57.

Soldevilla, M. S., Wiggins, S. M., and Hildebrand, J. A. (2010a). Spatial and temporal patterns of Risso's dolphin echolocation in the Southern California Bight. *The Journal of the Acoustical Society of America*, 127(1):124–132.

Soldevilla, M. S., Wiggins, S. M., and Hildebrand, J. A. (2010b). Spatio-temporal comparison

of Pacific white-sided dolphin echolocation click types. *Aquatic Biology*, 9(1):49–62.

Stewart, J. D., Joyce, T. W., Durban, J. W., Calambokidis, J., Fauquier, D., Fearnbach, H., Grebmeier, J. M., Lynn, M., Manizza, M., and Perryman, W. L. (2023). Boom-bust cycles in gray whales associated with dynamic and changing Arctic conditions. *Science*, 382(6667):207–211.

Suryan, R. M., Arimitsu, M. L., Coletti, H. A., Hopcroft, R. R., Lindeberg, M. R., Barbeaux, S. J., Batten, S. D., Burt, W. J., Bishop, M. A., and Bodkin, J. L. (2021). Ecosystem response persists after a prolonged marine heatwave. *Scientific reports*, 11(1):6235.

Szesciorka, A. R., Ballance, L. T., Širović, A., Rice, A., Ohman, M. D., Hildebrand, J. A., and Franks, P. J. S. (2020). Timing is everything: Drivers of interannual variability in blue whale migration. *Scientific Reports*, 10(1):7710.

Tanaka, K. R., Van Houtan, K. S., Mailander, E., Dias, B. S., Galginaitis, C., O'Sullivan, J., Lowe, C. G., and Jorgensen, S. J. (2021). North Pacific warming shifts the juvenile range of a marine apex predator. *Scientific reports*, 11(1):3373.

Thomas, L., Buckland, S. T., Rexstad, E. A., Laake, J. L., Strindberg, S., Hedley, S. L., Bishop, J. R., Marques, T. A., and Burnham, K. P. (2010). Distance software: design and analysis of distance sampling surveys for estimating population size. *Journal of Applied Ecology*, 47(1):5–14.

Thompson, A. R., Bjorkstedt, E. P., Bograd, S. J., Fisher, J. L., Hazen, E. L., Leising, A., Santora, J. A., Satterthwaite, E. V., Sydeman, W. J., and Alksne, M. (2022). State of the California Current Ecosystem in 2021: Winter is coming? *Frontiers in Marine Science*, 9:958727.

Thompson, A. R., Swalethorp, R., Alksne, M., Santora, J. A., Hazen, E. L., Leising, A., Satterthwaite, E., Sydeman, W. J., Anderson, C. R., Auth, T. D., Baumann-Pickering, S., Baumgardner, T., Bjorkstedt, E. P., Bograd, S. J., Bowlin, N. M., Burke, B. J., Daly, E. A., Dewar, H., Field, J. C., Fisher, J. L., Garfield, N., Gidding, A., Goericke, R., Golightly, R., Gomez-Ocampo, E., Gomez-Valdes, J., Hildebrand, J. A., Jacobson, K. C., Jacox, M. G., Jahncke, J., Johns, M., Jones, J. M., Lavaniegos, B., Mantua, N., McChesney, G. J., Medina, M. E., Melin, S. R., Miranda, L. E., Morgan, C. A., Nickels, C. F., Orben, R. A., Porquez, J. M., Preti, A., Robertson, R. R., Rudnick, D. L., Sakuma, K. M., Schacter, C. R., Schroeder, I. D., Scopel, L., Snodgrass, O. E., Thompson, S. A., Warzybok, P., Whitaker, K., Watson, W., Weber, E. D., and Wells, B. (2024). State of the California Current Ecosystem report in 2022: a tale of two La Ninas. *Frontiers in Marine Science*, 11.

Thorne, L. H., Heywood, E. I., and Hirtle, N. O. (2022). Rapid restructuring of the odontocete community in an ocean warming hotspot. *Global Change Biology*, 28(22):6524–6540.

van Weelden, C., Towers, J. R., and Bosker, T. (2021). Impacts of climate change on cetacean distribution, habitat and migration. *Climate Change Ecology*, 1:100009.

Wernberg, T., Thomsen, M. S., Burrows, M. T., Filbee-Dexter, K., Hobday, A. J., Holbrook, N. J., Montie, S., Moore, P. J., Oliver, E. C., and Sen Gupta, A. (2025). Marine heatwaves as hot spots of climate change and impacts on biodiversity and ecosystem services. *Nature Reviews Biodiversity*, 1(7):461–479.

Williams, R. and Thomas, L. (2007). Distribution and abundance of marine mammals in the coastal waters of British Columbia, Canada. *J. Cetacean Res. Manage.*, 9(1):15–28.

Zaba, K. D. and Rudnick, D. L. (2016). The 2014–2015 warming anomaly in the Southern California Current System observed by underwater gliders. *Geophysical Research Letters*, 43(3):1241–1248.

4.6 Supplementary Material

4.6.1 S1 Survey Metadata

Table 4.6. Survey effort for each CalCOFI cruise in the study area. Trackline length is the total on-effort, on-transect distance surveyed within the southern CalCOFI grid. Observer height is the height of the observation platform above the waterline for the ship used during a given cruise.

Cruise	Season	Start date	End date	Trackline (km)	Observer height (m)
CC2004-07	Summer	13 Jul 2004	26 Jul 2004	1340.6	11.0
CC2004-11	Fall	02 Nov 2004	16 Nov 2004	920.7	13.0
CC2005-01	Winter	05 Jan 2005	18 Jan 2005	905.4	8.1
CC2005-04	Spring	16 Apr 2005	30 Apr 2005	1218.2	8.1
CC2005-07	Summer	02 Jul 2005	15 Jul 2005	1354.8	8.1
CC2005-11	Fall	05 Nov 2005	19 Nov 2005	869.7	8.1
CC2006-02	Winter	04 Feb 2006	21 Feb 2006	1146.2	11.0
CC2006-04	Spring	02 Apr 2006	16 Apr 2006	1315.3	8.1

Continued on next page

Table 4.6 continued from previous page

Cruise	Season	Start date	End date	Trackline (km)	Observer height (m)
CC2006-07	Summer	09 Jul 2006	23 Jul 2006	474.5	8.1
CC2006-10	Fall	22 Oct 2006	02 Nov 2006	612.5	13.0
CC2007-01	Winter	13 Jan 2007	29 Jan 2007	979.3	11.0
CC2007-04	Spring	02 Apr 2007	14 Apr 2007	638.5	11.0
CC2007-07	Summer	28 Jun 2007	12 Jul 2007	695.3	8.1
CC2007-11	Fall	03 Nov 2007	17 Nov 2007	428.0	8.1
CC2008-01	Winter	08 Jan 2008	24 Jan 2008	764.1	11.0
CC2008-03	Spring	25 Mar 2008	06 Apr 2008	463.2	11.0
CC2008-08	Summer	14 Aug 2008	29 Aug 2008	1256.3	8.1
CC2008-10	Fall	15 Oct 2008	28 Oct 2008	1120.7	8.1
CC2009-01	Winter	08 Jan 2009	22 Jan 2009	1391.6	8.1
CC2009-03	Spring	08 Mar 2009	21 Mar 2009	906.5	11.0
CC2009-07	Summer	15 Jul 2009	30 Jul 2009	1419.2	17.0
CC2009-11	Fall	07 Nov 2009	22 Nov 2009	939.2	8.1
CC2010-01	Winter	13 Jan 2010	30 Jan 2010	854.5	8.1
CC2010-08	Summer	30 Jul 2010	15 Aug 2010	1220.0	17.0
CC2010-11	Fall	28 Oct 2010	10 Nov 2010	979.6	8.1
CC2011-01	Winter	13 Jan 2011	29 Jan 2011	1059.3	8.1
CC2011-08	Summer	27 Jul 2011	11 Aug 2011	1284.1	8.1
CC2011-10	Fall	17 Oct 2011	30 Oct 2011	949.3	8.1
CC2012-02	Winter	28 Jan 2012	03 Feb 2012	499.5	8.1
CC2012-03	Spring	25 Mar 2012	03 Apr 2012	692.1	13.8
CC2012-07	Summer	03 Jul 2012	25 Jul 2012	1405.1	11.0

Continued on next page

Table 4.6 continued from previous page

Cruise	Season	Start date	End date	Trackline (km)	Observer height (m)
CC2012-10	Fall	20 Oct 2012	03 Nov 2012	973.4	8.1
CC2013-01	Winter	11 Jan 2013	26 Jan 2013	888.1	13.8
CC2013-04	Spring	07 Apr 2013	25 Apr 2013	858.7	13.8
CC2013-07	Summer	07 Jul 2013	21 Jul 2013	1339.5	8.1
CC2013-11	Fall	10 Nov 2013	24 Nov 2013	862.6	8.1
CC2014-02	Winter	29 Jan 2014	04 Feb 2014	465.9	13.8
CC2014-04	Spring	03 Apr 2014	15 Apr 2014	838.1	11.0
CC2014-11	Fall	09 Nov 2014	21 Nov 2014	1095.1	8.1
CC2015-01	Winter	16 Jan 2015	31 Jan 2015	983.8	8.1
CC2015-04	Spring	05 Apr 2015	18 Apr 2015	1077.7	8.1
CC2015-07	Summer	11 Jul 2015	24 Jul 2015	1340.7	7.1
CC2015-11	Fall	29 Oct 2015	11 Nov 2015	986.9	7.1
CC2016-01	Winter	07 Jan 2016	23 Jan 2016	1002.9	13.3
CC2016-04	Spring	02 Apr 2016	17 Apr 2016	1217.9	13.8
CC2016-07	Summer	11 Jul 2016	25 Jul 2016	1267.1	11.0
CC2016-11	Fall	07 Nov 2016	20 Nov 2016	864.5	10.4
CC2017-01	Winter	06 Jan 2017	19 Jan 2017	1021.2	13.3
CC2017-04	Spring	29 Mar 2017	14 Apr 2017	1362.0	13.8
CC2017-08	Summer	01 Aug 2017	15 Aug 2017	1397.6	10.4
CC2017-11	Fall	10 Nov 2017	23 Nov 2017	888.9	10.4
CC2018-02	Winter	02 Feb 2018	09 Feb 2018	665.5	13.8
CC2018-04	Spring	06 Apr 2018	21 Apr 2018	1097.2	13.8
CC2018-06	Summer	09 Jun 2018	23 Jun 2018	1246.0	10.4

Continued on next page

Table 4.6 continued from previous page

Cruise	Season	Start date	End date	Trackline (km)	Observer height (m)
CC2018-10	Fall	14 Oct 2018	28 Oct 2018	1079.1	10.4
CC2019-02	Winter	07 Feb 2019	12 Feb 2019	371.3	13.3
CC2019-04	Spring	02 Apr 2019	16 Apr 2019	778.8	13.3
CC2019-07	Summer	12 Jul 2019	26 Jul 2019	1391.2	8.1
CC2019-11	Fall	05 Nov 2019	17 Nov 2019	595.3	7.1
CC2020-01	Winter	05 Jan 2020	20 Jan 2020	922.5	13.3
CC2021-07	Summer	19 Jul 2021	01 Aug 2021	1041.8	10.4
CC2022-04	Spring	12 Apr 2022	22 Apr 2022	417.9	13.3
CC2022-08	Summer	14 Aug 2022	29 Aug 2022	1141.2	8.1
CC2022-11	Fall	06 Nov 2022	18 Nov 2022	416.7	10.4
CC2023-01	Winter	07 Jan 2023	15 Jan 2023	378.9	13.3
CC2023-03	Spring	26 Mar 2023	17 Apr 2023	697.5	13.3
CC2023-11	Fall	05 Nov 2023	17 Nov 2023	590.1	10.4
CC2024-01	Winter	20 Jan 2024	30 Jan 2024	606.8	13.3
CC2024-03	Spring	27 Mar 2024	10 Apr 2024	744.5	13.3
CC2024-07	Summer	28 Jul 2024	10 Aug 2024	1014.7	10.4
CC2024-11	Fall	19 Nov 2024	23 Nov 2024	181.2	10.4
CC2025-01	Winter	04 Jan 2025	22 Jan 2025	592.4	13.3
CC2025-03	Spring	21 Mar 2025	14 Apr 2025	906.9	13.3
CC2025-07	Summer	20 Jul 2025	27 Jul 2025	569.1	10.4
CC2025-11	Fall	09 Nov 2025	16 Nov 2025	249.7	10.4

4.7 S2 Detection functions

Table 4.7. Summary of CalCOFI visual survey effort by season.

Season	Cruises	Trackline (km)
Winter	19	15,499
Spring	17	15,231
Summer	19	22,199
Fall	20	15,603
Total	**75**	**68,532**

Table 4.8. Candidate detection function models evaluated for each species, ranked by AIC. The selected model for inference is marked with †. For Dall's porpoise, Pacific white-sided dolphin, and bottlenose dolphin the AIC-best model was not selected because the fitted hazard-rate function produced an unrealistic spike in detection probability near zero distance; the selected model is marked with ‡ in those species' panels. Adjustment terms: Cos = cosine; Poly = simple polynomial. Covariates retained in the scale parameter.

Model	Covariates	AIC	ΔAIC
Mysticetes			
Blue whale			
Uniform + Cos(1)†	—	2169.4	0.00
Half-normal	—	2170.0	0.60
Uniform + Cos(2)	—	2170.3	0.88
Half-normal	sea state	2170.5	1.02
Hazard-rate	—	2170.8	1.35
Half-normal	group size	2170.9	1.42
Hazard-rate	group size	2171.1	1.67
Half-normal	swell	2172.0	2.52
Half-normal + Cos(1)	—	2172.0	2.59
Hazard-rate	observer ht.	2172.4	2.92
Hazard-rate	swell	2172.8	3.33

Continued on next page

Table 4.8 continued from previous page

Model	Covariates	AIC	ΔAIC
Hazard-rate + Poly(1)	—	2172.8	3.35
Half-normal	observer ht.	2173.1	3.69
Uniform	—	2226.0	56.56
Hazard-rate	sea state	2232.0	62.54
Fin whale			
Half-normal[†]	sea state, group size, observer ht.	3484.1	0.00
Half-normal	sea state, group size, observer ht., swell	3484.7	0.58
Half-normal	sea state, group size	3485.9	1.78
Half-normal	sea state, group size, swell	3486.2	2.07
Hazard-rate	sea state, group size, observer ht.	3491.7	7.55
Hazard-rate	sea state, group size, observer ht., swell	3492.1	7.98
Hazard-rate	sea state, group size	3492.3	8.16
Hazard-rate	sea state, observer ht.	3492.6	8.50
Half-normal	sea state	3492.9	8.77
Half-normal	sea state, swell	3492.9	8.78
Hazard-rate	sea state	3493.1	8.98
Hazard-rate	sea state, group size, swell	3493.3	9.20
Hazard-rate	sea state, swell	3494.3	10.21
Half-normal	sea state, observer ht.	3494.6	10.54
Hazard-rate	swell	3496.1	12.01
Half-normal	swell	3496.5	12.38
Half-normal + Cos(1)	—	3501.0	16.89
Hazard-rate	group size	3501.1	17.01

Continued on next page

Table 4.8 continued from previous page

Model	Covariates	AIC	ΔAIC
Half-normal	group size	3501.9	17.76
Hazard-rate	—	3502.4	18.28
Hazard-rate	observer ht.	3502.6	18.47
Uniform + Cos(2)	—	3503.5	19.43
Uniform + Cos(3)	—	3503.6	19.45
Hazard-rate + Poly(1)	—	3503.6	19.47
Half-normal	—	3503.7	19.56
Uniform + Cos(1)	—	3505.5	21.42
Half-normal	observer ht.	3507.2	23.10
Uniform	—	3595.8	111.74
Humpback whale			
Half-normal[†]	swell, observer ht., sea state	3044.2	0.00
Uniform + Cos(1)	—	3044.5	0.36
Uniform + Cos(2)	—	3045.2	1.06
Half-normal	swell, observer ht.	3045.6	1.42
Half-normal	sea state, swell, observer ht., group size	3045.9	1.77
Half-normal	swell	3046.0	1.78
Hazard-rate	—	3046.1	1.96
Half-normal	swell, sea state	3046.1	1.97
Hazard-rate	group size	3046.4	2.21
Half-normal	swell, group size	3046.7	2.58
Half-normal	—	3046.8	2.60
Hazard-rate	swell	3047.2	3.04

Continued on next page

Table 4.8 continued from previous page

Model	Covariates	AIC	ΔAIC
Half-normal	swell, observer ht., group size	3047.4	3.19
Half-normal + Cos(1)	—	3047.4	3.22
Half-normal	group size	3047.8	3.64
Hazard-rate	sea state	3047.9	3.77
Hazard-rate + Poly(1)	—	3048.1	3.96
Hazard-rate	observer ht.	3048.2	4.04
Half-normal	sea state	3048.7	4.53
Half-normal	observer ht.	3049.1	4.88
Uniform	—	3082.2	37.98
Gray whale			
Half-normal + Cos(1)[†]	—	951.7	0.00
Hazard-rate	—	952.1	0.38
Half-normal + Cos(2)	—	952.6	0.91
Half-normal	—	952.7	0.98
Uniform + Cos(1)	—	952.9	1.25
Hazard-rate	swell	953.3	1.59
Half-normal	swell	953.6	1.91
Hazard-rate	group size	953.8	2.16
Uniform + Cos(2)	—	953.9	2.18
Hazard-rate + Poly(1)	—	953.9	2.25
Hazard-rate	sea state	954.0	2.35
Half-normal	sea state	954.5	2.86
Half-normal	group size	954.6	2.91

Continued on next page

Table 4.8 continued from previous page

Model	Covariates	AIC	ΔAIC
Hazard-rate	observer ht.	954.8	3.12
Half-normal	observer ht.	955.5	3.80
Uniform	—	965.1	13.43
Odontocetes			
Short-beaked common dolphin			
Hazard-rate†	sea state, group size	6332.8	0.00
Hazard-rate	sea state, group size, swell	6333.9	1.07
Hazard-rate	sea state	6334.1	1.24
Hazard-rate	sea state, swell	6335.5	2.69
Hazard-rate	sea state, group size, observer ht.	6336.5	3.69
Hazard-rate	sea state, observer ht.	6338.0	5.15
Hazard-rate + Poly(1)	—	6344.5	11.67
Hazard-rate	group size	6353.9	21.06
Hazard-rate	swell	6356.6	23.75
Hazard-rate	—	6357.3	24.48
Half-normal + Cos(2)	—	6359.5	26.73
Hazard-rate	observer ht.	6360.0	27.23
Uniform + Cos(3)	—	6374.4	41.56
Half-normal + Cos(1)	—	6378.7	45.86
Half-normal	sea state, group size	6401.8	68.98
Half-normal	sea state, group size, swell	6402.2	69.37
Half-normal	sea state	6402.6	69.83

Continued on next page

Table 4.8 continued from previous page

Model	Covariates	AIC	ΔAIC
Half-normal	sea state, swell	6402.7	69.90
Half-normal	sea state, group size, observer ht.	6403.5	70.73
Half-normal	sea state, observer ht.	6404.4	71.60
Half-normal	swell	6408.6	75.80
Uniform + Cos(2)	—	6411.9	79.04
Half-normal	group size	6415.0	82.23
Half-normal	—	6416.6	83.77
Half-normal	observer ht.	6418.8	85.99
Uniform + Cos(1)	—	6443.4	110.61
Uniform	—	6761.6	428.76
Long-beaked common dolphin			
Half-normal[†]	group size	1022.8	0.00
Half-normal	—	1024.4	1.59
Half-normal	group size, swell	1024.6	1.78
Half-normal	group size, sea state	1024.6	1.80
Uniform + Cos(1)	—	1024.9	2.15
Half-normal + Cos(1)	—	1025.5	2.75
Hazard-rate	group size	1025.9	3.13
Half-normal	group size, observer ht.	1026.3	3.48
Half-normal	sea state	1026.3	3.55
Half-normal	swell	1026.4	3.59
Hazard-rate	—	1026.7	3.87
Uniform + Cos(2)	—	1026.7	3.90

Continued on next page

Table 4.8 continued from previous page

Model	Covariates	AIC	ΔAIC
Hazard-rate + Poly(1)	—	1027.1	4.28
Hazard-rate	group size, swell	1027.5	4.67
Hazard-rate	group size, sea state	1027.9	5.11
Half-normal	observer ht.	1028.1	5.29
Hazard-rate	swell	1028.6	5.79
Hazard-rate	sea state	1028.6	5.86
Hazard-rate	group size, observer ht.	1029.4	6.60
Hazard-rate	observer ht.	1030.3	7.51
Uniform	—	1047.6	24.78
Risso's dolphin			
Hazard-rate[†]	group size, sea state	836.9	0.00
Half-normal	sea state	836.9	0.00
Half-normal	sea state, group size	838.1	1.26
Half-normal	sea state, swell	838.9	1.99
Half-normal	sea state, observer ht.	840.3	3.38
Half-normal	swell	840.8	3.96
Hazard-rate	group size, swell	841.1	4.25
Hazard-rate	group size	841.5	4.63
Hazard-rate	swell	841.6	4.74
Half-normal	group size	842.4	5.51
Half-normal	—	843.4	6.52
Hazard-rate	group size, observer ht.	843.9	7.02
Uniform + Cos(1)	—	843.9	7.06

Continued on next page

Table 4.8 continued from previous page

Model	Covariates	AIC	ΔAIC
Hazard-rate	—	845.1	8.22
Half-normal + Cos(1)	—	845.2	8.29
Uniform + Cos(2)	—	845.3	8.39
Half-normal	observer ht.	846.4	9.56
Hazard-rate + Poly(1)	—	847.1	10.21
Hazard-rate	observer ht.	848.5	11.64
Uniform	—	850.8	13.92
Hazard-rate	sea state	856.0	19.08
Hazard-rate	sea state, group size, swell	860.8	23.92
Bottlenose dolphin			
Hazard-rate	observer ht.	778.8	0.00
Hazard-rate	observer ht., sea state	779.6	0.73
Hazard-rate	observer ht., group size	780.1	1.29
Hazard-rate	observer ht., swell	780.3	1.41
Half-normal + Cos(1)[‡]	—	780.7	1.82
Hazard-rate	—	781.6	2.80
Uniform + Cos(3)	—	782.1	3.25
Half-normal + Cos(2)	—	782.4	3.58
Hazard-rate + Poly(1)	—	782.7	3.82
Hazard-rate	sea state	782.7	3.90
Hazard-rate	group size	782.9	4.08
Hazard-rate	swell	783.5	4.61
Half-normal	—	786.0	7.19

Continued on next page

Table 4.8 continued from previous page

Model	Covariates	AIC	ΔAIC
Uniform + Cos(2)	—	786.2	7.34
Half-normal	group size	786.5	7.68
Half-normal	swell	787.8	8.99
Half-normal	sea state	788.0	9.14
Half-normal	observer ht.	788.7	9.91
Uniform + Cos(1)	—	789.2	10.33
Uniform	—	822.4	43.61
Pacific white-sided dolphin			
Hazard-rate	sea state	974.2	0.00
Hazard-rate	sea state, group size	975.6	1.39
Hazard-rate	sea state, observer ht.	976.7	2.49
Half-normal‡	sea state	976.9	2.75
Half-normal	sea state, swell	978.1	3.92
Half-normal	sea state, group size	978.7	4.49
Hazard-rate	swell	980.2	6.00
Half-normal	sea state, observer ht.	980.6	6.44
Hazard-rate	—	985.3	11.17
Hazard-rate + Poly(1)	—	986.8	12.62
Hazard-rate	group size	987.3	13.16
Hazard-rate	observer ht.	987.7	13.55
Half-normal	swell	989.2	15.07
Half-normal + Cos(1)	—	989.3	15.09
Uniform + Cos(3)	—	990.4	16.28

Continued on next page

Table 4.8 continued from previous page

Model	Covariates	AIC	ΔAIC
Half-normal	—	991.5	17.36
Uniform + Cos(2)	—	991.8	17.62
Half-normal	group size	993.0	18.82
Half-normal	observer ht.	993.1	18.98
Uniform + Cos(1)	—	993.5	19.29
Uniform	—	1034.0	59.79
Hazard-rate	sea state, swell	1042.0	67.79
Dall's porpoise			
Hazard-rate	observer ht.	911.2	0.00
Hazard-rate	observer ht., swell	912.9	1.76
Hazard-rate	observer ht., sea state	913.1	1.93
Hazard-rate	observer ht., group size	913.2	2.00
Hazard-rate	sea state	915.7	4.58
Hazard-rate	—	917.6	6.41
Hazard-rate	group size	917.8	6.63
Hazard-rate	swell	918.1	6.90
Hazard-rate + Poly(1)	—	919.3	8.16
Half-normal‡	sea state	925.4	14.20
Half-normal + Cos(1)	—	925.9	14.77
Half-normal	—	926.1	14.92
Uniform + Cos(2)	—	926.2	15.02
Half-normal	sea state, group size	926.4	15.29
Half-normal	sea state, swell	927.4	16.20

Continued on next page

Table 4.8 continued from previous page

Model	Covariates	AIC	ΔAIC
Half-normal	group size	927.5	16.33
Half-normal	swell	927.5	16.39
Uniform + Cos(3)	—	927.7	16.57
Uniform + Cos(1)	—	927.8	16.65
Half-normal	sea state, observer ht.	929.3	18.18
Half-normal	observer ht.	929.7	18.57
Uniform	—	965.9	54.79

Table 4.9. Goodness-of-fit statistics for the selected detection function model for each species. CvM: Cramér–von Mises test statistic (W) and p-value. χ^2: Pearson chi-squared statistic, degrees of freedom (df), and p-value. $p > 0.05$ indicates no significant departure from the fitted model. Species marked ‡ used a non-AIC-best model.

	CvM		χ^2		
Species	W	p	χ^2	**df**	p
Mysticetes					
Blue whale	0.079	0.698	8.20	10	0.610
Fin whale	0.182	0.306	5.50	9	0.788
Humpback whale	0.098	0.594	11.32	8	0.184
Gray whale	0.022	0.995	1.62	5	0.899
Odontocetes					
Short-beaked common dolphin	0.243	0.198	39.23	17	0.002
Long-beaked common dolphin	0.077	0.713	7.58	6	0.271
Risso's dolphin	0.046	0.900	6.73	3	0.081
Bottlenose dolphin‡	0.050	0.875	1.28	5	0.937
Pacific white-sided dolphin‡	0.647	0.017	7.82	6	0.251
Dall's porpoise‡	0.465	0.049	7.87	5	0.164

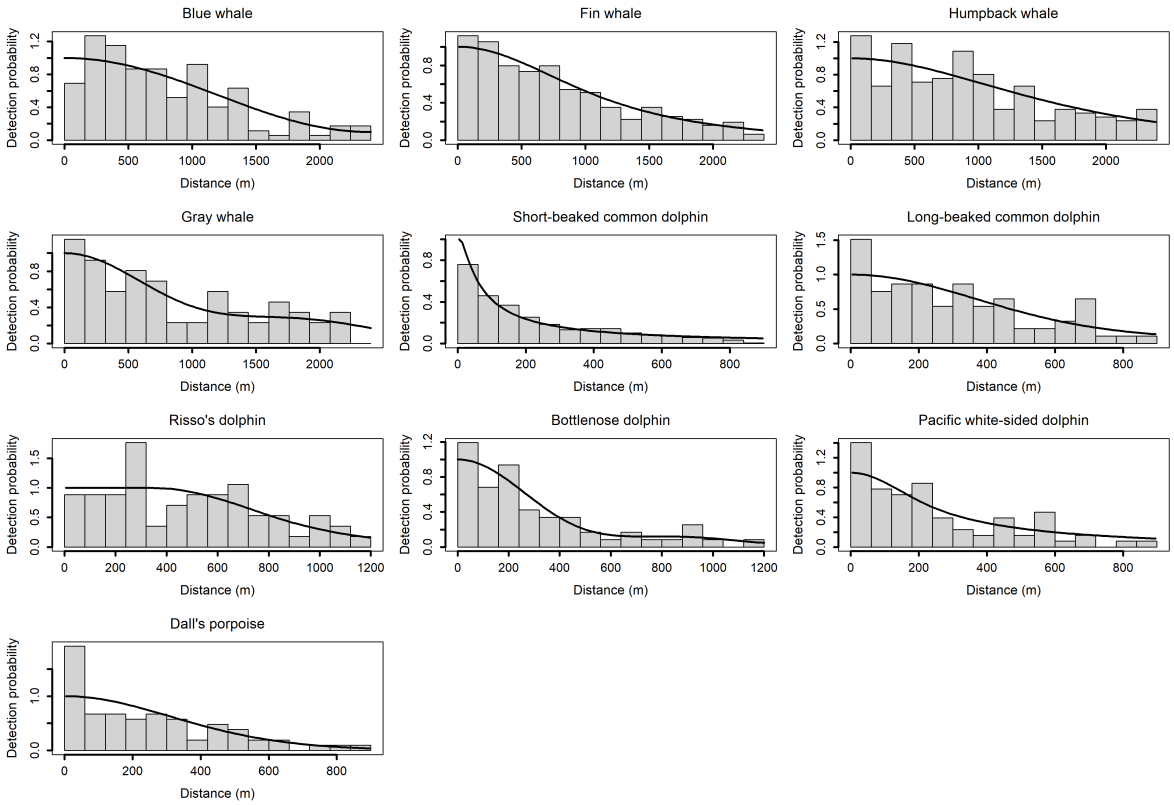


Figure 4.9. Fitted detection functions for the ten cetacean species analyzed, with scaled histograms of observed perpendicular distances. Mysticetes are shown in the top two rows and odontocetes in the bottom two rows. The solid curve is the fitted detection function; histogram bars are proportional to the fraction of detections in each distance bin, scaled to the estimated detection probability at zero distance.

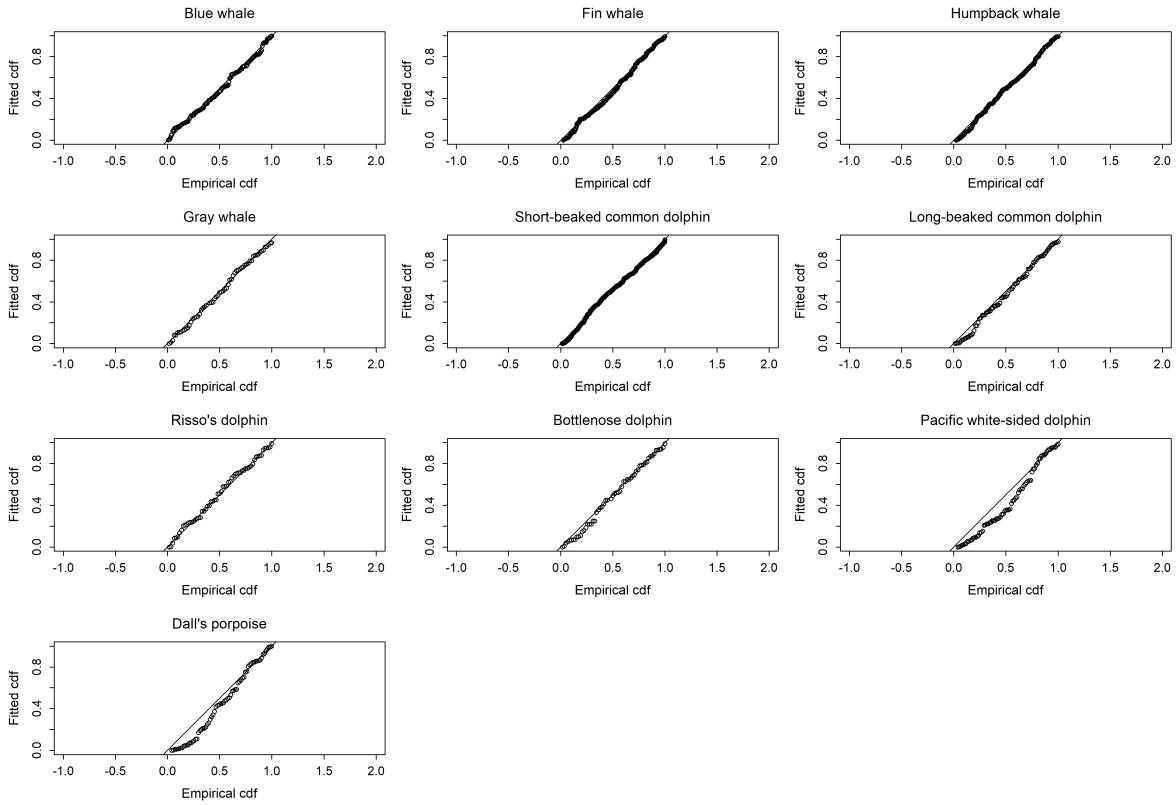


Figure 4.10. Quantile–quantile plots for the fitted detection functions. Points are probability-integral-transform scores of the observed perpendicular distances plotted against expected uniform quantiles; perfect fit falls on the 1:1 diagonal (dashed line). Panel order matches Fig. 4.9.

4.8 S3 Sea surface temperature regression results

Table 4.10. Bootstrap mean regression slope and R^2 for the relationship between annual density (animals per 1,000 km^2) and annual mean SST anomaly (°C) for each species. Slopes are the change in density per 1°C increase in SST anomaly. 95% CIs are from the 2.5th and 97.5th percentiles of the bootstrap distribution. Species whose slope 95% CI excludes zero are indicated with an asterisk.

Species	Slope	95% CI (slope)	R^2
Mysticetes			
Blue whale	+0.08	−0.57 to +0.74	0.013
Fin whale	−0.08	−1.26 to +1.09	0.021
Gray whale	+0.93	−0.30 to +2.73	0.123
Humpback whale*	+1.00	+0.02 to +1.94	0.019
Odontocetes			
Long-beaked common dolphin*	+553	+66 to +1916	0.204
Short-beaked common dolphin	+290	−92 to +781	0.132
Pacific white-sided dolphin	−6.3	−16.8 to +2.0	0.045
Risso's dolphin	+10.8	−8.2 to +63.1	0.134
Bottlenose dolphin	+7.2	−9.5 to +29.7	0.030
Dall's porpoise*	−13.3	−25.1 to −4.5	0.226

Chapter 5

Integrating marine mammal visual and acoustic surveys through a shared latent density model

5.1 Abstract

Passive acoustic monitoring can observe animal acoustic occurrence continuously and in weather conditions where other modalities are infeasible, but converting acoustic occurrence to density requires a cue rate: the number of calls produced per animal per unit time. In cetacean research, cue rates are usually estimated from small samples of tagged or localized animals, a laborious process that depends on precisely attributing each call to a known caller and is difficult to extrapolate to population-level estimates. Baleen whale cue rates also vary seasonally and with behavioral state, making reliable cue rate estimation an ongoing challenge for acoustic-based baleen whale density estimation. Existing approaches to combine observational data streams for species distribution modeling typically fit models for each data type separately and then combine resulting estimates after the fact, which requires every stream to independently estimate the same underlying metric. Because acoustic detections cannot be converted to density without an already-estimated cue rate, visual and acoustic data are rarely combined in such ensemble-style models for baleen whales. We developed a joint Bayesian species distribution model that links visual line-transect and passive acoustic survey data through a single shared

latent log-density field. Density varies with environmental covariates and space rather than season, so seasonal patterns in the acoustic data can reflect the cue rate rather than a shift in density. We tested the model's ability to recover known density surfaces and cue rates using simulated data matched to common acoustic occurrence observation types: multi-call-level detections (blue and fin whales) and presence/absence detections (humpback whales). The model recovered both density and cue/presence rate parameters across all three simulations. We then applied the model to 20 years of concurrent visual and acoustic California Cooperative Oceanic Fisheries Investigation (henceforth, CalCOFI) survey data for blue, fin, and humpback whales in the southern California Current Ecosystem, producing species-specific density surfaces and the first model-based seasonal cue and presence rate estimates for these populations. This approach bypasses the need for external cue rate estimates wherever paired visual and acoustic survey data exist, and provides a transferable method to estimate animal density and detection-process parameters from multi-modal wildlife surveys.

5.2 Introduction

Ecosystem monitoring increasingly uses data collected across many platforms. Camera traps, acoustic recorders, satellite tags, environmental DNA, and line-transect surveys may now exist in a single study system. Combining these data sources is valuable, but difficult, because each one measures a different variable related to a population's occurrence. Several statistical approaches address this. Data pooling reduces every dataset to a lowest-common-denominator format, then fits one model to the combined result (Isaac et al., 2020). For instance, acoustic and visual detections of Dall's porpoise have been merged into a combined dataset of encounters per survey segment and fit with a generalized additive model (Fleming et al., 2018). Model-based data integration instead builds observation submodels for each data source and links them through a shared latent state (Fithian et al., 2015; Koshkina et al., 2017; Isaac et al., 2020).

Passive acoustic monitoring (PAM) is one of the fastest-growing observation platforms in

marine ecology because deploying acoustic moorings or gliders can increase monitoring effort in regions and seasons where other modalities cannot reach (Cauchy, 2023; Posdaljian et al., 2022). PAM can record continuously and may capture the occurrence of cryptic, nocturnal, far-away, or deep diving animals that are rarely encountered through other modalities (Baumann-Pickering et al., 2014). But converting acoustic detections to a common metric, such as animal density, requires a cue rate. The cue rate is the average number of acoustic cues produced per animal per unit time (Marques et al., 2013). Raw detection or presence-absence counts can document relative change over time, but without a cue rate they cannot say how many animals produced those detections. This matters because density, not just presence, is what most conservation and management decisions require. Species distribution models (SDMs), which relate environmental covariates to a species' occurrence or density to predict its distribution and abundance (Becker et al., 2016, 2019), are the standard tool used to make these decisions.

Visual line-transect surveys use distance sampling to estimate density and abundance (Buckland et al., 2001, 2015), and are the standard input data for marine mammal SDMs (Becker et al., 2016, 2019, 2020; Forney et al., 2012). But visual surveys are limited to daylight hours and require costly ship time, leaving long stretches of time and space unobserved. Combining visual and PAM data seems like an obvious solution, but without an acoustic cue rate estimated from external studies, the two cannot be combined to predict density.

A reliable cue rate is not easy to estimate. For cetaceans, cue rates are usually estimated from small samples of tagged or acoustically localized animals (Marques et al., 2009, 2013), or from vessel or aerial encounters with visually confirmed calling animals (Marques et al., 2011; Garcia et al., 2025), both labor-intensive processes that depend on attributing each call to a known caller and are difficult to extrapolate to the population-level. This is especially hard for baleen whales, whose calls can propagate over hundreds of kilometers (Širović et al., 2007; Alksne et al., 2026), increasing the chance a detected call came from a conspecific rather than the individual being monitored (Zeh et al., 2024). Furthermore, baleen whales produce multiple

call types associated with different behavioral states (McDonald et al., 2006; Oleson et al., 2007; Širović et al., 2017; Oleson et al., 2014). Song, for instance, is the stereotyped signal used to acoustically monitor most baleen populations, and is produced only by males (Oleson et al., 2007; Croll et al., 2002; Payne and McVay, 1971; Darling and Berube, 2001). Thus an acoustic density estimate built from song risks only representing the singing portion of the population.

Several studies have combined visual and acoustic cetacean records with or without integrating them into a single model. Long-term acoustic presence records of Baird's beaked whale have been plotted against historical sightings to compare distribution patterns descriptively (Rios et al., 2026). Separately trained species distribution models have been combined in an ensemble to predict cetacean density from visual line-transect and PAM data (Frasier et al., 2021), and visual and acoustic detections have been combined in a mark-recapture distance sampling approach to correct for availability bias (Sigourney et al., 2023). In the southern California Current Ecosystem, visual and acoustic encounter rates for blue whales have been estimated using a generalized additive model (Oleson et al., 2007). A joint model linking aerial line-transect and PAM data through a shared latent density surface has been applied to North Atlantic right whales in a two day case study, where an average cue rate was estimated jointly with density (Schliep et al., 2024), but that model did not link cue rate to season or behavioral state.

We build a joint species distribution model that links visual line-transect and PAM data through a single shared latent density surface, letting a seasonally varying cue rate be estimated from the acoustic likelihood. This approach is motivated by our interest in combining 20 years of concurrent visual and acoustic survey data collected through the California Cooperative Oceanic Fisheries Investigations (CalCOFI), one of the longest running marine ecosystem timeseries in the world. Our goal is to build integrated species distribution models for blue, fin, and humpback whales to improve our understanding of their seasonal distribution and density on a key eastern North Pacific foraging ground. However, the call-specific average cue rates of these populations

are unknown, therefore, to date, acoustic data has not been incorporated to such models. In our model, cue rate is allowed to vary by season because these populations are migratory and have distinct acoustic behavioral states across the year (Szesciorka et al., 2020; Oleson et al., 2007; Oestreich et al., 2020; Ryan et al., 2019). The visual survey likelihood anchors absolute density (Campbell et al., 2015), thus, the acoustic likelihood can estimate whatever seasonal, call-type-specific cue rate is needed to explain the observed counts given that density. Latent density varies with environmental covariates commonly used in baleen whale SDMs (Becker et al., 2016), allowing our model to serve as a joint SDM and estimate call-type-specific seasonal cue rates. By anchoring our cue rate estimates against CalCOFI's visual density estimates, we aim to capture a regional cue rate that includes whales that never sing and those that were not calling during the survey, which is what is needed to convert an acoustic call density estimate into an estimate of animal density.

We implement this model in a joint Bayesian framework to link two separate processes informing the same underlying latent state (Pacifici et al., 2017; Miller et al., 2019; Fletcher et al., 2019). We first validated the joint model structure using simulated data with known density surfaces and cue rates, then applied the model to the full CalCOFI record to estimate seasonal density surfaces, environmental response curves, and seasonal cue and presence rates for blue, fin, and humpback whales in the southern California Current Ecosystem.

5.3 Methods

Here we develop a joint Bayesian model that estimates acoustic cue rate as a model parameter by joining visual and acoustic data through a shared latent density surface. We pooled all visual and acoustic observations across the full CalCOFI survey record (2004–2024) and density was modeled as a function of four environmental covariates (sea surface temperature, sea surface height, salinity, chlorophyll-*a*), shared by both data streams. Cue rate has its own seasonal intercept and is estimated separately, while density does not have a seasonal intercept.

Therefore, environmental covariates are the only part of the model through which density can vary from one season to the next.

We built one model architecture and applied it separately to blue, fin, and humpback whales, each with a different set of call types. We validated the model on simulated data with known relationships between the environmental data and density and known cue rates. After confirming its ability to recover the given parameter values, we applied it to the 20 year CalCOFI dataset to compute seasonal cue rates, seasonal density surfaces, and environmental response curves from the fitted parameters for each species.

5.3.1 Multi-modal survey data

Our study area consists of the core CalCOFI survey grid spanning six transect lines that run perpendicular to the coast between San Diego and Point Conception, California, with stations spaced approximately 37 km apart inshore of the 2,000 m isobath and 74 km apart offshore, extending up to 600 km from shore (Campbell et al., 2015). We used data from 68 CalCOFI cruises conducted quarterly between 2004 and 2024 with concurrent visual and passive acoustic effort. Acoustic and visual metadata can be Chapter 2 and Chapter 3 Supplementary Material. Seasons were defined as winter: December–February; spring: March–May; summer: June–August; fall: September–November.

Visual line-transect surveys were conducted in passing mode during daylight hours on CalCOFI cruises, with two trained observers searching using 7×50 binoculars. Effort was restricted to Beaufort sea state ≤ 5 and visibility ≥ 1 km. For each sighting, observers recorded species identity, group size, binocular reticle distance, and bearing relative to the bow, from which perpendicular sighting distance was calculated. On-effort trackline was divided into subsegments of approximately 10 km to serve as the spatial unit of analysis for the density surface model, with any remainder length distributed evenly across subsegments of that transect. A total of 10,468 10 km visual subsegments were available across all cruises. Species-specific detection functions were fit using the multiple-covariate distance sampling (MCDS) framework in the

`Distance` package in R (Buckland et al., 2001, 2015) and details of key function selection, covariates, and model selection are provided in Chapter 3 Supplementary Material, which analyzed the 2004-2024 CalCOFI line-transect record to estimate long-term visual density trends. The fitted detection functions were used to estimate species-specific subsegment-level detection probabilities, $\hat{p}$, which entered the visual likelihood as a fixed offset.

Passive acoustic recordings were collected by sonobuoys deployed at CalCOFI stations. Most recordings lasted around two hours and recordings only took place during the day. Blue whale (B, D calls) and fin whale (20 Hz, 40 Hz calls) detections were generated by a Faster R-CNN deep-learning detector, and full detector architecture, training, and evaluation are described in Alksne et al. (2026). Across 68 cruises, 1,743 sonobuoy deployments contributed to the blue and fin whale acoustic records. Humpback whale detections were generated using the convolutional neural network of Allen et al. (2021), run on omnidirectional sonobuoy recordings, with detector output scores averaged into 1-minute bins and thresholded to produce a per-minute presence/absence record. Detector outputs were verified against manually reviewed deployments from five CalCOFI cruises to generate precision–recall curves (Supplemental Figure 5.9), estimate detection thresholds, and estimate false positive and false negative rates. The omnidirectional sonobuoy acoustic record had 1,586 deployments. For each signal type, a station-level detection area was computed from range-dependent parabolic-equation propagation modeling (RAMGEO) and received-level thresholding, following Alksne et al. (2026). Automated detections were corrected for species- and call-type-specific false positive and false negative rates (Supplemental Table 5.3), based on precision and recall on held-out evaluation data, before entering the likelihood.

Sea surface temperature (SST), sea surface height (SSH), sea surface salinity, and chlorophyll-*a* were used as environmental covariates as they are the standard input to marine mammal species distribution models (Becker et al., 2016, 2019, 2022). In the southern California Current Ecosystem, SST is strongly seasonal and tracks cold, upwelled water that drives

productivity (Croll et al., 2005; Fiedler et al., 1998), SSH reflects mesoscale circulation linked to prey aggregation (Dorman et al., 2015; Croll et al., 2005), salinity is associated with distinct water masses (Jacox et al., 2016), and chlorophyll-*a* tracks productivity (Fiedler et al., 1998). SST, SSH, and salinity came from the Hybrid Coordinate Ocean Model (HYCOM; Chassignet et al., 2007) global reanalysis (https://www.hycom.org/). Chlorophyll-*a* came from NOAA ERDDAP (https://coastwatch.pfeg.noaa.gov/erddap/) and was log-transformed to reduce its right skew. For visual transect subsegments and acoustic stations used in model fitting, covariate fields were matched to the nearest observation location and date. For the prediction grid, covariate values were averaged over each two-week cruise window. All four covariates were standardized to zero mean and unit variance from the combined visual and acoustic training data.

5.3.2 Model overview

We developed a Bayesian joint model that links visual and acoustic observations through a single shared latent log-density field (Figure 5.4), following a joint-likelihood approach in which both observation types are modeled as noisy functions of one shared latent process rather than being fit separately (Pacifici et al., 2017; Miller et al., 2019; Fletcher et al., 2019). Visual and acoustic detections have their own likelihoods and nuisance parameters but both inform the same environmental and spatial structure.

We fit this architecture independently to each of the three species rather than building a single joint model across species. A multispecies joint model would require specifying a cross-species covariance structure for the spatial random fields, on top of the complexity of each species already having a distinct acoustic likelihood and call-type structure, which we determined was beyond the scope of this analysis.

We modeled the log of expected whale density because the log transform keeps predictions positive and reflects the multiplicative relationship between environmental drivers and whale density that is typical of marine mammal species distribution models (Becker et al., 2016, 2022). For each species, log density at location i was modeled as an intercept and centered

nonlinear environmental responses:

$$\log D_i = \mu + \sum_{k=1}^{4} \left[f_k(x_{ik}) - \bar{f}_k \right], \tag{5.1}$$

where $\bar{f}_k$ are the sample means of $f_k(x_{ik})$ across the training data and μ is the mean log-density. μ was given a lognormal prior centered on independent density estimates for the three baleen whale species from habitat-based density estimates (Becker et al., 2019) (Table 5.1).

Each environmental response f_k was modeled using a cubic B-spline basis with 4 functions per covariate, with a second-order random-walk prior on the spline coefficients penalizing curvature (Eilers and Marx, 1996). Four basis functions per covariate were chosen to capture unimodal or bimodal habitat associations across the range of covariate values. The P-spline smoothing standard deviation was given a weakly informative Half-Normal(0,1) prior for each covariate (Table 5.1).

Given the latent density surface, the expected number of whale groups detected in visual transect subsegment i was modeled as

$$n_i \sim \text{NegBinomial}\left(\frac{D_i}{\bar{s}} \hat{p}_i A_i,\ \phi_v \right), \tag{5.2}$$

where $D_i = \exp(\log D_i)$ from Equation 5.1, $\bar{s}$ is expected group size, A_i is the surveyed area of the subsegment, and ϕ_v is the negative-binomial overdispersion parameter (Table 5.1). The subsegment-specific detection probability, $\hat{p}_i = g(0)\,\hat{p}_i^{\perp}$, is the product of $g(0)$, the trackline detection probability, fixed at 0.91 for all three species (Barlow and Forney, 2007), and $\hat{p}_i^{\perp}$, the probability of detection integrated over perpendicular distance from the fitted detection function. We used a negative binomial rather than a Poisson likelihood to account for overdispersion ϕ_v.

Group size was modeled separately from group counts because the two values arise from different processes (Sigourney et al., 2020). The detection process determines how many groups are seen per unit area, while social behavior determines how many animals are in each

group. Group size, recorded for each sighting event, was modeled with its own shifted negative-binomial likelihood (Table 5.1). Because group size is always at least one, we modeled $s_g - 1$ so that the response is centered at zero:

$$(s_g - 1) \sim \text{NegBinomial}(\bar{s} - 1,\ \phi_s). \tag{5.3}$$

The acoustic likelihood links the latent density field to the sonobuoy data through call-type-specific observation processes. For each acoustic station i and call type, a false positive/negative correction factor was defined as:

$$c_{i,\text{type}} = (1 - \text{FN}_{\text{type}})/(1 - \text{FP}_{\text{type}}). \tag{5.4}$$

For each species, call counts or presence counts were modeled with independent negative-binomial likelihoods because baleen whale calling behavior is bursty and spatially clustered:

$$x_{i,\text{type}} \sim \text{NegBinomial}\left(D_i\, \beta_{\text{type}}[m_i]\, A_{i,\text{type}}\, T_i\, c_{i,\text{type}},\ \phi_{\text{type}}\right), \tag{5.5}$$

where $\beta_{\text{type}}[m_i]$ is the season-specific cue rate (calls/presence per whale per hour), $A_{i,\text{type}}$ is the call-type-specific detection area, T_i is recording duration (hours), $m_i \in \{1,2,3,4\}$ indexes season, and ϕ_{type} is the overdispersion parameter (Table 5.1). Published acoustic cue rate estimates are sparse for the call types in question, so our priors were weakly informative and set to be the same in every season. For fin whale 20 Hz calls, we used the mean call production rate reported by Stimpert et al. (2015), 4.8 calls per whale per hour, as the prior mean, with a log-standard deviation of 1 (Table 5.1). No published cue rate exists for eastern North Pacific blue whale B or D calls, so we set the mean to 2 calls per whale per hour, near the lower end of the mean hourly production rates reported across behavioral states for these call types by Lewis et al. (2018), with a log-standard deviation of 1 for both call types across all seasons (Table 5.1). No estimate was available for fin whale 40 Hz calls, so we assumed the same prior mean as blue whale D

calls, since both are associated with similar behavioral states (Oleson et al., 2007; Romagosa et al., 2021). No estimate was available for humpback whale presence rate, so we used a uniform prior between 0 and 60 minutes per whale per hour (Table 5.1).

5.3.3 Simulation and model fitting

Before fitting the model to any data, we performed prior predictive checks Conn et al. (2018). For each species, we drew 1000 parameter sets jointly from every prior in the model, propagated them through the model's generative equations using the real survey design, meaning the same station locations, environmental covariate values, effort, and detection areas as the real data, and confirmed that the resulting simulated visual and acoustic counts fell in a plausible range relative to the observed counts (Supplemental Figure 5.11, 5.12, 5.13).

Before fitting the model to the real 20-year dataset, we validated its structure using simulation (Talts et al., 2020; Conn et al., 2018). For each species, we generated $M = 10$ independent synthetic datasets using the real survey design, but with all response variables redrawn from the model's own generative process at known parameter values. True values for the density intercept and seasonal cue or presence rates were set equal to the literature-derived prior means used in the real analysis. No literature presence-rate estimate exists for humpback whales, so its true seasonal presence-minute rate was instead a hand-picked constant within its uninformative Uniform(0, 60) prior's range. Environmental responses were assigned hand-specified values, identical in magnitude across species and differing only in the sign of each covariate's effect per species 5.4 which we based on previous estimated relationships between these species and the same environmental covariates (Hazen et al., 2017; Becker et al., 2017; Scales et al., 2017; Becker et al., 2019). We fit the Stan model (Carpenter et al., 2017) to each simulated replicate dataset. For every parameter we calculated coverage, the proportion of trials whose posterior credible interval contained the true simulated value (Talts et al., 2020). Season- and the spline basis-function-specific parameters were pooled across their four members before computing coverage, so a group's reported coverage is a single proportion

over 40 trials rather than four separately-computed rates. We used a CI target of 70%. We also calculated contraction, which represents how much more precise the posterior is than the prior, calculated as $1 - (\sigma_{\text{post}}/\sigma_{\text{prior}})^2$, where σ is the standard deviation of the parameter's distribution. Contraction close to 1 indicates the data narrowed the posterior relative to the prior. Contraction is not defined for the environmental spline coefficients, whose prior scale (σ_{spl}) is an estimated hyperparameter. Lastly, we calculated the signed bias between the posterior mean and the true simulated value for every parameter. After verifying that the prior predictive checks and simulation recovered expected counts and parameter values, we fit the model to the real 20 year dataset.

Each species-specific model was fit in Stan (v2.21) via `rstan`, using four chains of 2,000 iterations each (1,000 warmup), for a total of 4,000 posterior draws. Convergence was assessed for every estimated parameter using the potential scale reduction statistic ($\hat{R} < 1.01$ for all parameters; Vehtari et al., 2021) together with visual inspection of chain traces for key parameters, namely the density intercept, spline smoothing standard deviations, seasonal call rates, and overdispersion parameters. The 4,000 retained posterior draws were used for all downstream prediction and uncertainty quantification.

We evaluated model fit for each species using posterior predictive checks (Vehtari et al., 2021; Conn et al., 2018). For each of 1,000 thinned posterior draws, replicated datasets y^{rep} were simulated from the observation-level predictive distributions, using that draw's latent density field and its cue-rate and overdispersion parameters. We assessed two aspects of fit for each species and data stream. First, we used the proportion of zero counts, $T(y) = \frac{1}{N}\sum_i 1(y_i = 0)$, as a test statistic targeting whether the model reproduced the degree of zero-inflation in the data Conn et al. (2018). Second, we used the total count, $T(y) = \sum_i y_i$, to assess whether the model reproduced the correct overall magnitude, separated by season and spatial region within the CalCOFI survey grid, using four quadrants defined by splitting the grid at CalCOFI Line 86.7 (north/south) and Station 60 (inshore/offshore, applied along every line). We used the Bayesian

p-value $p_B = \Pr(T(y^{\text{rep}}) \geq T(y^{\text{obs}}))$ to compare each replicated statistic to its observed value for each test.

For each of the 4,000 posterior draws, the latent log-density field was evaluated at every CalCOFI grid location, using that draw's spline coefficients. For the seasonal prediction grid, environmental covariates at each grid cell were averaged across days within a cruise, and density was predicted for each cruise and then averaged across all cruises in a given season. We summarized the resulting seasonal distribution as the posterior median predicted density at each grid cell, with uncertainty expressed as the 95% credible interval across draws. To characterize each species' response to individual environmental covariates, we computed marginal response curves for each covariate, where the corresponding spline term was evaluated in isolation across the covariate's observed range and centered to zero mean over the training data, isolating that covariate's estimated additive contribution to log-density together with its 95% credible interval. We summarized the posterior distribution of the season-specific acoustic cue-rate parameter ($\beta_{\text{type}}[m]$) for each call type as the posterior median and 95% credible interval by season.

5.4 Results

5.4.1 Model performance

Across $M = 10$ simulated replicates per species, the model recovered known parameter values for the seasonal cue rates, density intercepts, and environmental spline coefficients. Overall coverage of the 70% posterior credible interval, averaged across every estimated parameter, was 60.3% for blue whales (29 parameters), 68.6% for fin whales (29 parameters), and 55.0% for humpback whales (24 parameters) 5.5. Pooling each cue rate's four seasonal values across all $M = 10$ replicates, blue whale B-call rates had 65% coverage with contraction averaging 98.7% and mean bias -0.036 calls/whale/hr; D-call rates had 62% coverage, 98.7% contraction, and mean bias -0.040 calls/whale/hr. Fin whale 20-Hz rates had 88% coverage, 99.6% contraction, and mean bias 0.040 calls/whale/hr; 40-Hz rates had 78% coverage, 99.6%

contraction, and mean bias 0.034 calls/whale/hr. Humpback presence-minute rates had 62% coverage, 100.0% contraction, and mean bias 0.167 presence-minutes/whale/hr. Contraction well above zero and coverage at or above the 70% target indicates these estimates are informed by the simulated acoustic and visual likelihoods rather than reproducing the prior. The density intercept μ recovered with 80%, 90%, and 70% coverage (blue, fin, humpback; contraction 98.8%, 99.8%, and 99.7%; mean bias 0.032, -0.007, and -0.032 on the log-density scale). The environmental spline coefficients recovered less consistently than the cue rates or μ, and chlorophyll-*a* was the weakest of the four covariates in every species (Supplemental Table 5.5), likely because it is strongly right skewed even after the log transformation, which makes it difficult for the basis functions to estimate.

For the model fit to the 20-year dataset, all the chains converged and the potential scale reduction statistic $\hat{R}$ was < 1.01 for all parameters. Posterior predictive checks, comparing observed against model-predicted visual and acoustic counts, indicated adequate fit for most conditions tested. For the proportion-of-zeros statistic, pooled across seasons, six of the eight species/stream combinations fell well within the expected central 90% predictive interval (Bayesian p-values between [0.05, 0.95]) and those that didn't were barely outside of it (Supplemental Table 5.6). For the total-count statistic, stratified by season and CalCOFI quadrant, most of the 16 season-by-region strata per stream fell within the calibrated range (Figure 5.5; Supplemental Table 5.7). For those that didn't, they were generally concentrated in offshore regions or seasons where the true counts were zero or close to zero and the posterior ranges were often just beyond the true value. Several strata were systematically over or under predicted where high counts would be expected. For instance, blue whale D-call counts were skewed towards over-prediction in the summer months in the southern inshore quadrant ($T_{\text{obs}} = 495$ vs. $T_{\text{pred}} = 1403$, though $p_B = 0.882$ was still in the expected range). Fin whale 40 Hz counts were over-predicted across three of four summer quadrants, with the northern offshore quadrant exceeding the expected threshold (Supplemental Table 5.7). For the humpback whale winter

acoustic strata, the northern offshore quadrant was under predicted ($T_{\text{obs}} = 1174$ vs. $T_{\text{pred}} = 337$, $p_B = 0.001$) while the northern inshore quadrant was over predicted ($T_{\text{obs}} = 275$ vs. $T_{\text{pred}} = 810$, $p_B = 0.998$), and the winter visual northern inshore quadrant was also over predicted ($T_{\text{obs}} = 32$ vs. $T_{\text{pred}} = 95$, $p_B = 1$).

5.4.2 Environmental drivers, species distributions, and seasonal cue rates

Each species had a distinct response to the environmental covariates (Figure 5.6). Blue whale density increased with warmer SST, and the 95% credible interval excluded zero across the entire observed range. Fin whale density showed a weak, unimodal response to SST, peaking near 16°C, with the interval excluding zero only where data were the most dense. Humpback whale density decreased with SST, and the interval excluded zero across all of the data range. Blue and fin whale density showed identically sloped negative responses to SSH and the credible interval did not include zero. Humpback whale density showed no response to SSH, with the interval including zero throughout. The weakest relationships across species were with salinity, where each species had a weakly positive slope but the 95% CIs included zero. Chlorophyll-*a* responses were weakly positive for fin and blue whales with the interval including zero for most of the range, and positive for humpback whales although the tails changed direction at the very edges of the range of the data.

The spatial-seasonal distributions were distinct for each species (Fig. 5.7). Predicted blue whale density ranged from 0.0000253 to 0.00963 animals/km^2 and was low across the region in winter and spring, with density peaking in summer months inshore of the continental slope and near the southern Channel Islands, and declining again in the fall. Fin whale density ranged from 0.0000280 to 0.0136 animals/km^2 and peaked further offshore from blue whales in the summer and near the northern and southern Channel Islands and off Point Conception. Following the summer months, fin whale density gradually declined to its lowest density in winter, followed by an increase in spring transitioning back into summer. Humpback whale

density was concentrated in coastal waters above Point Conception, with an expansion into the Southern California Bight in winter and spring, and contraction during summer and fall. Humpback whale predicted density was the greatest of the three species, ranging from 0.000793 to 0.0598 animals/km^2 just off Point Conception.

Posterior seasonal cue rate estimates for all three species and call types are in Figure 5.8 and Table 5.2. The blue whale B-call cue rate was similar in fall and winter, near zero in spring, and peaked at 0.80 in summer. D-call cue rates were near zero in winter, rose in spring, peaked at 0.13 in summer, and declined in fall. Fin whale 20-Hz cue rates were highest in fall and declined throughout winter and spring, falling to near zero in summer. Fin whale 40-Hz cue rates were low throughout the year, with a peak of 0.17 in summer. Humpback whale minute-level presence rates peaked at 0.09 in winter and declined through spring and summer, with an increase in fall.

5.5 Discussion

We show that acoustic cue rates can be estimated jointly with density from concurrent visual and passive acoustic surveys, and we apply the method to three baleen whale species with distinct acoustic observation structures. Because our cue rate estimates are anchored to CalCOFI's visual density estimates rather than to known-calling individuals, they represent a regional average cue rate that includes whales that never sing and those that were not calling at the time of survey. This is what allows the model to convert acoustic call density into animal density, rather than into an estimate that only accounts for a handful of actively calling whales. A joint model has previously estimated a cue rate for North Atlantic right whales in a two day case study, doing so by including tag data to resolve the identifiability between unknown surfacing rates and unknown acoustic cue rates (Schliep et al., 2024). In aerial surveys, the probability of a whale being at the surface is an unknown parameter that must be accounted for because the time window of observation is narrow from a fast-moving plane. With this unknown, as well as the unknown acoustic cue rate, neither visual counts nor acoustic counts can estimate

animal density, and both conversion factors cannot be estimated in the same model without additional information. Schliep et al. (2024) therefore added an additional likelihood from tag data, which provided independent estimates of surfacing rate and cue rate. Our approach, by contrast, assumes animal density in the survey area can be estimated from the visual likelihood. Because a ship moves much more slowly than a plane, we assume surface availability bias will not affect the detection probability.

Some additional assumptions and potential biases in the cue rate estimates are as follows. Because CalCOFI surveys are conducted in passing mode rather than closing mode, some proportion of large whale sightings are unidentified to the species level, and our visual likelihood did not include or account for these, which may bias the densities lower than they truly are (Campbell et al., 2015). We assume the trackline detection probability matches Barlow and Forney (2007), meaning that regardless of survey conditions, the probability of seeing an animal given that it is directly on the trackline is constant, which does not always hold true (Barlow, 2015). We assume the acoustic detection area at a given station is constant, even though sound propagation ranges are known to be affected by environmental conditions (Helble et al., 2013b,a) and change seasonally and interannually Miotto (2025). Lastly, the recorders used in our study are only deployed during the day. Blue, fin, and humpback whales sing more often at night (Wiggins et al., 2005; Baggett et al., 2026), so our cue rates may underestimate the true 24-hour regional average.

Blue whale B calls are associated with song, which increases in presence in the southern California Current Ecosystem as animals shift from feeding to breeding behavior (Oleson et al., 2007; Širović et al., 2015). Males are thought to sing to attract mates or mitigate antagonistic interactions between conspecifics (Oleson et al., 2007; Cholewiak et al., 2018). B call cue rate was highest in summer, lower in fall, and lowest in spring and winter. CalCOFI's fall cruises sample after peak singing activity has already occurred (Širović et al., 2015; Szesciorka et al., 2020), so the fall cue rate may be an underestimate of what it would be in September or October,

when the greatest proportion of the population is singing. The lower winter and spring estimates are consistent with documented seasonal singing patterns (Širović et al., 2015; Oleson et al., 2007), as blue whales leave the feeding grounds and song activity declines (Oestreich et al., 2020; Szesciorka et al., 2020; Širović et al., 2015), or arrive on the feeding grounds and begin producing D calls, which are associated with foraging (Oleson et al., 2007) rather than song. Alksne et al. (2026) observed that blue whale B call inter-call intervals are stable in CalCOFI sonobuoy recordings across seasons, suggesting the seasonal pattern we observe in cue rate more likely reflects a change in the proportion of whales singing rather than a change in how quickly individual singers call. Lewis et al. (2018) report average call production rates for blue whales classified by behavioral state. For B calls, both singular calls and calls produced within song ranged on average between 1 and 6 calls per hour, and our weakly informative prior mean of 2 was set based on this range. Our posterior median in summer, 0.8, is lower than most of Lewis et al. (2018) estimates, but we did not separate by behavioral state, only recorded during the day, and our estimates include offshore recordings, where calling activity is lower (Alksne et al., 2026). D call cue rate was highest in summer, lower in spring, and lowest in fall and winter, suggesting that peak foraging-related acoustic activity overlaps with peak visual density in the region. The B and D call cue rates had different seasonal patterns, and both differ from their shared prior mean, indicating the acoustic and visual likelihoods are informing the estimates. Posterior predictive checks for total B call counts recovered the true value in most strata, with some over-prediction in offshore summer and fall quadrants, and in spring and winter quadrants, all regions and seasons where observed counts were low. Our zero-count test statistic showed the model performed well overall, though it slightly underestimated the proportion of zeros in the B call counts, which likely contributes to the over-prediction in strata where counts are typically low or zero. For D calls, the model tended to over-predict counts, and the zero-test statistic also underestimated zero-inflation slightly. A zero-inflated model could be explored in future work to address this.

Fin whale 20 Hz calling peaks during fall and winter (Širović et al., 2015; Oleson et al., 2014), consistent with the seasonal pattern in our cue rate estimates. Acoustically tracked, actively singing fin whales in Hawaiian waters have reported 20 Hz cue rates with a median of 131 calls per whale per hour (Helble et al., 2020), and a North Atlantic dataset of tracked singers showed individual tracks ranging from 90 to 332 calls per whale per hour (Guazzo et al., 2024). The prior mean (4.8) used in our study instead came from Stimpert et al. (2015), an average based on ten whales, some of which were silent, in California. Our fall peak is at 1.5 calls per whale per hour, far below these actively-singing rates, which again is expected since our estimate represents a regional average rate across whales that are and are not singing. The seasonal peak in fin whale 20 Hz cue rates does not align with the peak in visual density, which occurs in the summer months (Campbell et al., 2015). Summer had the lowest 20 Hz cue rate, consistent with this being a period when animals are primarily engaged in foraging rather than singing (Širović et al., 2015; Oleson et al., 2014). Oleson et al. (2014) documented a fin whale song type in this region for which inter-call intervals increased from August through April before resetting the following year. An increasing inter-call interval predicts a decreasing cue rate, since a longer gap between calls means fewer calls produced per unit time. Our seasonal cue rate estimates decrease across this same window, peaking in fall and winter and reaching their lowest point in spring. We cannot distinguish how much of the seasonal decline could be attributed to lengthening inter-call intervals versus a change in the proportion of the population engaged in singing behavior, since either mechanism, or some combination of the two, could produce the same seasonal change in our cue rate estimates. However, the mismatch between visual and acoustic 20 Hz seasonal densities suggests that a change in the proportion of singing whales is the more parsimonious explanation. Širović et al. (2017) also found that inter-call intervals for fin whale song type lengthened across years in Southern California, from 2004 to 2012. We report a single pooled seasonal cue rate estimated jointly across our 20 year record. Modeling the interannual changes documented by Širović et al. (2017) was beyond the scope

of this analysis, but could be an avenue for future work. Fin whale 40 Hz cue rate peaked in summer, similar to the blue whale D call pattern, consistent with both call types being linked to foraging behavior Romagosa et al. (2021) and peaking during peak visual density. Posterior predictive checks showed more 40 Hz calls predicted than observed and zero proportions were under estimated, again suggesting a zero-inflation model could improve estimates in the future.

For humpback whales, we used the convolutional neural network of Allen et al. (2021) and converted its output to minute level presence to reduce the influence of individual detection outliers. This gives us a seasonal presence rate rather than a call level cue rate for humpback whales. Many acoustic detection pipelines have a similar type of output, and the results show that our approach works with minute-level presence-absence data. The detector does not distinguish between song and other call types, so we cannot separate breeding related calls from foraging-related ones. Humpback presence rate peaked in winter, matching known song phenology in the region (Vu, 2015; Ryan et al., 2019, 2025). Unlike blue and fin whales, the humpback presence rate did not drop to near zero in any season. This may be because our presence rate is capturing both song and foraging calls, which are produced at different times of year. Our spatiotemporal visual and acoustic data show more offshore calling activity in winter than in other seasons, contributing to this seasonal peak. Posterior predictive checks under-predicted offshore and over-predicted inshore in winter, which may suggest that the true acoustic presence rate is not spatially uniform in winter, possibly because the population's proportional song cue rates are greater offshore than inshore in this season.

Our results show that each species produces different calls at different rates throughout a year. Blue whales arrive in spring, ramp up D call production through summer, which decline through fall. Song-associated B calls also ramp up in summer and decline through fall, though again we acknowledge that our survey design misses the peak singing period. Fin whale 20 Hz call production ramps up in fall and continues through winter. Humpback acoustic presence ramps up in fall, peaks in winter, and continues into spring. The seasonal peaks are offset

across species, which may suggest acoustic partitioning of a shared foraging ground driven by differences in breeding season timing. Two studies of blue, fin, and humpback whale song, one using CalCOFI data (Vu, 2015), and another in the Monterey Bay (Ryan et al., 2025), found similar seasonal structure across species. Our results convert the previously described seasonal acoustic patterns of these three species into seasonally varying regional-average cue rates, which can hopefully be used in future studies to convert acoustic density to animal density.

Our seasonal cue rate estimates can support future PAM-only density estimation for these three populations. Because our cue rates are anchored to visual density rather than to tagged individuals, they reflect calling behavior across animals that were never tagged, never sing, or were not calling during the survey. Using density instead of raw counts means each survey type's detection process, and the animals or calls it missed, is accounted for before cue rate is estimated. Because we use a Bayesian joint framework, uncertainty from both detection processes is propagated through to the cue rate estimates, so future PAM-based density estimates built from them would have associated uncertainty.

Our joint model also produces species-specific density surfaces, which we can compare against existing spatial distribution work. Existing SDMs for cetaceans along the U.S. West Coast typically use visual survey data from summer and fall survey effort (Becker et al., 2016, 2019). CalCOFI's quarterly cruises add winter and spring coverage and have been used in recent modeling efforts for some species (Becker et al., 2017, 2025). Our seasonal-spatial predictions align with previous habitat-based distribution models and biologically important areas (BIAs) for each species (Calambokidis et al., 2024; Becker et al., 2017, 2019, 2016). Blue whale density peaks near the southern Channel Islands in summer, overlapping with known feeding areas (Calambokidis et al., 2015, 2024) and prior habitat models (Becker et al., 2022). Although, our model predicts lower densities near the northern Channel Islands than most previous estimates (Becker et al., 2017, 2019, 2016). Density increases with SST, similar to Hazen et al. (2017) habitat model, but since our model of latent density aggregates across all seasons rather than

separately modeling winter and spring from summer and fall, like Hazen et al. (2017) did, it may be learning to favor warm SST too strongly, which would under-predict density at the northern Channel Islands, since that area stays cold and productive year-round. Fin whale density peaks in the summer further offshore than blue whales, and the high density regions align with BIAs (Calambokidis et al., 2015, 2024). Fin whale density also decreases with SSH, similar to blue whale. Blue whales are krill specialists (Croll et al., 2005; Fiedler et al., 1998), while fin whales switch between krill and forage fish (Croll et al., 2005). The shared SSH response suggests both species are tracking dense prey aggregations, since SSH is tied to upwelling and the mesoscale eddies and fronts that aggregate prey (Croll et al., 2005; Dorman et al., 2015), which has been documented in other studies (Fahlbusch et al., 2022). Humpback whale density is concentrated near Point Conception, and expands south in winter and spring and contracts in summer and fall, matching Becker et al. (2017)'s CalCOFI winter/spring model. The high seasonal densities around Point Conception also align with humpback feeding BIAs along the coast (Calambokidis et al., 2015, 2024).

The same joint structure could be used with continuous PAM as the model does not require acoustic and visual data to be collected at the same time. Visual survey days could anchor density and cue rate as in this study, while a continuous acoustic record, from a glider or fixed recorder, could cover the gaps and be converted to density using the estimated cue rate. However, doing so would assume the density and cue rate relationship learned on visual survey days remain representative of conditions during the gaps between them. Alternatively, visual survey days could also be replaced with SDM-predicted visual density estimates at the acoustic recording location, allowing cue rate to be estimated continuously in the acoustic record. Cue rate could also be modeled as a function of environmental conditions, in addition to or instead of season. Beyond passive acoustics, this architecture could apply to any paired data stream where one is anchored by a known process and the other by an unknown scaling parameter. Environmental DNA is one example. CalCOFI has recently begun collecting large-volume water

samples for eDNA alongside visual transects (Wisely et al., 2026), and the same model structure could estimate an eDNA scaling factor jointly with visual survey density.

As multi-modal data collection for ecosystem monitoring continues to grow, methods are needed that integrate modalities to address pressing biodiversity threats. One barrier is the missing scaling factor that lets one stream estimate the metric of another, whether acoustic, visual, genetic, or otherwise. Our approach shows that parameter does not need to be assumed from an unrelated study. It can be solved for directly, using the data already being collected.

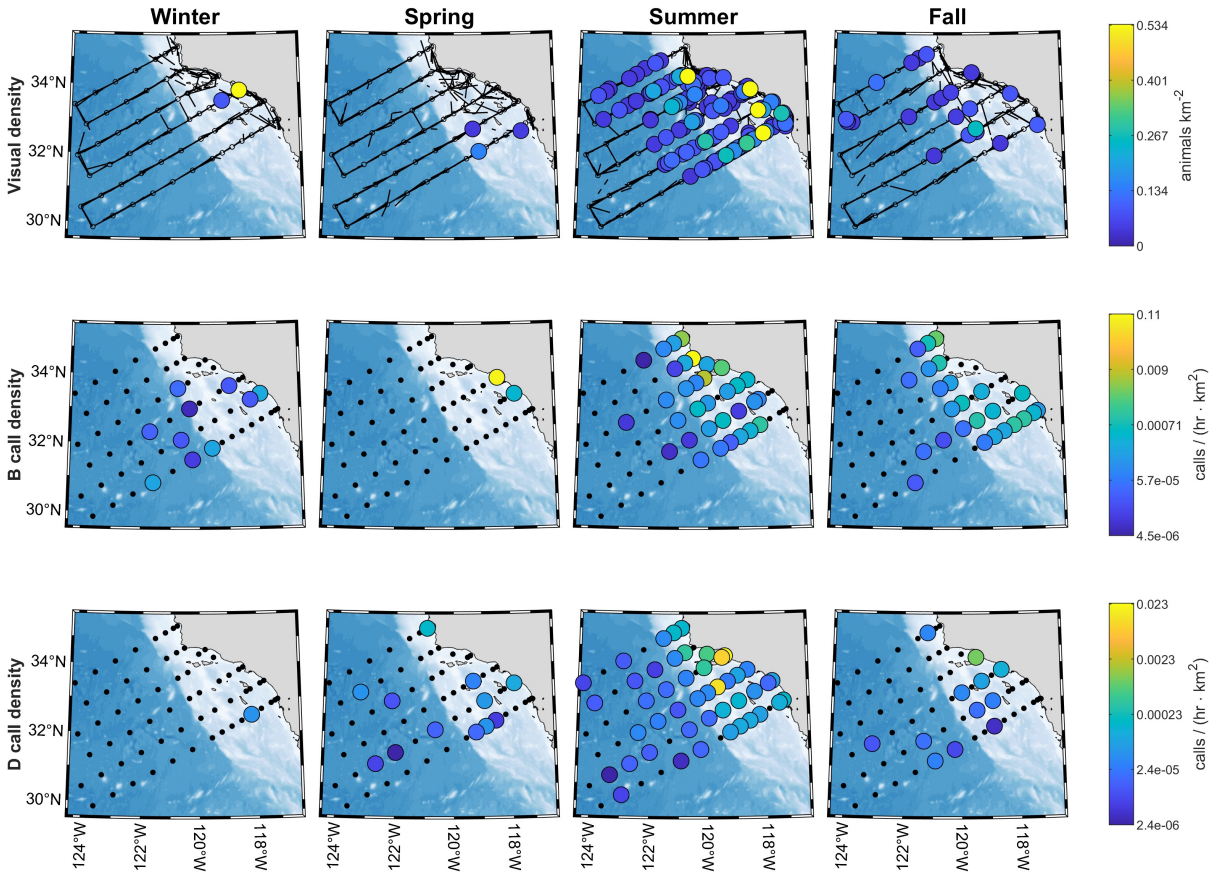


Figure 5.1. Seasonal spatial distribution of blue whale segment-level density estimates and acoustic density estimates of blue whale B and D calls across the CalCOFI survey grid, 2004–2024. For the visual data, each on-effort segment with a sighting is given a colored circle, were the colors are scaled by density. Low densities are in blue and high densities are in yellow. Segments with effort but no sightings are shown as black lines. Acoustic densities are shown with the same color scaling and each circle represents the total acoustic density at a given station for a given season. Stations with no detections of a given call type are black circles.

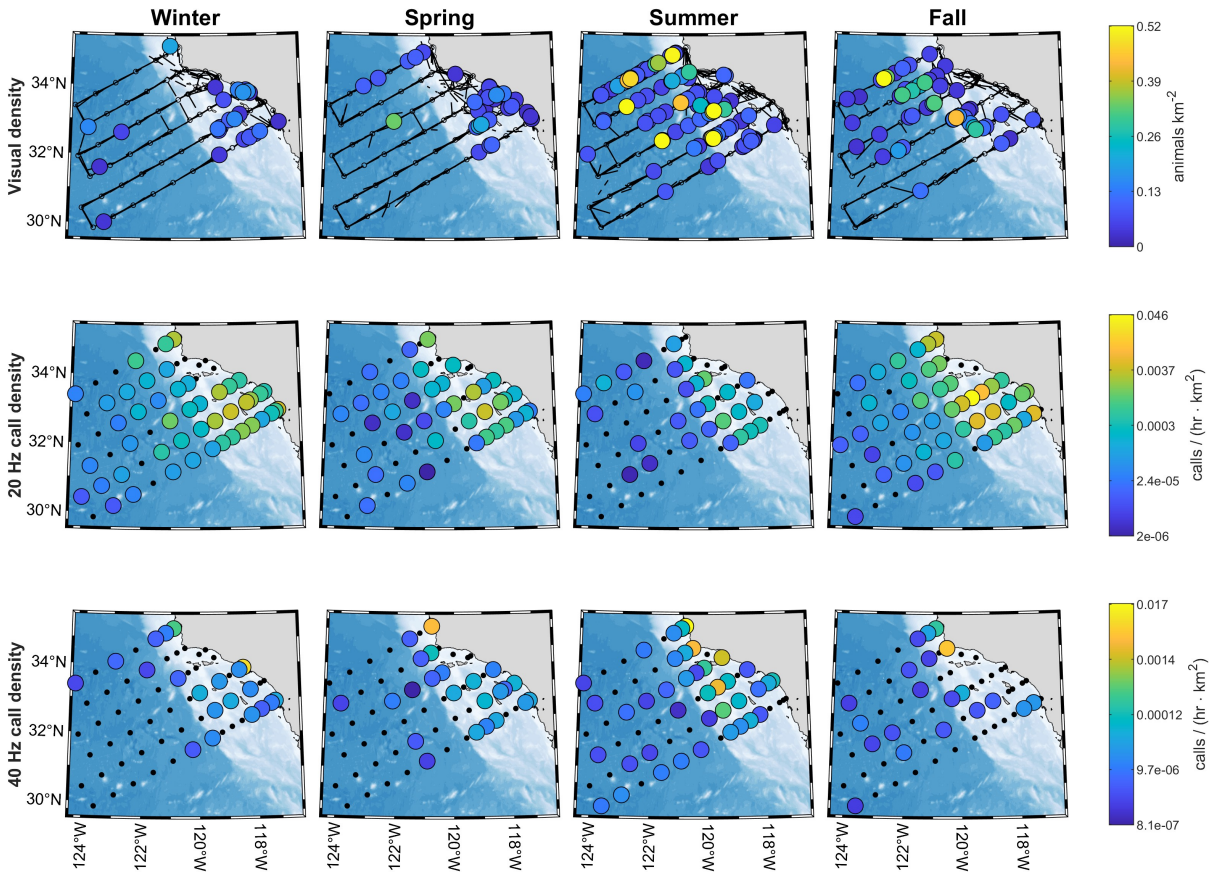


Figure 5.2. Seasonal spatial distribution of fin whale segment-level density estimates and acoustic density estimates of fin whale 20 Hz and 40 Hz calls across the CalCOFI survey grid, 2004–2024. For the visual data, each on-effort segment with a sighting is given a colored circle, were the colors are scaled by density. Low densities are in blue and high densities are in yellow. Segments with effort but no sightings are shown as black lines. Acoustic densities are shown with the same color scaling and each circle represents the total acoustic density at a given station for a given season. Stations with no detections of a given call type are black circles.

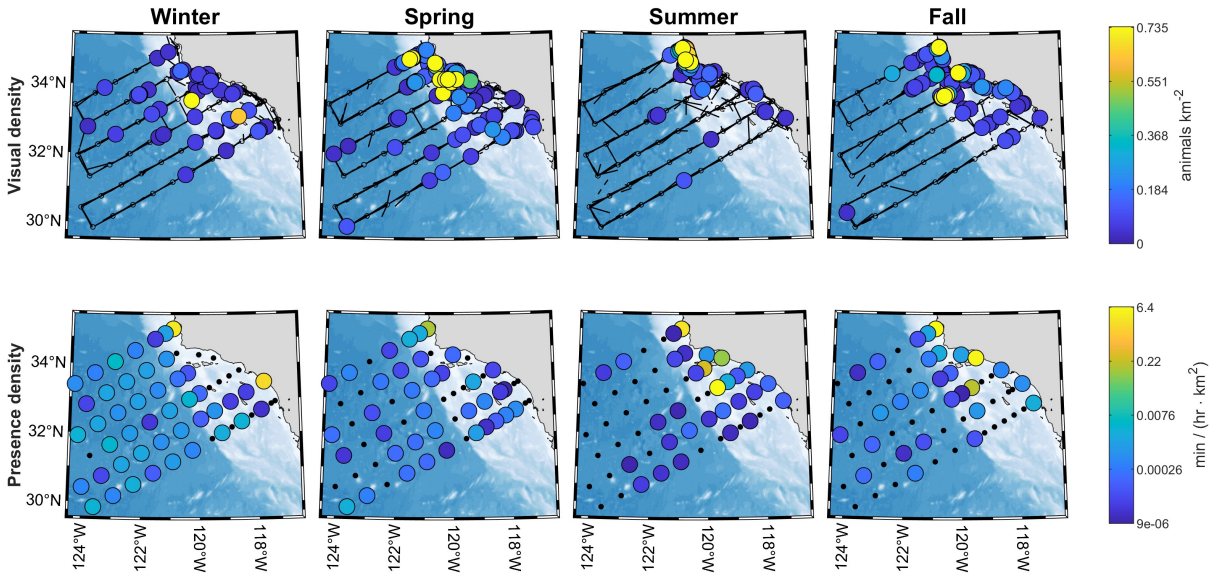


Figure 5.3. Seasonal spatial distribution of humpback whale segment-level density estimates and acoustic presence density estimates of across the CalCOFI survey grid, 2004–2024. For the visual data, each on-effort segment with a sighting is given a colored circle, were the colors are scaled by density. Low densities are in blue and high densities are in yellow. Segments with effort but no sightings are shown as black lines. Acoustic densities are shown with the same color scaling and each circle represents the total acoustic density at a given station for a given season. Stations with no detections of a given call type are black circles.

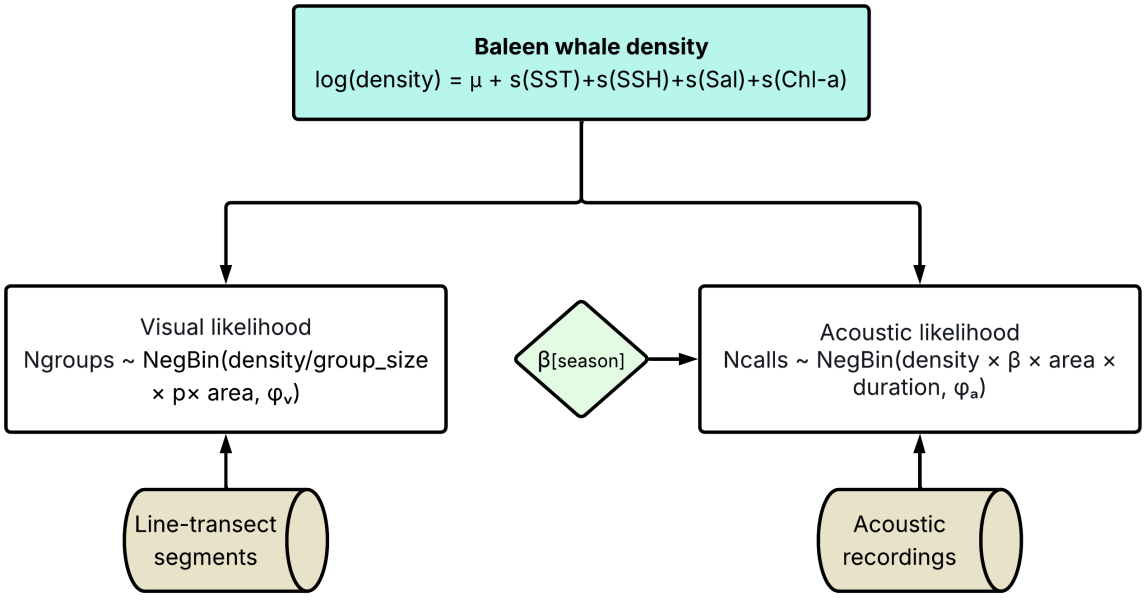


Figure 5.4. Schematic of the joint Bayesian model linking visual line-transect and passive acoustic survey data through a shared latent log-density field.

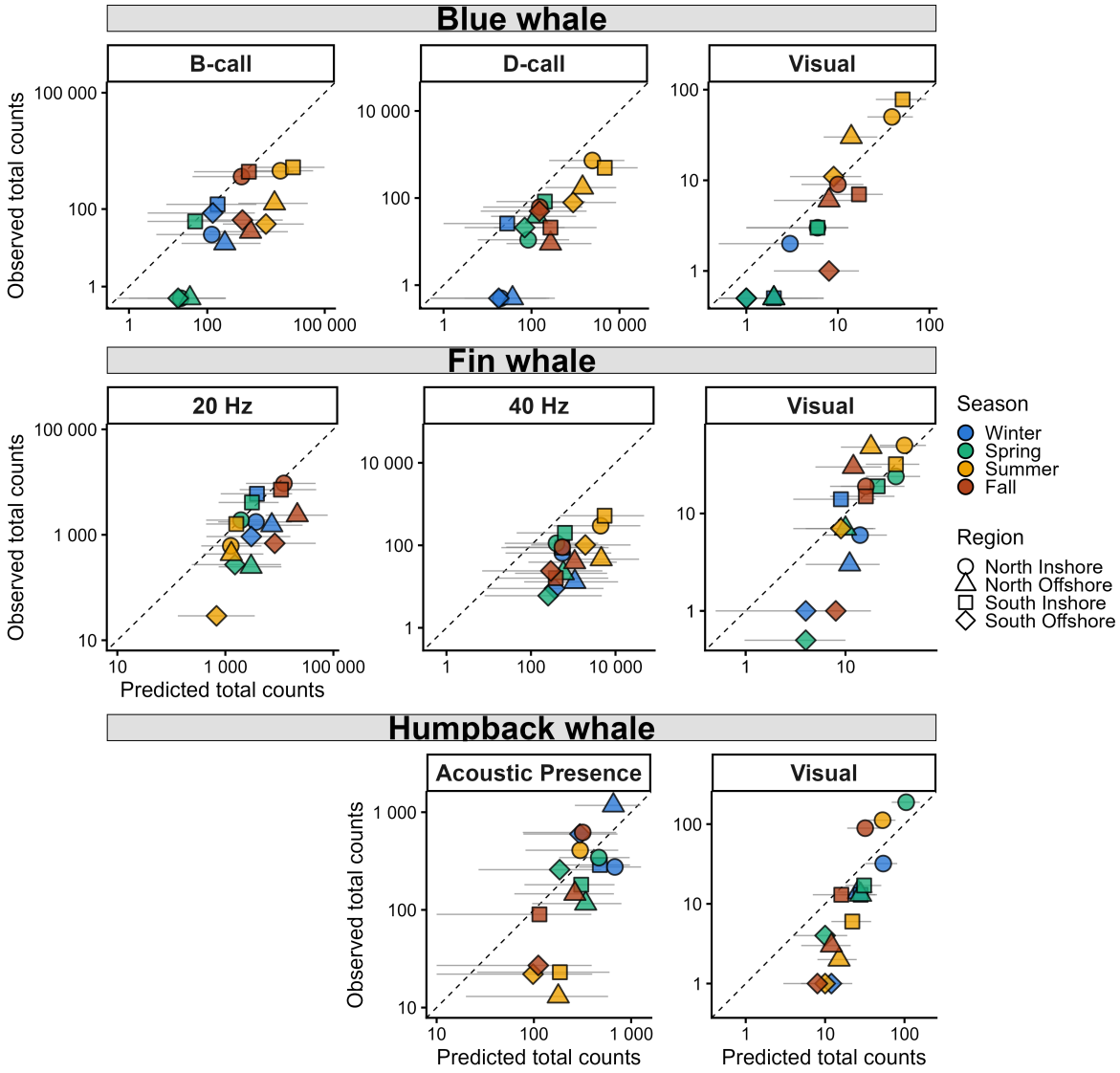


Figure 5.5. Posterior predictive checks comparing observed and model-predicted total counts (log-log scale), by species, call type or visual detection, season, and CalCOFI quadrant. Points are colored by season and shaped by quadrant (north/south, inshore/offshore). Horizontal gray bars show the 95% posterior predictive interval for each point. The dashed line marks 1:1 agreement between observed and predicted counts.

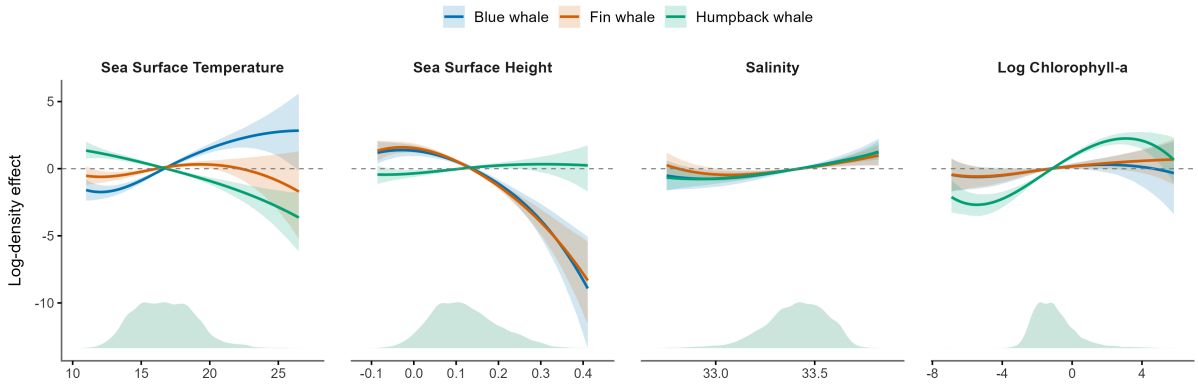


Figure 5.6. Posterior marginal response of species-specific log-density to sea surface temperature, sea surface height, salinity, and chlorophyll-*a*, with 95% credible intervals. Gray-green shading shows the kernel density estimate of each environmental variable, indicating the distribution of observed conditions.

Table 5.1. All prior distributions used in the joint model. Priors are the same across the three species unless a species-specific value is given, and the same across all four seasons for the seasonal cue/presence rate $\beta_{\text{type}}[m]$ priors. For lognormal priors, the location parameter is offset by $-0.5\sigma^2$ so that the stated value is the prior mean instead of its median.

Parameter	Prior	Definition
μ	$\text{Lognormal}(\log(0.0008) - 0.5, 1)$	Log-density intercept (blue whale)
	$\text{Lognormal}(\log(0.0093) - 0.5, 1)$	Log-density intercept (fin whale)
	$\text{Lognormal}(\log(0.0031) - 0.5, 1)$	Log-density intercept (humpback whale)
γ_{1k}, γ_{2k}	$\text{Normal}(0, 1)$	Spline coefficients, per environmental covariate
$\sigma_{\text{spl},k}$	$\text{Half-Normal}(0, 1)$	P-spline smoothing SD, per environmental covariate
ϕ_v	$\text{Half-Normal}(0, 10)$	Visual NegBin overdispersion
ϕ_{type}	$\text{Half-Normal}(0, 10)$	Acoustic NegBin overdispersion, per call type
$\bar{s} - 1$	$\text{Exponential}(1)$	Mean group size minus 1
ϕ_s	$\text{Exponential}(1)$	Group-size NegBin overdispersion
$\beta_{\text{type}}[m]$	$\text{Lognormal}(\log(2) - 0.5, 1)$	Blue whale B call cue rate
	$\text{Lognormal}(\log(2) - 0.5, 1)$	Blue whale D call cue rate
	$\text{Lognormal}(\log(4.8) - 0.5, 1)$	Fin whale 20 Hz cue rate
	$\text{Lognormal}(\log(2) - 0.5, 1)$	Fin whale 40 Hz cue rate
	$\text{Uniform}(0, 60)$	Humpback presence rate

Table 5.2. Posterior median seasonal cue/presence rates with 95% CI by species and call type. Units are calls/whale/hr for blue and fin whale, min/whale/hr for humpback whale.

Species	Call type	Winter	Spring	Summer	Fall
Blue whale	B-call	0.26 (0.10–0.76)	0.03 (0.01–0.10)	0.80 (0.37–1.93)	0.36 (0.17–0.86)
Blue whale	D-call	0.02 (0.01–0.08)	0.05 (0.02–0.15)	0.13 (0.06–0.30)	0.04 (0.02–0.13)
Fin whale	20 Hz	0.69 (0.41–1.28)	0.28 (0.17–0.52)	0.06 (0.03–0.09)	1.52 (0.94–2.68)
Fin whale	40 Hz	0.11 (0.03–0.42)	0.06 (0.02–0.20)	0.18 (0.07–0.48)	0.07 (0.02–0.23)
Humpback whale	Presence min	0.09 (0.06–0.12)	0.04 (0.03–0.06)	0.03 (0.02–0.05)	0.05 (0.03–0.07)

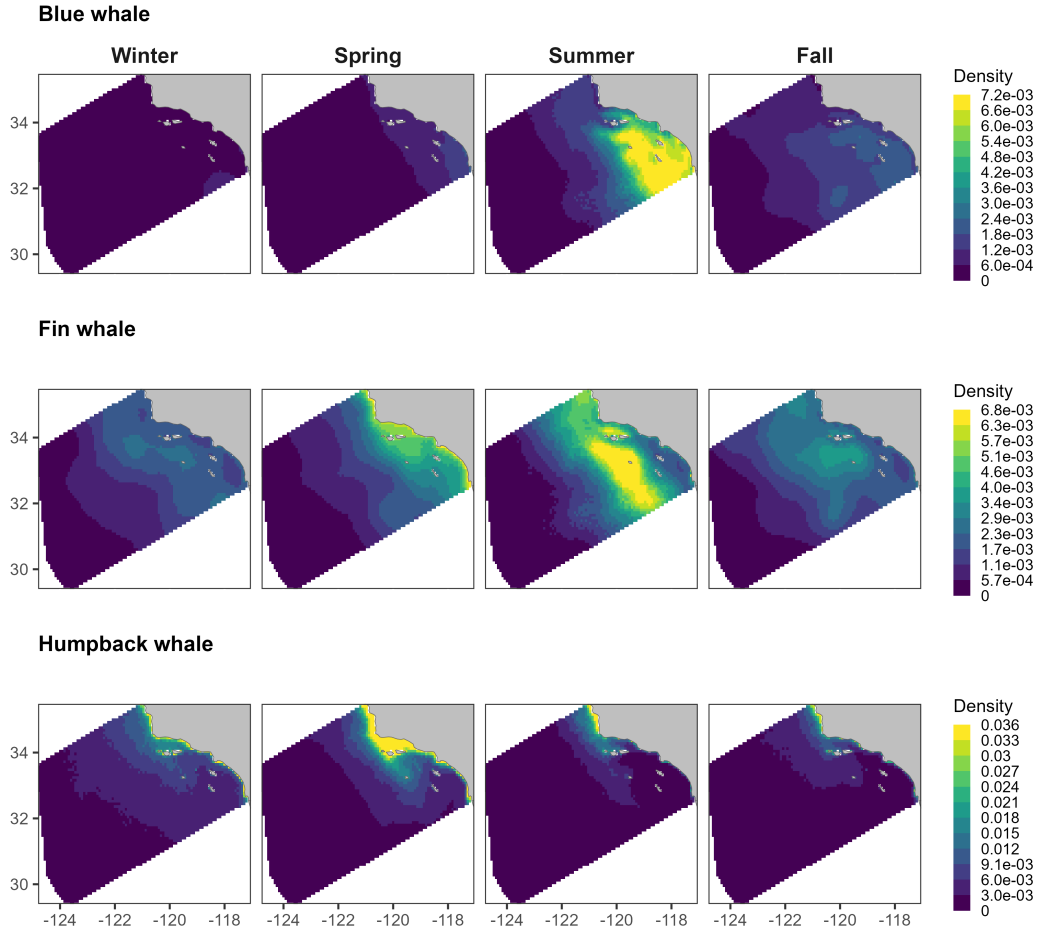


Figure 5.7. Posterior median seasonal density surfaces (animals/km^2) for blue, fin, and humpback whales across the CalCOFI study area. Density was predicted separately for each cruise, then averaged within season. At each grid cell, density is summarized as the median across 4,000 posterior draws.

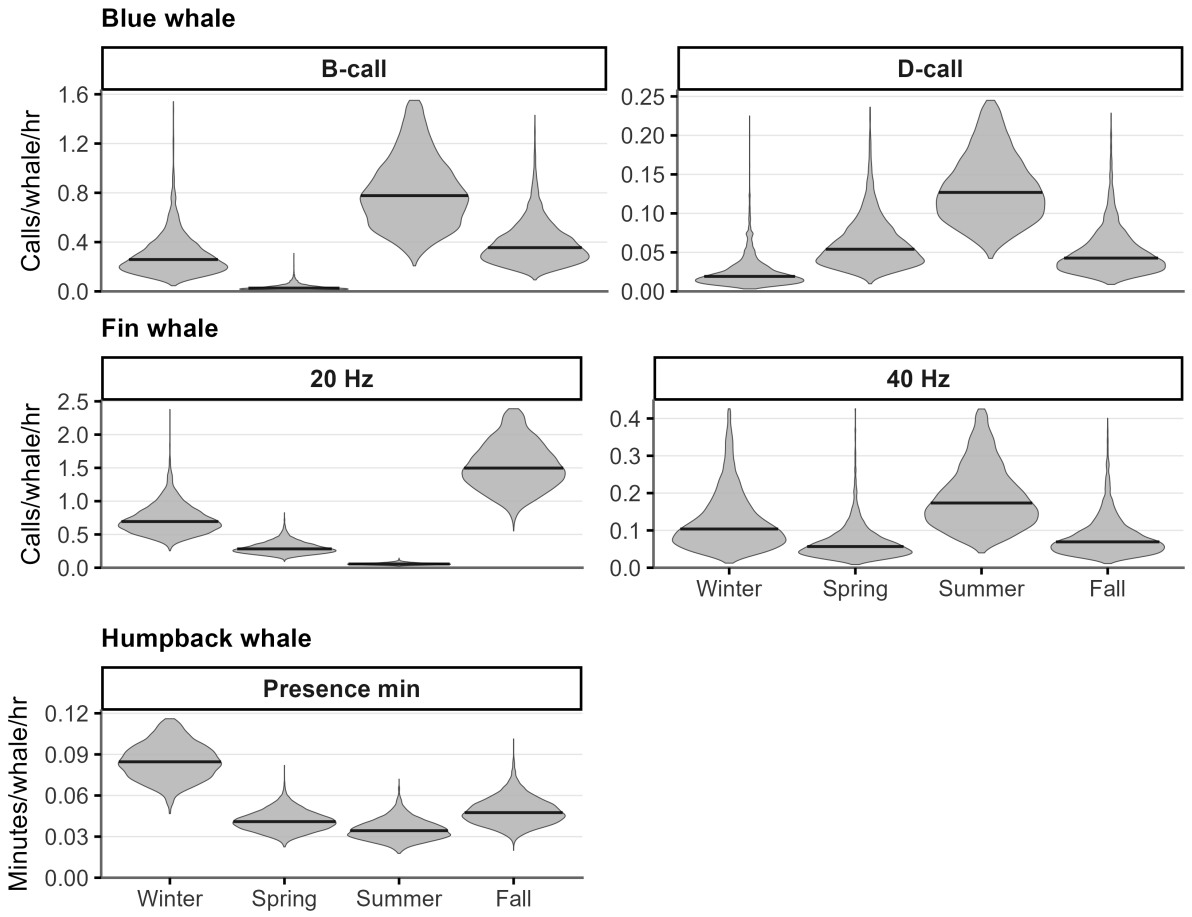


Figure 5.8. Posterior seasonal cue and presence rates ($\beta_{\text{type}}[m]$) for blue, fin, and humpback whales. Violins show the full posterior distribution for each season; horizontal lines mark the posterior median. Units are calls/whale/hr for blue and fin whale call types and minutes/whale/hr for humpback whale presence.

Bibliography

Alksne, M. N., Roch, M. A., Frasier, K. E., Hildebrand, J. A., Andres, S., Adesanya, D., Baggett, L. M., Jones, J. M., Liu, X., Širović, A., Zhang, X., Zingale, J., and Baumann-Pickering, S. (2026). Application of deep learning to estimate blue and fin whale call density in the southern California Current Ecosystem. *Under Review*.

Allen, A. N., Harvey, M., Harrell, L., Jansen, A., Merkens, K. P., Wall, C. C., Cattiau, J., and Oleson, E. M. (2021). A convolutional neural network for automated detection of humpback whale song in a diverse, long-term passive acoustic dataset. *Frontiers in Marine Science*, 8:607321.

Baggett, L. M., Posdaljian, N., ZoBell, V. M., Andres, J. F., Pickering, L. P., Schriber, N. E., Alksne, M. N., Lenssen, K. L., Thayre, B. J., and Baumann-Pickering, S. (2026). Baseline soundscapes and bioacoustic considerations relevant to floating offshore wind development along the U.S. West Coast. *Under Review*.

Barlow, J. (2015). Inferring trackline detection probabilities, g(0), for cetaceans from apparent densities in different survey conditions. *Marine Mammal Science*, 31(3):923–943.

Barlow, J. and Forney, K. A. (2007). Abundance and population density of cetaceans in the California Current ecosystem. *Fishery Bulletin*, 105:509–526.

Baumann-Pickering, S., Roch, M. A., Brownell, Robert L., J., Simonis, A. E., McDonald, M. A., Solsona-Berga, A., Oleson, E. M., Wiggins, S. M., and Hildebrand, J. A. (2014). Spatio-temporal patterns of beaked whale echolocation signals in the North Pacific. *PLoS ONE*, 9(1):e86072.

Becker, E. A., Carretta, J. V., Forney, K. A., Barlow, J., Brodie, S., Hoopes, R., Jacox, M. G., Maxwell, S. M., Redfern, J. V., Sisson, N. B., Welch, H., and Hazen, E. L. (2020). Performance evaluation of cetacean species distribution models developed using generalized additive models and boosted regression trees. *Ecology and Evolution*, 10(12):5759–5784.

Becker, E. A., Forney, K. A., Fiedler, P. C., Barlow, J., Chivers, S. J., Edwards, C. A., Moore, A. M., and Redfern, J. V. (2016). Moving towards dynamic ocean management: How well do modeled ocean products predict species distributions? *Remote Sensing*, 8(2):149.

Becker, E. A., Forney, K. A., Miller, D. L., Barlow, J., Rojas-Bracho, L., Urbán R, J., and Moore, J. E. (2022). Dynamic habitat models reflect interannual movement of cetaceans within the California Current Ecosystem. *Frontiers in Marine Science*, 9:829523.

Becker, E. A., Forney, K. A., Redfern, J. V., Barlow, J., Jacox, M. G., Roberts, J. J., and Palacios, D. M. (2019). Predicting cetacean abundance and distribution in a changing climate. *Diversity and Distributions*, 25(4):626–643.

Becker, E. A., Forney, K. A., Thayre, B. J., Debich, A. J., Campbell, G. S., Whitaker, K., Douglas, A. B., Gilles, A., Hoopes, R., and Hildebrand, J. A. (2017). Habitat-based density models for three cetacean species off southern California illustrate pronounced seasonal differences. *Frontiers in Marine Science*, 4:121.

Becker, E. A., Forney, K. A., Thayre, B. J., Whitaker, K., Hoopes, R., Jones, J. M., Hildebrand, J. A., and Moore, J. (2025). Evaluating seasonal vs. spatial extrapolation for cetacean distribution models in the California Current. *Marine Mammal Science*.

Buckland, S. T., Anderson, D. R., Burnham, K. P., Laake, J. L., Borchers, D. L., and Thomas, L. (2001). *Introduction to Distance Sampling: Estimating Abundance of Biological Populations*. Oxford University Press.

Buckland, S. T., Rexstad, E. A., Marques, T. A., and Oedekoven, C. S. (2015). *Distance Sampling: Methods and Applications*. Springer.

Calambokidis, J., Kratofil, M. A., Palacios, D. M., Lagerquist, B. A., Schorr, G. S., Hanson, M. B., Baird, R. W., Forney, K. A., Becker, E. A., Rockwood, R. C., and Hazen, E. L. (2024). Biologically important areas II for cetaceans within U.S. and adjacent waters – West Coast region. *Frontiers in Marine Science*, 11:1283231.

Calambokidis, J., Steiger, G. H., Curtice, C., Harrison, J., Ferguson, M. C., Becker, E., DeAngelis, M., and Van Parijs, S. M. (2015). Biologically important areas for selected cetaceans within U.S. waters – West Coast region. *Aquatic Mammals*, 41(1):39–53.

Campbell, G. S., Thomas, L., Whitaker, K., Douglas, A. B., Calambokidis, J., and Hildebrand, J. A. (2015). Inter-annual and seasonal trends in cetacean distribution, density and abundance off southern California. *Deep-Sea Research Part II*, 112:143–157.

Carpenter, B., Gelman, A., Hoffman, M. D., Lee, D., Goodrich, B., Betancourt, M., Brubaker, M., Guo, J., Li, P., and Riddell, A. (2017). Stan: a probabilistic programming language. *Journal of Statistical Software*, 76(1):1–32.

Cauchy, P. (2023). Gliders for passive acoustic monitoring of the oceanic environment. *Frontiers in Remote Sensing*, 4:1106533.

Chassignet, E. P., Hurlburt, H. E., Smedstad, O. M., Halliwell, G. R., Hogan, P. J., Wallcraft, A. J., Baraille, R., and Bleck, R. (2007). The HYCOM (HYbrid Coordinate Ocean Model) data assimilative system. *Journal of Marine Systems*, 65(1-4):60–83.

Cholewiak, D. M., Sousa-Lima, R. S., and Cerchio, S. (2018). Songbird dynamics under the sea: acoustic interactions between humpback whales suggest song mediates male interactions. *Royal Society Open Science*, 5(2):171298.

Conn, P. B., Johnson, D. S., Williams, P. J., Melin, S. R., and Hooten, M. B. (2018). A guide to Bayesian model checking for ecologists. *Ecological Monographs*, 88(4):526–542.

Croll, D. A., Clark, C. W., Acevedo, A., Tershy, B., Flores, S., Gedamke, J., and Urban, J. (2002). Only male fin whales sing loud songs. *Nature*, 417(6891):809.

Croll, D. A., Marinovic, B., Benson, S., Chavez, F. P., Black, N., Ternullo, R., and Tershy, B. R. (2005). From wind to whales: trophic links in a coastal upwelling system. *Marine Ecology Progress Series*, 289:117–130.

Darling, J. D. and Berube, M. (2001). Interactions of singing humpback whales with other males. *Marine Mammal Science*, 17(3):570–584.

Dorman, J. G., Sydeman, W. J., García-Reyes, M., Zeno, R. A., and Santora, J. A. (2015). Modeling krill aggregations in the central-northern California Current. *Marine Ecology Progress Series*, 528:87–99.

Eilers, P. H. C. and Marx, B. D. (1996). Flexible smoothing with B-splines and penalties. *Statistical Science*, 11(2):89–121.

Fahlbusch, J. A., Czapanskiy, M. F., Calambokidis, J., Cade, D. E., Abrahms, B., Hazen, E. L., and Goldbogen, J. A. (2022). Blue whales increase feeding rates at fine-scale ocean features. *Proceedings of the Royal Society B: Biological Sciences*, 289(1981):20221180.

Fiedler, P. C., Reilly, S. B., Hewitt, R. P., Demer, D., Philbrick, V. A., Smith, S., Armstrong, W., Croll, D. A., Tershy, B. R., and Mate, B. R. (1998). Blue whale habitat and prey in the California Channel Islands. *Deep-Sea Research Part II*, 45(8-9):1781–1801.

Fithian, W., Elith, J., Hastie, T., and Keith, D. A. (2015). Bias correction in species distribution models: pooling survey and collection data for multiple species. *Methods in Ecology and Evolution*, 6(4):424–438.

Fleming, A. H., Yack, T., Redfern, J. V., Becker, E. A., Moore, T. J., and Barlow, J. (2018). Combining acoustic and visual detections in habitat models of Dall's porpoise. *Ecological Modelling*, 384:198–208.

Fletcher, R. J. J., Hefley, T. J., Robertson, E. P., Zuckerberg, B., McCleery, R. A., and Dorazio, R. M. (2019). A practical guide for combining data to model species distributions. *Ecology*, 100(6):e02710.

Forney, K. A., Ferguson, M. C., Becker, E. A., Fiedler, P. C., Redfern, J. V., Barlow, J., Vilchis, I. L., and Ballance, L. T. (2012). Habitat-based spatial models of cetacean density in the eastern Pacific Ocean. *Endangered Species Research*, 16(2):113–133.

Frasier, K. E., Garrison, L. P., Soldevilla, M. S., Wiggins, S. M., and Hildebrand, J. A. (2021). Cetacean distribution models based on visual and passive acoustic data. *Scientific Reports*, 11:8896.

Garcia, M. L., Tolkova, I., Madhusudhana, S., Rahaman, A., Baker, C. S., Mayo, C. A., Hudak, C. A., and Klinck, H. (2025). Acoustic abundance estimation for Critically Endangered North Atlantic right whales in Cape Cod Bay, Massachusetts, USA. *Endangered Species Research*, 56:101–115.

Guazzo, R. A., Stevenson, D. L., Edell, M. K., Gagnon, G. J., and Helble, T. A. (2024). A decade of change and stability for fin whale song in the North Atlantic. *Frontiers in Marine Science*, 11:1278068.

Hazen, E. L., Palacios, D. M., Forney, K. A., Howell, E. A., Becker, E., Hoover, A. L., Irvine, L., DeAngelis, M., Bograd, S. J., Mate, B. R., and Bailey, H. (2017). WhaleWatch: a dynamic management tool for predicting blue whale density in the California Current. *Journal of Applied Ecology*, 54(5):1415–1428.

Helble, T. A., D'Spain, G. L., Campbell, G. S., and Hildebrand, J. A. (2013a). Calibrating passive acoustic monitoring: correcting humpback whale call detections for site-specific and time-dependent environmental characteristics. *Journal of the Acoustical Society of America*, 134(5):EL400–EL406.

Helble, T. A., D'Spain, G. L., Hildebrand, J. A., Campbell, G. S., Campbell, R. L., and Heaney, K. D. (2013b). Site specific probability of passive acoustic detection of humpback whale calls from single fixed hydrophones. *Journal of the Acoustical Society of America*, 134(3):2556–2570.

Helble, T. A., Guazzo, R. A., Alongi, G. C., Martin, C. R., Martin, S. W., and Henderson, E. E. (2020). Fin whale song patterns shift over time in the central north pacific. *Frontiers in Marine Science*, 7:587110.

Isaac, N. J. B., Jarzyna, M. A., Keil, P., Dambly, L. I., Boersch-Supan, P. H., Browning, E., Freeman, S. N., Golding, N., Guillera-Arroita, G., Henrys, P. A., Jarvis, S., Lahoz-Monfort, J., Pagel, J., Pescott, O. L., Schmucki, R., Simmonds, E. G., and O'Hara, R. B. (2020). Data

integration for large-scale models of species distributions. *Trends in Ecology & Evolution*, 35(1):56–67.

Jacox, M. G., Hazen, E. L., and Bograd, S. J. (2016). Optimal environmental conditions and anomalous ecosystem responses: constraining bottom-up controls of phytoplankton biomass in the California Current System. *Scientific Reports*, 6:27612.

Koshkina, V., Wang, Y., Gordon, A., Dorazio, R. M., White, M., and Stone, L. (2017). Integrated species distribution models: combining presence-background data and site-occupancy data with imperfect detection. *Methods in Ecology and Evolution*, 8(4):420–430.

Lewis, L. A., Calambokidis, J., Stimpert, A. K., Fahlbusch, J., Friedlaender, A. S., McKenna, M. F., Mesnick, S. L., Oleson, E. M., Southall, B. L., Szesciorka, A. R., and Širović, A. (2018). Context-dependent variability in blue whale acoustic behaviour. *Royal Society Open Science*, 5(8):180241.

Marques, T. A., Munger, L., Thomas, L., Wiggins, S., and Hildebrand, J. A. (2011). Estimating North Pacific right whale Eubalaena japonica density using passive acoustic cue counting. *Endangered Species Research*, 13(3):163–172.

Marques, T. A., Thomas, L., Martin, S. W., Mellinger, D. K., Ward, J. A., Moretti, D. J., Harris, D., and Tyack, P. L. (2013). Estimating animal population density using passive acoustics. *Biological Reviews*, 88(2):287–309.

Marques, T. A., Thomas, L., Ward, J., DiMarzio, N., and Tyack, P. L. (2009). Estimating cetacean population density using fixed passive acoustic sensors: an example with Blainville's beaked whales. *Journal of the Acoustical Society of America*, 125(4):1982–1994.

McDonald, M. A., Hildebrand, J. A., and Wiggins, S. M. (2006). Increases in deep ocean ambient noise in the Northeast Pacific west of San Nicolas Island, California. *Journal of the Acoustical Society of America*, 120(2):711–718.

Miller, D. A. W., Pacifici, K., Sanderlin, J. S., and Reich, B. J. (2019). The recent past and promising future for data integration methods to estimate species' distributions. *Methods in Ecology and Evolution*, 10(1):22–37.

Miotto, C. (2025). *Acoustic Detection Ranges of Blue Whale (Balaenoptera musculus) D Calls Under Changing Ocean Conditions*. Thesis, UC San Diego.

Oestreich, W. K., Fahlbusch, J. A., Cade, D. E., Calambokidis, J., Margolina, T., Joseph, J., Southall, B. L., McKenna, M. F., Goldbogen, J. A., and Ryan, J. P. (2020). Animal-borne metrics enable acoustic detection of blue whale migration. *Current Biology*, 30(23):4773–4779.e3.

Oleson, E. M., Calambokidis, J., Burgess, W. C., McDonald, M. A., LeDuc, C. A., and Hildebrand, J. A. (2007). Behavioral context of call production by eastern North Pacific blue whales. *Marine Ecology Progress Series*, 330:269–284.

Oleson, E. M., Širović, A., Bayless, A. R., and Hildebrand, J. A. (2014). Synchronous seasonal change in fin whale song in the North Pacific. *PLoS ONE*, 9(12):e115678.

Pacifici, K., Reich, B. J., Miller, D. A. W., Gardner, B., Stauffer, G., Singh, S., McKerrow, A., and Collazo, J. A. (2017). Integrating multiple data sources in species distribution modeling: a framework for data fusion. *Ecology*, 98(3):840–850.

Payne, R. and McVay, S. (1971). Songs of humpback whales. *Science*, 173(3997):585–597.

Posdaljian, N., Soderstjerna, C., Jones, J. M., Solsona-Berga, A., Hildebrand, J. A., Westdal, K. H., Ootoowak, A. J., and Baumann-Pickering, S. (2022). Changes in sea ice and range expansion of sperm whales in the Eclipse Sound region of Baffin Bay, Canada. *Global Change Biology*, 28(12):3860–3870.

Rios, A., Alksne, M., Frasier, K. E., and Baumann-Pickering, S. (2026). Long-term passive acoustic monitoring captures spatiotemporal patterns of an elusive deep-diving predator across the eastern North Pacific. Under Review.

Romagosa, M., Pérez-Jorge, S., Cascão, I., Mouriño, H., Lehodey, P., Pereira, A., Marques, T. A., Matias, L., and Silva, M. A. (2021). Food talk: 40-Hz fin whale calls are associated with prey biomass. *Proceedings of the Royal Society B*, 288(1954):20211156.

Ryan, J. P., Cline, D. E., Joseph, J. E., Margolina, T., Santora, J. A., Kudela, R. M., Chavez, F. P., Pennington, J. T., Wahl, C., Michisaki, R., Benoit-Bird, K., Forney, K. A., Stimpert, A. K., DeVogelaere, A., Black, N., and Fischer, M. (2019). Humpback whale song occurrence reflects ecosystem variability in feeding and migratory habitat of the northeast Pacific. *PLoS ONE*, 14(9):e0222456.

Ryan, J. P., Oestreich, W. K., Benoit-Bird, K. J., Waluk, C. M., Rueda, C. A., Cline, D. E., Zhang, Y., Cheeseman, T., Calambokidis, J., and Fahlbusch, J. A. (2025). Audible changes in marine trophic ecology: Baleen whale song tracks foraging conditions in the eastern North Pacific. *Plos one*, 20(2):e0318624.

Scales, K. L., Schorr, G. S., Hazen, E. L., Bograd, S. J., Miller, P. I., Andrews, R. D., Zerbini, A. N., and Falcone, E. A. (2017). Should i stay or should i go? modelling year-round habitat suitability and drivers of residency for fin whales in the California Current. *Diversity and Distributions*, 23(10):1204–1215.

Schliep, E. M., Gelfand, A. E., Clark, C. W., Mayo, C. A., McKenna, B., Parks, S. E., Yack,

T. M., and Schick, R. S. (2024). Assessing marine mammal abundance: a novel data fusion. *Annals of Applied Statistics*, 18(4):3071–3090.

Sigourney, D. B., Chavez-Rosales, S., Conn, P. B., Garrison, L., Josephson, E., and Palka, D. (2020). Developing and assessing a density surface model in a Bayesian hierarchical framework with a focus on uncertainty: insights from simulations and an application to fin whales (Balaenoptera physalus). *PeerJ*, 8:e8226.

Sigourney, D. B., DeAngelis, A., Cholewiak, D., and Palka, D. (2023). Combining passive acoustic data from a towed hydrophone array with visual line transect data to estimate abundance and availability bias of sperm whales (Physeter macrocephalus). *PeerJ*, 11:e15850.

Širović, A., Hildebrand, J. A., and Wiggins, S. M. (2007). Blue and fin whale call source levels and propagation range in the Southern Ocean. *Journal of the Acoustical Society of America*, 122(2):1208–1215.

Širović, A., Oleson, E. M., Buccowich, J., Rice, A., and Bayless, A. R. (2017). Fin whale song variability in southern California and the Gulf of California. *Scientific Reports*, 7:10126.

Širović, A., Rice, A., Chou, E., Hildebrand, J. A., Wiggins, S., and Roch, M. (2015). Seven years of blue and fin whale call abundance in the Southern California Bight. *Endangered Species Research*, 28.

Stimpert, A. K., DeRuiter, S. L., Falcone, E. A., Joseph, J., Douglas, A. B., Moretti, D. J., Friedlaender, A. S., Calambokidis, J., and Goldbogen, J. A. (2015). Sound production and associated behavior of tagged fin whales (Balaenoptera physalus) in the Southern California Bight. *Animal Biotelemetry*, 3:23.

Szesciorka, A. R., Ballance, L. T., Širović, A., Rice, A., Ohman, M. D., Hildebrand, J. A., and Franks, P. J. S. (2020). Timing is everything: Drivers of interannual variability in blue whale migration. *Scientific Reports*, 10:7710.

Talts, S., Betancourt, M., Simpson, D., Vehtari, A., and Gelman, A. (2020). Validating bayesian inference algorithms with simulation-based calibration. *arXiv preprint arXiv:1804.06788*.

Vehtari, A., Gelman, A., Simpson, D., Carpenter, B., and Burkner, P.-C. (2021). Rank-normalization, folding, and localization: an improved R-hat for assessing convergence of MCMC (with discussion). *Bayesian Analysis*, 16(2):667–718.

Vu, E. T. A. (2015). *Habitat use of calling baleen whales in the southern California Current Ecosystem*. Thesis, UC San Diego.

Wiggins, S. M., Oleson, E. M., McDonald, M. A., and Hildebrand, J. A. (2005). Blue whale

(Balaenoptera musculus) diel call patterns offshore of southern California. *Aquatic Mammals*, 31(2):161–168.

Wisely, E., Patin, N., Alksne, M. N., Dinasquet, J., Swalethorp, R., Bowlin, N., McKaughan, G., Coden, F., Satterthwaite, E., Baumann-Pickering, S., and Semmens, Brice, X. (2026). Continuous large-volume active transect sampling improves detection of rare marine vertebrate eDNA across large spatial scales. *Under Review*.

Zeh, J. M., Perez-Marrufo, V., Adcock, D. L., Jensen, F. H., Knapp, K. J., Robbins, J., Tackaberry, J. E., Weinrich, M., Friedlaender, A. S., Wiley, D. N., and Parks, S. E. (2024). Caller identification and characterization of individual humpback whale acoustic behaviour. *Royal Society Open Science*, 11(3):231608.

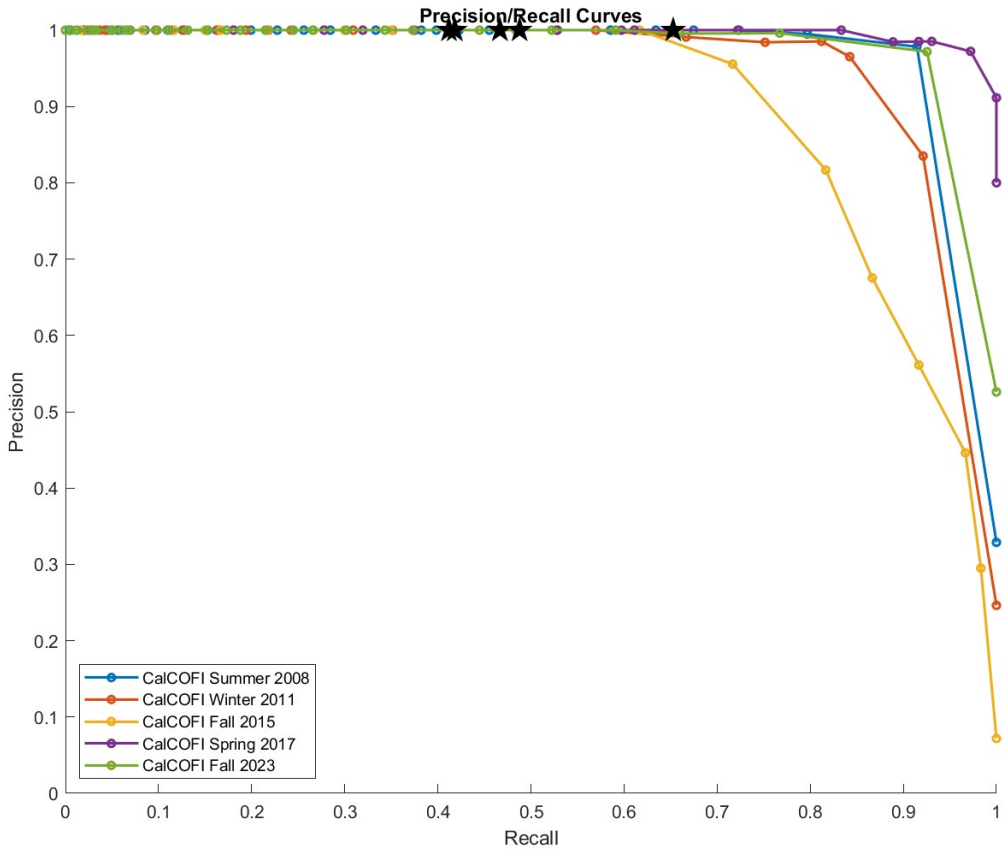


Figure 5.9. Precision-recall curve for the Allen et al. (2021) humpback whale acoustic detector, in 0.01 score bins, evaluated against five manually reviewed CalCOFI cruises. A score threshold of 0.2 was selected, and precision and recall in each dataset at this threshold is denoted by the black stars.

5.6 Supplementary Material

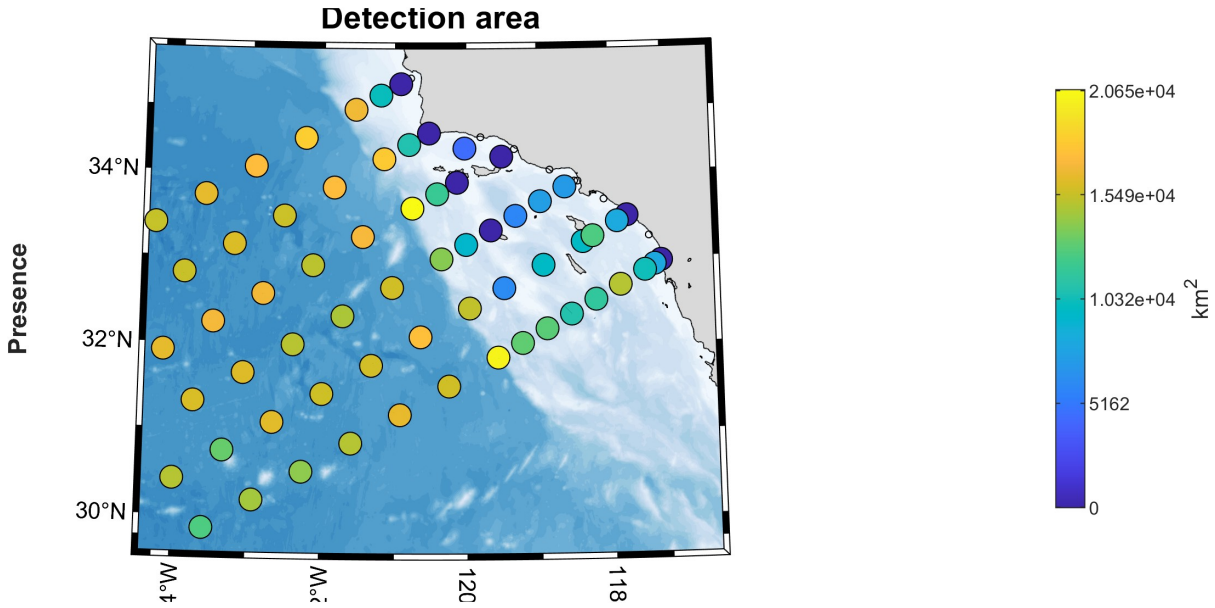


Figure 5.10. Station-level modeled detection area estimates for humpback whales, computed from received-level thresholding at 100 dB.

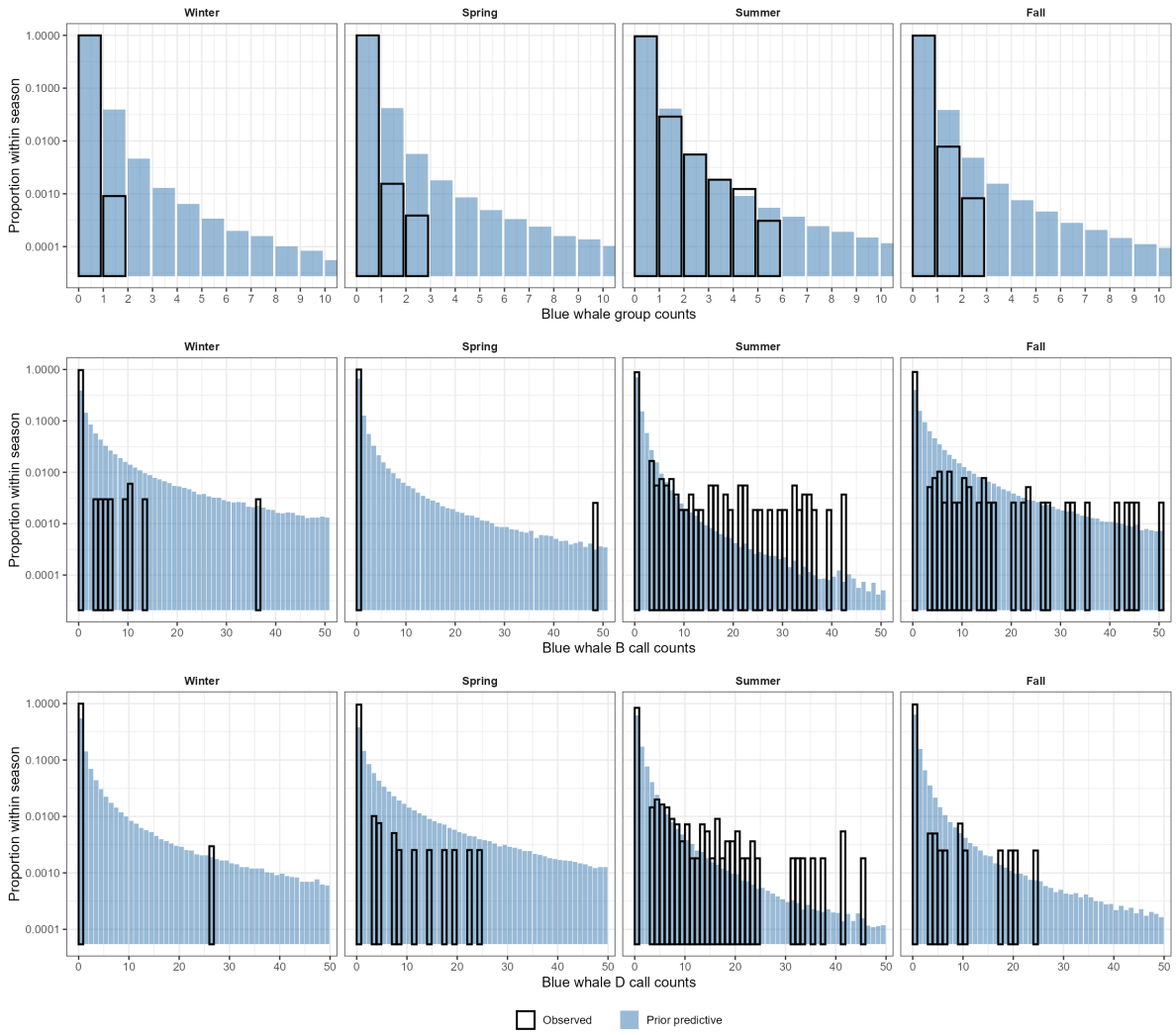


Figure 5.11. Prior predictive check: blue whale. Overlaid observed vs. prior-predictive frequency distributions by season, for visual group counts and each acoustic call type.

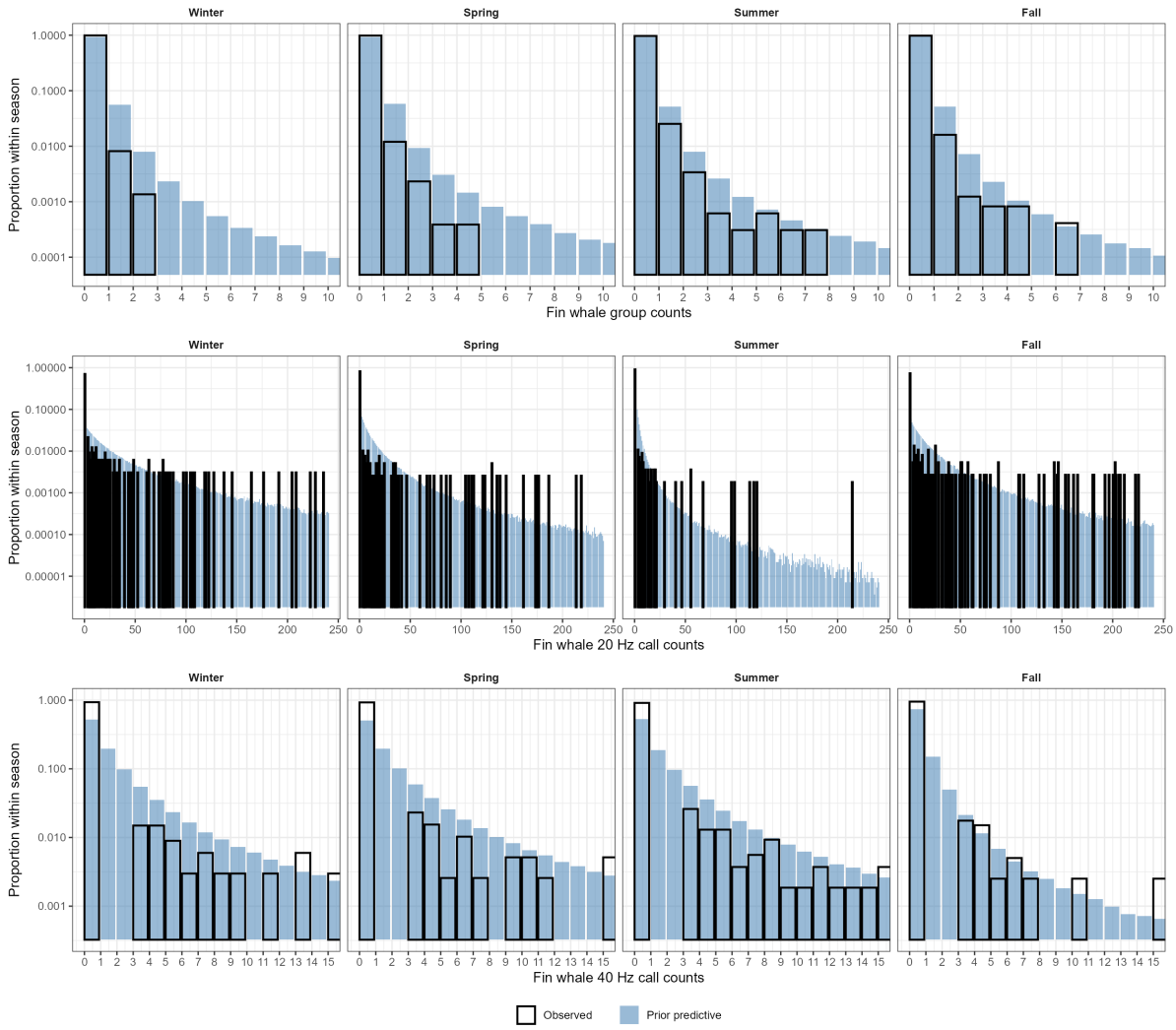


Figure 5.12. Prior predictive check: fin whale. Overlaid observed vs. prior-predictive frequency distributions by season, for visual group counts and each acoustic call type.

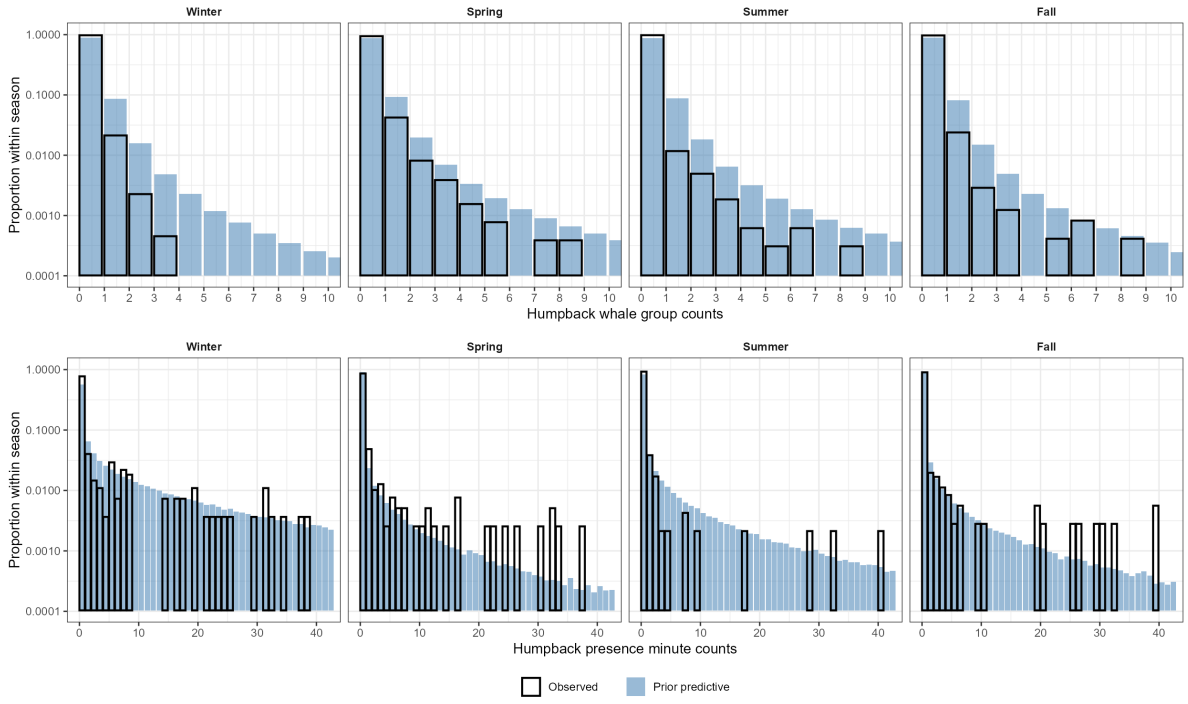


Figure 5.13. Prior predictive check: humpback whale. Overlaid observed vs. prior-predictive frequency distributions by season, for visual group counts and acoustic presence minutes.

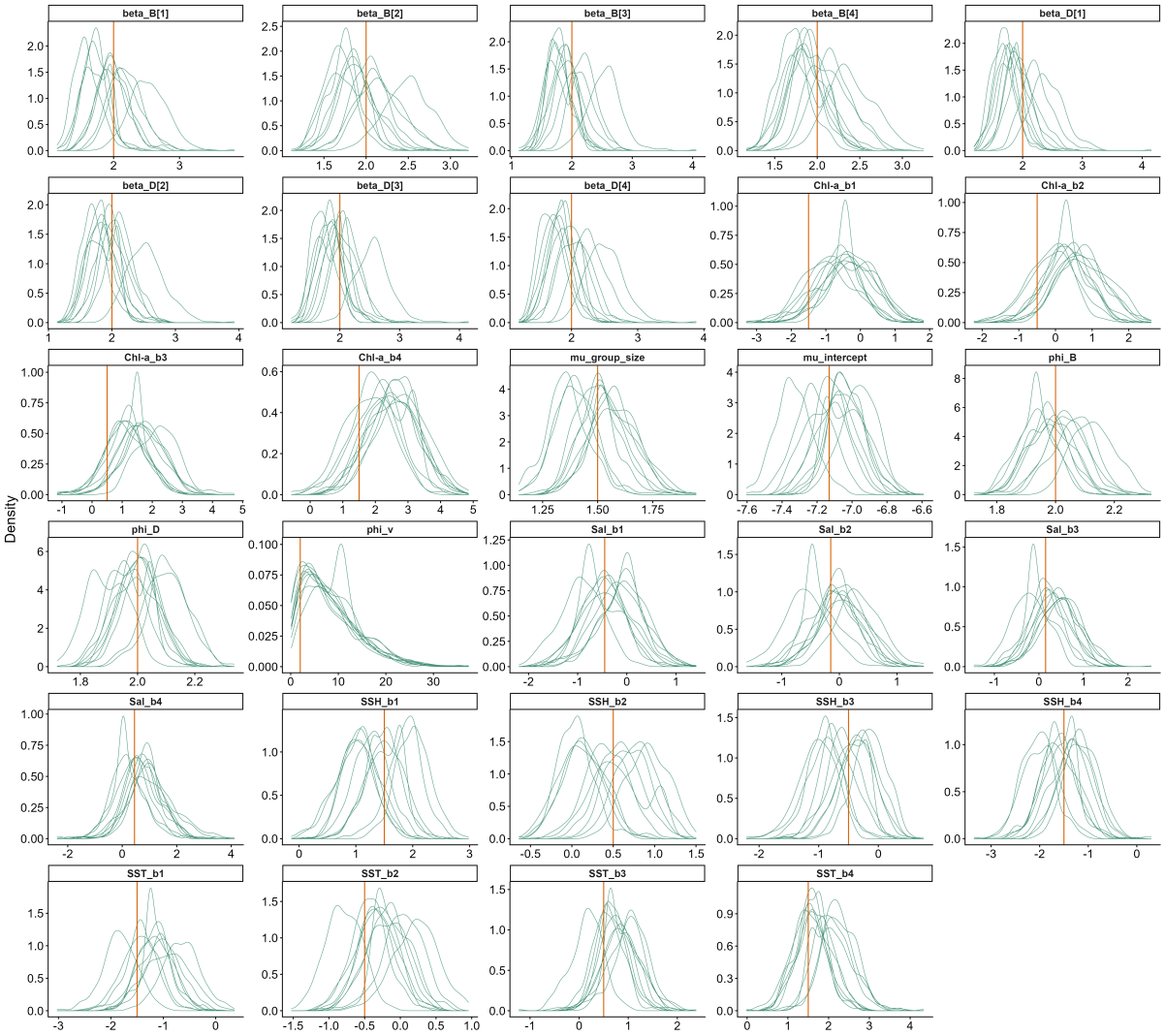


Figure 5.14. Posterior distributions of all recovered parameters across the $M = 10$ simulated replicates for the blue whale model. Each teal curve is one replicate's posterior density for that parameter and the vertical orange line is the true value used to simulate that replicate's data. Each environmental covariate (SST, SSH, salinity, log-chlorophyll-a) has four B-spline basis-function coefficients, β_B[season]/β_D[season] are the seasonal B-call/D-call rates. A parameter recovers well when the true value falls within the bulk of posterior mass across replicates, and poorly when the replicates' posteriors are shifted away from it in a consistent direction.

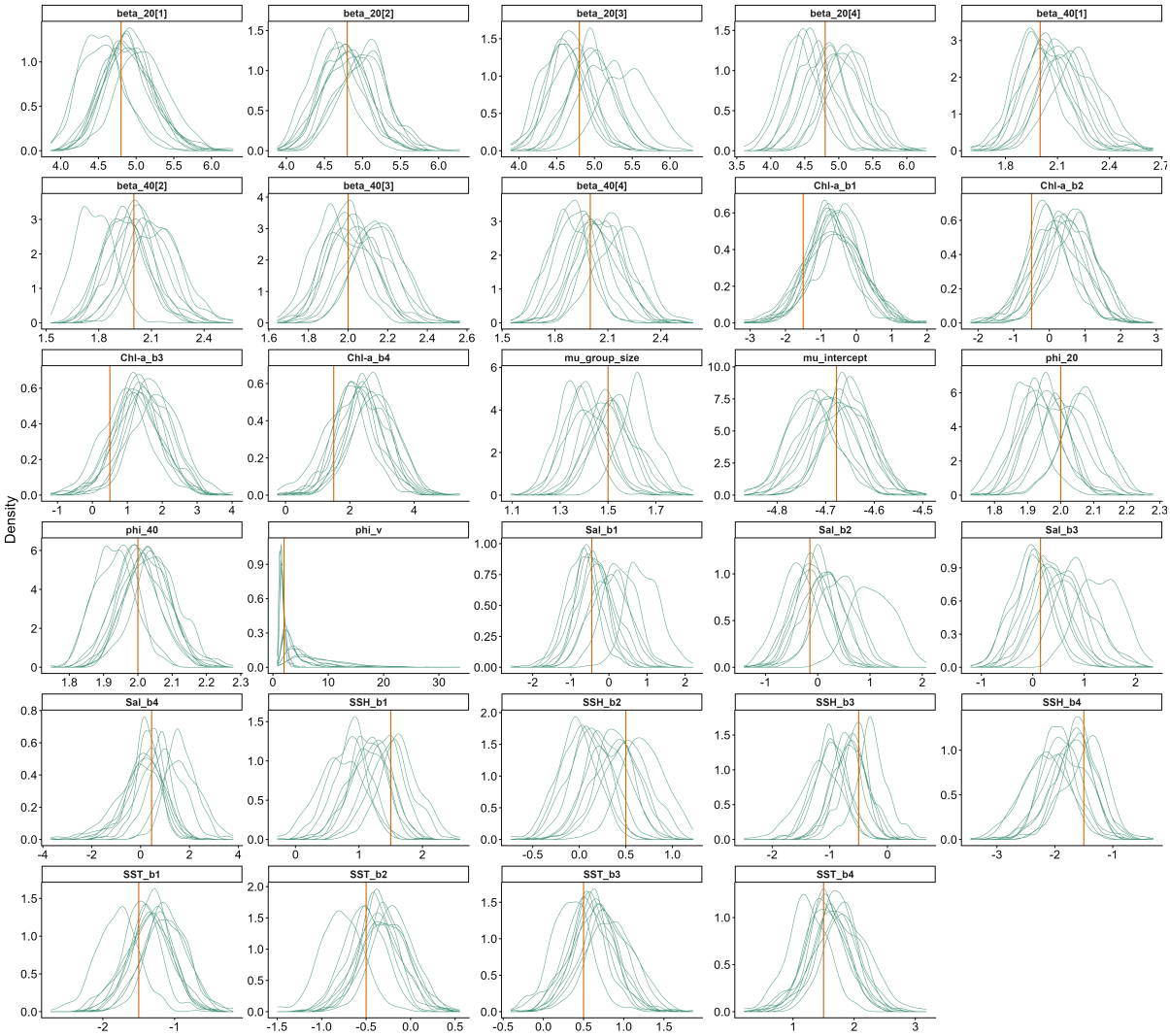


Figure 5.15. Posterior distributions of all recovered parameters across the $M = 10$ simulated replicates for the fin whale model. Each teal curve is one replicate's posterior density for that parameter and the vertical orange line is the true value used to simulate that replicate's data. Each environmental covariate (SST, SSH, salinity, log-chlorophyll-a) has four B-spline basis-function coefficients, β_20Hz[season]/β_40Hz[season] are the seasonal 20 Hz-call/40 Hz-call rates. A parameter recovers well when the true value falls within the bulk of posterior mass across replicates, and poorly when the replicates' posteriors are shifted away from it in a consistent direction.

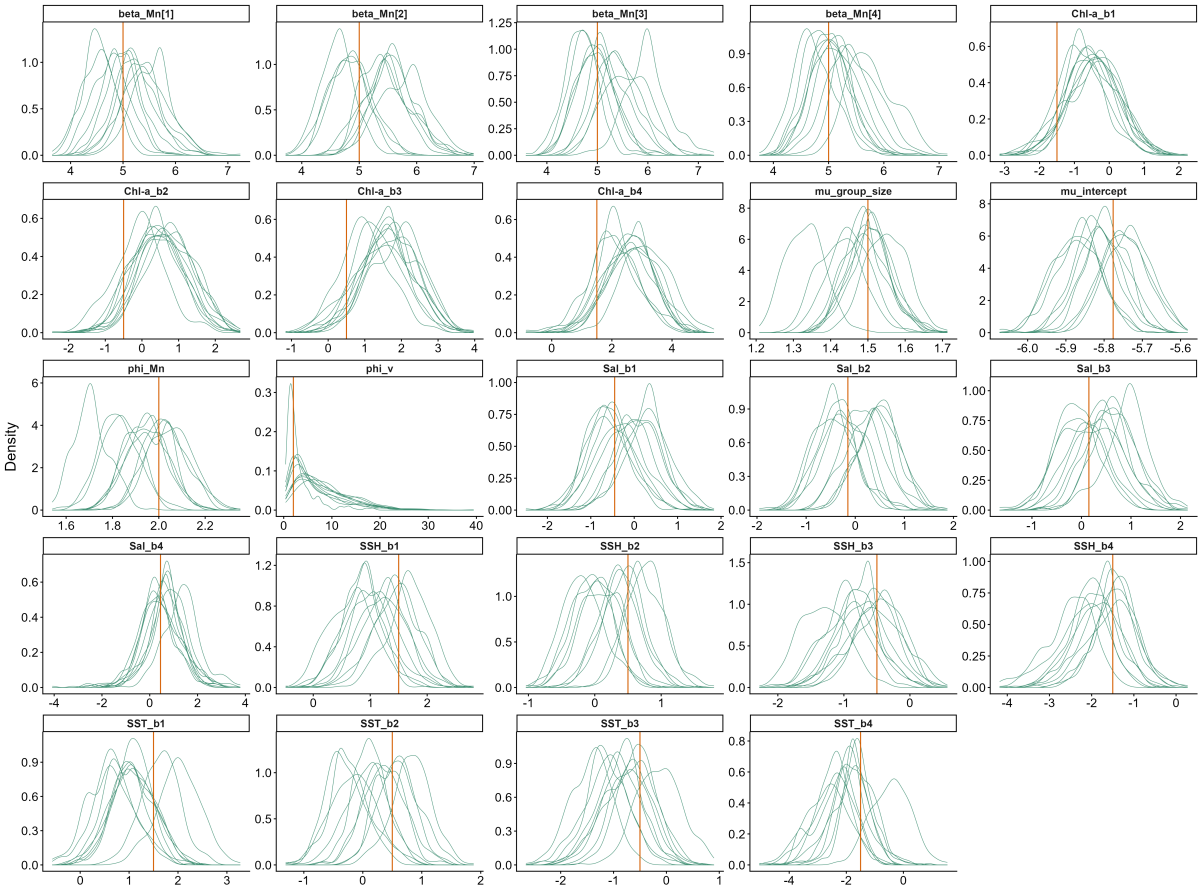


Figure 5.16. Posterior distributions of all recovered parameters across the $M = 10$ simulated replicates for the humpback whale model. Each teal curve is one replicate's posterior density for that parameter and the vertical orange line is the true value used to simulate that replicate's data. Each environmental covariate (SST, SSH, salinity, log-chlorophyll-a) has four B-spline basis-function coefficients, β_{Mn}[season] is the seasonal acoustic presence rate. A parameter recovers well when the true value falls within the bulk of posterior mass across replicates, and poorly when the replicates' posteriors are shifted away from it in a consistent direction.

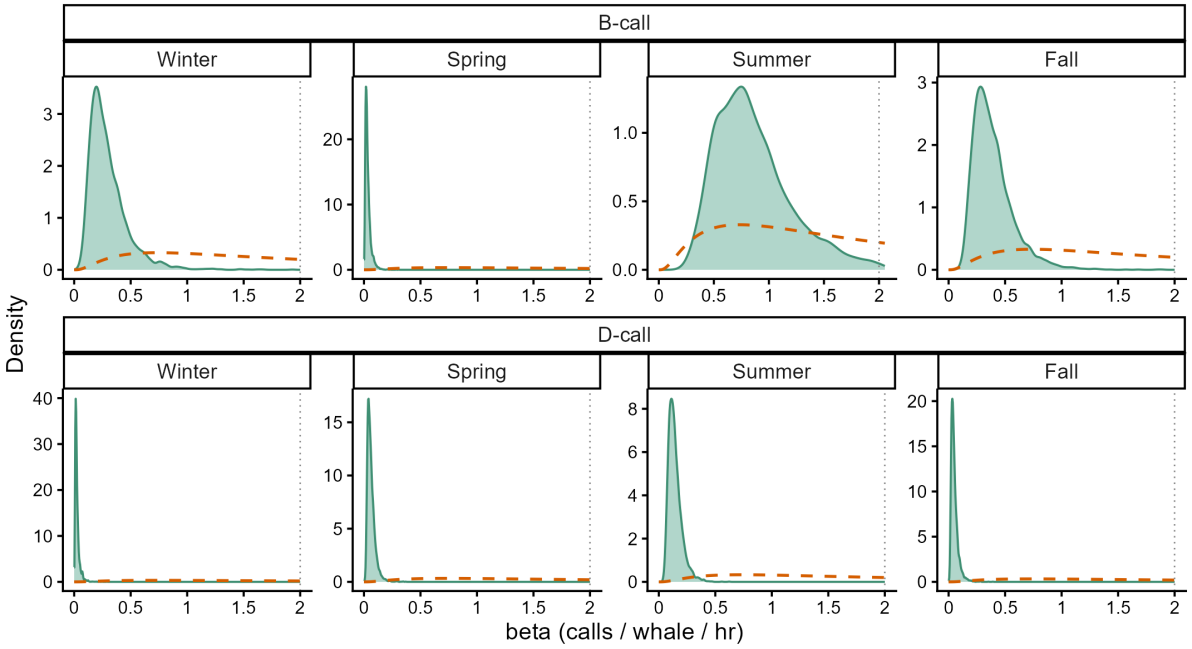


Figure 5.17. Prior vs. posterior comparison for blue whale seasonal call rates (β_B, β_D).

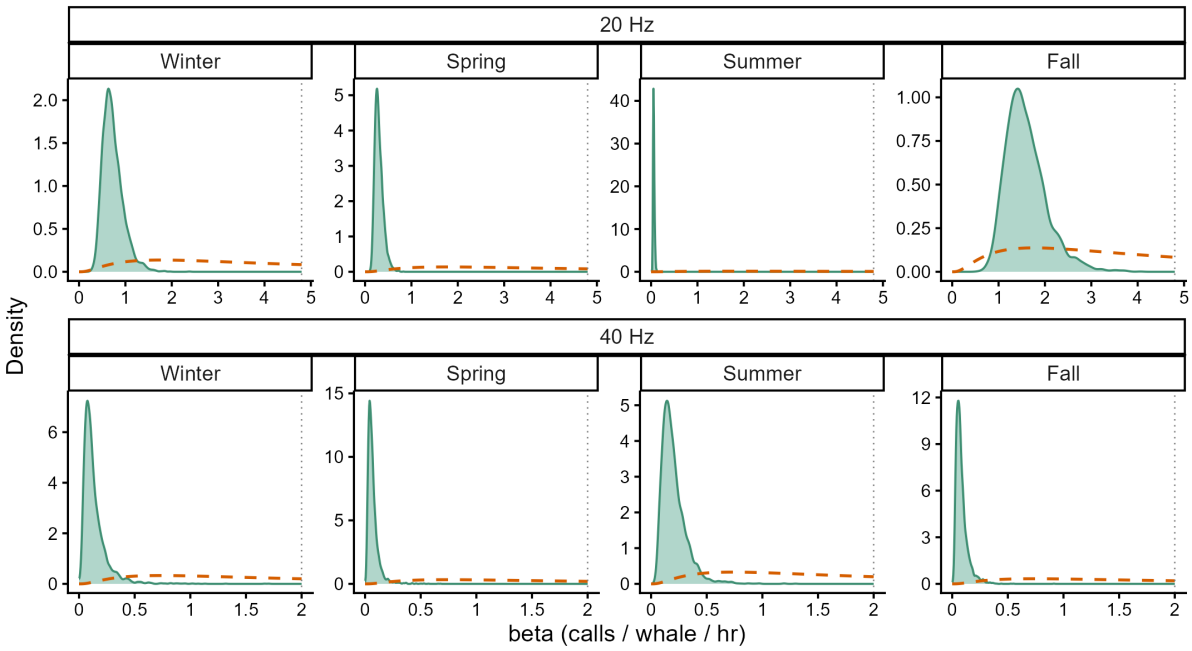


Figure 5.18. Prior vs. posterior comparison for fin whale seasonal call rates (β_{20}, β_{40})

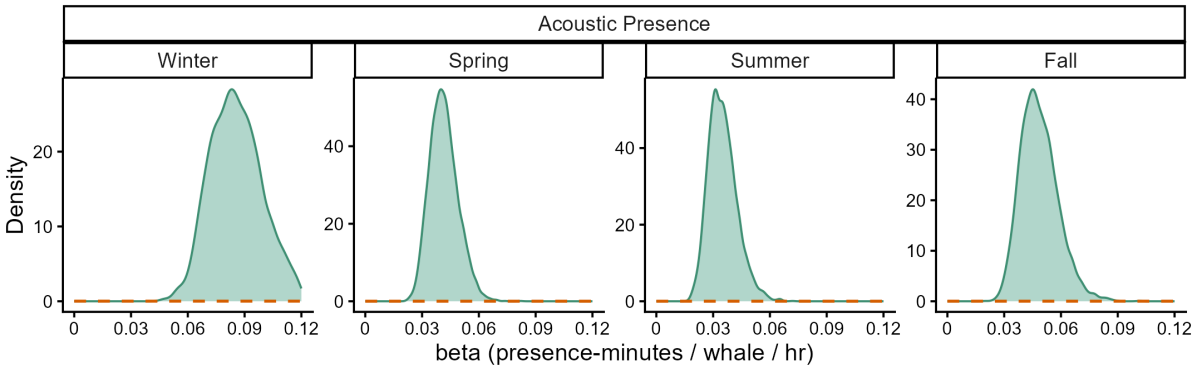


Figure 5.19. Prior vs. posterior comparison for the humpback whale seasonal presence-minute rate (β_{Mn})

Table 5.3. False negative (FN) and false positive (FP) rates used to correct acoustic call and presence counts for each species and call type, estimated from precision and recall from automated acoustic detection algorithms for each call type as described in the main text

Species	Call/signal type	FN	FP
Blue whale	A call	0.293	0.293
Blue whale	B call	0.486	0.174
Blue whale	D call	0.186	0.206
Fin whale	20 Hz call	0.268	0.141
Fin whale	40 Hz call	0.369	0.449
Humpback whale	Presence minutes	0.513	0

Table 5.4. True parameter values assigned for the simulation-based validation (Table 5.5). β_{type} is a single values applied to all four seasons. γ_{env} rows give the four B-spline basis-function coefficients for that covariate, all four are monotonic across basis functions. Blue and fin whale used identical values for every covariate, humpback whale used the same values for SSH, salinity, and chlorophyll-*a*, but the opposite-sign SST coefficients.

Species	Parameter	True value
Blue whale	μ (density intercept)	0.0008 whales/km^2
Blue whale	β_B (B-call rate)	2.0 calls/whale/hr
Blue whale	β_D (D-call rate)	2.0 calls/whale/hr
Blue whale	γ_{env} (SST)	$(-1.50, -0.50, 0.50, 1.50)$
Blue whale	γ_{env} (SSH)	$(1.50, 0.50, -0.50, -1.50)$
Blue whale	γ_{env} (Salinity)	$(-0.45, -0.15, 0.15, 0.45)$
Blue whale	γ_{env} (Chlorophyll-*a*)	$(-1.50, -0.50, 0.50, 1.50)$
Fin whale	μ (density intercept)	0.0093 whales/km^2
Fin whale	β_{20} (20 Hz rate)	4.8 calls/whale/hr
Fin whale	β_{40} (40 Hz rate)	2.0 calls/whale/hr
Fin whale	γ_{env} (SST)	$(-1.50, -0.50, 0.50, 1.50)$
Fin whale	γ_{env} (SSH)	$(1.50, 0.50, -0.50, -1.50)$
Fin whale	γ_{env} (Salinity)	$(-0.45, -0.15, 0.15, 0.45)$
Fin whale	γ_{env} (Chlorophyll-*a*)	$(-1.50, -0.50, 0.50, 1.50)$
Humpback whale	μ (density intercept)	0.0031 whales/km^2
Humpback whale	β_{Mn} (presence-minute rate)	5.0 presence-min/whale/hr*
Humpback whale	γ_{env} (SST)	$(1.50, 0.50, -0.50, -1.50)$
Humpback whale	γ_{env} (SSH)	$(1.50, 0.50, -0.50, -1.50)$
Humpback whale	γ_{env} (Salinity)	$(-0.45, -0.15, 0.15, 0.45)$
Humpback whale	γ_{env} (Chlorophyll-*a*)	$(-1.50, -0.50, 0.50, 1.50)$

Table 5.5. Simulation-based recovery of the density intercept (μ), seasonal cue/presence rates (β_{type}), and environmental spline coefficients, across $M = 10$ simulated replicates per species. Coverage is the proportion of trials whose 70% posterior credible interval contained the true simulated value. Contraction is $1 - (\sigma_{\text{post}}/\sigma_{\text{prior}})^2$ which it is not estimated for the spline coefficients because their prior uses a second-order random-walk (P-spline), which is estimated from the data. Mean bias is the signed posterior-mean-minus-true difference, averaged across replicates.

Parameter	**Species**	**Coverage (%)**	**Contraction (%)**	**Mean bias**
Density intercept μ	Blue whale	80	98.8	0.032
Density intercept μ	Fin whale	90	99.8	-0.007
Density intercept μ	Humpback whale	70	99.7	-0.032
B-call rate β_B	Blue whale	65	98.7	-0.036
D-call rate β_D	Blue whale	62	98.7	-0.040
20 Hz rate β_{20}	Fin whale	88	99.6	0.040
40 Hz rate β_{40}	Fin whale	78	99.6	0.034
Presence-minute rate β_{Mn}	Humpback whale	62	100.0	0.167
Chl-*a* spline coefficients	Blue whale	25	–	0.933
SSH spline coefficients	Blue whale	52	–	-0.078
SST spline coefficients	Blue whale	55	–	0.286
Salinity spline coefficients	Blue whale	95	–	0.139
Chl-*a* spline coefficients	Fin whale	22	–	0.882
SSH spline coefficients	Fin whale	57	–	-0.277
SST spline coefficients	Fin whale	80	–	0.132
Salinity spline coefficients	Fin whale	78	–	0.235
Chl-*a* spline coefficients	Humpback whale	15	–	1.011
SSH spline coefficients	Humpback whale	60	–	-0.292
SST spline coefficients	Humpback whale	52	–	-0.349
Salinity spline coefficients	Humpback whale	72	–	0.199

Table 5.6. Posterior predictive check for the proportion-of-zeros statistic, pooled across seasons. $p_{\text{zero,obs}}$ and $p_{\text{zero,pred}}$ are the observed and posterior-predictive-median proportion of zero counts; the interval is the 95% posterior predictive interval on that proportion. p_B is the Bayesian p-value (proportion of posterior predictive draws with a zero-proportion at or below the observed value).

Species	**Stream**	**Obs.**	**Pred.**	**95% PI**	p_B
Blue whale	Visual	0.986	0.983	[0.979, 0.986]	0.067
Blue whale	B-call	0.916	0.920	[0.901, 0.937]	0.695
Blue whale	D-call	0.927	0.932	[0.914, 0.947]	0.727
Fin whale	Visual	0.980	0.976	[0.972, 0.979]	0.024
Fin whale	20 Hz	0.784	0.783	[0.757, 0.809]	0.489
Fin whale	40 Hz	0.915	0.926	[0.909, 0.943]	0.907
Humpback whale	Visual	0.968	0.964	[0.959, 0.968]	0.061
Humpback whale	Acoustic	0.857	0.880	[0.858, 0.901]	0.982

Table 5.7. Posterior predictive check for the total-count statistic, stratified jointly by season and CalCOFI quadrant (North/South × Inshore/Offshore). T_{obs} is the observed total count in that stratum; T_{pred} is the posterior-predictive median with its 95% interval; p_B is the Bayesian p-value (proportion of posterior predictive draws $\geq T_{\text{obs}}$). Strata with $p_B \leq 0.05$ or $p_B \geq 0.95$ are marked with an asterisk.

Stream	Season	Quadrant	T_{obs}	T_{pred}	95% PI	p_B
Blue whale						
Visual	Winter	North Inshore	2	9	[3, 18]	0.998*
Visual	Winter	North Offshore	0	3	[0, 8]	1.000*
Visual	Winter	South Inshore	0	5	[1, 11]	1.000*
Visual	Winter	South Offshore	0	1	[0, 4]	1.000*
Visual	Spring	North Inshore	3	12	[4, 24]	0.996*
Visual	Spring	North Offshore	0	4	[0, 10]	1.000*
Visual	Spring	South Inshore	3	7	[2, 15]	0.943
Visual	Spring	South Offshore	0	1	[0, 5]	1.000*
Visual	Summer	North Inshore	50	77	[44, 133]	0.949
Visual	Summer	North Offshore	30	14	[5, 28]	0.014*
Visual	Summer	South Inshore	78	60	[31, 110]	0.200
Visual	Summer	South Offshore	11	6	[1, 14]	0.125
Visual	Fall	North Inshore	9	29	[14, 53]	1.000*
Visual	Fall	North Offshore	6	9	[3, 19]	0.815
Visual	Fall	South Inshore	7	29	[14, 54]	1.000*
Visual	Fall	South Offshore	1	5	[1, 14]	0.990*
B-call	Winter	North Inshore	22	94	[7, 633]	0.875
B-call	Winter	North Offshore	13	62	[5, 347]	0.918
B-call	Winter	South Inshore	132	85	[7, 507]	0.337

continued on next page

Table 5.7 continued from previous page

Stream	**Season**	**Quadrant**	T_{obs}	T_{pred}	**95% PI**	p_B
B-call	Winter	South Offshore	79	23	[1, 303]	0.166
B-call	Spring	North Inshore	0	5	[0, 44]	1.000*
B-call	Spring	North Offshore	0	5	[0, 47]	1.000*
B-call	Spring	South Inshore	48	9	[1, 59]	0.039*
B-call	Spring	South Offshore	0	2	[0, 18]	1.000*
B-call	Summer	North Inshore	971	1185.5	[205, 5312]	0.604
B-call	Summer	North Offshore	140	402.5	[83, 1886]	0.887
B-call	Summer	South Inshore	1192	1550	[322, 6484]	0.640
B-call	Summer	South Offshore	41	140	[13, 980]	0.872
B-call	Fall	North Inshore	687	474	[45, 2696]	0.341
B-call	Fall	North Offshore	26	309	[49, 1746]	0.998*
B-call	Fall	South Inshore	918	616	[48, 3564]	0.334
B-call	Fall	South Offshore	52	113.5	[9, 1091]	0.747
D-call	Winter	North Inshore	0	8	[0, 66]	1.000*
D-call	Winter	North Offshore	0	5	[0, 42]	1.000*
D-call	Winter	South Inshore	26	8	[0, 55]	0.133
D-call	Winter	South Offshore	0	2	[0, 25]	1.000*
D-call	Spring	North Inshore	11	95	[6, 928]	0.947
D-call	Spring	North Offshore	38	84	[7, 695]	0.759
D-call	Spring	South Inshore	83	162	[13, 1411]	0.740
D-call	Spring	South Offshore	21	29	[1, 309]	0.597
D-call	Summer	North Inshore	729	1066.5	[155, 5228]	0.673
D-call	Summer	North Offshore	174	352	[44, 1594]	0.800

continued on next page

Table 5.7 continued from previous page

Stream	Season	Quadrant	T_{obs}	T_{pred}	95% PI	p_B
D-call	Summer	South Inshore	495	1403	[244, 6148]	0.882
D-call	Summer	South Offshore	79	120.5	[7, 1154]	0.648
D-call	Fall	North Inshore	62	129	[11, 934]	0.736
D-call	Fall	North Offshore	9	87	[11, 602]	0.979*
D-call	Fall	South Inshore	21	191	[14, 1332]	0.956*
D-call	Fall	South Offshore	50	31	[1, 321]	0.361
Fin whale						
Visual	Winter	North Inshore	6	30	[15, 54]	1.000*
Visual	Winter	North Offshore	3	12	[4, 24]	0.998*
Visual	Winter	South Inshore	14	17	[7, 34]	0.725
Visual	Winter	South Offshore	1	2	[0, 6]	0.835
Visual	Spring	North Inshore	24	55	[31, 96]	0.995*
Visual	Spring	North Offshore	7	14	[6, 26]	0.954*
Visual	Spring	South Inshore	19	26	[12, 47]	0.806
Visual	Spring	South Offshore	0	2	[0, 6]	1.000*
Visual	Summer	North Inshore	50	78	[45, 128]	0.948
Visual	Summer	North Offshore	48	24	[12, 42]	0.010*
Visual	Summer	South Inshore	32	51	[28, 95]	0.940
Visual	Summer	South Offshore	7	4	[0, 10]	0.133
Visual	Fall	North Inshore	19	36	[20, 61]	0.983*
Visual	Fall	North Offshore	30	14	[6, 26]	0.012*
Visual	Fall	South Inshore	15	34	[18, 61]	0.994*
Visual	Fall	South Offshore	1	3	[0, 9]	0.968

continued on next page

Table 5.7 continued from previous page

Stream	**Season**	**Quadrant**	T_{obs}	T_{pred}	**95% PI**	p_B
20 Hz	Winter	North Inshore	1753	3314.5	[682, 12485]	0.802
20 Hz	Winter	North Offshore	1518	3007	[797, 12733]	0.847
20 Hz	Winter	South Inshore	5996	2848.5	[680, 11410]	0.151
20 Hz	Winter	South Offshore	926	546.5	[104, 1992]	0.227
20 Hz	Spring	North Inshore	1897	1459.5	[333, 5078]	0.355
20 Hz	Spring	North Offshore	247	1394	[361, 5328]	0.994*
20 Hz	Spring	South Inshore	4103	2122	[610, 7179]	0.136
20 Hz	Spring	South Offshore	272	280	[68, 1054]	0.516
20 Hz	Summer	North Inshore	616	758	[217, 2468]	0.644
20 Hz	Summer	North Offshore	432	490	[147, 1958]	0.589
20 Hz	Summer	South Inshore	1601	775.5	[251, 2168]	0.086
20 Hz	Summer	South Offshore	29	79	[21, 299]	0.947
20 Hz	Fall	North Inshore	9442	5956	[1440, 18397]	0.247
20 Hz	Fall	North Offshore	2354	5769	[1784, 18226]	0.929
20 Hz	Fall	South Inshore	7188	5516.5	[1073, 21813]	0.351
20 Hz	Fall	South Offshore	689	891	[217, 3231]	0.639
40 Hz	Winter	North Inshore	65	74	[5, 450]	0.562
40 Hz	Winter	North Offshore	13	73	[8, 464]	0.943
40 Hz	Winter	South Inshore	88	74	[6, 503]	0.444
40 Hz	Winter	South Offshore	9	13	[0, 89]	0.646
40 Hz	Spring	North Inshore	112	96	[8, 574]	0.438
40 Hz	Spring	North Offshore	21	93	[10, 537]	0.928
40 Hz	Spring	South Inshore	200	141.5	[17, 666]	0.341

continued on next page

Table 5.7 continued from previous page

Stream	Season	Quadrant	T_{obs}	T_{pred}	95% PI	p_B
40 Hz	Spring	South Offshore	6	18	[1, 108]	0.852
40 Hz	Summer	North Inshore	298	667.5	[100, 3521]	0.816
40 Hz	Summer	North Offshore	46	463	[79, 2785]	0.993*
40 Hz	Summer	South Inshore	522	754	[110, 3867]	0.669
40 Hz	Summer	South Offshore	102	75	[11, 419]	0.360
40 Hz	Fall	North Inshore	90	84	[8, 456]	0.482
40 Hz	Fall	North Offshore	39	75	[10, 406]	0.758
40 Hz	Fall	South Inshore	16	71	[6, 512]	0.901
40 Hz	Fall	South Offshore	24	11	[0, 70]	0.245
Humpback whale						
Visual	Winter	North Inshore	32	95	[64, 139]	1.000*
Visual	Winter	North Offshore	14	16	[8, 27]	0.706
Visual	Winter	South Inshore	13	15	[7, 25]	0.719
Visual	Winter	South Offshore	1	8	[2, 15]	0.998*
Visual	Spring	North Inshore	188	147	[103, 208]	0.096
Visual	Spring	North Offshore	13	22	[12, 35]	0.972*
Visual	Spring	South Inshore	17	16	[8, 27]	0.415
Visual	Spring	South Offshore	4	8	[3, 16]	0.950*
Visual	Summer	North Inshore	112	83	[57, 116]	0.042*
Visual	Summer	North Offshore	2	13	[6, 22]	0.999*
Visual	Summer	South Inshore	6	15	[7, 25]	0.985*
Visual	Summer	South Offshore	1	9	[3, 16]	0.999*
Visual	Fall	North Inshore	89	53	[36, 74]	0.002*

continued on next page

Table 5.7 continued from previous page

Stream	**Season**	**Quadrant**	T_{obs}	T_{pred}	**95% PI**	p_B
Visual	Fall	North Offshore	3	8	[3, 16]	0.989*
Visual	Fall	South Inshore	13	13.5	[6, 22]	0.592
Visual	Fall	South Offshore	1	7	[2, 14]	1.000*
Acoustic	Winter	North Inshore	275	809.5	[406, 1353]	0.998*
Acoustic	Winter	North Offshore	1174	336.5	[98, 757]	0.001*
Acoustic	Winter	South Inshore	288	296	[86, 622]	0.518
Acoustic	Winter	South Offshore	598	185.5	[39, 516]	0.015*
Acoustic	Spring	North Inshore	321	357.5	[127, 730]	0.623
Acoustic	Spring	North Offshore	100	185	[31, 528]	0.793
Acoustic	Spring	South Inshore	181	167	[26, 426]	0.448
Acoustic	Spring	South Offshore	258	98	[6, 342]	0.079
Acoustic	Summer	North Inshore	394	271	[73, 641]	0.236
Acoustic	Summer	North Offshore	13	113	[10, 406]	0.969*
Acoustic	Summer	South Inshore	23	101	[7, 395]	0.902
Acoustic	Summer	South Offshore	22	61	[1, 303]	0.801
Acoustic	Fall	North Inshore	620	302.5	[93, 664]	0.039*
Acoustic	Fall	North Offshore	146	113	[12, 356]	0.359
Acoustic	Fall	South Inshore	90	72.5	[3, 306]	0.431
Acoustic	Fall	South Offshore	27	60	[1, 273]	0.729